

Sheffield Hallam University

Strategies for the examination of Alzheimer's disease amyloid precursor protein isoforms.

NEWTON, Jillian R.A.

Available from the Sheffield Hallam University Research Archive (SHURA) at:

<http://shura.shu.ac.uk/20769/>

A Sheffield Hallam University thesis

This thesis is protected by copyright which belongs to the author.

The content must not be changed in any way or sold commercially in any format or medium without the formal permission of the author.

When referring to this work, full bibliographic details including the author, title, awarding institution and date of the thesis must be given.

Please visit <http://shura.shu.ac.uk/20769/> and <http://shura.shu.ac.uk/information.html> for further details about copyright and re-use permissions.

101 766 217 7



SHEFFIELD HALLAM UNIVERSITY
LEARNING CENTRE
COLLEGIATE CRESCENT
SHEFFIELD S10 2BP

REFERENCE

ProQuest Number: 10702871

All rights reserved

INFORMATION TO ALL USERS

The quality of this reproduction is dependent upon the quality of the copy submitted.

In the unlikely event that the author did not send a complete manuscript and there are missing pages, these will be noted. Also, if material had to be removed, a note will indicate the deletion.



ProQuest 10702871

Published by ProQuest LLC (2017). Copyright of the Dissertation is held by the Author.

All rights reserved.

This work is protected against unauthorized copying under Title 17, United States Code
Microform Edition © ProQuest LLC.

ProQuest LLC.
789 East Eisenhower Parkway
P.O. Box 1346
Ann Arbor, MI 48106 – 1346



Strategies for the Examination of
Alzheimer's Disease
Amyloid Precursor Protein Isoforms

Jillian Rose Ann Newton

A thesis submitted in partial fulfilment of
the requirements of Sheffield Hallam
University for the degree of Doctor of
Philosophy

May 2004

Abstract

The principal aim of this research project has been the utilisation of various proteomic techniques in the investigation of the Alzheimer's disease amyloid precursor protein (APP) isoforms, namely APP₆₉₅, APP₇₅₁ and APP₇₇₀. One of the most noticeable pathological characteristics of Alzheimer's disease is the presence of neuritic plaques in brain tissue. The chief protein constituent of neuritic plaques is the beta amyloid peptide. This peptide is proteolytically cleaved from APP, as such the interest in APP isoforms is great and a rapid detection method for the presence of each isoform would be a huge advantage to the research effort with regards to the determination and concentration in both diseased and non-diseased states. Two-dimensional gel electrophoresis and peptide mass fingerprinting are two of the most important techniques in the proteomics arena and both are investigated fully in this work. Retinoic acid induced Ntera 2 cells, derived from a human teratocarcinoma cell line, were the *in vitro* source of APP. Initial isolation of APP was performed by immunoprecipitation, using a monoclonal antibody raised to amino acids 1-17 of the β -amyloid peptide sequence, which is present in all three alpha secretase cleaved isoforms of interest. The next step was to separate whole APP into its isoform components by two-dimensional gel electrophoresis. The resulting protein spots were then subjected to peptide mass fingerprinting employing the different digest reagents, trypsin, endoproteinase Asp-N and formic acid. Initial distinction between the APP isoforms could be seen upon examination of theoretical *in silico* digests using the various digest reagents mentioned. The *in silico* digests revealed peptides unique to each isoform that in theory could be used as indicators of isoform presence.

Table of Contents

Contents	Page
Title Page	i
Abstract	ii
Table of contents	iii
1.0 Introduction	1
1.1 Alzheimer's Disease	2
1.2 Proteomics	22
1.21 Protein separation	24
1.211 Sodium dodecylsulphate polyacrylamide electrophoresis	24
1.212 Western blotting	26
1.22 In-gel digestion	29
1.23 Protein detection	33
1.231 Mass spectrometry	33
1.2311 Matrix assisted laser desorption ionisation-mass spectrometry	34
1.2312 Electrospray ionisation-mass spectrometry	45
1.24 Information Dependent Acquisition	59
1.25 Protein fragmentation	60
1.26 Protein modifications	65
1.27 Protein identification	68
1.271 Bioinformatics	68
1.28 Application of proteomics to the study of Alzheimer's disease	74
2.0 Experimental	76

3.454 Capillary LC/MS analysis of a two-dimensional in-gel Asp-N digestion of alpha secretase cleaved amyloid precursor protein standard, isoform 695	231
3.455 MALDI-MS analysis of a two-dimensional in-gel Asp-N digestion of alpha secretase cleaved amyloid precursor protein, isoform 770	235
3.456 Capillary LC/MS analysis of a two-dimensional in-gel Asp-N digestion of alpha secretase cleaved amyloid precursor protein, isoform 770	236
3.457 MALDI-MS analysis of a two-dimensional in-gel Asp-N digestion of alpha secretase cleaved amyloid precursor protein	240
3.458 Capillary LC/MS analysis of a two-dimensional in-gel Asp-N digestion of alpha secretase cleaved amyloid precursor protein	241
3.46 Two-dimensional in-gel formic acid digestion of bovine serum albumin and amyloid precursor protein	245
3.461 MALDI-MS analysis of a two-dimensional in-gel formic acid digestion of bovine serum albumin	245
3.462 Capillary LC/MS analysis of a two-dimensional in-gel formic acid digestion of bovine serum albumin	246
3.463 MALDI-MS analysis of a two-dimensional in-gel formic acid digestion of alpha secretase cleaved amyloid precursor protein standard, isoform 695	248
3.464 Capillary LC/MS analysis of a two-dimensional in-gel formic acid digestion of alpha secretase cleaved amyloid precursor protein standard, isoform 695	249
3.465 MALDI-MS analysis of a two-dimensional in-gel formic acid digestion of alpha secretase cleaved amyloid precursor protein, isoform 770	251
3.466 Capillary LC/MS analysis of a two-dimensional in-gel formic acid digestion of alpha secretase cleaved amyloid precursor protein, isoform 770	252
3.467 MALDI-MS analysis of a two-dimensional in-gel formic acid digestion of alpha secretase cleaved amyloid precursor protein	254

2.1 Reduction and alkylation of Ntera 2 conditioned media and Chinese hamster ovary (CHO) 770 cells	77
2.2 Immunoprecipitation of amyloid precursor protein	77
2.3 Standard Protein Solutions	78
2.4 One-dimensional SDS-PAGE	78
2.5 Two dimensional SDS-PAGE	84
2.6 Electro-transfer of proteins from polyacrylamide gels	86
2.7 Western Blotting	87
2.8 In-gel digestion	88
2.9 Mass spectrometry	91
2.91 Matrix assisted laser desorption ionisation-mass spectrometry	91
2.92 Liquid chromatography electrospray ionisation-mass spectrometry	92
2.93 Nanospray-mass spectrometry	94
3.0 Results and Discussion	95
3.1 Isolation of amyloid precursor protein isoforms from conditioned media	98
3.11 One-dimensional gel electrophoresis	100
3.111 One-dimensional gel electrophoresis of bovine serum albumin	100
3.112 Comparison of immunoprecipitation methods	100
3.113 Comparison of bead elution methods	102
3.114 Optimal concentration of AB10 primary antibody	104
3.115 One-dimensional gel electrophoresis of amyloid precursor protein isoforms	105
3.12 Two-dimensional gel electrophoresis	107
3.121 Two-dimensional gel electrophoresis of bovine serum albumin	107
3.122 Two-dimensional gel electrophoresis of amyloid precursor protein isoforms	108

3.1221 Two-dimensional gel electrophoresis of alpha secretase cleaved amyloid precursor protein standard, isoform 695	108
3.1222 Two-dimensional gel electrophoresis of alpha secretase cleaved amyloid precursor protein, isoform 770	110
3.1223 Two-dimensional gel electrophoresis of alpha secretase cleaved amyloid precursor protein	112
3.2 Examination of intact bovine serum albumin and amyloid precursor protein	114
3.21 MALDI-MS and nanospray analysis of intact bovine serum albumin	114
3.211 MALDI-MS of intact bovine serum albumin	114
3.212 Nanospray of intact bovine serum albumin	114
3.22 MALDI-MS and nanospray analysis of intact alpha secretase cleaved amyloid precursor protein standard, isoform 695	116
3.221 MALDI-MS of intact alpha secretase cleaved amyloid precursor protein standard, isoform 695	116
3.222 Nanospray of intact alpha secretase cleaved amyloid precursor protein standard, isoform 695	116
3.23 MALDI-MS and nanospray analysis of intact alpha secretase cleaved amyloid precursor protein, isoform 770	118
3.231 MALDI-MS of intact alpha secretase cleaved amyloid precursor protein, isoform 770	118
3.232 Nanospray of intact alpha secretase cleaved amyloid precursor protein, isoform 770	118
3.24 MALDI-MS and nanospray analysis of intact alpha secretase cleaved amyloid precursor protein	120
3.241 MALDI-MS of intact alpha secretase cleaved amyloid precursor protein	120
3.242 Nanospray of intact alpha secretase cleaved amyloid precursor protein	120

3.3 In-silico digestion of APP isoforms	122
3.4 Analysis by mass spectrometry of the in-gel digestion of bovine serum albumin and amyloid precursor protein	129
3.41 One-dimensional in-gel tryptic digestion of bovine serum albumin and amyloid precursor protein	131
3.411 MALDI-MS analysis of a one-dimensional in-gel tryptic digestion of bovine serum albumin	131
3.412 Capillary LC/MS analysis of a one-dimensional in-gel tryptic digestion of bovine serum albumin	134
3.413 MALDI-MS analysis of a one-dimensional in-gel tryptic digestion of alpha secretase cleaved amyloid precursor protein standard, isoform 695	137
3.414 Capillary LC/MS analysis of a one-dimensional in-gel tryptic digestion of alpha secretase cleaved amyloid precursor protein standard, isoform 695	141
3.415 MALDI-MS analysis of a one-dimensional in-gel tryptic digestion of alpha secretase cleaved amyloid precursor protein, isoform 770	146
3.416 Capillary LC/MS analysis of a one-dimensional in-gel tryptic digestion of alpha secretase cleaved amyloid precursor protein, isoform 770	149
3.417 MALDI-MS analysis of a one-dimensional in-gel tryptic digestion of alpha secretase cleaved amyloid precursor protein	153
3.418 Capillary LC/MS analysis of a one-dimensional in-gel tryptic digestion of alpha secretase cleaved amyloid precursor protein	156
3.42 One-dimensional in-gel Asp-N digestion of bovine serum albumin and amyloid precursor protein	160
3.421 MALDI-MS analysis of a one-dimensional in-gel Asp-N digestion of bovine serum albumin	160
3.422 Capillary LC/MS analysis of a one-dimensional in-gel Asp-N digestion of bovine serum albumin	163
3.423 MALDI-MS analysis of a one-dimensional in-gel Asp-N digestion of alpha secretase cleaved amyloid precursor protein standard, isoform 695	167

3.424 Capillary LC/MS analysis of a one-dimensional in-gel Asp-N digestion of alpha secretase cleaved amyloid precursor protein standard, isoform 695	170
3.425 MALDI-MS analysis of a one-dimensional in-gel Asp-N digestion of alpha secretase cleaved amyloid precursor protein, isoform 770	174
3.426 Capillary LC/MS analysis of a one-dimensional in-gel Asp-N digestion of alpha secretase cleaved amyloid precursor protein, isoform 770	175
3.427 MALDI-MS analysis of a one-dimensional in-gel Asp-N digestion of alpha secretase cleaved amyloid precursor protein	179
3.428 Capillary LC/MS analysis of a one-dimensional in-gel Asp-N digestion of alpha secretase cleaved amyloid precursor protein	180
3.43 One-dimensional in-gel formic acid digestion of bovine serum albumin and amyloid precursor protein	183
3.431 MALDI-MS analysis of a one-dimensional in-gel formic acid digestion of bovine serum albumin	183
3.432 Capillary LC/MS analysis of a one-dimensional in-gel formic acid digestion of bovine serum albumin	184
3.433 MALDI-MS analysis of a one-dimensional in-gel formic acid digestion of alpha secretase cleaved amyloid precursor protein standard, isoform 695	186
3.434 Capillary LC/MS analysis of a one-dimensional in-gel formic acid digestion of alpha secretase cleaved amyloid precursor protein standard, isoform 695	187
3.435 MALDI-MS analysis of a one-dimensional in-gel formic acid digestion of alpha secretase cleaved amyloid precursor protein, isoform 770	189
3.436 Capillary LC/MS analysis of a one-dimensional in-gel formic acid digestion of alpha secretase cleaved amyloid precursor protein, isoform 770	190
3.437 MALDI-MS analysis of a one-dimensional in-gel formic acid digestion of alpha secretase cleaved amyloid precursor protein	192

3.438 Capillary LC/MS analysis of a one-dimensional in-gel formic acid digestion of alpha secretase cleaved amyloid precursor protein	193
3.44 Two-dimensional in-gel tryptic digestion of bovine serum albumin and amyloid precursor protein	195
3.441 MALDI-MS analysis of a two-dimensional in-gel tryptic digestion of bovine serum albumin	195
3.442 Capillary LC/MS analysis of a two-dimensional in-gel tryptic digestion of bovine serum albumin	198
3.443 MALDI-MS analysis of a two-dimensional in-gel tryptic digestion of alpha secretase cleaved amyloid precursor protein standard, isoform 695	202
3.444 Capillary LC/MS analysis of a two-dimensional in-gel tryptic digestion of alpha secretase cleaved amyloid precursor protein standard, isoform 695	205
3.445 MALDI-MS analysis of a two-dimensional in-gel tryptic digestion of alpha secretase cleaved amyloid precursor protein, isoform 770	210
3.446 Capillary LC/MS analysis of a two-dimensional in-gel tryptic digestion of alpha secretase cleaved amyloid precursor protein, isoform 770	213
3.447 MALDI-MS analysis of a two-dimensional in-gel tryptic digestion of alpha secretase cleaved amyloid precursor protein	217
3.448 Capillary LC/MS analysis of a two-dimensional in-gel tryptic digestion of alpha secretase cleaved amyloid precursor protein	220
3.45 Two-dimensional in-gel Asp-N digestion of bovine serum albumin and amyloid precursor protein	224
3.451 MALDI-MS analysis of a two-dimensional in-gel Asp-N digestion of bovine serum albumin	224
3.452 Capillary LC/MS analysis of a two-dimensional in-gel Asp-N digestion of bovine serum albumin	225
3.453 MALDI-MS analysis of a two-dimensional in-gel Asp-N digestion of alpha secretase cleaved amyloid precursor protein standard, isoform 695	228

3.454 Capillary LC/MS analysis of a two-dimensional in-gel Asp-N digestion of alpha secretase cleaved amyloid precursor protein standard, isoform 695	231
3.455 MALDI-MS analysis of a two-dimensional in-gel Asp-N digestion of alpha secretase cleaved amyloid precursor protein, isoform 770	235
3.456 Capillary LC/MS analysis of a two-dimensional in-gel Asp-N digestion of alpha secretase cleaved amyloid precursor protein, isoform 770	236
3.457 MALDI-MS analysis of a two-dimensional in-gel Asp-N digestion of alpha secretase cleaved amyloid precursor protein	240
3.458 Capillary LC/MS analysis of a two-dimensional in-gel Asp-N digestion of alpha secretase cleaved amyloid precursor protein	241
3.46 Two-dimensional in-gel formic acid digestion of bovine serum albumin and amyloid precursor protein	245
3.461 MALDI-MS analysis of a two-dimensional in-gel formic acid digestion of bovine serum albumin	245
3.462 Capillary LC/MS analysis of a two-dimensional in-gel formic acid digestion of bovine serum albumin	246
3.463 MALDI-MS analysis of a two-dimensional in-gel formic acid digestion of alpha secretase cleaved amyloid precursor protein standard, isoform 695	248
3.464 Capillary LC/MS analysis of a two-dimensional in-gel formic acid digestion of alpha secretase cleaved amyloid precursor protein standard, isoform 695	249
3.465 MALDI-MS analysis of a two-dimensional in-gel formic acid digestion of alpha secretase cleaved amyloid precursor protein, isoform 770	251
3.466 Capillary LC/MS analysis of a two-dimensional in-gel formic acid digestion of alpha secretase cleaved amyloid precursor protein, isoform 770	252
3.467 MALDI-MS analysis of a two-dimensional in-gel formic acid digestion of alpha secretase cleaved amyloid precursor protein	254

3.468 Capillary LC/MS analysis of a two-dimensional in-gel formic acid digestion of alpha secretase cleaved amyloid precursor protein	255
4.0 Conclusions and future work	261
5.0 Appendices	267
5.1 Appendix 1 – Presentations and conferences attended	267
5.2 Appendix 2 - In-gel digestion	269
5.3 Appendix 3 – Mass spectrometry	271
5.4 Appendix 4 – Protein fragmentation	273
5.5 Appendix 5 – Protein modifications	276
5.6 Appendix 6 - Fluorescent stain, Ruthenium II bathophenanthroline	278
5.7 Appendix 7- Theoretical digest lists for APP isoforms	279
6.0 References	292
Acknowledgments	324

Proteomic techniques are utilised in this research for the investigation of the Alzheimer's disease amyloid precursor protein (APP) isoforms, namely the three isoforms implicated with Alzheimer's disease; APP₆₉₅, APP₇₅₁ and APP₇₇₀. This chapter provides a brief review of Alzheimer's disease giving the reader an overall view of the history, clinical and pathological characteristics, aetiology, treatment and research into Alzheimer's disease. This is followed by an introduction into proteomics covering the main techniques utilised in this science and finally the application of proteomics to Alzheimer's disease research.

1.1 Alzheimer's Disease

Alzheimer's disease was first described in 1906¹ by Alois Alzheimer, an Austrian physician. Whilst working on staining techniques for the cerebral cortex Alzheimer observed nerve cell loss, plaques and tangles in tissue derived from a 51-year-old sufferer of presenile dementia.

Alzheimer's disease (AD) is the most common single cause of dementia in the elderly. The number of afflicted individuals doubles every five years after the age of 60. It is seen in ~1% of 60 year olds, rising to a prevalence of >40% in 85 year olds². The disease typically begins in middle to late adult life and is noticeable from a series of clinical features, such as impairment of cognitive function (beginning with general forgetfulness and loss of recent or immediate recall), progressing to remote recall. It is a progressive, irreversible, neurodegenerative disorder, causing intellectual impairment, disorientation and eventually death. Sufferers show an inability to perform new and previously learned tasks that involve intellectual thinking and have impaired judgement and slowed responses. Mood swings are common, ranging from

euphoria to depression and anxiety and ending in a sullen vegetative state. Behaviour is uncharacteristic, often antisocial and disorientated. The disease gradually deteriorates over a period of five to fifteen years rendering patients bedridden and ending in death, either from organ failure or more commonly from complications arising from their bedridden state, such as bed sores and bladder infections. Whilst there are numerous pharmaceuticals accessible for the treatment of AD³ no cure is currently available⁴.

The pathological characteristics of AD include a profound loss of brain tissue, visible as valleys and troughs, rather than the clefts and fissures associated with healthy tissue. At a microscopic level an accumulation of fibrous proteins can be seen inside the cytoplasm of nerve cells within the cortex of the brain, forming dense neurofibrillary tangles. The cytoplasmic tangles are bundles of paired, helically wound, 10nm filaments (PHFs), combined with straight filaments⁵ (figure 1)⁶. Tangles are present mainly in the entorhinal cortex, hippocampus, amygdala, associated cortexes of the frontal, temporal and parietal lobes and subcortical nuclei that project into these regions. The principal protein subunit of PHFs is a hyperphosphorylated version of a protein known as tau,⁷ (figure 2a)⁸, whose normal physiological role is the assembly of the microtubule skeleton and cellular transport, a function that is abolished by hyperphosphorylation⁹. Normally occurring tau is highly soluble but hyperphosphorylation renders it insoluble causing it to aggregate in tangles, often complexed with ubiquitin. Ubiquitinated tangles are also a feature of

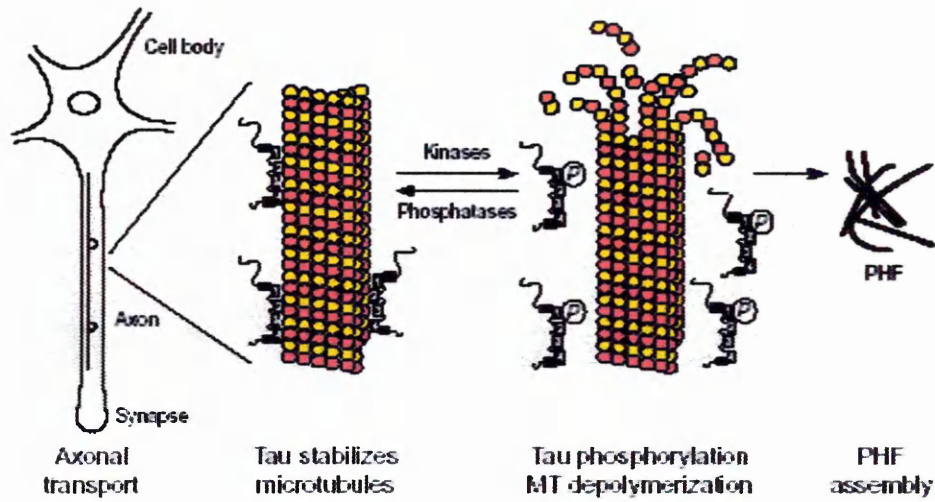
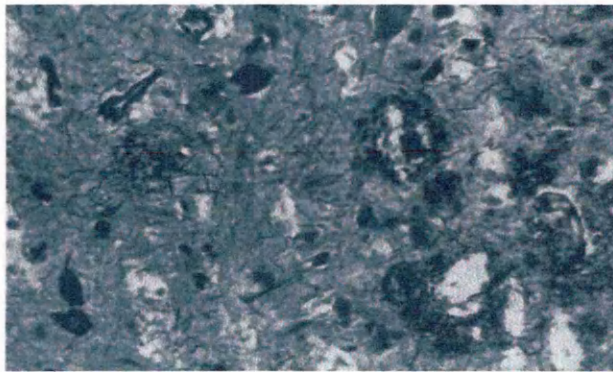


Figure 1⁶. Scheme showing a possible link between axonal transport, microtubules and tau in Alzheimer's disease.

(a)



(b)

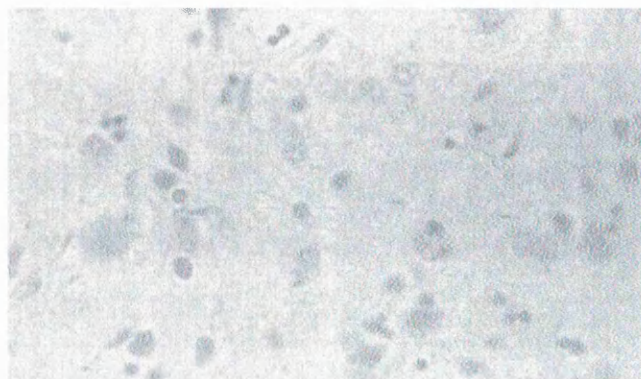


Figure 2⁸. (a) Neurofibrillary tangles characteristic of Alzheimer's disease, containing the hyperphosphorylated forms of tau, (b) Extracellular amyloid plaques characteristic of Alzheimer's disease, composed principally of amyloid beta peptide.

other neuronal disorders, such as Parkinson's and Lewy body disease. It is thought that the presence of ubiquitin may be an attempt to degrade the tangles by action of the proteasome, if this is the case, however, it is largely unsuccessful. The other pathological representation of AD most currently and enthusiastically researched is the presence of senile or neuritic plaques (figure 2b), seen as an aggregation of fibrous proteins within the extracellular space. The major protein constituent of these plaques is an insoluble, highly aggregating, 4kDa (39 to 43 amino acids) peptide, known as the beta amyloid ($A\beta$) peptide, first isolated and characterised by Glenner and Wong, 1984¹⁰. $A\beta$ plaque formation is mainly within the cerebral and limbic cortices, deposits are also found on the walls of meningeal and cerebral blood vessels¹¹. Plaques are present in two forms, fibrillar and non-fibrillar.

The non-fibrillar plaques present in AD brain are termed 'diffuse' and occur as insoluble clumps (8-10nm), granular in appearance and intermingled almost exclusively with non-fibrillar, 42-residue amyloidogenic $A\beta$ peptide ($A\beta_{42}$)¹². Diffuse plaques appear within regions of the AD brain, not generally concerned with the disease and also in healthy aged brains. The fibrillar forms of plaques are termed 'neuritic' plaques and exist solely within disease regions. These plaques are made up of a mixture of both the non-amyloidogenic $A\beta_{40}$ and the amyloidogenic $A\beta_{42}$, yet strangely enough it is the non-amyloidogenic version of the peptide that predominates here (~90%).

Although primarily associated with the elderly the aetiology of AD is still unknown. There are ever increasing reports of early onset (EOAD)¹³, familial (FAD)¹⁴ and links to Down's syndrome¹⁵ suggesting a genetic aetiology, however, several other risk

factors are also apparent such as, metabolic disturbances, environmental origins, high blood pressure, bacterial/viral infections and head trauma, with genetic factors only accounting for around 5% of all cases³. One of the aspects that AD research has uncovered is the sheer complexity and multifactorial nature of this disease. The possibility cannot be ruled out, therefore, that genetics are more frequently involved than first thought, perhaps as an initial switch turned on, for example by the more obvious environmental, metabolic or bacterial factors. There are at least four genes implicated in the development of AD; the amyloid precursor protein (APP) gene, ApoE4 gene and the presenilin 1 (PS1) and 2 (PS2) genes, a list that is, however, by no means definitive^{16,17}. Individuals exhibiting two copies of the ApoE4 gene have been shown to be at a greater risk of developing late onset AD¹⁸ and both FAD and EOAD are strongly linked with mutations in the APP, PS1 and PS2 genes¹⁹. There are also chromosomal links as opposed to just the gene loci themselves, the most prominent example being the association with Down's syndrome²⁰. A single gene on the long arm of chromosome 21 (21q21) codes APP and was cloned in 1987 by Tanzi *et al*²¹. This area is duplicated in Down's syndrome and studies have shown this to be true in cases of AD²², providing evidence for the 'gene dosage' hypothesis, where it is thought that over expression due to duplication of the genes is causative of the disease, yet several other studies have shown this phenomenon to be unrepeatabe^{23,24}.

In 1987 Kang *et al*²⁵ isolated and sequenced a 695 residue protein, using a probe designed from the *N*-terminus of the A β peptide. Initially termed the precursor of A β peptide, later referred to as the amyloid precursor protein (APP). APP is part of a large family of transmembrane and secreted proteins, whose constitutive expression and evolutionary conservation is seen in many cell types. The heterogeneity of APP

arises from both alternative splicing and post-translational processing, including the addition of *N*- and *O*- linked sugars, phosphates and sulphates. The mammalian APP family has three members; APP and APP-like proteins, APLP1 and APLP2²⁶. APP exists in both secreted and membrane bound forms. Membrane bound APP is a type I integral membrane protein, whose primary structure strongly resembles a cell surface receptor with a signal sequence, a single transmembrane domain and a small cytoplasmic tail. The gene has 19 exons²⁷, of which exons 7, 8 and 15 can be alternatively spliced producing at least 10 protein isoforms (table 1)²⁸. The three most relevant isoforms with respect to AD are APP₆₉₅ restricted to the central nervous system (CNS), APP₇₅₁ and APP₇₇₀ both expressed in peripheral and CNS tissues (figure 3). All three contain the full length A β peptide and therefore have the ability to be processed into the potentially amyloidogenic A β peptide. APP₇₇₀ is the full length protein, APP₇₅₁ lacks exon 8 that codes for a 19 residue domain with homology to the MRC OX-2 antigen found on the membrane of neurons and thymocytes²⁹. APP₆₉₅ lacks both exon 8 and exon 7, the latter coding for a 57-residue domain bearing homology to a serine protease inhibitor of the Kunitz type (KPI)³⁰. The serine protease inhibitory quality of the KPI containing isoforms, APP₇₅₁ and APP₇₇₀ uncovers the function of these isoforms present in platelets, where they are involved in the inhibition of factors of the coagulation cascade. Splice variants lacking exon 15 along with various combinations of exons 7 and 8 are referred to as leukocyte derived APP's (L-APP's) because of their initial identification from peripheral lymphocytes³¹, however, expression has since been observed in almost all tissues³². Exon 15 codes for an 18 residue domain proximal to the A β peptide region, excision of this exon results in a chondroitin-sulphate-glycosaminoglycan attachment site. Attachment of this moiety results in a high molecular mass APP called appican³³ involved in the

adhesion of neural cells to the extracellular matrix and possible regulation of neurite outgrowth within the brain.

Isoform	Main cell types expressing the isoforms in brain
APP695	Neurons >> other cells
APP714	Meninges, glia, endothelia, neurons
APP751	Neurons > other cells
APP770	Meninges, glia, endothelia, > neurons
L-APP	Lymphocytes, microglia. Not in neurons
APP365	Unknown
APP563	Unknown

Table 1. Localisation of APP mRNA isoforms in human brain

After synthesis on the ribosomes APP is co-translationally translocated into the endoplasmic reticulum (ER) by its signal peptide where *N*-glycosylation occurs. The next stage is maturation through the central secretory pathway to the trans-Golgi network (TGN) and it is here that *O*-glycosylation and sulphation occurs releasing the mature molecule (figure 4). Phosphorylation either takes place within the post-Golgi network or at the cell surface. Only a small fraction of the holoprotein actually reaches the cell surface the majority being degraded within the secretory pathway³⁴.

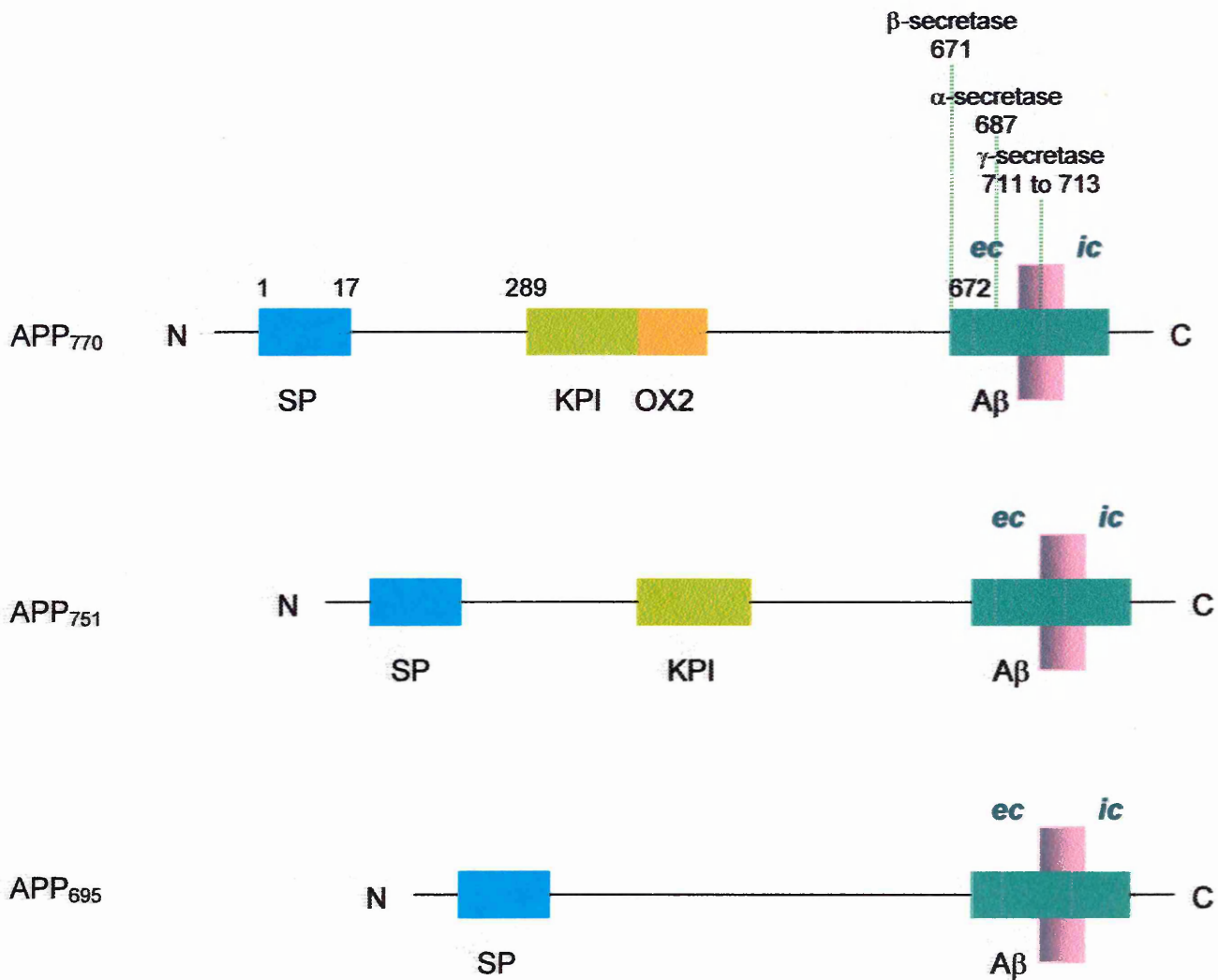


Figure 3. Schematic diagram of APP₇₇₀, APP₇₅₁ and APP₆₉₅, showing regions distinct to each isoform and the cleavage site for α, β and γ secretase (all amino acid residues APP₇₇₀ numbering). Abbreviations: Aβ, beta amyloid sequence; *ec*, extracellular domain; *ic*, intracellular domain; KPI, Kunitz type protease inhibitor; OX2, OX2 homology domain.

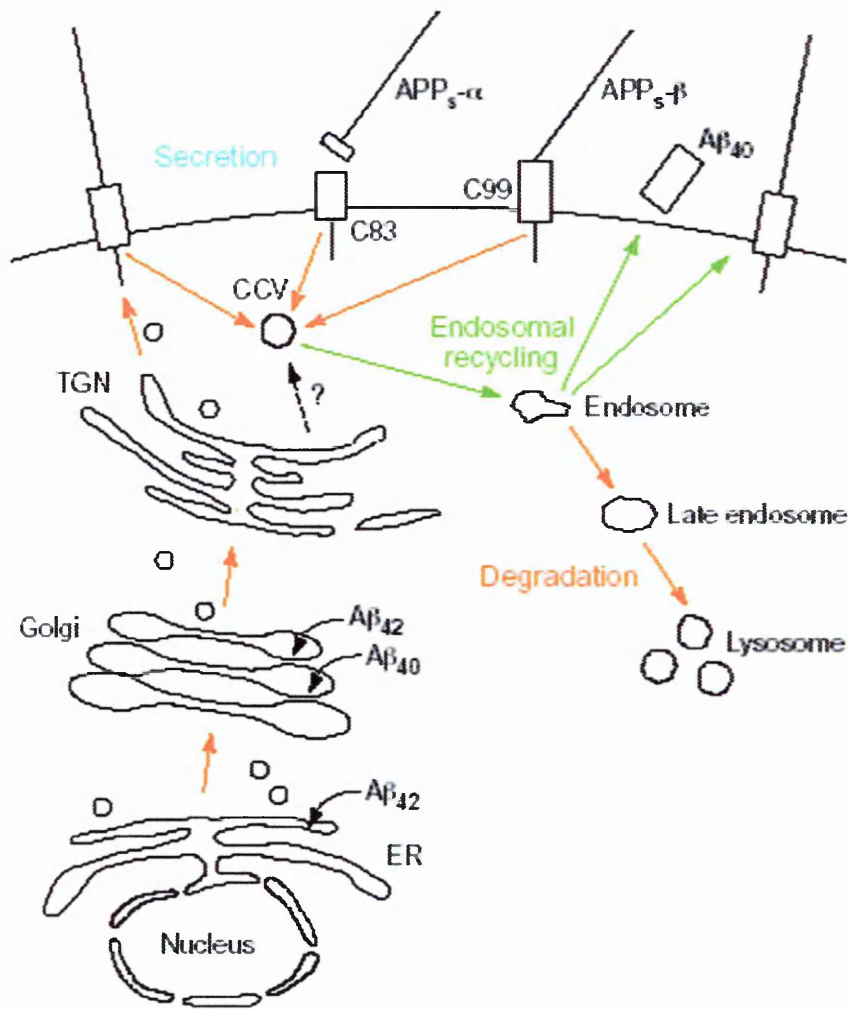


Figure 4⁶. Principal trafficking routes of APP.

APP has several different cleavage pathways performed by α , β and γ secretase (figure 5)³⁵. Proteolysis of APP performed by α -secretase requires the molecule to be membrane bound. It was initially thought that this principal secretory cleavage event occurred only at the cell surface, however, it is now believed to take place also within the late Golgi and trans-Golgi networks. Cleavage by α -secretase releases soluble APP (APPs- α) into the extracellular space whilst the C-terminus is internalised and degraded by endosomes and lysosomes. Any uncleaved APP present at the cell surface is rapidly internalised into clathrin-coated vesicles (CCV's) entering the

endosomal system and degradation³⁶. The α -secretase cleavage site is within the A β domain and as such precludes the formation of the A β peptide. It was originally thought that the A β peptides were only formed as a result of aberrant processing³⁷ but it is now known that they are part of normal APP metabolism³⁸. Formation of A β peptides involves cleavage by β and γ secretase. β -secretase cleavage occurs within the ER and as with α -secretase acts only upon the membrane bound molecule, yielding the A β N-terminus and releasing the truncated form of soluble APP (APPs- β) from the cell. The C-terminus of A β is formed by cleavage with γ secretase and results in A β_{1-40} , non-amyloidogenic peptide or A β_{1-42} , amyloidogenic peptide. It is uncertain whether production of the peptides arises from two independent γ -secretase enzymes, as it is believed that A β_{1-42} is generated in the ER and intermediate Golgi and A β_{1-40} in the trans-Golgi³⁹.

The proteolytic mechanism of α -secretase may have helped to uncover its true identity. APP processing involves both constitutive and regulated components with activation by either protein kinase C (PKC) or other second messenger cascades. Research into the ADAM (A Disintegrin And Metalloprotease) enzymes uncovered three family members as strong candidates; ADAM 10,⁴⁰; ADAM 9⁴¹ and ADAM 17 also known as tumour necrosis factor-converting enzyme (TACE)⁴². TACE knockout mice showed deficits in APP secretion and cotransfection of ADAM 9 and 10 with APP resulted in increased secretion of soluble α cleaved APP. Positive identification of β -secretase came in 1999 with the simultaneous publications from four independent groups^{43,44,45,46}. Using separate approaches all four groups revealed β -secretase to be a novel aspartic protease termed BACE (beta site APP cleaving

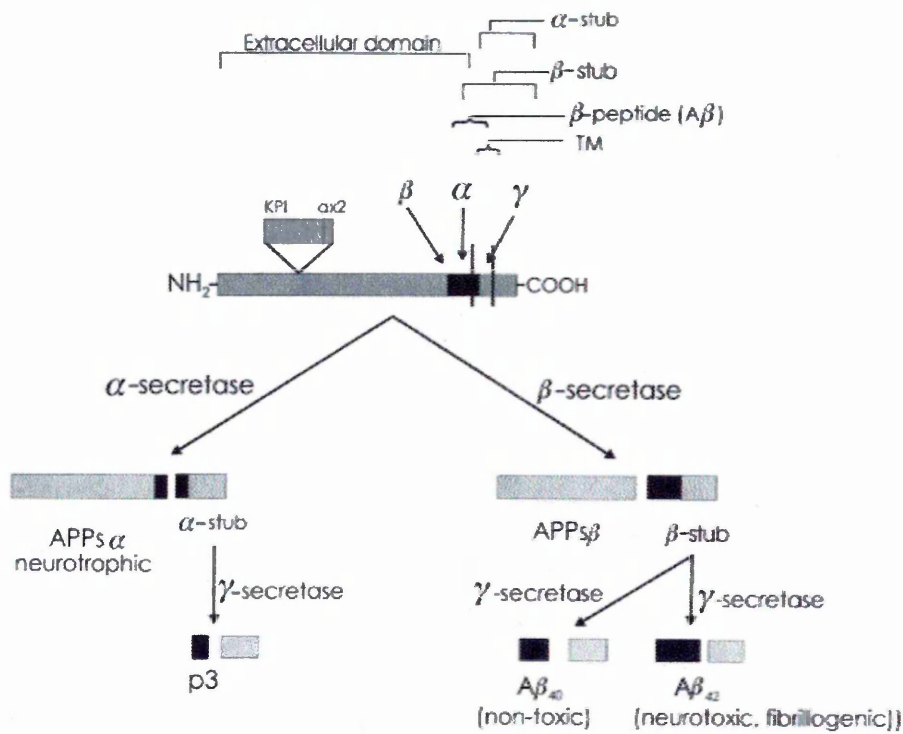


Figure 5³⁵. Proteolytic cleavage pathway of APP. α -secretase cleaves within the $A\beta$ sequence (shown in black) between residues Lys₆₈₇ and Leu₆₈₈, liberating APPs- α . The other pathway involves β and γ -secretases. β -secretase cleaves between Met₆₇₁ and Asp₆₇₂ and γ -secretase cleaves after Ile₇₁₂, Thr₇₁₄ or Val₇₁₅ to generate $A\beta_{40}$, $A\beta_{42}$ or $A\beta_{43}$ respectively.

enzyme). BACE is a type I integral membrane protein, highly expressed in brain tissue and found to have a higher affinity for APP forms with the Swedish mutation known to be causative in FAD. Evidence exists that γ -secretase is either the membrane protein presenilin 1⁴⁷ or that presenilins are important cofactors in APP cleavage⁴⁸ and that activity is due to a multiprotein complex⁴⁹ (figure 6)⁵⁰.

Although many of APP's structural domains are now well documented (figure 7)⁵¹, giving an excellent insight into its possible functionalities (table 2)⁵⁰ they are as yet still poorly understood. Its overall structure suggests a role as a receptor or growth factor⁵² but functionality research has been confused by the presence of both secreted and membrane bound forms, most of the work being centred upon secreted APP as

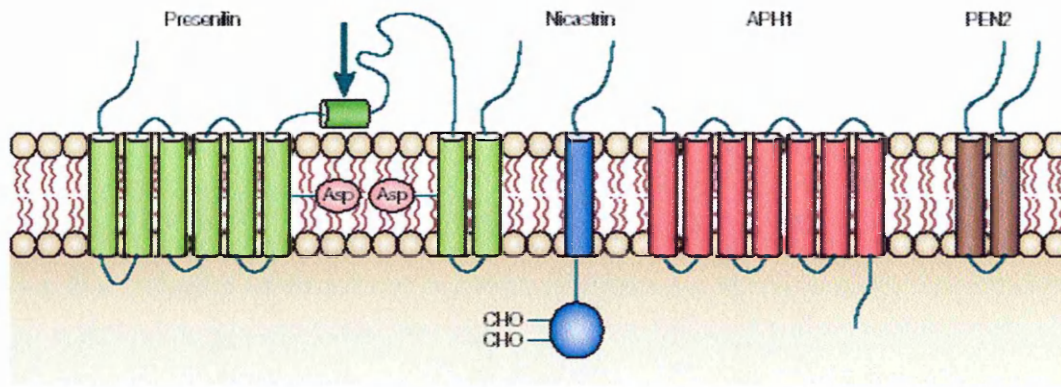


Figure 6⁵⁰. Components of the γ -secretase complex⁵⁰. The complex is made up of at least four integral membrane proteins. The active site is thought to reside in presenilin, which is cleaved into two pieces, indicated by the arrow, that remain associated as heterodimers. Glycosylated Nicastrin, APH1 and PEN2 proteins associate with the dimers and are required for protease activity.

Activity	Proposed function
Binds and reduces copper Binds zinc	Metal ion homeostasis
Stimulates neurite out growth and synaptogenesis	Regulation of neurite outgrowth and/or synaptic plasticity
Binds HSPG, glypican, collagen and laminin	Regulation of neurite outgrowth
Stimulates cell extracellular matrix adhesion	Mediator of cell matrix and cell-cell interactions
Stimulates mitogenesis, MAP kinases and G ₀ proteins	Regulation of cell proliferation, differentiation and survival
Alters cGMP levels, calcium homeostasis and K ⁺ channel activation	Neuroprotection
Protects against excitotoxicity, hyperglycaemia and brain ischaemia	
Serine protease inhibition	Regulation of blood coagulation

Table 2⁵⁰. Activities and corresponding function of APP⁵².

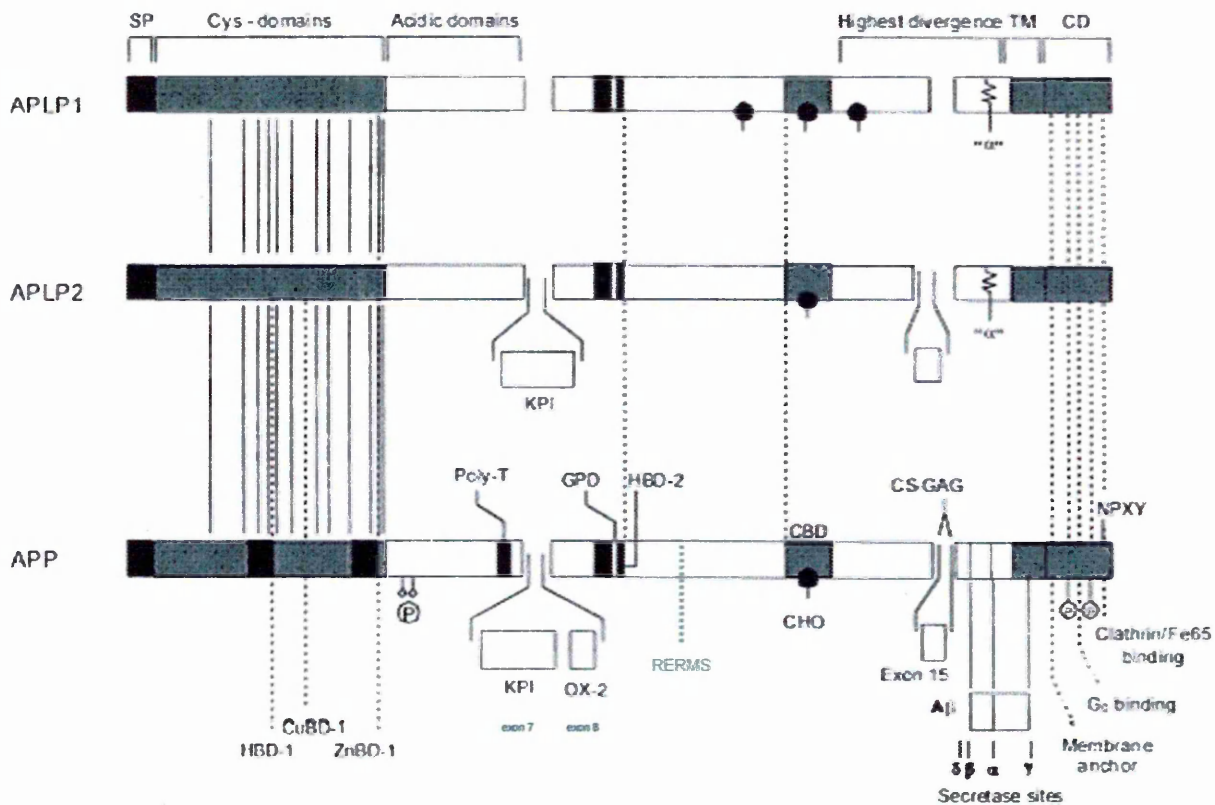


Figure 7⁵¹. The structural domains and binding motifs of the APP superfamily members. The solid vertical lines signify cysteine residues. The broken vertical lines corresponding to APP sequences conserved in the amyloid precursor-like protein (APLP) molecules. Abbreviations: α , alpha secretase site; ' α ', homologous to alpha secretase site for release of the ectodomain; β , beta secretase site; CD, cytoplasmic domain; CBD, collagen binding domain; CHO, N-linked attachment site; CS-GAG, chondroitin sulphateglycosaminoglycan; CuBD-1, copper binding domain 1; cys, cysteine; δ , delta secretase site; γ , gamma secretase site; GPD, growth promoting domain; HBD-1, heparin binding domain 1; HBD-2, heparin binding domain 2; KPI, Kunitz type protease inhibitor; NPXY, asparagines-proline-any amino acid-tyrosine; OX-2, OX-2 homology domain; poly T, poly threonine; P, phosphorylation site; SP, signal peptide; TM, transmembrane domain; ZnBD, zinc binding domain 1.

detection of membrane bound proved problematic⁵³. Jung *et al*⁵⁴ demonstrated using flow cytometry the presence of APP on the cell surface of neurons and it is now believed that both secreted and membrane bound APP have distinct functions in neuronal development and as receptors, the membrane bound version acting upon

signals from the extracellular matrix to the interior of the cell. Secreted APP is thought to exert neuronal survival by lowering intracellular calcium levels⁵⁵ the site of neuroprotection localised to residues 666-687 (APP₇₇₀ numbering). This domain is present within APPs- α but not APPs- β and as such suggests a possible reason for the different processing events. Other functional sub-domains identified are the RERMS sequence possibly involved in growth promotion⁵⁶ and two heparin binding sites, HBD1⁵⁷ and HBD2⁵⁸ at residues 96-110 and 316-337 respectively. Heparin is a member of the glycosaminoglycan family involved in cytokine action, cell-adhesion, enzyme catalysis and regulating the structure and function of basement membranes. Williamson et al⁵⁹ showed how the binding of heparin-like molecules, such as glypican and perlecan modulated APP induced neurite outgrowth. The highly conserved zinc (II) binding domain between residues 181-200⁶⁰ has been shown to modulate heparin binding. This along with the findings of abnormal zinc (II) metabolism in AD and Downs syndrome⁶¹ and the presence of perlecan in amyloid plaques⁶² may be relevant in the pathology of AD and the early stages of plaque formation. Other metal binding sites at residues 135-155 bind Cu (II) and reduce it to Cu(I), with the subsequent oxidation of cysteine residues at 144 and 158, resulting in the formation of new intramolecular disulphide bridges⁶³. This is believed to play an important role in anti-oxidant defence, disparities in which could have causative effects for late onset AD, where aging coupled with environmental effects exacerbate A β peptide formation. The best understood APP domain with respect to both structure and function is the KPI site present in APP₇₇₀, APP₇₅₁ and APLP2 also termed APP_{KPI} isoforms. Involved in the coagulation cascade within platelets this serine protease inhibitor domain inhibits factors IXa, X and XIa. Johnson *et al* 1990⁶⁴ showed that the APP₇₅₁/APP₆₉₅ ratio was increased in the hippocampal and neocortical tissues during

Alzheimer's disease, suggesting a prevalence of alternatively spliced mRNAs during neurodegeneration and that the KPI domain itself is somehow involved in amyloid plaque build up.

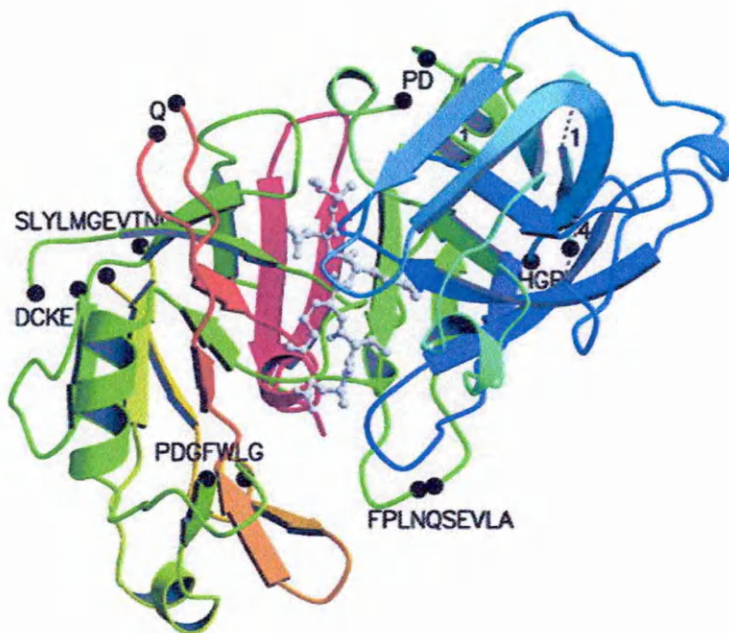
The generation of A β peptides was initially thought to be involved in AD pathology but is now known to be physiologically normal. Both A β_{1-40} and A β_{1-42} are lipophilic metal chelators with the capacity to reduce Cu(II) and Fe(III), A β_{1-42} being the most effective and binding to lipoproteins, apolipoprotein E and J and high density lipoprotein inhibiting their metal catalysed oxidation. A β_{1-42} has also been shown to be involved in phagocyte activation within the brain⁶⁵, eliciting inflammatory responses as well as being active in tau aggregation and phosphorylation, of which both activities could be instrumental in the disease cascade.

It is well understood that A β plaques are a significant marker in AD, however, there are several angles from which the aetiology of AD may be approached, yet the collection and succession of proteins involved is so widespread and complicated that a simple cascade covering every eventuality will probably never be found. Are the A β plaques a cause or consequence of some other genetic or metabolic disturbance? Is an alteration or increase in APP processing the key to AD? Or is it a deviation in the cleavage pathway? It was essentially thought that APP₆₉₅ was the most important isoform in AD, relative to APP₇₅₁ and APP₇₇₀, due to its abundance within the CNS, however, further studies show that this may not be the case. Research continues in order to find a cure for this debilitating disease but as might be expected with such a complex and multifactorial condition the list of therapeutic targets is extremely diverse. As A β peptides are a principal feature of AD they are a natural goal.

Inhibition or modulation of the proteases involved in A β formation, namely β and γ secretase being obvious approaches. Although the three-dimensional structure of β -secretase has been determined in complex with its substrate, APP (figure 8a)⁶⁶ and APP derived substrates (figure 8b) this only demonstrated further the difficulties in finding an inhibitor. The relatively big active site with two active aspartate residues currently only has large substrate inhibitors developed (figure 9)⁶⁷ thus limiting their ability to penetrate the blood brain barrier. This, however, is not the case for γ -secretase and inhibitors capable of passing through the membrane are more readily available (figure 10) due to the hydrophobicity of the active site. Cleavage of APP by γ -secretase is within the transmembrane domain and as such its active site needs to be hydrophobic a quality that aids passage across membranes and that inhibitors also possess. Clinical testing of inhibitors, however, is hindered by possible side effects on signal proteins such as the Notch receptor⁶⁸ showing the fundamental need of high specificity.

Extensive research into the inflammatory aspects of AD has uncovered the effect of non-steroidal anti-inflammatory drugs (NSAIDs) upon γ -secretase specificity increasing its propensity towards A β ₁₋₄₀ formation⁶⁹, the non-amyloidogenic peptide. NSAIDs have no observed effect on Notch activity and are already known to be safe in humans prompting their passage into clinical trials.

(a)



(b)

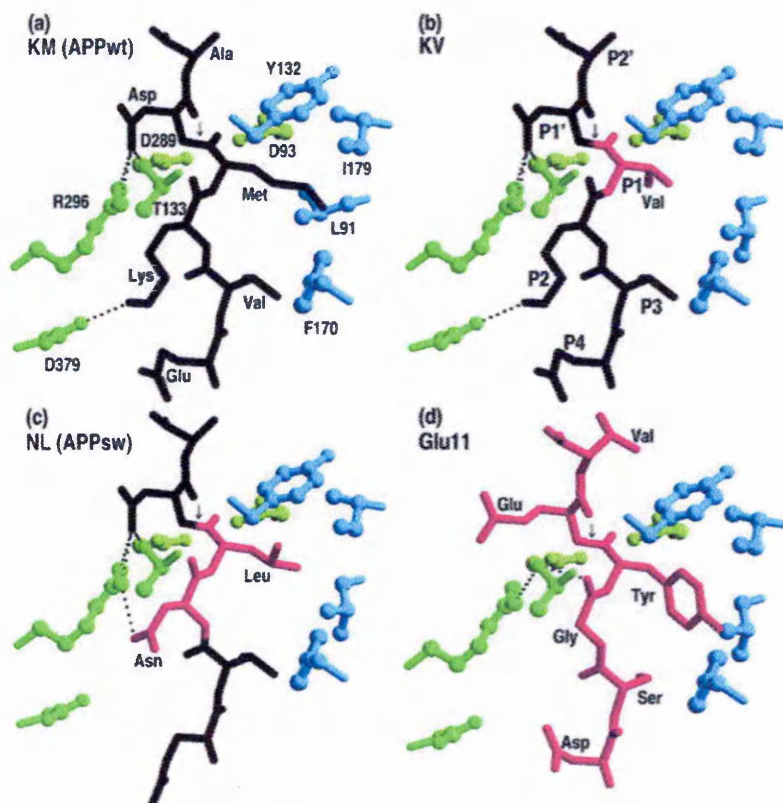


Figure 8⁶⁶. (a) The comparative model of the human β secretase shown with the APP substrate peptide in the active site, (b) Models of β secretase with APP derived substrates.

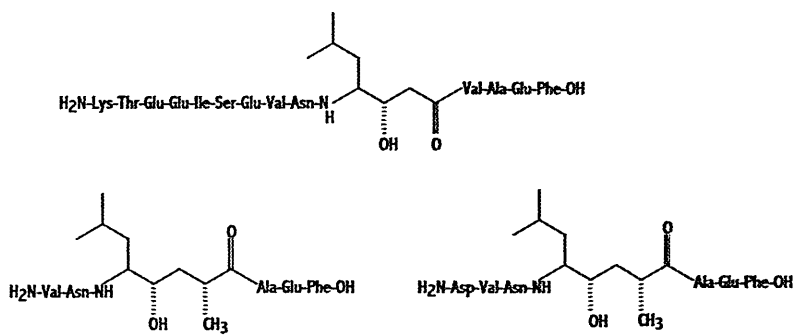


Figure 9⁶⁷. β -secretase inhibitors. All three compounds are transition state mimics that contain a hydroxyl group which co-ordinates with the two active site aspartates of β -secretase.

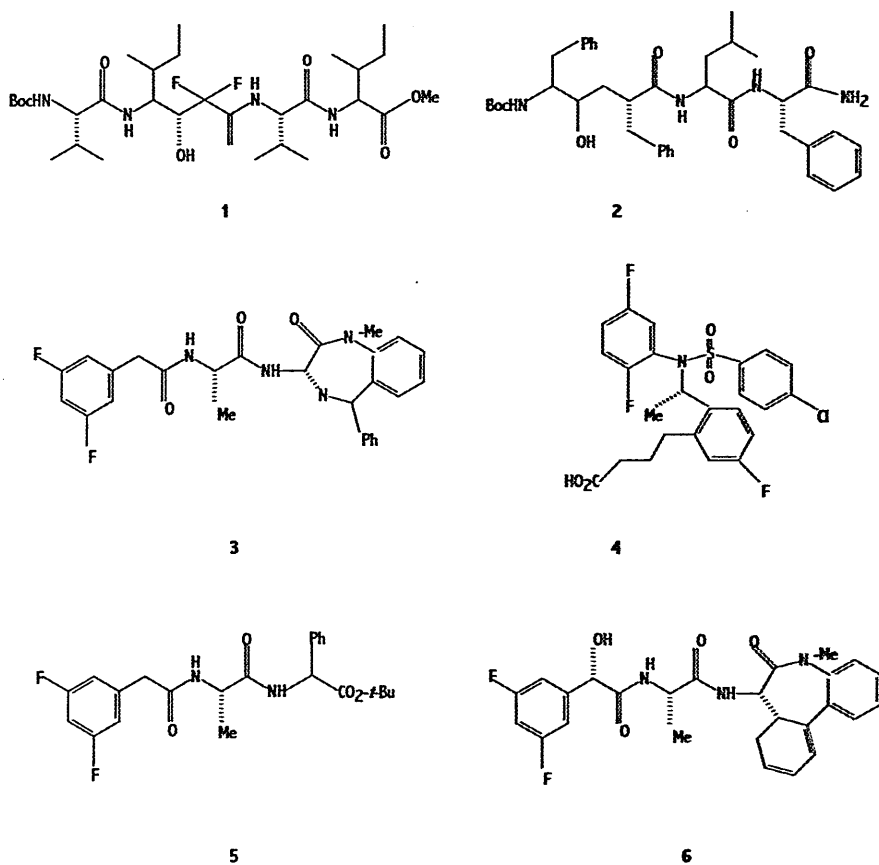


Figure 10⁶⁷. γ -secretase inhibitors. These include transition state mimics (1 and 2); benzodiazepines (3); sulphonamides (4); dipeptides (5); and benzocaprolactams (6).

Considering that the amount of APP cleaved from the membrane is divided between α and β -secretase pathways, it is not unreasonable to state that stimulation of one route will decrease APP availability for the other. A β peptides are not produced from APPs- α so stimulation of this route will decrease the peptide formation. Muscarinic agonists⁷⁰ are able to stimulate α -secretase by activation of PKC, however, side effects involving the over activation of muscarinic receptors may prove problematic. Enhanced A β clearance from the cerebral cortex or prevention of oligomerisation have been reported^{71,72} by active immunisation with A β and passive immunisation with A β antibodies. Results were promising showing a redistribution of A β peptides into the periphery, loss of plaques and other AD neuropathological changes. Early clinical trials for active immunisation, however, uncovered an unacceptable inflammatory reaction of the CNS in a low percentage of subjects but the use of passive immunisation is still a possibility. Another clearance strategy targets a protein involved in plaque protection, serum amyloid P (SAP). Reduction of SAP using analogues of proline dimers showed a marked decrease in the serum levels of plaques in both mice and humans⁷³.

The genetic link of the ApoE4 gene, which codes for a protein involved in lipid binding, indicates a possible connection between high cholesterol levels and late onset AD⁷⁴. It has been observed that sufferers of high cholesterol administered with cholesterol biosynthesis inhibitors such as statins have a lower incidence of AD⁷⁵ and decreased A β production. This was also reported both *in vitro* and *in vivo*⁷⁶ and conversely the administration of high cholesterol diets to rabbits increased A β production⁷⁷. Cholesterol lowering drugs are well tolerated and as such clinical trials are ongoing, as are trials for metal chelators like clioquinol⁷⁸. A β peptides are

lipophilic metal ion chelators. Both Cu(II) and Zn(II) are known to be involved in A β aggregation and as such sequestration of these ions may help to prevent A β deposits. Other therapeutic strategies involve interactions upstream of A β formation, for example the inhibition of APP expression⁷⁹, modulation of tau phosphorylation and the use of antioxidants, neuroprotectants and neurotrophic agents. The current status of functional curative therapeutics with the ability to slow conjugative decline is non-existent, the only validated treatments being those for AD symptoms such as acetylcholinesterase inhibitors, serotonin antagonists, benzodiazepines and non-prescription medicines, such as vitamin E and melatonin.

1.2 Proteomics⁸⁰

The 20th century has seen remarkable advances in biomedical research, leading to the prevention and cure of many previously incurable diseases. Certain conditions, however, such as autoimmune deficiency syndrome (AIDS), tuberculosis, malaria, multiple sclerosis and Alzheimer's still remain problematic. One of the reasons for this is the inability of researchers to unravel the elaborate interactions of proteins and genes at the genomic level. A major step towards reaching this goal was the recent publication of the human genome sequence⁸¹, and the sequences for many infectious organisms. Proteomics is a relatively new area of research allowing a more detailed and complete understanding of disease by systematically studying the proteins expressed by a cell. It has been driven by the dramatic increase in technology, creating rapid advances in protein identification with respect to speed and sensitivity. Structural conformation, abundance, modifications and involvement in multi-protein complexes are all studied by this science.

A protein's role is reflected by its interaction with other molecules, thus the identification of a protein with respect to its cellular environment is critical to its understanding. Alternative splice events and post-translational modifications can lead to multiple protein forms. The estimated 35000-80000 genes predicted in the human genome, therefore, could easily produce at least several hundred thousand proteins. Since proteins perform most cellular functions, proteomics can give a more complete picture of the organism and as such it is more advantageous to study gene function by proteomics rather than studying protein function from genomic and transcriptive data.

The techniques in proteomics embrace, separation science for the purification of proteins and peptides, analytical science for their subsequent identification and quantitation and bioinformatics for data management and analysis of results. The fundamental strategy involves separation of protein mixtures by either one-dimensional sodium dodecylsulphate polyacrylamide gel electrophoresis (1D-SDS-PAGE) or two-dimensional electrophoresis (2DE). Two-dimensional electrophoresis is the principal technique in proteomics, due to its unrivalled resolving power enabling the separation of isoforms and modified proteins, quite often when referring to 2DE, proteomics is often the term used instead. Excision of the protein bands or spots from 1D-SDS-PAGE or 2DE followed by proteolytic digestion of the intact proteins using specific cleavage reagents is the next step. The cleavage pattern of these reagents is specific to the protein and yields a collection of peptide masses known as the 'fingerprint' of that particular protein. These masses can then be detected by mass spectrometry and the measured values identified by comparison with the theoretical values available in protein databases. The new breed of mass spectrometric techniques, namely matrix assisted laser desorption ionisation-mass spectrometry (MALDI-MS) and electrospray ionisation-mass spectrometry (ESI-MS), play a vital role in the proteomics scenario, offering sensitivity, resolution, accuracy and automation thus permitting speed of identification. Sample preparation prior to mass spectrometry is also of paramount importance and likewise advances in sample clean up and separation techniques have occurred. These advances have had an increasing impact on the understanding of cellular processes and discovery of disease markers. This is obviously a simplified illustration of proteomics, which in reality encompasses many wide ranging techniques, such as chromatography, capillary

electrophoresis, antibody technology and isotopic or radio-labelling for quantitative purposes.

1.21 Protein separation

1.211 Sodium dodecylsulphate polyacrylamide electrophoresis

Electrophoresis is the process by which charged molecules are moved by application of an electric field, moving according to their charge, shape and size. Sodium dodecylsulphate polyacrylamide gel electrophoresis (SDS-PAGE) utilises this in the separation of proteins according to their molecular weight. SDS is an anionic detergent that denatures proteins, producing flexible protein rods with a net negative charge. Molecular weight is a linear function of peptide chain length, therefore, in sieving gels the proteins are separated by molecular weight as opposed to charge or shape. There are two types of buffer system utilised in SDS-PAGE, continuous and discontinuous. Continuous is the simplest, using only one buffer for both the tank and gel. The discontinuous system has a stacking gel and a resolving or separating gel, both gels and tank incorporating different buffers. Although set-up procedures for this type of gel are more laborious resolution is greater and it is less affected by sample precipitation and aggregation. In 1970 Laemmli⁸² devised a discontinuous, denaturing buffer system in which treated proteins are concentrated in a stacking gel before entering the separating gel. The Laemmli method is now the most common system utilised in SDS-PAGE.

Two-dimensional electrophoresis (2DE)⁸³ is an extension of SDS-PAGE, allowing the separation of complex protein mixtures, extracted from cells, tissues and other biological samples. It involves two discrete steps: isoelectric focussing (IEF) and SDS-PAGE. The first step, IEF separates proteins according to their isoelectric point (pI), the second step, as previously explained separates by molecular weight. Proteins are amphoteric, carrying a positive, negative or zero charge dependent upon the pH of their environment. The net protein charge is the sum of all the negative and positive charges present on its amino acid side chains and carboxyl terminus. The isoelectric point (pI) is the specific pH at which the protein charge is zero. The presence of a pH gradient is critical to IEF; this is achieved by the use of immobilised pH gradients in a gel format known as a dry strip. In a pH gradient under the influence of an electric field a protein will migrate to where its charge is zero. A protein with a net positive charge will move towards the cathode, becoming progressively less positive as it reaches its pI. Likewise, a protein that is negatively charged will move towards the anode, becoming less negative as it reaches its pI. If diffusion from the pI occurs the pH immediately causes a regain of charge and the protein will then return to its pI. This focussing effect concentrates proteins at their pI, allowing separation on the basis of very small differences in pI. 2DE offers unrivalled sensitivity and resolution in the separation of protein mixtures but in the same instance it is time consuming and requires manual dexterity in order to achieve reproducibility. The SDS-PAGE step resolves proteins further, allowing separation of individual proteins, splice variants and proteins differing due to post-translational modifications.

Separated proteins are then visualised by various means, depending upon concentration. Quite often cellular proteins are low in concentration and as such the necessity for more sensitive staining methods has arisen. Traditionally colloidal Coomassie blue and silver staining were the methods of choice but quite often Coomassie was not sensitive enough and silver staining although sensitive involves many steps and is not fully compatible with mass spectrometry. The development of imaging systems has allowed fluorescent detection to come to the fore with a new generation of fluorescent stains such as Sypro orange, Sypro red⁸⁴ and Sypro ruby⁸⁵, which have proven themselves to be comparably sensitive to silver staining yet affording ease and speed of application and compatibility with mass spectrometry. The disadvantages of 2DE are its incompatibility with hydrophobic and low abundance proteins, it is time consuming, limited by the dynamic range of the staining procedure and only semi-quantitative. Scanning densitometry⁸⁶ can measure and compare 2DE spots but the data obtained is questionable due to reproducibility problems.

1.212 Western blotting

Blotting was first introduced in 1975 by Southern⁸⁷ in the transfer of DNA to membranes termed “Southern blotting”. Consistency of nomenclature followed with the transfer of RNA being called “Northern blotting” and “Western blotting” describing the transfer of proteins to membranes. Western blotting has established itself as a highly sensitive technique for the detection and identification of proteins using antibodies (figure 11). Protein mixtures separated by SDS-PAGE are transferred from the gel onto a thin membrane support. The membrane binds and immobilises

proteins in the same configuration as the gel. Nitrocellulose or polyvinylidene difluoride (PVDF) membranes are the most common but there are several different types available all offering distinct properties⁸⁸. Nitrocellulose affords good sensitivity, resolution and low background noise but is mechanically fragile. PVDF, however, is a more robust membrane with a high protein binding capacity. Transfer onto the membrane is either electrophoretically, by applying an electric field in a suitable buffered environment or by simple diffusion, using weights and a suitable buffer system (figure 12). The latter is ideal for the transfer of proteins directly from IEF dry strips⁸⁹. The membrane blot is then exposed to a solution of antibodies specific to the protein in question. Once bound the antibodies themselves are detected. Detection quite often involves a species-specific enzyme-linked secondary antibody with an appropriate chromogenic substrate, offering a detectable colour change upon reaction. This method is simple to perform but the chemicals involved may sometimes be hazardous and fading of the initial result occurs with time. An alternative approach is the use of chemiluminescence detection (ECL), which is more sensitive, affording reliable quantitation, fast processing, repeated film exposures and the capacity of blot stripping allowing reprocessing for different antigens. Although Western blotting adds another step of protein purification after SDS-PAGE, electrophoretic transfer is almost quantitative with very little sample loss occurring and proteins are transferred free of buffers and other contaminants such as SDS. It has, therefore, been exploited as a means of sample clean-up prior to MALDI-MS enabling protein extraction, proteolytic digestion of excised membrane bands and provides a robust sample support^{90,91} found to be particularly compatible with ionisation by IR laser desorption⁹².

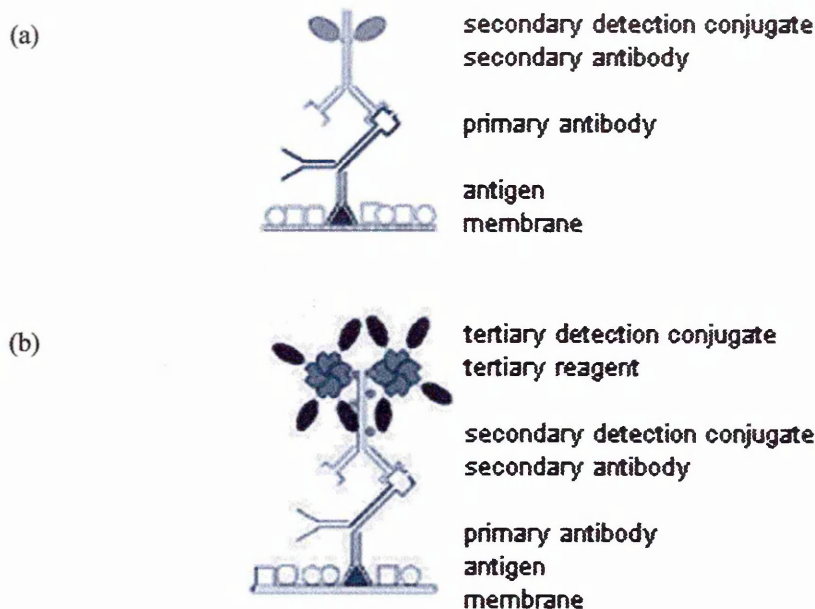


Figure 11⁹³. Indirect detection of blotted antigens. (a) Basic detection. The antigen specific primary antibody is detected by a species-specific secondary antibody, conjugated to a detection molecule or Protein A or G. Detection molecules include enzymes, such as horse radish peroxidase or alkaline phosphatase, fluorophores, colloidal gold and radioisotopes. (b) Enhanced detection. A ligand such as biotin is conjugated to the species-specific secondary antibody. A tertiary detection system with a suitable detection component then binds to the ligand.

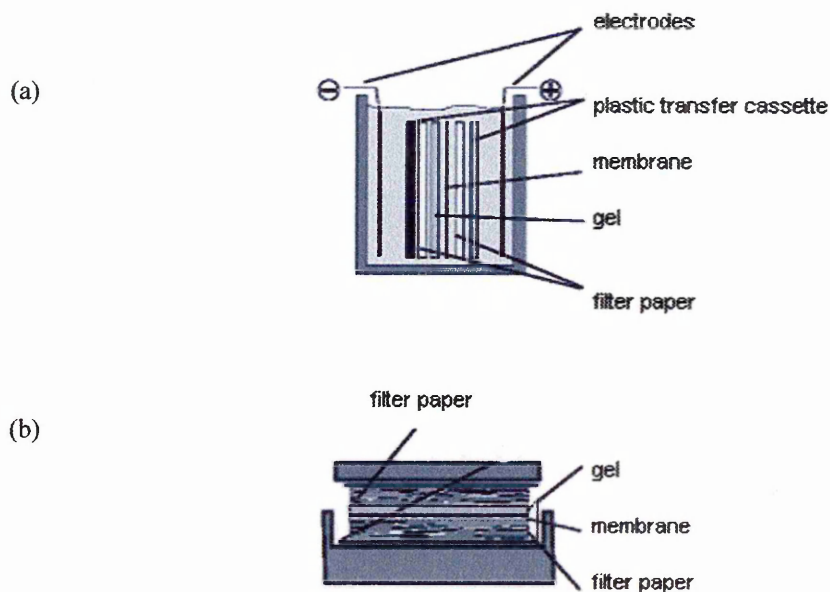


Figure 12⁹³. Blotting transfer systems. (a) Electrophoretic transfer. (b) Passive transfer

1.22 In-gel digestion

The technique of peptide mass mapping (PMM) or fingerprinting was introduced in 1993^{94,95,96,97}. It involves cleavage of the intact protein, using specific reagents, followed by mass determination of the generated peptides and subsequent identification of the protein by matching the measured peptide masses with calculated masses of a theoretical digest based on protein sequence databases. Protein determination and structure analysis is less complex and more accurate when performed upon peptides derived from the larger protein. There are many cleavage reagents available, including chemicals such as formic acid and cyanogen bromide (CNBr), however, the most common reagents used are endoprotease enzymes, due to their inherent specificity, safety and ease of use. Endoproteases create peptides from intact proteins by cleaving particular peptide bonds with varying degrees of specificity⁹⁸. The specificity of the most frequently used reagents (table 3) is well established⁹⁹. Proteins of known sequence can, therefore, be digested using the most convenient protease. The complexity and number of peptides created is proportional to the number of targeted peptide bonds present and size of the intact protein.

Much research has been aimed towards achieving complete digestions with full sequence coverage. Peptide peak intensities vary significantly, however, and 40% to 60% coverage is typical as cleavage is often hampered or prevented. Problems encountered include insolubility of the enzyme or substrate and substrate resistance to cleavage. These issues can be overcome by solvent variation and denaturation of the protein substrate, which allows ease of enzyme entry to the active sites. There are several methods of denaturing proteins including SDS, urea, and reducing agents such

as mercaptoethanol and dithiothreitol followed by alkylation. The latter method is routinely used in 2DE and the in-gel digestion of proteins separated by one-dimensional SDS-PAGE, particularly those in low concentration. Cysteine residues within proteins readily react with one another forming disulphide bonds that are part of a protein's tertiary structure. Reduction breaks these bonds, destroying the tertiary formation and alkylation caps them preventing reformation (figure 13).

There are many digestion procedures available within the literature, protocols have been developed to ensure optimal protease activity, however, these are not boundless and deviations away from the norm can sometimes achieve better results.

Reagent	Cleavage	Does not cleave	N or C terminus
Arg-C	R	P	C
Asp-N	D	-	N
Chymotrypsin	F/W/Y/L	P	C
CnBr	M	-	C
Elastase	G/A/S/V/L/I	-	C
Formic acid	D	-	N or C
Glu-C Ammonium bicarbonate	E	P	C
Glu-C Phosphate	E/D	P	C
Lys-C	K	P	C
Pepsin	F/L/E	V/A/G	C
Trypsin	K/R	P	C

Table 3. Common cleavage reagents and their cleavage rules. For amino acid nomenclature see appendix 4, table 1.

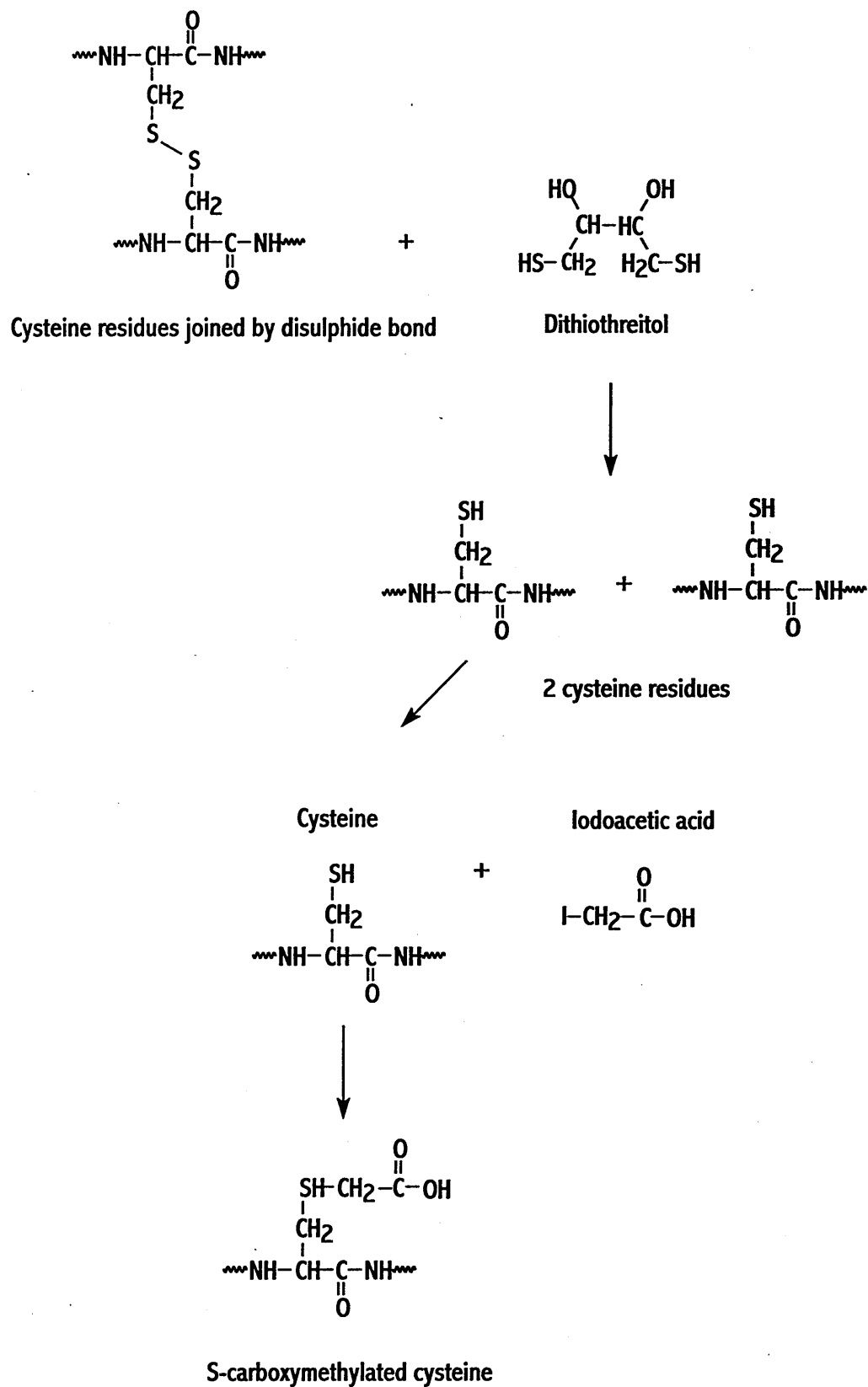


Figure 13. Reduction and carboxymethylation of cysteine residues

Proteolysis is most often done at 37°C but generally most enzymes work well between 20°C and 50°C. Optimal pH, on the other hand, is usually within a narrow range and should be adhered to. Reaction times range from 2 to 24 hours depending upon the protease used and whether the substrate is in solution or gel. Longer incubation times are necessary for in-gel digests in order to facilitate protease entry into the pores of the gel. Prolonging incubation times, however, provides no advantage whatsoever and generally if a reaction has not worked in the specified time it is due to incorrect enzyme to substrate ratio or experimental errors. On the whole in-gel digests have a much better recovery of peptides compared to digests performed upon membranes¹⁰⁰.

Trypsin is often the protease of choice in peptide mass mapping due to its cost, reliability and specificity, although it is known to suffer from autolysis. The presence of autolysis peaks (appendix 2, table 1) can be problematic, particularly in low level samples as they can overshadow the analyte peaks. Using the correct enzyme to substrate ratio to ensure no excess enzyme or using a higher-grade modified porcine trypsin can reduce autolysis. Alternative proteases may be used which do not exhibit the same degree of autolysis, such as Lys-C or Asp-N but these have their own problems such as expense and missed cleavages. Other notable contaminants are keratin digest peaks (appendix 2, table 2). Keratin is ubiquitous and as such methods to prevent contamination are often necessary. These include the use of gloves and a laminar flow hood for all experimental manipulations¹⁰¹. Another critical parameter is the absorption of peptides to the sample tubes and other surfaces this again can be particularly difficult when working in the femtomole range. Sample loss can be

prevented, somewhat by careful quantitative handling, use of silanised tubes and addition of organic solvents to the digestion buffer to aid solubility. In the MALDI-MS of un-separated peptides altering the composition and acidity of matrix solvents or the matrix itself has also been known to improve results.

1.23 Protein detection

1.231 Mass spectrometry

Mass spectrometry (MS) was traditionally a technique for the structural characterisation of small, volatile molecules (<500Da). Biopolymers such as proteins, polysaccharides and nucleic acids, were either too large and involatile or suffered from thermal decomposition during the harsh ionisation process. The invention and development over the last 20 years of so called 'soft' ionisation techniques, such as secondary ion mass spectrometry (SIMS), fast atom bombardment-mass spectrometry (FAB-MS)¹⁰², plasma desorption-mass spectrometry (PDMS)^{103,104} and the natural progression of MS research towards the analysis of biological molecules, led to the development in the late 1980s of electrospray ionisation-mass spectrometry (ESI-MS)¹⁰⁵ and matrix assisted laser desorption ionisation-mass spectrometry (MALDI-MS)¹⁰⁶. Both of these techniques show accuracy and sensitivity for the mass and structural analysis of high molecular weight compounds such as peptides, proteins, glycoconjugates and synthetic polymers.

1.2311 Matrix assisted laser desorption ionization mass spectrometry

The MALDI-MS technique resulted from years of research into the use of lasers for biomolecule ionisation. In 1988 Karas and Hillenkamp described the ultraviolet laser desorption (UVD) of biomolecules over 10,000 Daltons, following the lead of Tanaka *et al*¹⁰⁷, who reported the desorption of proteins up to 34,000 Daltons and oligomers of lysozyme containing up to seven monomers, using a pulsed N₂ laser and a matrix of fine metal powder dispersed in glycerol. Karas and Hillenkamp demonstrated by co-crystallising analyte molecules with a large molar excess of a UV absorbing material, how large proteins could be ionised. They expanded the previously achieved molecular weight range up to 67,000 Daltons using an ultraviolet laser, operating at a wavelength of 266nm and an aqueous solution of nicotinic acid as the matrix. The obvious advantage of this technique created great interest and refinement was rapid, utilising different laser wavelengths¹⁰⁸ and new matrices^{109,110}. Within two years Karas, Bahr and Hillenkamp¹¹¹ were routinely analyzing proteins within the 100,000 Dalton range with subpicomole sensitivity.

The key to ionisation in this technique is the incorporation of the sample with an excess of matrix that absorbs within the wavelength of the laser. The sample does not need to have a matching absorption peak because the matrix material absorbs the laser radiation, some of which is passed onto the sample. When the laser radiation strikes the matrix crystals, sublimation occurs, expanding both the matrix and sample into the gaseous phase, where photo-ionisation is thought to cause ionisation of the sample by gas phase photon reactions (figure 14). Typically nitrogen lasers are used in commercial instruments operating at the UV wavelength of 337nm, however, infrared

lasers (2.94 μm) have proved invaluable for the analysis of proteins directly from membranes¹¹². The principal step in analysis by MALDI-MS is sample preparation and choice of matrix. A good matrix should provide the correct molecular surrounding to promote ionisation of the sample yet be insignificant in its contribution to the mass spectrum. The co-crystallisation of sample and matrix is performed by mixing solutions of each and allowing crystallisation through solvent evaporation, it is necessary to ensure, therefore, compatibility of the solvent systems. Matrices shown to be routinely useful at 337nm are the organic acids, 2,5-dihydroxybenzoic acid (DHB) and α -cyano-4-hydroxycinnamic acid (α CHCA) each one having its own advantages (appendix 3, table 1). Quite often a matrix is chosen because of its compatibility with a protein or peptide molecular weight but other aspects such as sensitivity, analyte adduct contamination¹¹³, internal energy production¹¹⁴, sample homogeneity¹¹⁵ and background noise generation are all important factors.

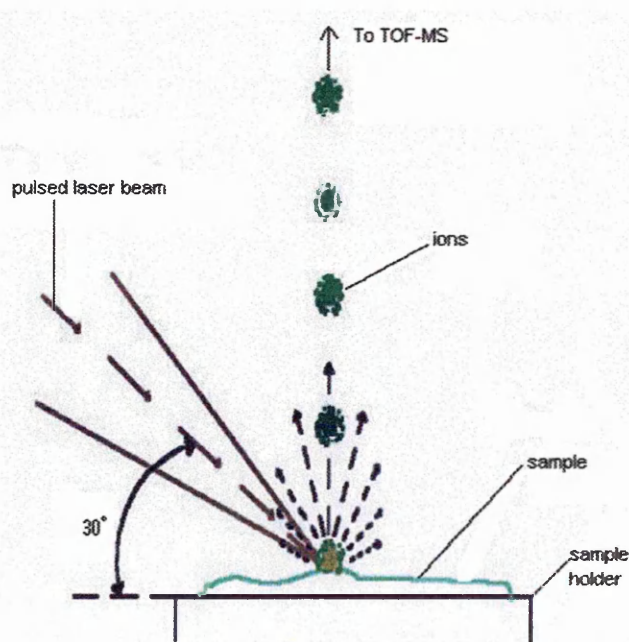


Figure 14. A laser pulse strikes the surface of the matrix/analyte, depositing energy, which is absorbed by the matrix. Some of this energy is passed onto the analyte. The matrix/analyte lattice is broken down and both the analyte and the matrix are forced into the gaseous phase, where ionisation occurs. Ions are then pumped into the analyser of the mass spectrometer.

Once the desired matrix and solvent system are decided upon, a large molar excess of matrix solution is combined with the analyte. The optimum volume ratio of matrix to analyte should be in the range of about 10^2 to 10^4 in the final deposit. Normally 0.5 to 1.0 μl is applied to the sample target, which is usually made of stainless steel but may be coated with gold or a non-conducting surface. After evaporation of the solvent the target can then be introduced into the MALDI source.

The MALDI technique is relatively tolerant of contaminants such as salts and buffers, which quite often remain in biological samples. This is partially due to the 'self cleaning' process encountered during crystallisation of the sample/analyte lattice. Improvements in spectral quality can be achieved, however, if contaminants remain problematic. Clean up procedures include cold water washes of the analyte/matrix crystals or analyte clean-up techniques using chromatographic material polymerised into pipette tips (ZipTips, Millipore). The ion species formed by MALDI are principally singly charged, intact molecules providing ease of structural determination.

Following ionisation the molecules go on to the mass spectrometer, which in effect organises the masses prior to detection (figure 15). The most common type of mass spectrometer coupled with MALDI is the time-of-flight (TOF) instrument¹¹⁶. These are ideally suited for use in systems generating a pulsed ion beam, in this case caused by a laser shot. Another advantage of TOF analysers is their lack of upper mass limits, allowing the detection of molecules in excess of 300,000Da¹¹⁷, a parameter necessary

in MALDI due to the creation of mainly singly charged molecules. TOF analysers measure the time it takes for the ions to pass through a field free drift tube at constant acceleration voltage¹¹⁸. They operate on the principle that ions of the same kinetic energy will move with different velocities depending on their m/z values. This can be expressed mathematically as: -

$$E = \frac{1}{2}mv^2 \quad \text{Equation 1}$$

Where: E = kinetic energy of ion

m = mass of ion

v = velocity of ion

Equation 1 can also be rearranged to give velocity in terms of kinetic energy and m/z:-

$$v = (2E/m)^{0.5} \quad \text{Equation 2}$$

If the distance from the point of ion formation to the detector at some fixed point is

d_L , then the time-of-flight (TOF) will be given as follows: -

$$\text{TOF} = d_L/v = d_L/(2E/m)^{0.5} \quad \text{Equation 3}$$

Thus ions of a greater mass will travel slower than lighter ones, therefore, reaching the detector later.

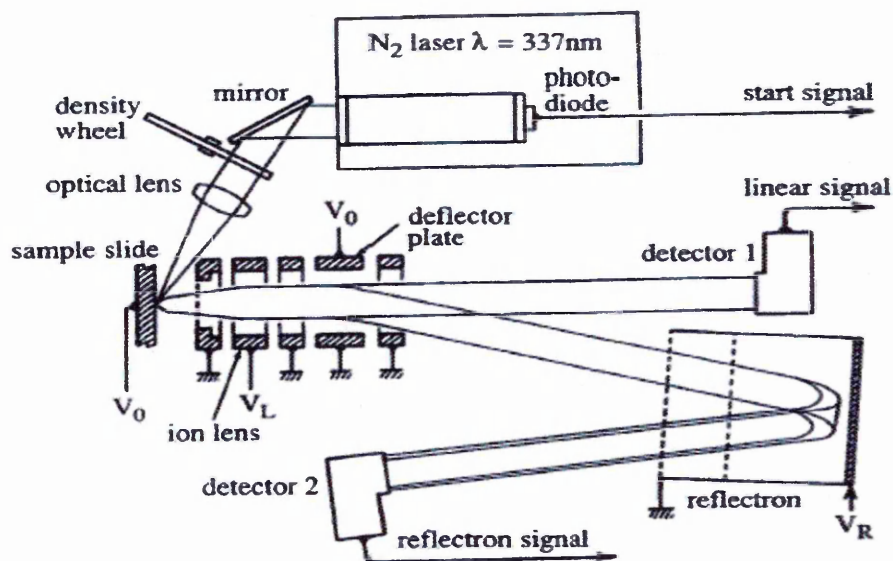


Figure 15¹¹⁹. Schematic diagram of a MALDI-TOF mass spectrometer with both linear and reflectron detection.

Although the MALDI technique provided many advantages, initially mass accuracy and sensitivity were low, mainly due to the energy spread of ions during ionisation. Factors contributing to the energy differentiation were collisions between sample and matrix ions during expansion into the gaseous phase and inhomogeneity at the surface of the sample. Vorm *et al*¹²⁰ improved resolution, accuracy and achieved attomole sensitivity by preparing thin sample/matrix layers and using volatile matrix solvents for fast evaporation. Jespersen *et al* attained similar results by reducing the size of sample spots from micro to nanolitre volumes¹²¹. These innovations emphasised the significance of sample preparation but when considering instrumental improvements four of the most important innovations have been the introduction of pulsed or

delayed ion extraction, reflectron TOF analysers, orthogonal MALDI and tandem mass spectrometry.

Delayed extraction introduced in 1995 by Brown and Lennon^{122,123} reduces the number and energy of collisions in the expanding plume, dramatically increasing resolution. It was based on the idea of 'time lag focussing', first described in 1955 by Wiley and McLaren¹²⁴. Ions generated in the extraction field are delayed or 'switched off', this delay allows the ions to spread out into the extraction gap according to their own velocity. Upon acceleration the ions spread out in space gaining different total kinetic energies, compensating for initial ion velocity distribution and therefore resolution. Previous laser designs operated with a short laser pulse, typically 1-5 ns, producing discrete ion packets in the ion source, which were then continuously extracted by application of a large static electric potential of around 25-30kV. The incorporation of pulsed ion extraction, (initially increasing pulse times to around 20 ns) with high accelerating potentials (up to 30kV), vastly enhanced mass resolution for both small and large molecules. Delayed extraction corrects for the energy spread of ions prior to the analyser, whereas the reflectron corrects this phenomenon within the analyser.

There are two types of TOF analyser, the linear TOF (figure 16a) and the reflectron TOF (figure 16b). The basic linear instrument consists of an ion source, flight tube and detector, all of which, with the exception of the laser are under vacuum pressures of 10^{-5} to 10^{-8} Torr. Ions follow a straight field free path between the ion source and

the detector. Limitations of this instrument are poor mass accuracy and low resolution, operating at a resolving power of ~ 450-600 for peptides and 50-400 for proteins. This means that the isotopic envelope of a peptide or peptides that only differ in mass by a few Daltons cannot be resolved. The resolving power (R) of a TOF instrument can be simply defined as: -

$$R = \frac{\text{mass of peak}}{\text{width of peak at } \frac{1}{2} \text{ height}} \quad \text{Equation 4}$$

Reflectron based TOF instruments include an ion mirror within the flight path, which helps to improve resolution and mass accuracy¹²⁵.

Despite the MALDI pulsed ion beam providing a well-defined start for TOF measurement, the quality of pulsation affects both resolution and accuracy and although delayed extraction improved upon beam pulsing to a certain extent problems were still seen, including complex calibration routines, detector saturation after each laser shot and problems controlling the laser fluence¹²⁶. In 1998 Krutchinsky and colleagues¹²⁷ achieved a higher level of decoupling, converting the pulsed MALDI ion beam into a quasi-continuous beam allowing orthogonal injection into the TOF analyser. Previously several groups^{128,129} had developed this technique in the combination of ESI with reflectron TOF analysers. In contrast to scanning instruments, nearly all the ions formed were detected and the small energy spread of

ions afforded mass resolution in excess of 10,000. Orthogonal MALDI with collisional cooling created a continuous beam by decreasing the time lapse between the laser pulses to nanoseconds, such that ion packets continuously flowed due to the rapidity of laser pulse. The quasi-continuous MALDI ion beam was comparable to the continuous ESI ion beam with regards to space and velocity distributions, thus giving orthogonal MALDI high resolution throughout an entire spectrum and comparable mass accuracy to that seen in ESI orthogonal TOF mass spectra.

Decomposition of the sample is often seen with MALDI. Ions with sufficient internal energy may fragment, either in the ion source, referred to as 'prompt fragmentation' or after the ion source, known as metastable or post source decay (PSD)¹³⁰. PSD is the most abundant and quite often results in poor resolution in linear instruments. The origin of PSD peak broadening lies in the energetics of fragmentation. In order to fragment the ions must have sufficient internal or activation energy for the reaction. The fragment ions will be at a lower energy than the transition state for the reaction, leaving some excess energy within the system. Following the laws of dynamics, this energy must be dissipated, so it is passed onto the fragments, slightly altering their velocities and in turn their arrival time at the detector. The reflectron acts as an ion-focussing device, correcting for the kinetic energy variation of the fragments. When ions hit the reflectron they are slowed down until they stop, turned around and accelerated towards a second detector. Ions of greater energy reach the detector first and penetrate into the reflectron, ions of a lesser energy, however, reach the detector later but do not penetrate the reflectron as deeply, allowing them to 'catch up' and creating focussed packets of ions rather than an unresolved spread. The reflectron

TOF can differentiate fragment ions from their precursors or parent ions. Although both are the same velocity they have different kinetic energy values. Equation 5 gives the kinetic energy value of a fragment (E_f) with respect to its parent ion¹³¹.

$$E_f = E_p f_m \quad (f_m = m_F/m_P) \quad \text{Equation 5}$$

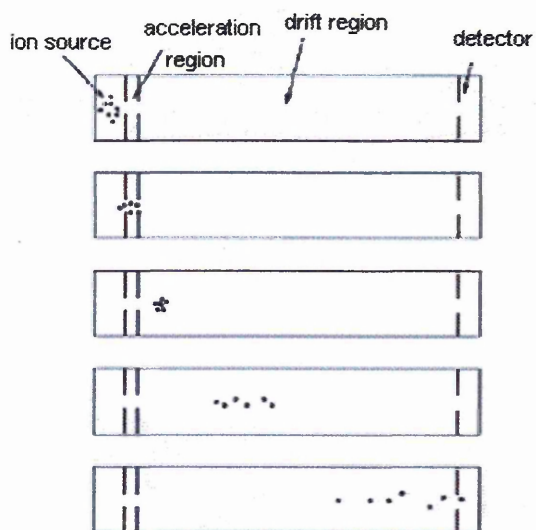
Where: E_p = kinetic energy of precursor ion

m_F = mass of the fragment ion

m_P = mass of the precursor ion

Thus if the parent ion arrives at the detector at time t_p , the arrival of the fragment t_f , can be made equal to t_p by lowering the potential of the reflectron to a value of t_f/t_p . So by scanning reflectron potentials it is possible to determine the m/z of the fragment ions by noting at which potential the fragment ion flight time is equal to that of the parent.

(a)



(b)

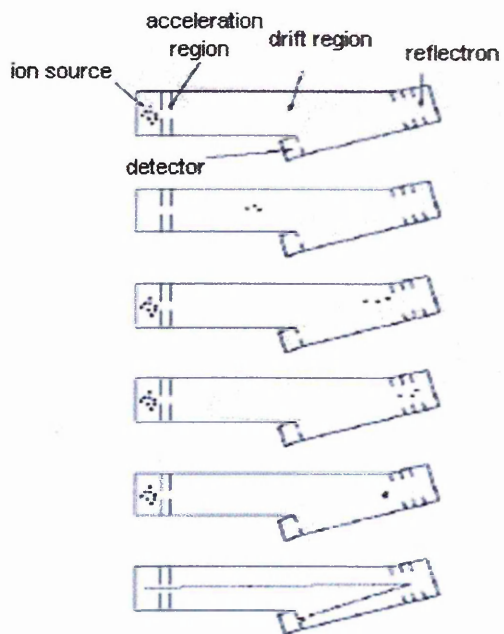


Figure 16¹¹⁹ (a). Schematic diagram of a linear TOF-MS shows how ions of the same molecular weight but different kinetic energy arrive at the detector at different times, resulting in peak broadening. (b) In the reflectron TOF-MS ions of greater kinetic energy reach the reflectron first and penetrate more deeply than their less energetic counterparts, giving them time to 'catch up' and acting as an ion focussing device.

The exploitation of PSD allowed the development of MALDI-MS for protein sequencing and gaining structural information. Kaufmann *et al* demonstrated how the resolving capabilities of the reflectron could discriminate between fragment ions and also by changing the reflector voltage complete PSD fragment ion spectrum could be acquired in segments¹²⁶. This development, nevertheless, was not without its problems that included complex fragmentation patterns, lack of computer algorithms for interpretation, and the resolving characteristics of delayed extraction reducing the rate of PSD fragmentation by at least one order of magnitude. Methods to improve fragmentation evolved with the addition of a collision cell and introduction of an inert gas, such as Argon generating collisionally induced dissociation (CID), peptide derivatisation methods^{132,133} and use of different analysers^{134,135,136} but the most important innovation to date has been the development of MALDI-MS/MS, namely the coupling of the MALDI source to a hybrid quadrupole time-of-flight mass spectrometer^{137,138,139} discussed later.

1.2312 Electrospray ionisation mass spectrometry

The principles of electrospray ionisation (ESI) were first proposed in 1974 by Beuhler *et al*¹⁴⁰, who stated that sufficient rapid energy transfer onto a molecule could cause vaporisation without decomposition. In 1989 Fenn and coworkers¹⁴¹ utilised this idea in the development of an instrument capable of ionising molecules up to 130,000 Daltons at atmospheric pressure, using a quadrupole mass analyser with an upper molecular weight limit of 4000 Daltons. Electrospray generates a very fine liquid aerosol via electrostatic charging. A liquid is passed through a fine nozzle, syringe or capillary, to which a charge is applied. As the liquid is forced through the nozzle it begins to form droplets, which are forced to hold more and more charge until they become unstable. The tiny charged droplets are less than 10µm in diameter with an attraction for a potential surface of opposite charge to land on. As they move about solvent molecules evaporate from the surface of the droplets. When the liquid begins to exit the tip of the needle it forms a conical shape known as the Taylor cone¹⁴², this formation occurs because the conical shape is able to hold more charge than a sphere. Desolvation decreases the size of the droplets causing the distance between the electrical charges within to shrink. If they cannot find a surface upon which to dissipate their charge a critical point is reached where no more electrical charge can be held and at the tip of the cone the liquid is blown apart into a fine plume of charged droplets. Lord Rayleigh first noted this phenomenon in 1882¹⁴³ and from then on it was termed 'Rayleigh instability', derived from the number of surface charges, Q_R that exist on a droplet of radius R_R :-

$$Q_R = 8\pi (\epsilon_0 \gamma R_R^3)^{1/2} \quad \text{Equation 6}$$

A principal characteristic of ESI is the formation of multiply charged ion species, two models attest the exact mechanism by which multiple charging occurs, the first charged residue mechanism¹⁴⁴ states that a series of droplet break-ups ends in the formation of a droplet with only one ion. Upon solvent evaporation the ion may be released into the gaseous phase. In the second model, termed ion evaporation,¹⁴⁵ the generation of gas phased ions is thought occur from small highly charged droplets. Repulsion of the charged ion by the other charges within the droplet may push the ion out of the droplet, after which solvent evaporation forms the gaseous ions. The second model also provides an explanation for the formation of multiply charged ions. The transfer of solution phase to gaseous phase is a strongly endothermic process, if the energy necessary to break a C-C bond was applied in one package over a short period of time, the act of freeing an organic ion from solvent molecules could also lead to fragmentation, however, desolvation in ESI occurs gradually by thermal energy at relatively low temperatures. Figure 17 shows the three main steps occurring in the ESI process. The ions are then sampled into the high vacuum region of the mass spectrometer. ESI is a continuous ionisation method and as such can be easily adapted to several different types of mass analysers and generally produces multiply charged ions. Multiple charging is particularly useful for the analysis of large molecules such as proteins as it lowers the m/z values to ranges that can easily be measured by a number of mass analysers. The number of charges acquired by a molecule is roughly equivalent to the number of sites of possible proton attachment, typically ESI generates ions that carry one charge per 1000 Daltons, the ion series for a protein, even a large protein, will fall in the m/z range of 800 to 3000 Daltons. The molecular mass of a protein is then determined by looking at the observed masses of any two adjacent ions in the series¹⁴⁶. Normally these calculations are automatically performed

by the data system, using deconvolution algorithms, which transform the m/z axis into a molecular mass axis enabling ease of interpretation and presentation. Since each multiply charged peak provides an independent measure of the molecular mass of the protein, an ion series from a single experiment provides a measure of mass precision. Most often ESI is coupled with quadrupole or triple quadrupole analysers but others including ion trap (ITMS)^{147,148}, TOF¹⁴⁹, and Fourier transform ion cyclotron mass spectrometry (FTMS)¹⁵⁰ are employed.

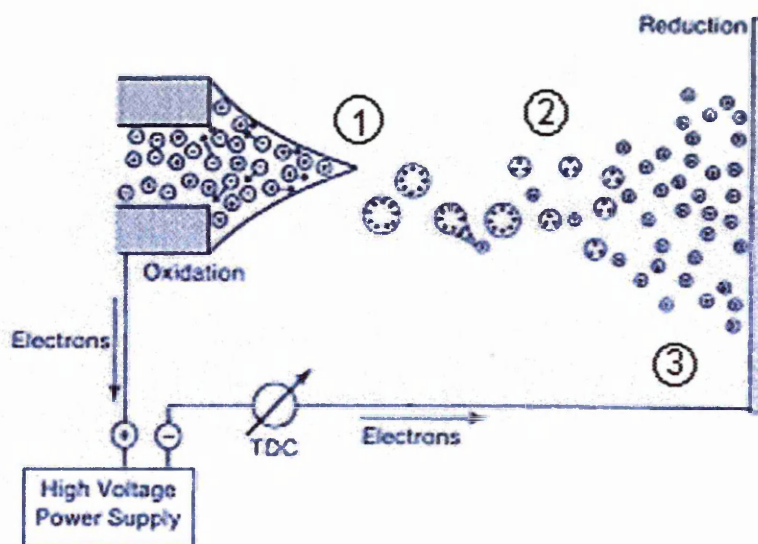


Figure 17¹⁵¹. Schematic of the electrospray process. (1) The production of charged droplets at the capillary tip. (2) Shrinkage of the charged droplets by solvent evaporation and repeated droplet disintegrations leading to very small highly charged droplets capable of producing gas phase ions. (3) Production of gas phase ions from the very small highly charged droplets.

Quadrupole mass spectrometry achieves mass separation by establishing an electric field in which ions of a particular m/z have a stable trajectory. A quadrupole consists of four parallel metal rods or quadrupoles through which ions are passed (figure 18). The trajectory of an ion through a quadrupole is complex, comprising characteristic

frequencies as they drift down the quadrupoles. By varying the strengths and frequencies of DC and RF voltages but keeping the precise DC to RF ratio, stable trajectories can be created allowing ions of specific m/z s to pass through the quadrupoles and be focused onto the detector, whilst deflecting others. Two opposite rods will have a potential of $+(U+V\cos(\omega t))$, the other two rods being $-(U+V\cos(\omega t))$, where U is a fixed potential and $(V\cos(\omega t))$ a radio frequency of amplitude V and frequency ω . When $\cos(\omega t)$ cycles with time, t , the applied voltages on opposite pairs of poles will vary in a sinusoidal manner but in opposite polarity. Along the central axis of the quadrupole assembly and the axis between each adjoining rod the resultant electric field is zero. In the transverse direction of the quadrupoles, an ion will oscillate amongst the poles in a complex fashion, depending on its m/z , the voltages U and V and the frequency, ω , of the alternating RF potential. By suitable choices of U ,

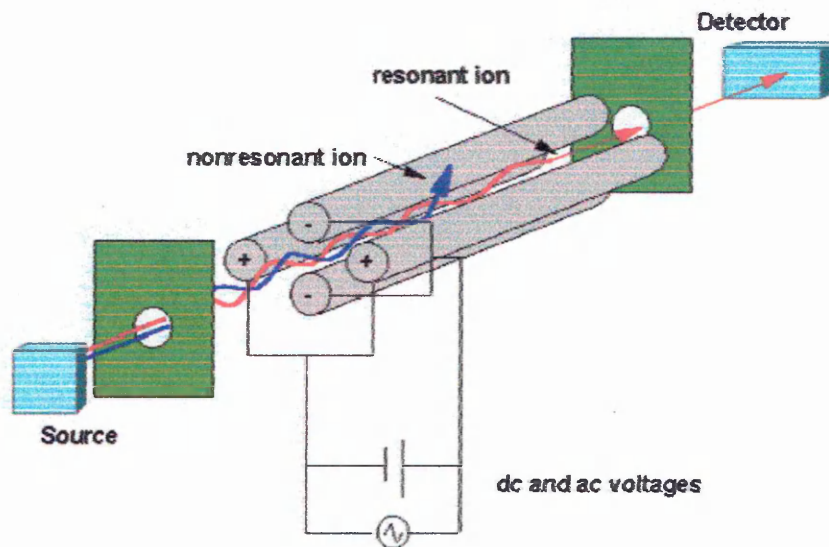


Figure 18¹⁵². Schematic diagram of a quadrupole mass analyser showing the four quadrupoles arranged so that the cross section forms two hyperbolae orthogonal to each other. The two rods of one hyperbola are connected electrically with a positive DC voltage. The other two surfaces are connected with a negative DC voltage. Application of an RF voltage at a fixed frequency, which has amplitude that oscillates between positive and negative, is also applied to all four surfaces. Ions of different m/z values are accelerated into the quadrupole field that separates ions as a function of a given DC and RF amplitude ratio.

V and ω only ions of one m/z will oscillate through the quadrupole mass analyser to the detector. All other ions will have greater amplitude of oscillation causing them to strike one of the rods. In practice, the frequency ω is fixed with typical values being 1-2MHz. The length and diameter of the poles will determine the mass range and ultimate resolution that can be achieved by the quadrupole assembly. The maximum range, however, normally attained is approximately 4000 Daltons and a resolution of around 2000. Mass resolution is dependant upon the number of RF cycles an ion experiences in the field, more cycles, better resolution, however, this has an effect on the signal of selected m/z s. The maximum mass (m) range of quadrupole may be calculated from the Mathieu parameters¹⁵³: -

$$m = \frac{eU}{a\pi^2 f^2 r_0^2} \quad \text{and} \quad m = \frac{eV}{2q\pi^2 f^2 r_0^2} \quad \text{Equation 7}$$

Where: m = maximum mass

e = electron charge

r_0 = field radius

U = maximum DC voltage between pole pairs

V = maximum zero to peak amplitude of the radio frequency applied between pole pairs

f = frequency of the RF

and for a quadrupole operated in the first stability region: -

$$a = 0.237$$

and $q = 0.706$

Equation 7 shows how the mass range may be increased; either by increasing both U and V respectively, decreasing r_0 , or by decreasing f but changes such as this can sometimes cause low resolution and loss of sensitivity¹⁵⁴.

As with any ionisation technique the observation of analyte ions is optimal when samples are free from contamination. Although ESI is tolerant to low levels of buffers, salts and detergents, they have the potential to either suppress analyte ions or form adducts with the analyte, giving rise to ambiguous mass measurements. Due to the liquid state of samples and ionisation occurring at atmospheric pressure ESI is ideally suited to coupling with separation techniques such as capillary electrophoresis (CE) and high performance liquid chromatography (HPLC). Both systems provide a convenient online clean-up technique prior to ionisation.

Typical solvents used for proteins and peptides are a mixture of water, an organic modifier, such as acetonitrile and a low percentage (typically 0.05% to 0.1% by volume) of a volatile acid, such as formic, acetic or trifluoroacetic to enhance ionisation. It is fortuitous that such solvent systems are fully compatible with optimal

separation in reversed-phase liquid chromatography systems (RPLC). Not only does LC fractionate complex mixtures prior to MS providing analyte pre-concentration and purification, saving time and sample losses but LC/MS data can be searched for components in minor levels. In an LC/MS experiment, mass spectra are recorded continuously. It is, therefore, advantageous to identify regions of data that may contain useful spectra. The data system produces a plot of the total number of ions detected during each mass spectrum scan versus time, known as the total ion current (TIC). When investigating the presence of a specific component and where it elutes the data system can be requested to display a selected ion current trace for the specific masses and probable ion charge states.

Traditionally HPLC used flow rates in the order of 1ml /min yet most mass spectrometers could only handle a few $\mu\text{l}/\text{min}$ of solvent. In order to achieve the coupling of conventional LC systems to ESI a technique called Ionspray® (figure 19) was developed¹⁵⁵. Also referred to as 'pneumatically assisted electrospray' because the dispersion of the sample liquid is supported by an inert gas, usually nitrogen. The device allowed flow rates of 200 $\mu\text{l}/\text{min}$, complementary to 1mm internal diameter (ID) narrow bore LC columns. Introduction of heat around the spray column increasing the surrounding temperature to 250°C produced flow rates as high as 2ml/min thus allowing interfacing to most conventional LC columns.

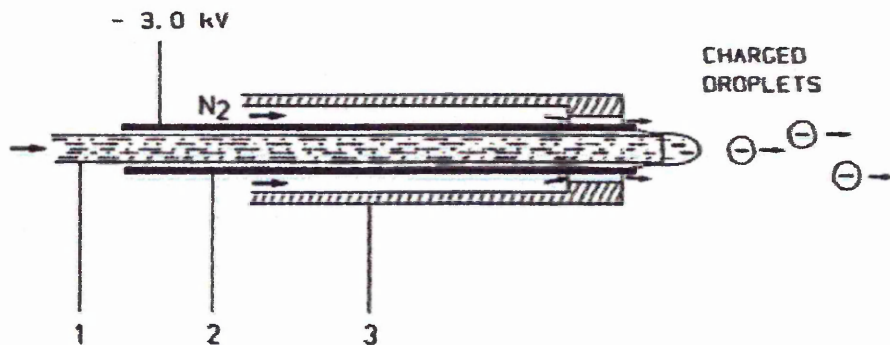


Figure 19¹⁵⁶. Schematic diagram of IonSpray®. 1 = 50 μ m internal diameter fused silica capillary. 2 = 200 μ m internal diameter SS-tubing. 3 = 0.8mm internal diameter PTFE tubing.

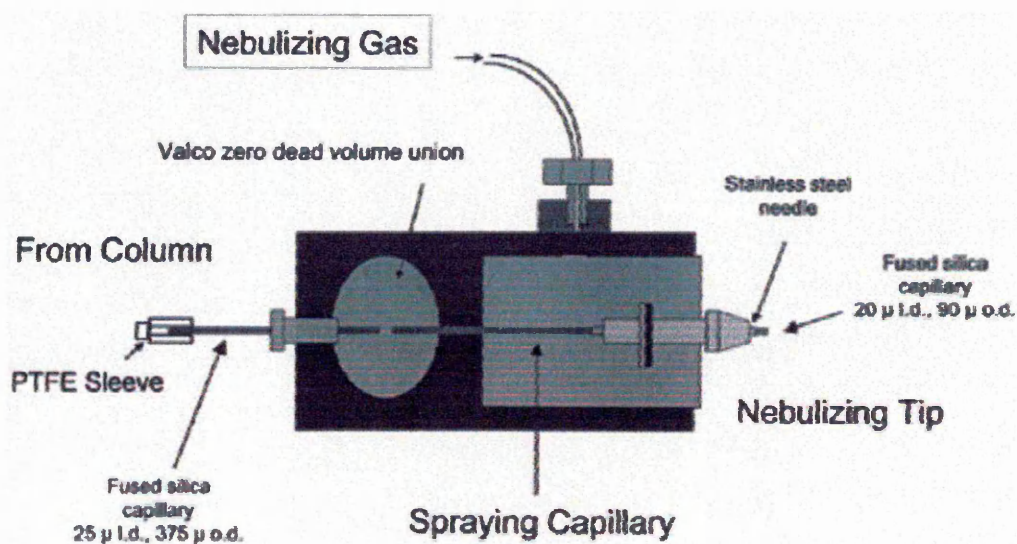


Figure 20¹⁵⁷. Nebulised nanospray electro spray allows analysis of low sample volumes.

The need to analyse biological samples in picomole concentrations or less brought about sample introduction techniques more amenable to small volumes. Nanospray (NS) (figure 20) was introduced by Wilm and Mann in 1994¹⁵⁸. Originally a gold-coated glass capillary that was drawn out at one end to give an orifice of only 1-2 μ m in diameter was used. The capillaries were loaded from the back with 0.5-5 μ l of sample solution and positioned in front of the mass spectrometer orifice at a distance of around 1-2mm. Voltages of 500-1000V applied to the capillary cause the sample solution to be drawn out by field forces, generating flow rates of about 20nl/min. Although this is an offline technique its advantage lies in extremely low sample consumption.

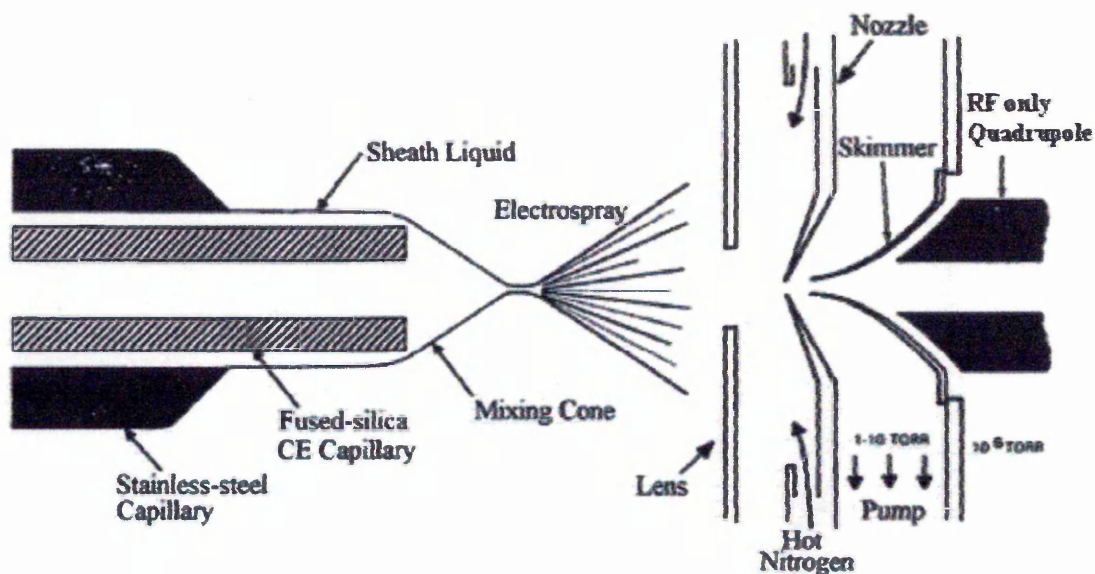


Figure 21¹⁵⁹. Schematic diagram of the sheath flow capillary.

The 'sheath flow' technique (figure 21), introduced in 1988 by Smith et al¹⁶⁰ allowed the coupling of capillary electrophoresis (CE) to ESI. Consisting of a fused silica capillary of 100µm ID, protruding about 0.2mm from a stainless steel tube of typically 0.25mm ID. The inner capillary carries the sample solution, whilst a 'sheath' liquid is fed through the outer capillary, to which a voltage is applied. Both liquids mix at the point of electrospray formation with flow rates of 0.25-1µl/min and 3-5µl/min respectively for the sample and sheath solutions. The use of a sheath flow allows flexibility of the solvent system and as the analyte is surrounded by the sheath liquid.

One of the most important innovations over the last thirty years, not only in quadrupole mass spectrometry but also in mass spectrometry itself, has been the development of tandem mass spectrometers. In these instruments the coupling of mass filters enables the detailed structural analysis of proteins^{161,162}. This methodology generically referred to as tandem mass spectrometry (MS/MS) can give complete or partial amino acid sequence information at the femtomole to picomole level for peptides containing up to 25 amino acid residues. In tandem mass spectrometry, two consecutive stages of mass analysis are used to detect secondary fragment ions that are formed from a particular precursor ion. The first stage is to isolate the peptide precursor of interest based on its m/z and the second stage to mass analyse the product ions formed from spontaneous or induced fragmentation of the selected precursor ion. Compared to Edman sequencing, MS/MS excels, as it is able to provide sequence information from peptides in complex mixtures due to the ability to select specific precursor m/z values. MS/MS can sequence peptides even when modifications are

present, is quicker than Edman sequencing because it is not a stepwise process and finally it is more sensitive. In triple quadrupole MS/MS (figure 22), a reaction or collision cell is positioned between the two quadrupoles, allowing the dissociation of ions¹⁶³. Collision cells involve the introduction of an inert gas and are typically constructed from a quadrupole without a DC voltage applied to the rods. This acts as a high pass mass filter allowing all ions above a set mass through the quadrupole. Enclosure of the cell allows higher pressures, permitting multiple low energy collisions creating sufficient activation for fragmentation. One of the main benefits of the quadrupole collision cell is the ability to focus ions after their interaction with the collision gas. The mass analysers can be set in different scanning modes, allowing the determination of structure and ions containing specific features¹⁶⁴. The simplest scanning mode is the 'product ion scan', where all fragments of a particular precursor are recorded, providing structural information. Here the first mass analyser is set to transmit only the precursor ion. The 'precursor ion scan' allows the first mass analyser to be scanned over a range of m/z values and sets the second analyser to transmit only one m/z .

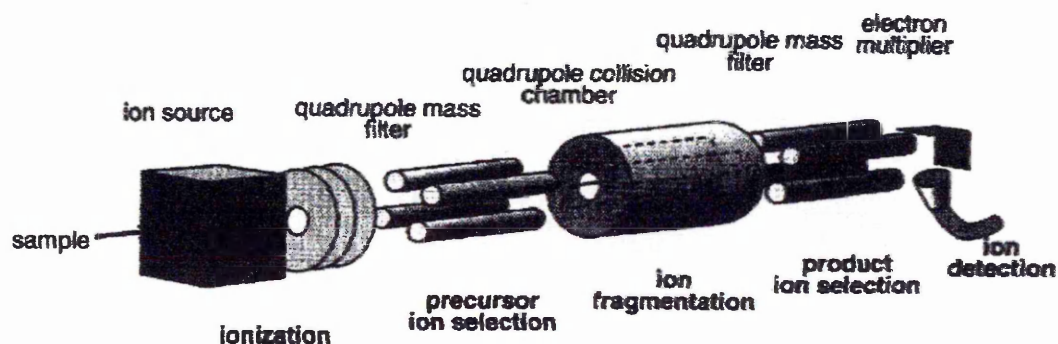


Figure 22¹⁵². Triple quadrupole MS/MS showing the basic set-up of the quadrupoles and their main functions.

This mode is particularly useful in the identification of structural motifs, such as glycosylation and phosphorylation. Other less common modes of scanning are the constant neutral ion loss scan and multiple reaction monitoring. Constant neutral loss looks at the loss of specific neutral moieties, both mass analysers are in the scanning mode but the second analyser is offset by the molecular weight of the moiety in question. Multiple reaction monitoring on the other hand fixes both analysers to look for parent and product ions in order to determine the presence of one analyte. Other tandem mass spectrometry instruments include the quadrupole ion trap mass spectrometer, time-of-flight/time-of-flight mass spectrometer and the hybrid quadrupole time-of-flight analyser (Qq-TOF). The reflectron time-of-flight mass spectrometer is sometimes referred to as a tandem system although this is not strictly true.

The Qq-Tof analyser will be focussed upon next, not only because of its inherent sensitivity, resolution and mass accuracy causing a notable impact upon the world of proteomics but because of its ability to be interfaced to both MALDI and ESI ionisation sources. In 1996 Morris *et al*¹⁶⁵ produced the first commercial ESI-Q-TOFs in which two of the quadrupoles, Q0 and Q2 were replaced with hexapoles but the operating procedure was the same. MALDI-Q-TOF coupling came four years later^{166,167}. Commonly termed Q-TOF, Q referring to the mass resolving quadrupole and TOF the time of flight element, whereas, q is noted only in an instrument capacity referring to the RF only collision cell. The instrumental arrangement can be easily described as a triple quadrupole system in which the third quadrupole (Q3) has been replaced by a TOF mass spectrometer. The Q-TOF configuration does, however, have

an additional RF quadrupole (Q0) affording collisional dampening. The fundamental instrumentation (figure 23) consists of three quadrupoles, Q0, Q1 and Q2, followed by reflecting TOF analysers with orthogonal injection. Ions enter Q0, where collisional cooling and focusing takes place. The 'cooled' ions are then transported through the quadrupoles for measurement of the whole mass spectrum in the TOF analyser. In single MS mode all three quadrupoles serve as RF only, the TOF analyser, generating high resolution, accuracy and the ability to record all ions in parallel without scanning, performs ion guiding and mass analysis. Q-TOF instruments have two modes of operation, product and precursor ion scans. In product ion scanning Q1 is operated as a mass filter, transmitting only the precursor ion of interest, which is accelerated into Q2, the collision cell where it undergoes CID upon interaction with the neutral collision gas molecules, typically argon or nitrogen. The resulting fragment ions and any remaining precursor are focused and cooled before entry into the TOF analyser. One of the main limitations of Q-TOF instruments is the lowered sensitivity in precursor ion scan mode relative to triple quadrupoles. Here the TOF analyser is fixed and does not need to record a full spectrum, thus the q-TOF is not benefiting from the simultaneous ion detection that TOF exploits. Although sensitivity may be lower than triple quadrupoles, Q-TOF compensates for this in other areas. In principle it is possible to carry out precursor scans for multiple ion products in one experiment and selection of the m/z fragment ion can be done with great resolution, thus increasing sensitivity and reducing chemical noise.

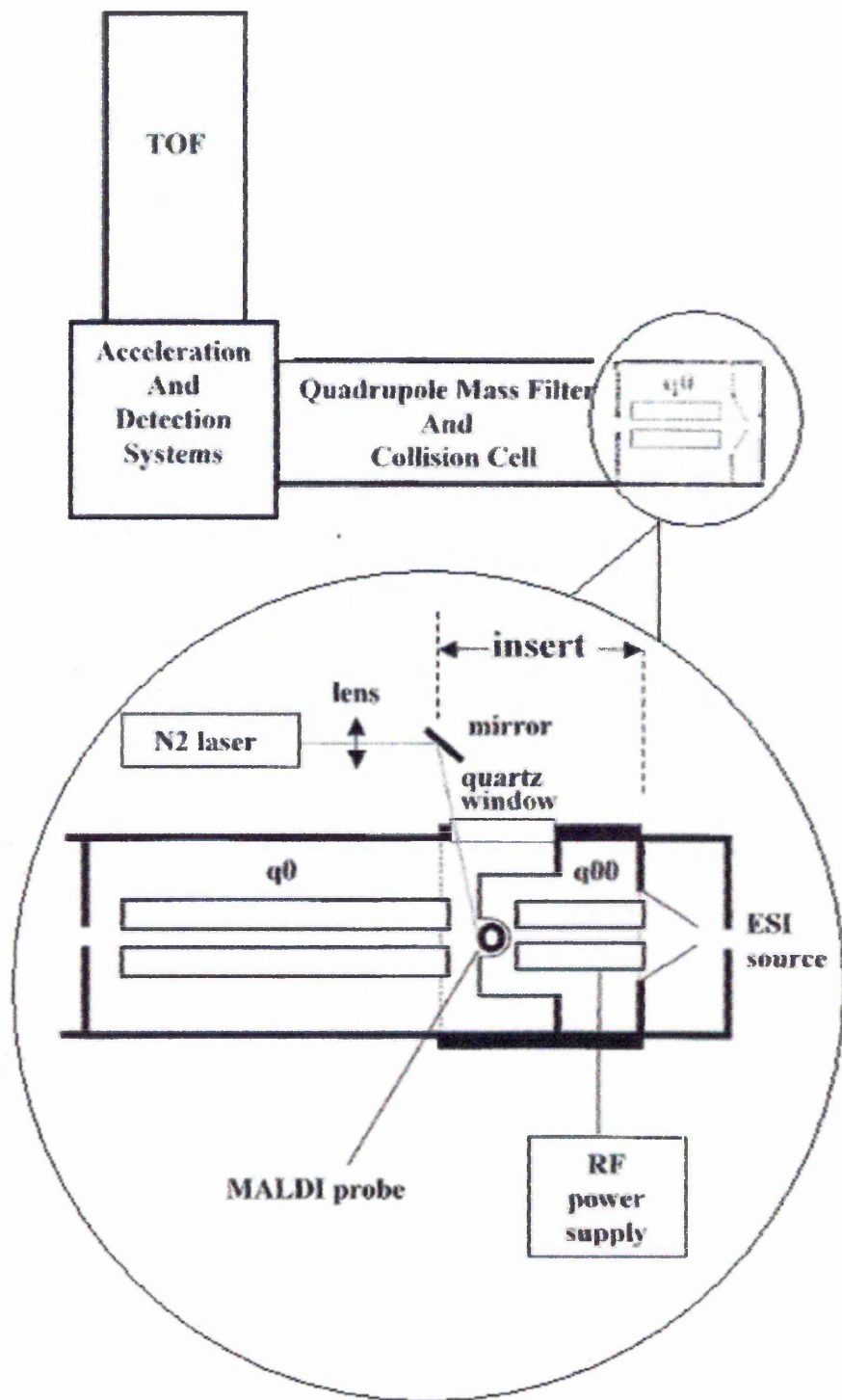


Figure 23¹⁶⁶. Schematic diagram of a Q-TOF mass spectrometer that can be rapidly switched between ESI and MALDI sources.

1.24 Information Dependent Acquisition (IDA)

IDA is a software functionality that allows automated high-throughput MS/MS screening of samples from TOF/MS and LC/MS, maximising the amount of data available from a single analysis. This feature automatically selects the most intense ions in a spectrum and performs MS/MS under optimal conditions. The survey scan of a sample will produce a peak list, which is then edited to remove any peaks that do not correspond to predetermined criteria. A fraction of the most intense remaining peaks will then be subjected to MS/MS. In order to get the most out of an IDA experiment it needs to be tailored with regards to the sample. This is performed by setting variables such as number of most intense peaks to be scanned; mass range, setting parameters within the area of interest; collision energy, more than one energy may be added to allow data optimisation, although some software packages include rolling collision energy, which looks at the m/z and charge state of each parent ion in order to determine its optimal collision energy; quad resolution, usually set at low allowing the isotopes of parent ions to enter the quadrupoles rather than just the C12 peak; charge state and intensity threshold. Predefining such parameters maximises the quantity and quality of information gathered uncovering data that otherwise may not be apparent. Initial LC/MS experiments performed by IDA give a set of chromatographic traces; the survey scan or total ion chromatograph (TIC), and extracted ion chromatograms (XICs). The XICs are created by looking at the first and second most intense peaks within the survey scan. For each a TIC of the product ion intensities generated by product ion scans is created. The peak list generated from these product ion scans are then automatically edited and MS/MS performed on up to eight ions at three different collision energies.

1.25 Protein fragmentation

The structure and function of proteins is permanently entwined, the three dimensional structure of a protein being directly dependant upon its specific primary sequence. Determination of amino acid sequences and detection of modifications, therefore, is a fundamental building block in the understanding of protein function. Until recently amino acid sequence determination was almost exclusively performed through the analysis of the encoding gene. Mass spectrometry, however, has revived sequence analysis of the gene product, using sequencing via peptide fragmentation.

The general structure of all amino acids is the same, their specificity inherited from the differences in the side chains or R groups, often termed as R₁, R₂, R₃ etc. (appendix 4, table 1). Fragmentation patterns of proteins and peptides are unique, decay within a mass spectrometer¹⁶⁸ occurring largely at the backbone amide bond, which joins the amino acids and resulting in fragments that are different in mass by one amino acid (figure 24). The difference in mass between two adjacent sequence ions of the same type defines the amino acid and of the twenty commonly occurring amino acids all but four have unique masses, the isomers leucine and isoleucine are identical and lysine and glutamine differ by only 0.04 Daltons. The occurrence of an anomalous mass not corresponding to any amino acid may be due to the presence of a post-translational modification.

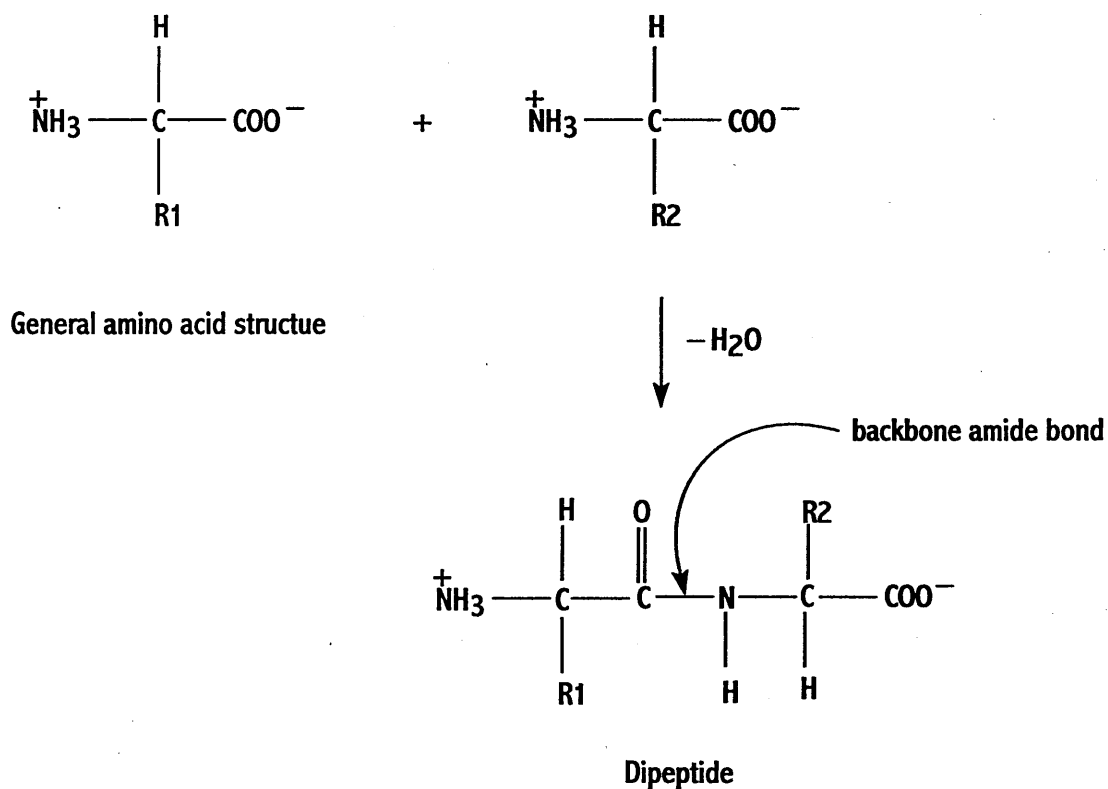


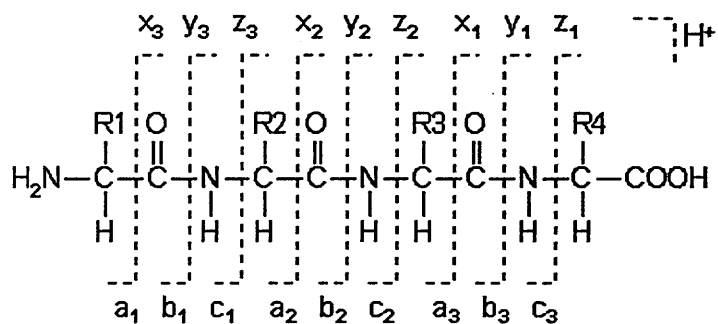
Figure 24. Amino acid structure and dehydration of two amino acids to form a dipeptide via the amide peptide bond. It is this bond that is fragmented in PSD, CID and MS/MS analysis.

Nomenclature for amino acid fragmentation was first proposed by Roepstorff and Fohlmann 1984¹⁶⁹ but this was later modified by Johnson *et al*¹⁷⁰. If the charge is retained on the N terminal fragment, the ion is classed as either *a*, *b* or *c*. If the charge is retained on the C terminal fragment the ion is referred to as *x*, *y* or *z* type. A subscript indicates the number of residues within the fragment (figure 25a). Internal cleavage may also occur, resulting in a more complex array of smaller fragments. Immonium ions are in this category (figure 26a), formed from *a* and *y* type cleavage giving a structure with a single side chain. This type of fragmentation is frequently observed from the amino acids tryptophan, tyrosine, phenylalanine, histidine and proline due to the steric pressure applied from their bulky side chains. Double

backbone cleavage of the *b* and *y* type forms another non-sequence specific ion, the amino acylium ion (figure 26b). Cleavage within the side chains at the beta carbon gives *d*, *v* and *w* ions (figure 26c), which can help to elucidate the isomeric structures of leucine and isoleucine. Every amino acid has its own characteristic fragmentation pattern, resulting in ions of various types (appendix 4, table 2) calculated using a general formulae (appendix 4, table 3) for fragment mass ions.

The method of fragmentation also dictates the type of ion produced. Low energy CID seen in triple quadrupole mass spectrometry give a predomination of *a*, *b* and *y* ions. In this type of fragmentation the loss of either ammonia (-17Da) or water (-18Da) is seen, denoted as *a*^{*}, *b*^{*} and *y*^{*} and *a*[°], *b*[°] and *y*[°] respectively. Low energy CID does not allow enough activation energy for the breakage of the stronger side chains and so *d* and *w* ions are not observed. High energy CID, however, creates all of the ions mentioned with the exception of ammonia and water losses. MALDI-TOF PSD fragmentation gives rise to *a*, *b* and *y* ions, however, if a collision gas is used patterns then resemble high energy CID, showing all types of cleavage along with ammonia and water losses. The presence of an internal proline can cause strong internal cleavage in PSD, extending from the proline residue towards the C terminus.

(a)



(b)

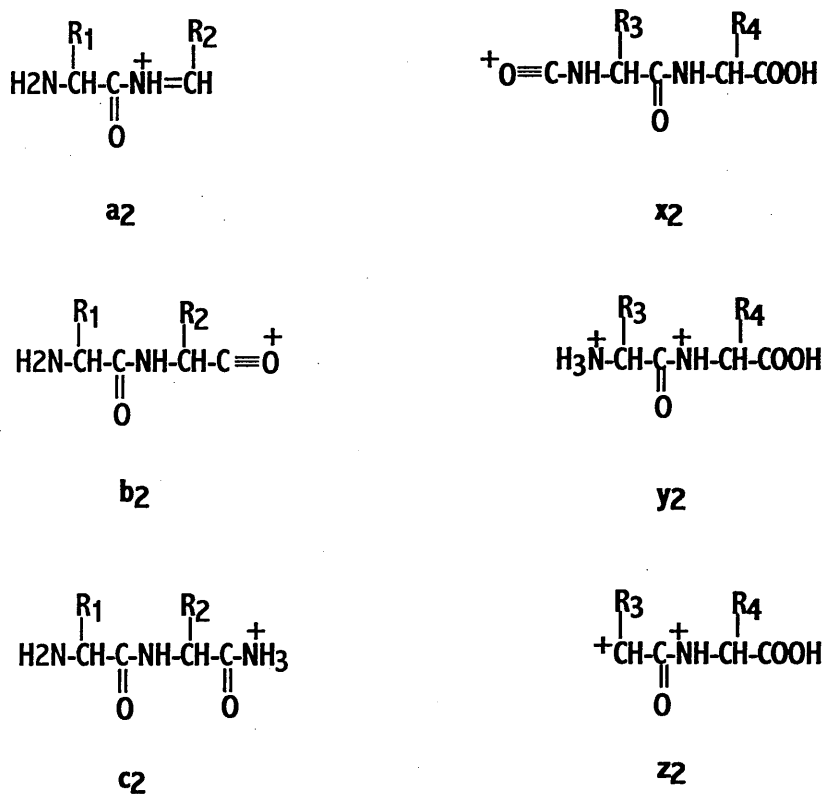
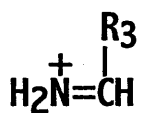
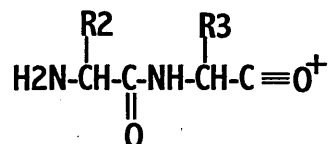


Figure 25¹⁷¹ (a) Peptide fragmentation patterns and their corresponding ion types. (b) In addition to the proton carrying charge, *c* and *y* ions take a proton from the precursor peptide creating the six singly charged structures shown. In ESI peptides may carry two or more charges, so the fragment ions may carry more than one charge.

(a)



(b)



(c)

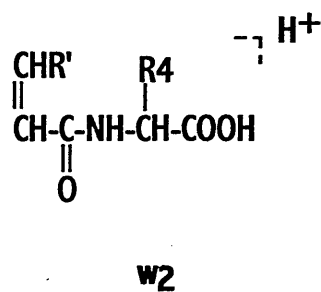
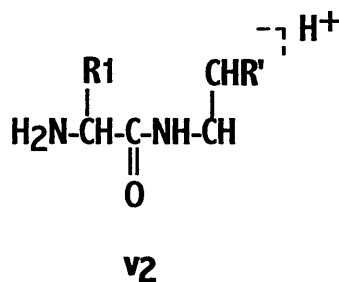
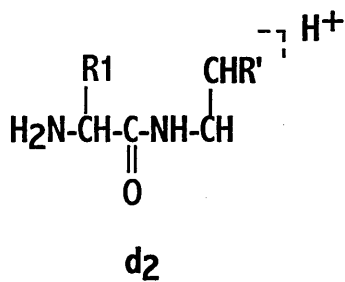


Figure 26¹⁷¹. Non-sequence specific internal cleavage ions. (a) Immonium ion. (b) Amino acylium ion. (c) Side chain cleavage resulting in *d*, *v* and *w* ions.

1.26 Protein modifications

Most proteins exhibit some form of modification, quite often translated proteins are inactive not becoming physiologically effective until a post-translational modification (PTM) has taken place. PTM's are important in the control of protein function, regulating enzyme activity, stabilising protein structures and altering the chemical functionality of a protein. As well as naturally occurring modifications proteins may also undergo accidental or deliberate adjustments during sample preparation. Principal examples being the accidental oxidation of methionine residues, due to oxidising agents such as ammonium persulphate present in polyacrylamide gels and carboxymethylation of cysteine residues, performed during sample work-up after reduction to prevent reformation of disulphide bonds (figure 13). It is important to be aware of such modifications (appendix 5, table 1) as the mass differences can create discrepancies if not noted in database searches.

Naturally occurring modifications as mentioned are an important characteristic of proteins, often unwanted modifications can result in a disease state and as such PTM research is extensive, the best method for identification and localisation being mass spectrometry. Most proteins undergo proteolytic cleavage during translation with removal of the signal peptide or terminal methionine transforming the inactive propeptide into its active counterpart. Post-translational phosphorylation is probably the most common PTM, quite often involved in the regulation of protein activity. One or more phosphate groups may be added and removed, acting as biological switches.

One of the most studied PTMs with regards to its disease causative status is glycosylation^{172,173}. Glycoproteins are proteins covalently linked to membrane associated carbohydrate groups, exclusively in the form of oligosaccharides. The predominant sugar groups attached are glucose, galactose, mannose, fructose, *N*-acetylgalactosaminyl (GalNac), *N*-acetylglucosaminyl (GlcNac) and *N*-acetylneuraminic acid (NANA). Protein linkage is either by *O*-glycosidic or *N*-glycosidic bonds, in mammalian cells the *N*-glycosidic bond is prominent. Attachment is within a consensus sequence of amino acids, N-X-S(T), where X is any amino acid except proline. Glycoproteins present on cell surfaces are important in cellular communication, maintenance of cell structure and self recognition by the immune system, enzyme deficiencies leading to erroneous glycosylation, therefore, can have profound physiological effects (table 4).

Disease	Enzyme Deficiency	Symptoms
Aspartylglycosaminuria	Aspartylglycosamidase	Progressive mental retardation, delayed speech and motor development, coarse facial features.
β -mannosidosis	β -mannosidase	Neurological defects and speech impairment
α -mannosidosis	α -mannosidase	Mental retardation, dystosis multiplex, hepatosplenomegaly, hearing loss and delayed speech.
GM ₁ gangliosidosis	β -galactosidase	Glycosphingolipid storage disease.
GM ₂ gangliosidosis	β -N-acetylhexosaminidases A and B	Glycosphingolipid storage disease.

Sialidosis	Neuraminidase	Myoclonus, congenital ascites, hepatosplenomegaly, coarse facial features, delayed mental and motor development.
Fucosidosis	α -fucosidase	Progressive motor and mental deterioration, growth retardation, coarse facial features, recurrent sinus and pulmonary infections.

Table 4¹⁷⁴. Glycosylation enzyme deficiencies leading to disease

1.27 Protein identification

1.271 Bioinformatics

Hwa Lim coined the term bioinformatics in the late 1980s but it wasn't until the 1990s and the advent of the human genome project that its usefulness came to the fore. The science of bioinformatics concerns the use of computers in biological research, forming an integral part of many research areas, including proteomics, genomics, transcriptomics, genetics and evolution. This new science uses databases and search engines for the storage and retrieval of information. Peptide libraries offer an invaluable means of providing functional information concerning protein interactions and protein modifying enzymes. Advances in proteomics wet chemistry have increased the amount of data available, however, this data needs to be analysed and as such bioinformatics has become an essential part of the research effort.

The elucidation of protein spots from gels is often the first analysis step in proteomics, carried out by peptide mass mapping. Sequence tagging or tandem MS may then be used to further characterise proteins, using the many on-line services available for protein identification. The use of databases for peptide mass mapping such as MS-Fit (figure 27) involves the input of experimentally generated peptide mass values for comparison against theoretical values. Other parameters included are mass tolerance, number of peptides required to match, cleavage reagent used and number of missed cleavage sites, monoisotopic or average masses, instrument used and choice of protein database (table 5), optional constraints include taxonomy,

Database: Instrument:

DNA Frame translation:

Search Hits: From: Filename:

Save Hits to file: Filename:

Species:

MW of Protein: (from Da to Da) All

Protein pI: (from to) All

Digest:

Max. # of missed cleavages:

Cysteines modified by:

N terminus: C terminus:

Sample ID (comment):

Max. Reported Hits:

Possible

Modifications

OR

Homology Mode (select any mode but identity)

Search mode:

Min. # matches with NO AA substitutions:

Peptide Mass shift: Da

Peptide masses are:

Min. # peptides required to match:

Report MOWSE Scores:

Pfactor:

Peptide Masses

mass tolerance: +/-

Mass (m/z)	Charge (z)
577.8	
835.8	
934.3	
1652.1	
1832.0	
2597.4	

Figure 27¹⁷⁵. Web page from MS-Fit for protein mass mapping. Internet protein databases now provide the amino acid sequences for over 200,000 proteins, information which is increasing daily.

protein molecular weight and pI, presence of any contaminating peaks and modifications. As the number of genomic sequences increases so does the accuracy of protein identification yet the uncertainty as to whether a protein possesses post-translational modifications can affect searches. The search may then be performed resulting in a display of search results in order of relevance, sometimes with a MOWSE score applied¹⁷⁶. MOWSE is an acronym of **M**olecular **W**eight **S**earch and was one of the first programs for identifying proteins by peptide mass mapping. It is an algorithm scoring system that takes into account all information given on the basis of considered importance, allowing rapid searching and retrieval of data from fully indexed libraries. Mowse inspired the development of many other programs and itself has been radically upgraded since its first development to encompass amino acid sequencing and MS/MS data. It was renamed in 1998 to MASCOT after collaboration of the Imperial Cancer Research Fund, UK with the bioinformatics company, Matrix Science.

Name	World-wide web address
Owl	http://www.biochem.ucl.ac.uk
Swiss Prot	http://www.expasy.ch
NCBI nr	http://ncbi.nlm.nih.gov

Table 5. Showing the three main protein databases utilised by most search programmes.

Name	World-wide web address	Application
AACompIdent	http://www.expasy.ch/tools/aacomp	Amino acid composition
AACompSim	http://www.expasy.ch/tools/aacsim	Amino acid composition
Amino Acid Information	http://prowl.rockefeller.edu/aainfo/contents.htm	Amino acid properties
CombSearch	http://www.expasy.ch/tools/combsearch/	Query system for several MS analysis programmes
Compute pI/Mw tool	http://www.expasy.ch/tools/pi_tool.html	Computation of pI and MW
Exact Mass Calculator	http://www.sisweb.com/cgi-bin/mass11.pl	Mass calculation
FindMod	http://www.expasy.ch/tools/findmod/	Prediction of post translational modifications
GlycoMod	http://www.expasy.ch/tools/glycomod/	Prediction of attached oligosaccharide structures
JPAT 2.2 API	http://www.pixelgate.net/mjones/java/jpat/jpat2/REA DME.html	Query system for several MS analysis programmes
Mascot	http://www.matrixscience.com/cgi/index.pl?page=../home.html	Peptide fingerprint and sequence tag analysis
MassSearch	http://cbrg.ing.ethz.ch/Server/MassSearch.html	Mass fragment search
Mass Spectrometer	http://www.sisweb.com/cgi-bin/mass8.pl	Generation of mass spectrum chart
MOWSE	http://www.hgmp.mrc.ac.uk/Bioinformatics/Webapp/mowse/	Peptide mass database
MS-Comp	http://prospector.ucsf.edu/ucsfhtml3.4/mscomp.htm	Amino acid composition comparison
MS-Digest	http://prospector.ucsf.edu/ucsfhtml3.4/msdigest.htm	Calculation of masses of protein cleavage products

MS-Edman	http:// prospector.ucsf.edu/ucsfhtml3.4/msedman.htm	Peptide tag mass and sequence search
MS-Fit	http:// prospector.ucsf.edu/ucsfhtml3.4/msfit.htm	Peptide mass fingerprinting
MS-Isotope	http:// prospector.ucsf.edu/ucsfhtml3.4/msiso.htm	Calculation of isotope patterns
MS-Product	http:// prospector.ucsf.edu/ucsfhtml3.4/msprod.htm	Calculation of masses of protein cleavage products
MS-Seq	http:// prospector.ucsf.edu/ucsfhtml3.4/msseq.htm	Peptide sequence tag analysis
MS-Tag	http:// prospector.ucsf.edu/ucsfhtml3.4/mstagfd.htm	Peptide sequence tag analysis
MultIdent	http://www.expasy.ch/toolsmultident/	Amino acid composition mass and sequence tag analysis
PepFrag	http://prowl.rockefeller.edu/prowl/pepfragch.html	Peptide sequence tag analysis
PeptideMass	http://www.expasy.ch/tools/peptide-mass.html	Peptide mass calculation
PepIdent	http://www.expasy.ch/tools/peptident.html	Peptide mass fingerprinting
PeptideSearch	http://www.mann.embl-heidelberg.de/GroupPages/PageLink/	Peptide mass and sequence analysis
ProteinProspector	http://prospector.ucsf.edu/	Query system for several MS analysis programmes
PROWL	http://prowl.rockefeller.edu/	Peptide mass and fragment ion search
TagIdent	http://www.expasy.ch/tools/tagident.html	Peptide mass and sequence analysis

Table 6. Mass spectrometry programmes on the Internet.

The most critical factor in database searching is the accuracy of peptide masses, accurate masses allow lower mass tolerance and, therefore, less ambiguous results. Table 6 shows some of the peptide mass mapping tools available on the Internet, along with other analysis tools such as protein molecular weight calculation, protein sequence tags, peptide sequence tags and amino acid composition.

2DE databases are available showing images of gels generated from various species, tissues, staining and experimental methods. Due to the diversity of image construction the usefulness with respect to comparison and quantification may be negligible, especially for low-level proteins. Qualitative and quantitative changes in protein expression can be observed by gel comparison using packages such as PDQuest (Biorad) and Melanie (GeneBio). Gels are scanned and processed to remove background noise prior to comparison. Care must be taken, however, to ensure experimental procedures are identical as inhomogeneities can arise from sample preparation, electrophoretic conditions and staining or unequal mobility within gel regions. Matching is performed either at the spot or pixel level and is laborious due to its lack of automation. This area is problematic, as is the need for database standardisation and both require attention to enable bioinformatics to proceed.

1.28 Application of proteomics to the study of Alzheimer's disease

The prevalence and lack of preventative treatment for Alzheimer's disease (AD) has made it a sensitive issue in the world of scientific research and one, which the use of proteomic methodology is ideally suited due to the increasing stream of possible causative protein targets. One of the most significant proteomic approaches must be surface enhanced laser desorption/ionisation time-of-flight mass spectrometry (SELDI-TOF MS) first introduced by Hutchens and Yip¹⁷⁷. This technique has since been utilised by Ciphergen in the production of the Protein Chip® system allowing selective analysis of proteins directly from biological samples within the femtomole range¹⁷⁸. Using antibodies specific to the A β peptide the Protein Chip® system was employed to investigate A β peptides present within lenses of AD patients suffering from cataracts. Expectedly the cataracts removed from AD patients showed a marked increase in the A β peptide compared to non-AD sufferers¹⁷⁹. Protein Chips® were used again to monitor the levels of proteins in the cerebrospinal fluid (CSF) of AD patients¹⁸⁰. Similarly CSF protein levels of AD patients and controls were investigated using the two-dimensional gel electrophoresis followed by mass spectrometry proteomic approach. The results were comparable to the Protein Chip® method, showing significant increases and decreases in CSF proteins present in CSF of AD patients¹⁸¹.

Although any successful research is significant the above work only shows the relative quantitation of proteins present in diseased verses non-diseased subjects. Recent work carried out by Merck Sharp & Dohme research laboratories, however, shows ultimate quantitation of A β ₁₋₄₀ and A β ₁₋₄₂ present within the brains of

transgenic mice using the SELDI- TOF approach in conjunction with a homogenous time resolved fluorescent immunoassay¹⁸².

Proteomics is now readily described as an effective new approach in the investigation of post-translationally¹⁸³ modified and oxidised proteins occurring in AD. The increased accumulation of oxidatively modified proteins present are well documented^{184, 185, 186, 187}. A phenotypic selection of a murine model of accelerated aging known as SAM (senescence accelerated mouse) was used to investigate the relationship between age associated oxidative stress on specific protein oxidation and age related learning and memory deficits¹⁸⁸. This study looked at the variation in oxidised proteins between 4 month and 12-month-old mice and illustrated the increase and decrease in oxidation and its effect upon enzyme activity. A major factor shown to affect the risk and progression of late onset AD is ApoE gene polymorphisms. Using two-dimensional electrophoresis and mass fingerprinting the Molecular Aging Unit, Texas, USA¹⁸⁹ showed how the ApoE gene product offers protection against age associated oxidative damage within the brain.

As well as the concentration and modification of AD related proteins their sub-cellular location is also important in the determination of function. Nicastrin is believed to be involved in the multiprotein complex involved in γ -secretase cleavage of APP and a recent study has shown the location of nicastrin to be within the lysosomal membrane¹⁹⁰ this result is notable as it may help to unravel the formation pathway of the A β peptide. None of the current AD research publications investigate APP isoform variation by proteomic methods and as such the work shown within this research is at present unique in its ability to detect APP and isolate isoform variations by mass fingerprinting.

2.1 Reduction and alkylation of Ntera 2 conditioned media and Chinese Hamster Ovary (CHO) 770 cells

2ml of 0.5M Tris-HCl, pH 7.4 was added to 20ml of Ntera 2 or CHO 770 media, then 1.3M dithiothreitol (DTT) (Sigma-Aldrich), to yield a final concentration of 10mM and the solution incubated at room temperature for 3h or overnight at 4°C. The reduced sulphydryl bonds were then subjected to alkylation, producing carboxymethyl cysteine residues by the addition of fresh sodium iodoacetic acid (Sigma-Aldrich), to a final concentration of 12.5ug/ml and incubation at room temperature for 1h. The necessary removal of excess reagents was performed by overnight dialysis of the resulting solution into excess de-ionised water. Removal of any insoluble material was performed by centrifugation (5 min at 10,000 rpm) prior to further use.

2.2 Immunoprecipitation of Amyloid Precursor Protein (APP)

Immunoprecipitation of APP was performed using the mouse monoclonal antibody AB10 (D.Parkinson, Biomedical Research Centre, Sheffield Hallam University) raised to amino acids 1-17 of the β amyloid peptide sequence and extracted using goat anti-mouse agarose beads (Sigma-Aldrich). 1ml of reduced and alkylated media was mixed with the primary antibody (400ul AB10/ml), 0.5M Tris-HCl, pH 7.4 (100ul/ml) and 40ul/ml of 50% slurry of goat anti-mouse agarose beads for 2h at room temperature. Initial optimisation of this method was performed comparing Protein G beads with the goat anti-mouse beads. The Protein G method was performed by substitution of 40 μ l/ml goat anti-mouse beads for 40 μ l/ml Protein G. The protein-antibody-bead complex was collected by centrifugation (3 min at 1500 rpm) then washed by adding 1ml Tris buffered saline (TBS) and centrifuging as before. Bead

elution was performed by incubation at 60°C for 10 min in a 50:50 100% urea/1×DTT solution (50µl), alternatively incubation in 100% urea (100µl) at 60°C for 1h. Immunoprecipitation was performed in 20ml batches and the resulting solutions were combined then concentrated by ultrafiltration (5000 rpm) with a Centricon 10 concentrator (Amicon) to a volume of around 10µl.

2.3 Standard Protein Solutions

Bovine serum albumin (Sigma-Aldrich) was made up as a 5.0µg/ml solution in 0.1M ammonium bicarbonate. The alpha secretase cleaved amyloid precursor protein standard, isoform 695 (Sigma-Aldrich) was purchased as a 0.15mg/ml solution in de-ionised water, which was further diluted 1 in 10 to give a 15.0 µg/ml solution

2.4 One-dimensional SDS-PAGE

2.41 Stock solutions

High quality de-ionised water (dH₂O) was used when making these solutions.

<i>Resolving Acrylamide</i>	<i>Final concentration</i>	<i>Amount</i>
<hr/>		
<i>(20% solution, 19:1 acrylamide/bis-acrylamide)</i>		
30%, 19:1 acrylamide/bis-acrylamide	20%	30ml
dH ₂ O		15ml

Stacking Acrylamide

(8% solution, 19:1 acrylamide/bis-acrylamide)

30%, 19:1 acrylamide/bis-acrylamide	8%	6.66ml
dH ₂ O		to 25ml

Resolving gel buffer (4x)

(1.5M tris.HCl pH 8.8, 50ml)

Tris (FW 121.1)	1.5M	9.1g
dH ₂ O		30ml
HCl	to pH 8.8	
dH ₂ O		to 50ml

Stacking gel buffer (4x)

(0.5M Tris.HCl pH 6.8, 50ml)

Tris (FW 121.1)	0.5M	3g
dH ₂ O		30ml
HCl	to pH 6.8	
dH ₂ O		to 50ml

Electrode buffer

0.025M Tris, 0.192M glycine, 0.1% SDS, pH 8.3, 2L)

Tris (FW 121.1)	0.025M	6g
Glycine (FW 75.07)	0.192M	28.8g
SDS	0.1%	2g

dH₂O

to 2L

10% SDS

SDS (FW 288.38)

10%

1g

dH₂O

to 10ml

5% Ammonium persulphate (APS)

Ammonium persulphate (FW 228.2)

5%

0.05g

dH₂O

to 1ml

Prepare just prior to use or store in aliquots at -20°C.

60% Glycerol

Glycerol

60%

30ml

dH₂O

20ml

5% Tetramethylethylenediamine (TEMED)

TEMED

5%

0.05ml

dH₂O

to 1ml

Sample buffer (2× DTT)

Dithiothreitol (DTT; FW 154.2)

0.2M

0.31g

10% SDS

2%

2ml

60% glycerol

24%

4ml

Stacking gel buffer (4×)		5ml
Bromophenol blue (2mg/ml)	0.01%	0.5ml

2.42 Additional Reagents

Prestained SDS-PAGE molecular weight protein standards; SDS-7B (Sigma-Aldrich), molecular weight range 26,600-180,000 Da (table 1); SDS-1B (Sigma-Aldrich), MW 58,000 Da and β -galactosidase (Sigma-Aldrich), MW 116,000 Da .

2.43 Equipment

BioRad Mini Protean II system

1.0 or 0.75mm thick combs and spacers

Glass plates

Water aspirator

Heater block

50ul Hamilton syringe

BioRad power supply

2.44 Table 7. SDS-7B Protein standards with approximate molecular weights

Source	Triosephosphate isomerase	Lactic Dehydrogenase	Fumarase	Pyruvate kinase	Fructose-6-phosphate kinase	β -galactosidase	α_2 -macroglobulin
MW, Da	26,600	36,500	48,500	58,000	84,000	116,000	180,000

2.45 Procedure

Preparation of the resolving gel

Clean, dry glass plates were assembled into the casting stand using either 0.75 or 1.0mm spacers. 6.5% gels (table 8) of 1mm thickness were used to resolve samples used for in-gel digestion due to increased loading capacity, whereas 0.75mm gels were used when subsequent Western blotting was to be carried out due to increased resolution. To pour two mini-gels the following solutions were mixed:

2.6ml resolving acrylamide (2×)

1.4ml dH₂O

2ml resolving gel buffer (4×)

2ml 60% glycerol

0.08ml 10% SDS

0.08ml 5% TEMED

After mixing the above and immediately prior to pouring the gels 0.08ml of APS was added to initiate the polymerisation reaction. After loading the gels were overlaid with dH₂O and allowed to set for approximately 1h.

2.46 Table 8. Resolving gel percentages

%	6.0	6.5	7.0	7.5	8.0	9.0	10.0
20% acrylamide (ml)	2.4	2.6	2.8	3.0	3.2	3.6	4.0
dH ₂ O (ml)	1.6	1.4	1.2	1.0	0.8	0.4	0.0

Preparation of the stacking gel

The resolving gel overlay was aspirated off before the insertion of relevant size Teflon comb. For two mini gels the following solutions were mixed:

2ml stack acrylamide (2×)

1ml 60% glycerol

1ml stacking gel buffer (4×)

0.04ml 10% SDS

0.04ml TEMED

After mixing the above and immediately prior to pouring the gels 0.04ml of APS was added to initiate the polymerisation reaction. The gels were poured ensuring no air bubbles were trapped between the teeth of the comb and polymerisation allowed for approximately 45mins.

Samples were prepared by mixing with sample buffer (50:50) and heating at 60°C for 30 mins. The combs were carefully removed from the gels and wells rinsed with dH₂O. The reservoirs of the tank were filled with electrode buffer ensuring coverage of sample wells then 20µl of prepared samples and markers 7 Blue and β-galactosidase (Sigma-Aldrich), were loaded into each well using a Hamilton syringe. Connection to the power supply, running at constant volts, 100V initially until the stacking gel was cleared then 150V for the remainder of the run.

Proteins subjected to in-gel digestion were visualised by overnight staining with SYPRO Ruby protein gel stain or the in-house equivalent (appendix E).

2.5 Two dimensional SDS-PAGE

2.51 Stock solutions

<i>Rehydration solution</i>	<i>Final concentration</i>	<i>Amount</i>
Urea (FW 60.06)	7M	21.9g
Thiourea (FW 79.12)	2M	7.9g
dH ₂ O		to 50ml
Do not heat to dissolve		
IPG buffer (same range as IPG strip)	0.5%	250µl

To 48ml of the above solution add 230mg , 60mM DTT and 2g (4% w/v) CHAPS and trace of bromophenol blue (0.002%). Store in 2.5ml aliquots at -20°C.

Post IEF equilibration buffer

Glycerol	20%	10ml
Tris (FW 121.1)	1.5M pH 8.8	12.5ml
Vortex to mix		
Urea (FW 60.06)	0.015M	18g
SDS (FW 288.38)	0.5%	1g
dH ₂ O		to 50ml

2.52 Equipment

Ettan IPGphor Isoelectric Focusing System

Immobiline DryStrips pH 3-10, linear.7cm long

BioRad Mini Protean II system

Glass plates

BioRad power supply

2.53 Procedure

The IPG strip holders were thoroughly cleaned and dried before pipetting 125 μ l rehydration solution into the strip holder, at a central point, ensuring even coverage and removing any large air bubbles. 15 μ l of sample was then added, 7.5 μ l to each side. The protective cover was removed from the dry strip starting at the acidic (pointed) end. The strip was positioned gel side down in the correct orientation within the strip holder, lowering the pointed end down first, slowly moving the strip back and forth along the surface of the solution to assure even and complete wetting. IPG cover fluid was then pipetted drop-wise over the whole strip, helping minimize evaporation and urea crystallization. The cover was placed on the strip holder, making certain the pressure blocks on the underside of the cover maintained a good contact with the electrodes. The strip holders were positioned correctly on the IEF platform with metal to metal contact, the following protocol programmed and IEF begun:

Step 1 – 12h rehydration

Step 2 – 30 min., 500V, 0.25kVh

Step 3 – 30 min., 1000V, 0.5 kVh

Step 4 – 1h 40min., 5000V, 7.5kVh

NB. For protocols with short running times it is possible that the voltage required may not be reached within the time allowed and so it may be better to programme in Volt hours rather than voltage and time.

After IEF the second dimension electrophoresis step was carried out using the standard SDS-PAGE methods described previously. The IPG strip was positioned between the glass plates upon the surface of the gel with the plastic backing against one of the glass plates ensuring no air bubbles were trapped before sealing with 1% agarose gel. The power was set at constant volts, 100V for the whole of the run. For in-gel digestion proteins were visualised by overnight staining with SYPRO Ruby protein gel stain or the in-house equivalent (Appendix E).

2.6 Electro-transfer of proteins from polyacrylamide gels

2.61 Stock solutions

<i>Transfer buffer</i>	<i>Final concentration</i>	<i>Amount of</i>
CAPS	10mM	2.2g
dH ₂ O		900ml
1M NaOH	pH 10.3	~2ml
Methanol		100ml

Dissolve CAPS in dH₂O, adjust to pH 10.3 with NaOH before adding methanol and stirring for 10 min.

2.62 Equipment

BioRad transfer cell with holder, cassette and two foam pads

Filter paper

Immobilon-P nitrocellulose membrane

Stirrer bar

2.63 Procedure

SDS-PAGE gels subjected to electrotransfer were generally run using 0.75mm spacers and combs as this allows greater resolution of proteins upon the membrane surface. The gel area to be transferred was cut out and immersed in transfer buffer for approximately 30 min. The apparatus was assembled with the gel sandwiched on top of the membrane and in between filter paper and foam pads. The cassette was inserted into the transfer holder ensuring the correct orientation. A stirrer bar and cooling pack was added before connection to the power supply running at constant current of 200mA for 60 min.

2.7 Western Blotting

Membranes were blocked in 5% non-fat dried milk in tris buffered saline (TBS) containing 0.01% Tween 20 (Blotto) for 30 min at room temperature before reaction with primary antibody for 1.5h. Washes with TBS followed for 3 × 5 min, then alkaline phosphatase linked secondary antibody in Blotto was added and reaction allowed to take place over 1h. Washes of 2 × 5 min with TBS and 1 × 5 min with dH₂O were carried out, then equal volumes of bromochloroindolyl (15mg/ml in 50:50

methanol:DMSO) and nitrobluetetrazolium (30mg/ml in methanol) in 100mM Tris HCl / 100mM NaCl / 5mM MgCl₂ (pH 9.5) added and staining allowed to develop. The reaction was stopped by the addition of water and membranes allowed to dry before visualisation.

2.8 In-gel digestion

2.81 Stock solutions

<i>Rehydration solution</i>	<i>Final concentration</i>	<i>Amount</i>
Ammonium bicarbonate (FW 79.06)	25mM	0.1g
dH ₂ O		50ml
<i>Dehydration solution</i>		
Ammonium bicarbonate (FW 79.06)	25mM	0.05g
dH ₂ O		25ml
Acetonitrile	50%	25ml
<i>Extraction solution</i>		
Trifluoroacetic acid (TFA)	5%	2.5ml
Acetonitrile	50%	25ml
dH ₂ O		to 50ml

Reduction solution

DTT (FW 154.2)	10mM	0.015g
----------------	------	--------

Dissolve in 25mM ammonium bicarbonate (10ml) aliquot and store at -20°C .

Alkylation solution

Iodoacetic acid (FW 207.9)	55mM	0.01g
----------------------------	------	-------

Dissolve in 25mM ammonium bicarbonate (1ml).

Digest reagents

<i>Trypsin</i>	pH 8.0	0.5 $\mu\text{g}/\text{ml}$
----------------	--------	-----------------------------

Dissolve in 25mM ammonium bicarbonate. Enzyme to protein ratio of 1:10.

<i>Endoproteinase Asp-N</i>	pH 4.0	40ng/ μl
-----------------------------	--------	---------------------

Dissolve in dH₂O. Enzyme to protein ratio of 1:20.

2% <i>Formic acid</i>	pH 2.0	200 μl
-----------------------	--------	-------------------

Acid to protein ratio 2:1 i.e. 200 μl of 2 % formic acid added to excised gel bands loaded with 100 μl protein.

2.82 Procedure

Ten protein bands or spots of interest were excised from the stained polyacrylamide gels for each digest. Each gel slice was cut into ~1mm pieces and placed into 0.65ml tubes. Parallel controls were also run by carrying out the digest procedure upon gel pieces from protein free regions. Dehydration solution, 100 μl , or enough to cover the gel pieces was added before vortexing for 3×10 min. The gel particles were dried for

~ 30 min in a freeze dryer before performing reduction and alkylation (figure 13) on bands from one-dimensional gels. Two-dimensional gels are already reduced and alkylated so this step is not necessary. The gel pieces were covered with 10mM DTT and reduced for 1h at 56°C then cooled to room temperature. Any excess DTT was pipetted off and replaced with equivalent amounts of 55mM iodoacetic acid before incubation in the dark at room temperature for ~45 min, with occasional vortexing. The gels pieces were then washed with 100µl rehydration solution, pH 8.0, for 10 min while vortexing then likewise with dehydration solution. The rehydration, dehydration step was then repeated. Any liquid phase was removed and the gel pieces freeze dried to complete dryness before rehydration of the gel pieces with digest reagent.

The enzyme volume needed for rehydration was calculated from the total gel volume excised (e.g., $2mm \times 4mm \times 1mm \text{ thickness} \times 3 \text{ lanes} = 24 \mu\text{l}$). The protein:enzyme ratio i.e. 1:10 for trypsin and 1:20 for Asp-N was calculated and the precise amount of enzyme added. Concentration of formic acid used, however, was calculated purely upon the starting volume of protein loaded (e.g. $20\mu\text{l protein} \times 3 \text{ lanes} = 60\mu\text{l}$, 2:1 acid:protein ratio, therefore 180µl formic acid added. After addition of the digest reagent the reaction was allowed to proceed for 16h at 37°C for enzymes and at 100°C for 2h for the formic acid digest.

The next step was the aqueous and organic extraction of the digest. Digests were centrifuged for 3 min at 1500 rpm, vortexed for 5 min before adding ~100µl dH₂O then vortexing, spinning (3 min at 1500 rpm) and sonicating for 5 min each. The aqueous solution was pipetted off into a clean 0.65ml tube, to which 5µl of the

organic extraction solution had been added. The gel was then subjected to an organic extraction by adding 50µl of extraction solution, vortexing for 10 min., then spinning (3min at 1500 rpm) and sonicating for 5 min. With the omission of sonication the last step was repeated two times. Both the aqueous and organic extracts were combined, vortexed and spun for 5 min each at 1500 rpm and the total volume reduced to ~10µl by freeze drying. 100µl of dH₂O was added before vortexing and freeze-drying to 10µl repeated and the final addition of 2-5µl extraction solution. Preliminary results showed whether or not further clean up was necessary by use of Millipore C₁₈ ZipTips.

2.9 Mass spectrometry

2.91 Matrix- assisted laser desorption ionisation-mass spectrometry (MALDI-MS)

Intact spectra were obtained on a Finnigan MAT Vision 2000 reflectron time-of-flight mass spectrometer equipped with a nitrogen laser (337nm), (Finnigan MAT GmbH, Bremen, Germany) at an accelerating voltage of 20kV. The digest spectra were obtained using an API QSTAR™ Pulsar Hybrid LC-MS-MS system (Applied Biosystems-MDS Sciex, Toronto, Canada) with the orthogonal MALDI ion source fitted and running at 5-15kV. A 10mg/ml 2,5-dihydroxybenzoic acid dissolved in 0.1% trifluoroacetic acid (TFA) and 10mg/ml 5-methoxysalicylic acid dissolved in 50:50 ethanol:water (9:1 v/v) matrix solution was used to obtain the intact protein spectra. The digest spectra were obtained using a solution of α -cyano-4-hydroxycinnamic acid (α CHCA) dissolved in 50% water (0.1% TFA added), 50%

acetonitrile. Samples for mass spectrometry were prepared by using 2 μ l protein solution mixed with 20 μ l matrix, of which 0.5 μ l was applied to the stainless steel target and allowed to air dry before insertion into the mass spectrometer.

2.92 Liquid chromatography electrospray ionisation-mass spectrometry (LC-ESI-MS)/ Information Dependant Acquisition (IDA).

All experiments were done on an API QSTAR™ Pulsar Hybrid LC-MS-MS system with a capillary LC interface. The LC system consisted of a LC Packings Ultimate™ nano-LC system equipped with a Famos™ autosampler (Dionex CA, USA). Separations were performed using a C18 “Pepmap” column (15cm \times 75 μ m o.d., 3 μ m particle size). A linear gradient over 55 minutes was carried out between eluents A (95% water [containing 0.1% formic acid]: 5% acetonitrile) and B (95% acetonitrile: 5% water [containing 0.1% formic acid]) at a flow rate of 0.2 μ l/min the gradient profile shown in table 9. Injection volume was 5 μ l of digest solution (2 μ l sample in 5 μ l 1% acetonitrile in water [containing 0.1% formic acid]).

All MS/MS experiments were performed using the IDA software (Analyst QS version, Sciex, Toronto, Canada). IDA allows automated high-throughput MS/MS screening of samples from TOF/MS and LC/MS, maximising the amount of data available from a single analysis (refer to section 1.24). Certain parameters are needed in order to build the acquisition method tailoring the analysis to the sample. Depending upon the type of experiment i.e. MALDI or LC, experimental parameters were set up in the correct hardware profile (MALDI or LC) from the acquisition method menu as follows:

Scan type –	TOF MS or product
Ion mode –	Positive
Collision energy –	0 invokes the rolling collision energy function (see section 1.24)
Ion mode -	positive
For ions greater than -	300.0 m/z
For ions smaller than -	1200.0 m/z
With charge state -	1 (MALDI) or 2 to 3 (LC-ESI)
Which exceeds -	3 counts
Switch after –	2 spectra
Quad resolution –	low
Ignore peaks within –	50.0 mmu
Declustering potention –	45.0
Focussing potential –	225.0
Argon CAD gas –	8.0
Ignore peaks within –	5.0 amu window
Survey scan accumulation -	1 second
Independent scan accumulation -	3 seconds

Monitoring the 8 most intense ions from the survey scan peak list for the MS/MS experiments:

Time (mins)	Flow rate ($\mu\text{l}/\text{min}$)	% A	% B
0.0	0.2	5.0	95.0
30.0	0.2	65.0	35.0
31.0	0.2	99.0	1.0
40.0	0.2	99.0	1.0
40.0	0.2	5.0	95.0
55.0	0.2	5.0	95.0

Table 9. The elution profile used for LC/ESI-MS of all samples. A =95% water [containing 0.1% formic acid]: 5% acetonitrile and B = 95% acetonitrile: 5% water [containing 0.1% formic acid].

2.93 Nanospray-mass spectrometry

All experiments were done on an API QSTARTM Pulsar Hybrid LC-MS-MS system with a ProtanaTM nanospray interface. Helium was used as a curtain gas at a flow rate of 0.25L/min. The capillary voltage was 1300V for all samples using fused silica capillaries (360 μm o.d., 20 μm i.d., 10 μm tip diameter) (PicotipsTM, NJ, USA).

Four different proteins are investigated here, two protein standards and two immunoprecipitated APP samples. The first standard protein examined was BSA due to its cost, availability, similarity in molecular weight to the APP samples and knowledge of expected results¹⁹¹. The second standard investigated was secreted alpha secretase cleaved APP isoform 695 (APP α_{695}) purchased from Sigma for use as a direct comparison with the immunoprecipitated APP α_{695} . The two samples, APP α_{770} and APP α were used as models of *in vivo* conditions. APP α_{770} was immunoprecipitated from Chinese hamster ovary cells¹⁹² (CHO 770) genetically modified to produce the APP $_{770}$ isoform only. APP α was immunoprecipitated from Ntera 2 cells¹⁹³, a teratocarcinoma cell line cell that differentiates into brain cells upon treatment with retinoic acid. The latter of the two samples secretes all three isoforms of interest (APP α_{695} , APP α_{751} and APP α_{770}) and as such acts as a more plausible model of *in vivo* conditions.

The results shown here are laid out in the general order that they were performed. The initial stages of this work involved the isolation of APP samples from the CHO 770 and Ntera 2 cell secretions (chapter 3.1). Once isolated these solutions were analysed intact by MALDI-MS and nanospray (chapter 3.2) or subjected to further purification by either one-dimensional (1D) electrophoresis or two-dimensional (2D) electrophoresis and Western analysis (chapters 3.11 and 3.12). Western blotting enabled the initial visualisation of proteins present within the 1D and 2D gels. Unlike the protein standards (BSA and APP α_{695}) whose starting concentrations were known the concentrations of the immunoprecipitated samples was unknown and could only be estimated by comparison of the staining densities of samples verses standards present on a gel. Quite often, however, the sample proteins remained undetected by

the staining technique employed (in-house fluorescent stain (appendices 6)), a major problem with low-level proteins. The staining method employed was an in-house equivalent to Sypro Ruby, which is comparative in sensitivity to silver staining¹⁹⁴ but does not suffer from the same problems such as staining inhomogeneity, time consuming application and adduct interference. Western blotting is inherently more sensitive than the staining technique employed detecting protein levels within the low attomole range and as such was able to visualise blotted proteins previously unseen upon the gel. When performing 2D gel separation two gels were run in parallel, one was subjected to Western analysis to detect the presence and position of the protein sample, this could then be used as a template for excision of the protein in question from the 2D gel.

Background work for the in-gel digestion and analysis by mass spectrometry came next and involved the *in silico* digestion of the APP isoforms (chapter 3.3). Each of the secreted APP isoform sequences was put into the ExPASy's peptide mass database as well as experimental parameters such as digest reagent, known modifications, mass range etc. A theoretical digest of the sequences then produced a list of peptides or theoretical mass fingerprint. Examination of these lists revealed the presence of isoform specific peptides (chapter 3.3, table 9). These unique peptides could then be used as 'tags' in the consequent in-gel digestions and analysis by mass spectrometry (chapter 3.4). Each experiment performed on the four samples is summarised in table 10 (chapter 3.4) with the exception of the intact data.

3.1 Isolation of amyloid precursor protein (APP) isoforms from conditioned media

The isolation of APP isoforms from conditioned media was carried out by one-dimensional and two-dimensional gel electrophoresis, the latter being a principal strategy in the separation of proteins due to its ability to resolve complex mixtures. The availability of several primary antibodies raised to various epitopes within APP isoforms (figure 28) enabled Western blot analysis to be performed upon the electrophoretic separations. Quite often when extracting proteins, low concentration is a major problem and even the most sensitive staining techniques are unable to detect all proteins within a gel. The infinite sensitivity and specificity of antibodies allows ultimate detection by Western blotting and so this technique was exploited as a primary detection method.

Initial electrophoresis work was performed using bovine serum albumin (BSA) as a standard (figure 29). The amyloid precursor protein isoforms needed to be isolated from conditioned media by immunoprecipitation prior to electrophoresis. Initial method development of this procedure involved the comparison of immunoprecipitation methods (figures 30(a), 30(b), 31(a) and 31(b)) and bead elution techniques (figures 32(a) and (b)). The optimal concentration of AB10 primary antibody (figure 33) with regards to achieving the optimal saturation of APP from the media was also determined before full investigation of APP isoforms. Samples were obtained from two different sources; chinese hamster ovary 770 (CHO770) cells excreting only APP α_{770} and Ntera 2 cells, a human teratocarcinoma cell line that excretes all three isoforms of interest (APP α_{695} , APP α_{751} and APP α_{770}). An alpha secretase cleaved APP α_{695} isoform (APP α_{695}) standard was purchased from Sigma for

use as a direct comparison. It should be noted that all electrophoretic separations of APP show the molecular weight of the isoforms to be around 116kDa when compared to the ladder of protein standards, instead of the desired 67,665kDa, 73,817kDa and 75940kDa for APP₆₉₅, APP₇₅₁ and APP₇₇₀ respectively. The slow running of APP isoforms may be due to glycosylation or phosphorylation affecting the charge on the molecules.

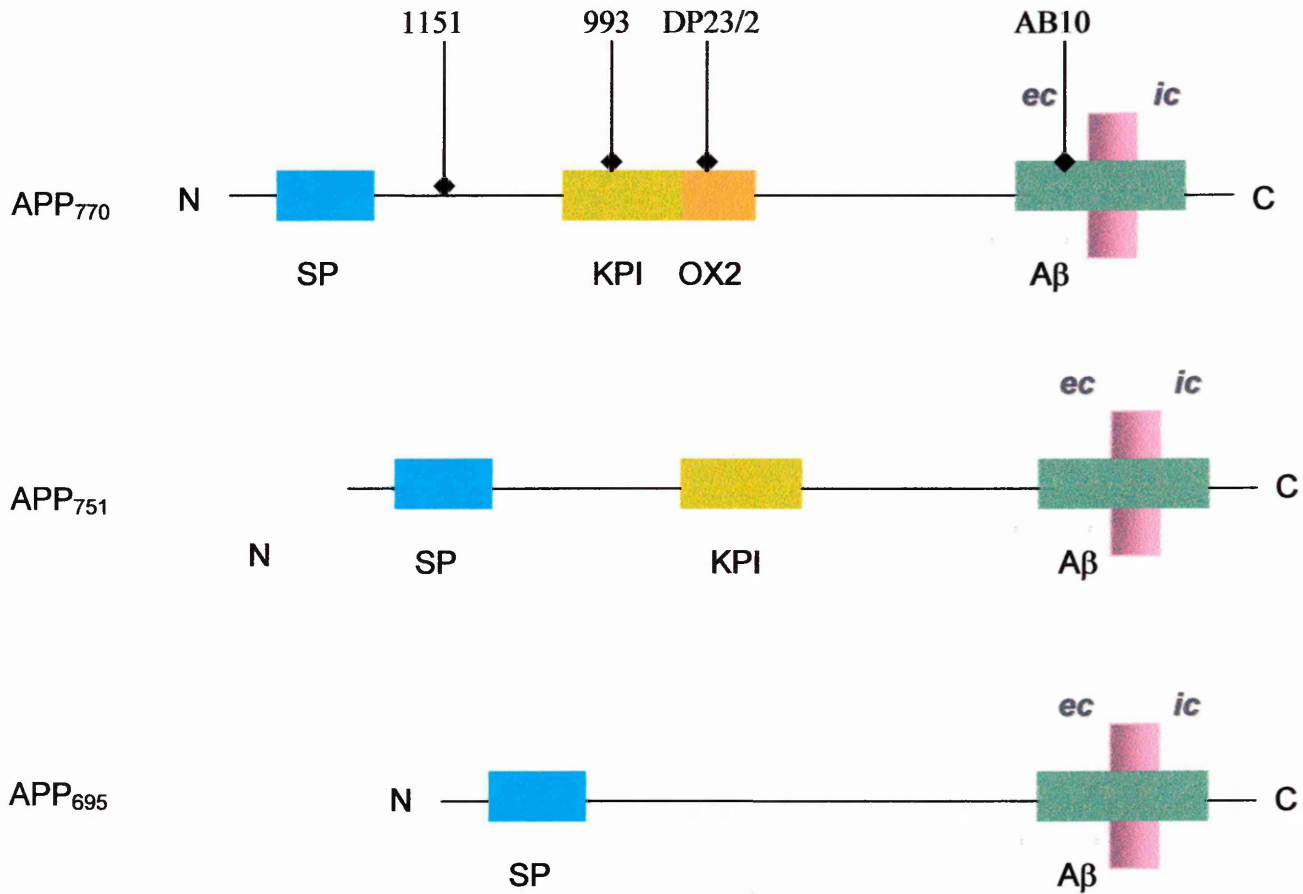


Figure 28. Schematic diagram of APP₇₇₀, APP₇₅₁ and APP₆₉₅, showing regions distinct to each isoform and the binding epitopes for the antibodies, 1151, 993, DP23/2 and AB10. The antibody, 1151 is raised to a sequence C terminal to the signal peptide, present in all three isoforms; 993 is raised to the KPI domain present in APP₇₇₀ and APP₇₅₁; DP23/2 is raised to the OX2 homology domain present only in APP₇₇₀; AB10 is raised to an epitope in 1-17 of the β amyloid peptide sequence. Abbreviations: Ab, beta amyloid sequence; CM, cell membrane; *ec*, extracellular domain; *ic*, intracellular domain; KPI, Kunitz type protease inhibitor; OX2, OX2 homology domain.

3.11 One-dimensional gel electrophoresis

3.111 One-dimensional gel electrophoresis of bovine serum albumin (BSA).

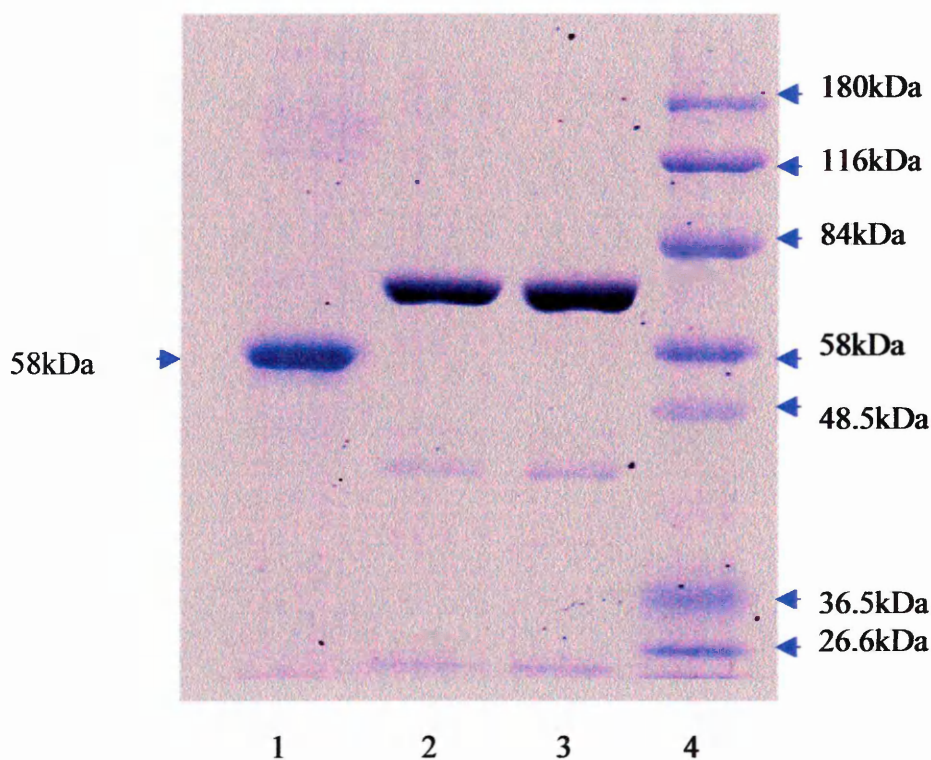


Figure 29. One-dimensional gel of BSA (lanes 2 and 3) stained with Coomassie and using 1-blue and 7-blue (Sigma) markers (lanes 1 and 4 respectively).

Bovine serum albumin (BSA, monoisotopic mass 66,389.86) was used as a standard due to its availability and similarity in molecular weight to the amyloid precursor protein isoforms ($APP_{\alpha 695}$, 67,665.55, $APP_{\alpha 751}$, 73,817.11, $APP_{\alpha 770}$, 75,940.25). Figure 29 shows a typical one-dimensional electrophoretic separation of BSA. The protein gel bands were then excised and subjected to in-gel digestion.

3.112 Comparison of immunoprecipitation methods

The usual precipitation method of APP from conditioned media was performed using mouse monoclonal antibody, AB10, raised to amino acids 1-17 of the β amyloid

peptide sequence, which is present in the alpha secretase cleaved isoforms of interest ($APP_{\alpha_{695}}$, $APP_{\alpha_{751}}$ and $APP_{\alpha_{770}}$). Extraction was then carried out using goat anti-mouse agarose beads (Sigma-Aldrich) and the protein-antibody-bead complex collected by centrifugation. In order to achieve optimal binding, therefore harvesting as much APP as possible, the use of a different extractant was considered. The goat anti-mouse secondary antibody adheres to both the Fc and FAB sites upon the primary antibody. Protein or antigen binding occurs at the antibody FAB portion and as such protein binding may be reduced if these sites are occupied by the goat anti-mouse molecule. Protein G, on the other hand, binds exclusively to the antibody Fc portion leaving free both FAB sites for optimal protein binding.

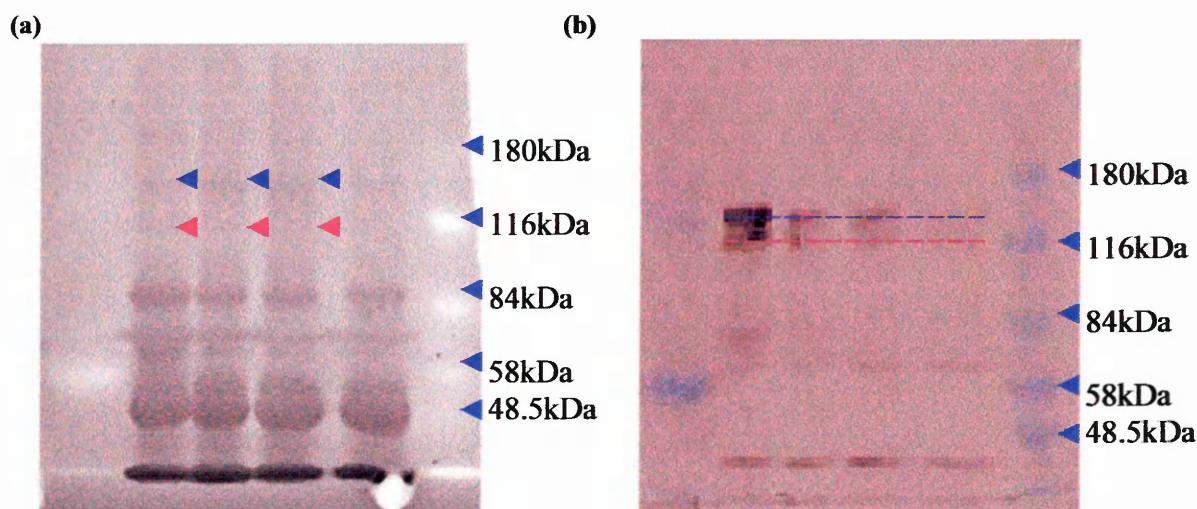


Figure 30. APP isolated from Ntera 2 cells using goat anti-mouse beads. (a) One-dimensional SDS-PAGE gel showing faint bands for the APP isoforms. (b) Western blot analysis using the primary antibody 1151 raised to an epitope C terminus to the signal peptide, which is present in all three isoforms. This gives the characteristic two band pattern shown, consisting of $APP_{\alpha_{695}}$ highlighted by the red dashed line and unresolved $APP_{\alpha_{751}}$ and $APP_{\alpha_{770}}$ isoforms highlighted by the blue dashed line.

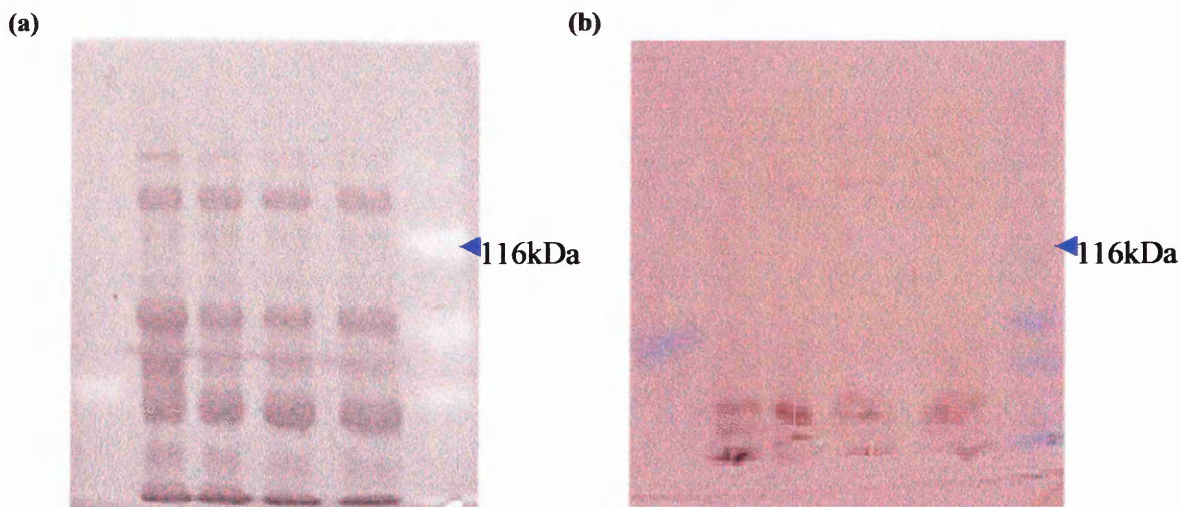


Figure 31. APP isolated from Ntera 2 cells using Protein G. (a) One-dimensional SDS-PAGE gel. (b) Western blot analysis again using the primary antibody 1151. This time, however, the APP isoforms are not visualised.

The Western blot shown in figure 30(b) of APP isolated from Ntera 2 cells using goat anti-mouse beads shows clearly the presence of all three isoforms, validating this method of extraction. The Western blot shown in figure 31(b), however, using Protein G does not show any measurable signs of APP isoforms, therefore substantiating the efficacy of the goat anti-mouse beads.

3.113 Comparison of bead elution methods

After collection of the protein-antibody-bead complex by centrifugation elution of the beads is performed. It was originally thought that the use of urea would be the best method for elution of the goat anti-mouse IgG beads rather than a 50:50 mixture of dithiothreitol (DTT) and urea, the rationale being that DTT may somehow interfere with the subsequent MALDI-MS analysis, however, this was not confirmed. Although earlier experiments demonstrated urea in high concentrations to have a deleterious effect upon MALDI-MS this could be combated by dialysis of eluted samples into dH₂O to remove excess urea.

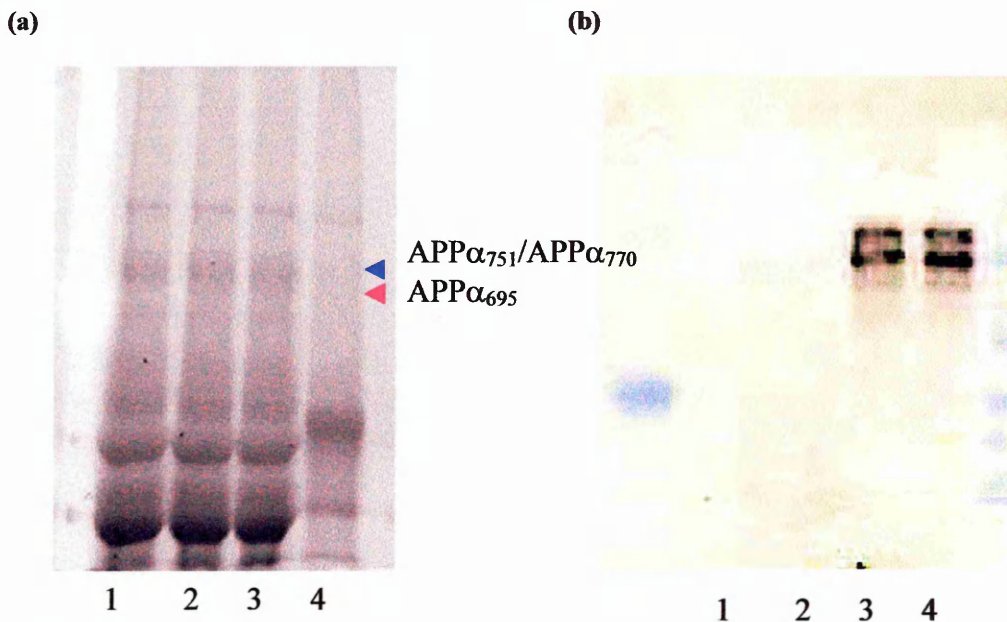


Figure 32. Comparison of bead elution techniques. (a) One-dimensional SDS-PAGE gel showing in lanes 1-3 bead elution using a 50:50 solution of DTT/urea and urea only in lane 4. (b) Western blot (using the antibody 1151, which pulls out all three isoforms of interest) showing urea only elution in lanes 1 and 2 and DTT/urea in lanes 3 and 4.

The comparison of elution techniques (figure 32) shows the addition of DTT far superior as it elutes greater concentrations of APP than urea alone. This is obvious in the Western analysis (figure 32b), which shows a lack of APP isoforms in lanes 1 and 2 resulting from the urea only elution, whereas the DTT/urea elution method gives strong staining (lanes 3 and 4). With low level proteins such as APP, concentration is always a problem so it is necessary not only to extract from the media as much of the protein as possible but also from that stage forward keep experimental steps to a minimum. The use of DTT improves in both these areas as it extracts more APP and cuts out the need for dialysis to remove excess urea, therefore facilitating protein isolation by cutting down on sample losses occurred during dialysis.

3.114 Optimal concentration of AB10 primary antibody.

In order to achieve optimal saturation of the antibody molecule immunoprecipitation was performed using increasing concentrations of AB10 and the resulting solutions subjected to one-dimensional SDS-PAGE followed by Western analysis (figure 33).

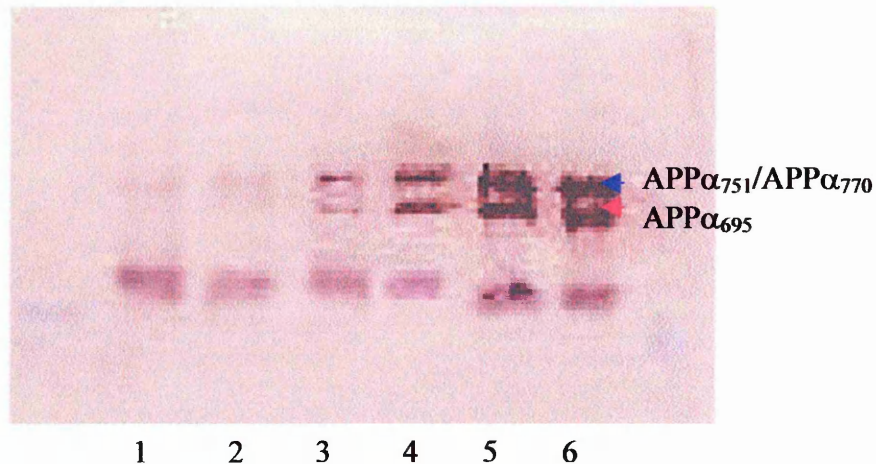


Figure 33. Western blot of APP isolated from Ntera 2 cells using the primary antibody AB10 (raised to an epitope within 1-17 of the A β peptide sequence, which is present in three isoforms). This gives the characteristic two band pattern shown consisting of APP α_{695} and unresolved APP α_{751} / APP α_{770} isoforms. Serial concentrations of AB10 added to 5ml of Ntera 2 solution are as follows; Lane 1- 0ml; Lane 2 -1ml; Lane 3 - 2ml; Lane 4 - 3ml; Lane 5 - 4ml; Lane 6 - 8ml.

The western analysis shown in figure 33 shows greatest staining in lane 5, using 4ml of AB10 primary antibody in the immunoprecipitation procedure. Increasing the volume of AB10 to 8ml as seen in lane 6 did not show darker staining and so from these results it was concluded that 4ml of AB10 to 5ml of Ntera2 solution is the optimal saturation concentration.

3.115 One-dimensional gel electrophoresis of amyloid precursor protein (APP) isoforms.

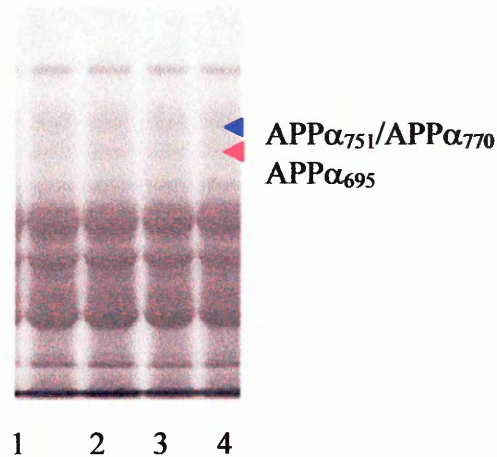


Figure 34. One-dimensional SDS-PAGE gel of APP isolated from Ntera 2 cells, which excretes all three isoforms of interest. This gel highlights the typical pattern seen in the one-dimensional analysis of this solution.

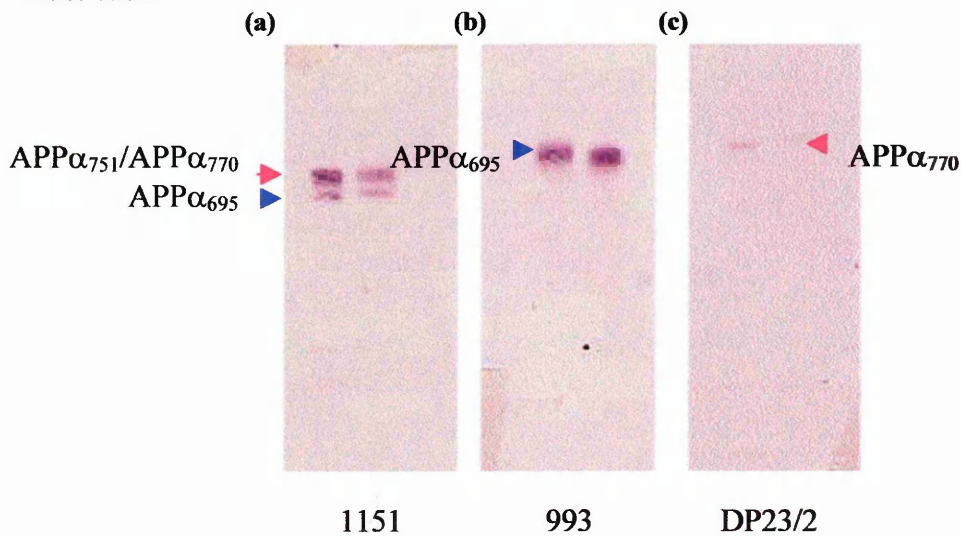


Figure 35. Western blots of APP excreted from Ntera 2 cells utilising primary antibodies raised to various epitopes within APP isoforms (figure 1). (a) 1151 is specific for all three isoforms, seen here is the general pattern showing two bands made up of APP_{770}/APP_{751} and APP_{695} in the faster running band. (b) 993 is specific to APP_{770} and APP_{751} and as expected only one band is seen consisting of both these isoforms. (c) DP23/2 is specific for APP_{770} only. The faint staining shown on the here correlates with the concentration of APP_{770} expected in cells i.e. APP_{770} is in relatively low concentration compared with APP_{695} and APP_{751} .

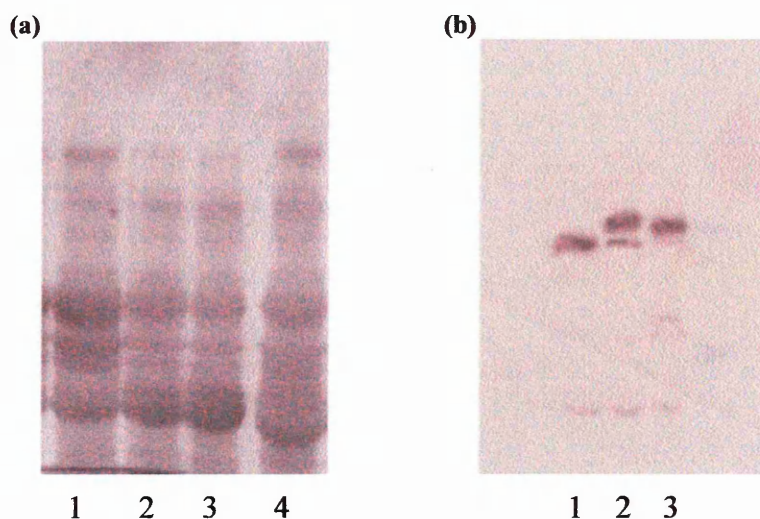


Figure 36. Comparison of APP isoforms. (a) One-dimensional SDS-PAGE gel of APP isoforms derived from three different sources. Lane 1 shows APP excreted from the CHO770 cells showing just one band for APP α_{770} . Lanes 2 and 3 shows the APP α_{695} standard. Lane 4 illustrates APP excreted from Ntera 2 cells with the expected 2 band pattern. (b) Western analysis of the afore mentioned solutions using 1151 antibody specific to all three isoforms (figure 28). Lane 1 shows the APP α_{695} standard. Lane 2 shows APP excreted from Ntera 2 cells. Lane 3 shows APP α_{770} excreted from the CHO770 cell line.

The preliminary determination of APP isoform presence within the one-dimensional gels was carried out by Western analysis. Due to the low concentration of APP the cell extractions were concentrated by Centricon adapter prior to running down a gel. The use of a sensitive staining technique was also employed for APP allowing the visualisation of isoform bands which could then be excised and subjected to in-gel digestion.

3.12 Two-dimensional gel electrophoresis

3.121 Two-dimensional gel electrophoresis of bovine serum albumin (BSA).

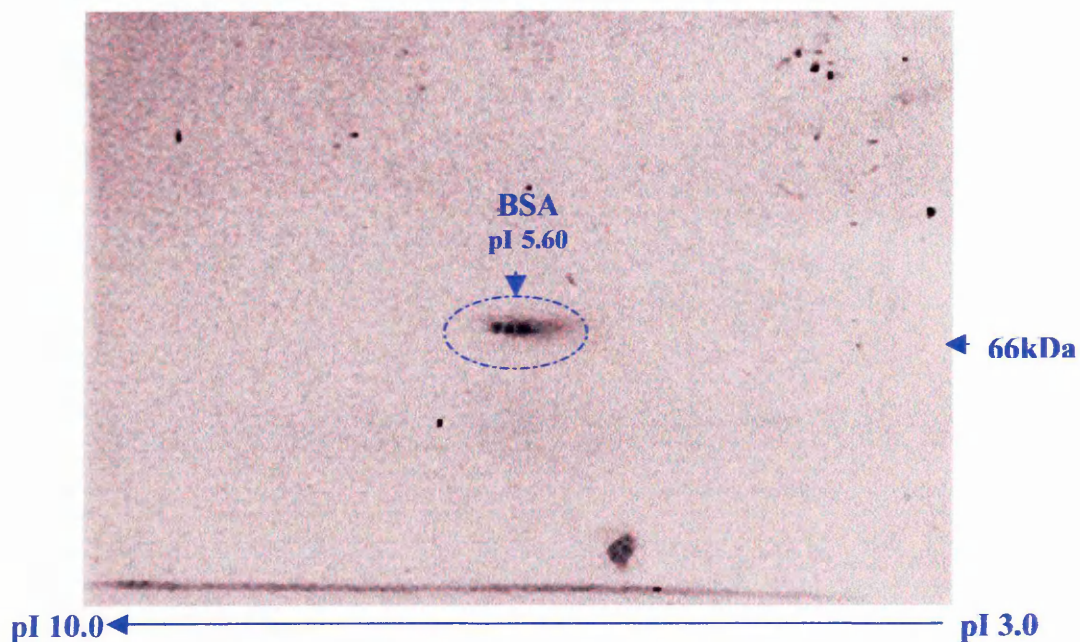


Figure 37. Two-dimensional gels of BSA using pH 3.0-10.0 dry-strips and performed on a 7cm gel.

Bovine serum albumin (BSA, monoisotopic mass 66,389.86) was used as a standard due to its availability and similarity in molecular weight to the amyloid precursor protein isoforms ($APP\alpha_{695}$, 67,665.55, $APP\alpha_{751}$, 73,817.11, $APP\alpha_{770}$, 75,940.25). Figure 37 shows a typical two-dimensional gel from which BSA was then excised and subjected to in-gel digestion.

3.122 Two-dimensional gel electrophoresis of amyloid precursor protein (APP) isoforms.

3.1221 Two-dimensional gel electrophoresis of alpha secretase cleaved amyloid precursor protein standard, isoform 695 (APP α_{695}).

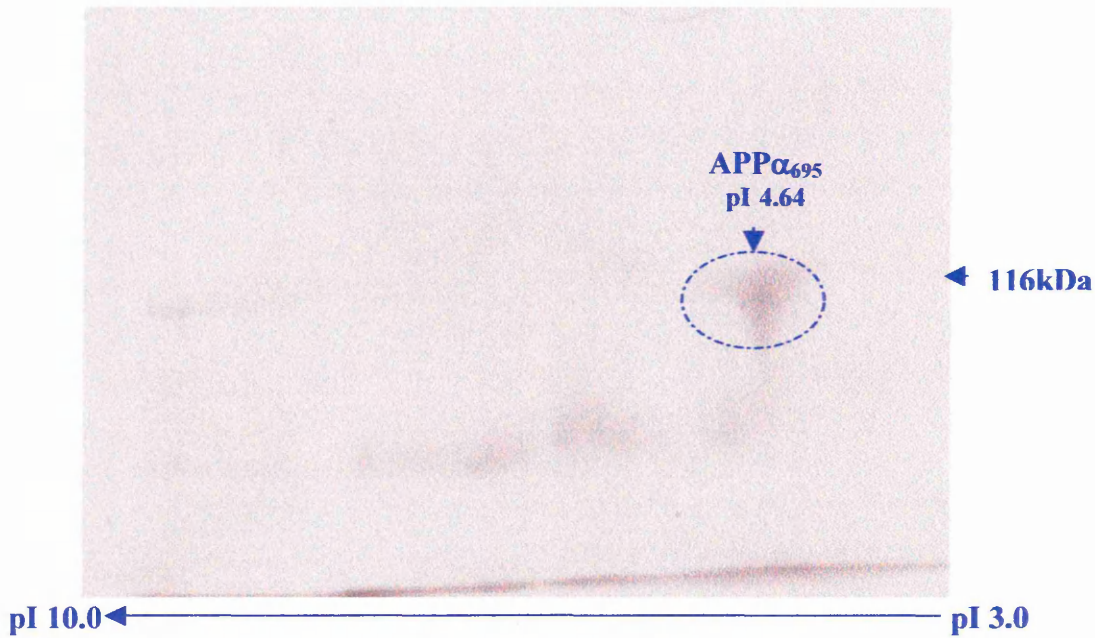


Figure 38. Two-dimensional gel of APP α_{695} standard using pH 3.0-10.0 dry strips and performed on a 7cm gel. The APP α_{695} standard could then be excised from the gel then subjected to an in-gel digestion.

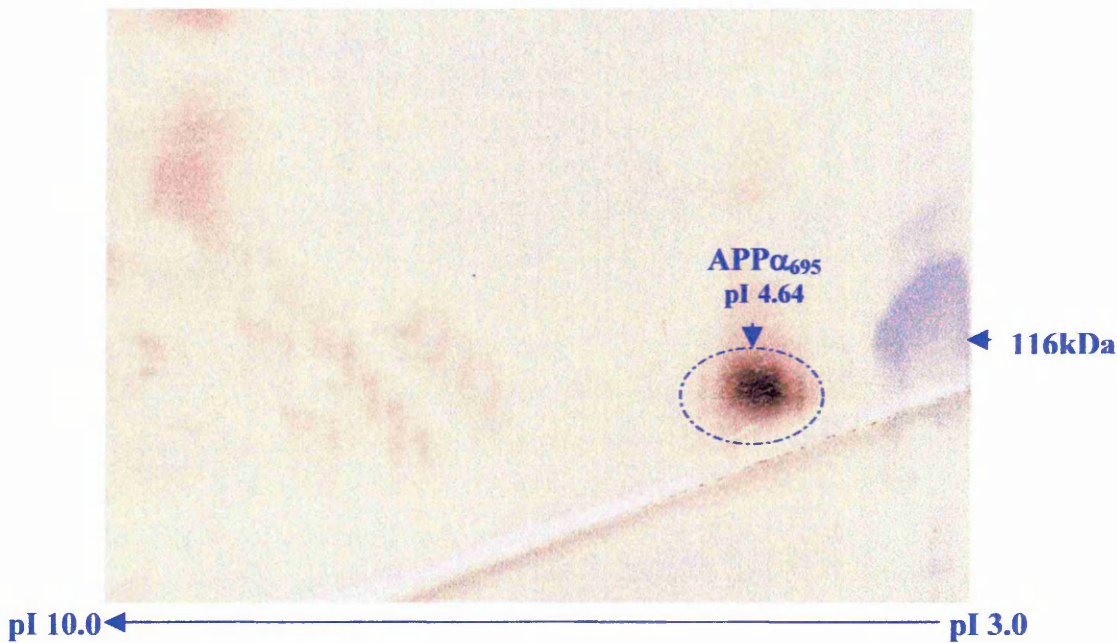


Figure 39. Western blot of a two-dimensional gel of the standard APP α_{695} identical to the one shown in figure 38. The antibody 1151 was used which reveals the presence of all three isoforms of interest.

The standard APP α_{695} isoform was subjected to two-dimensional analysis, which gave one major protein spot as expected at pI 4.64. This protein spot could then be in-gel digested to allow a direct comparison by mass spectroscopy.

3.1222 Two-dimensional gel electrophoresis of alpha secretase cleaved amyloid precursor protein, isoform 770 (APP α_{770}).

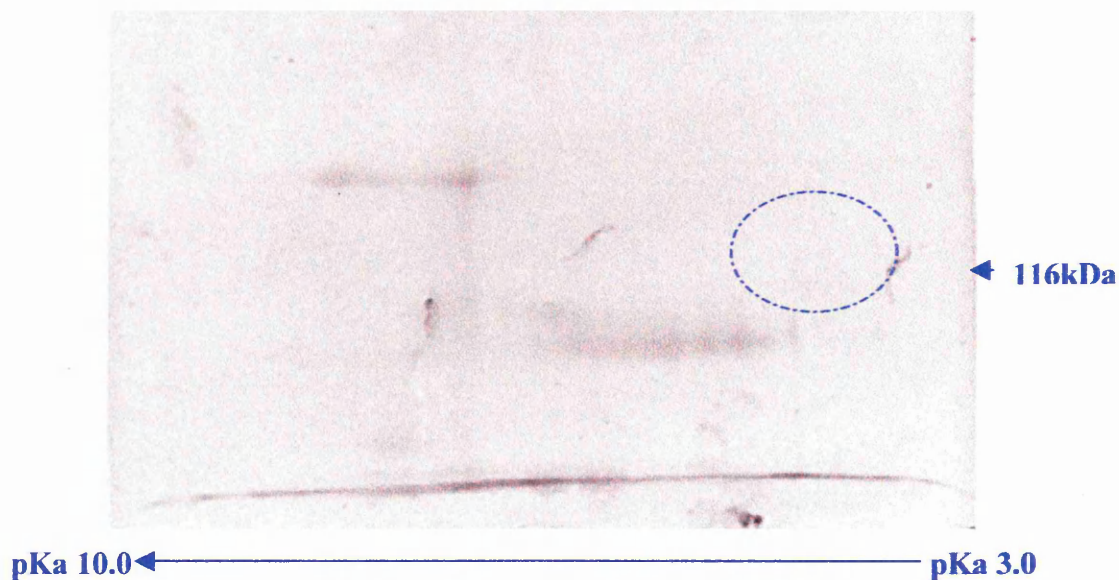


Figure 40. Two-dimensional gel of APP α_{770} isoform extracted from CHO 770 cell line. The circle highlights the area in which APP α_{770} is expected.

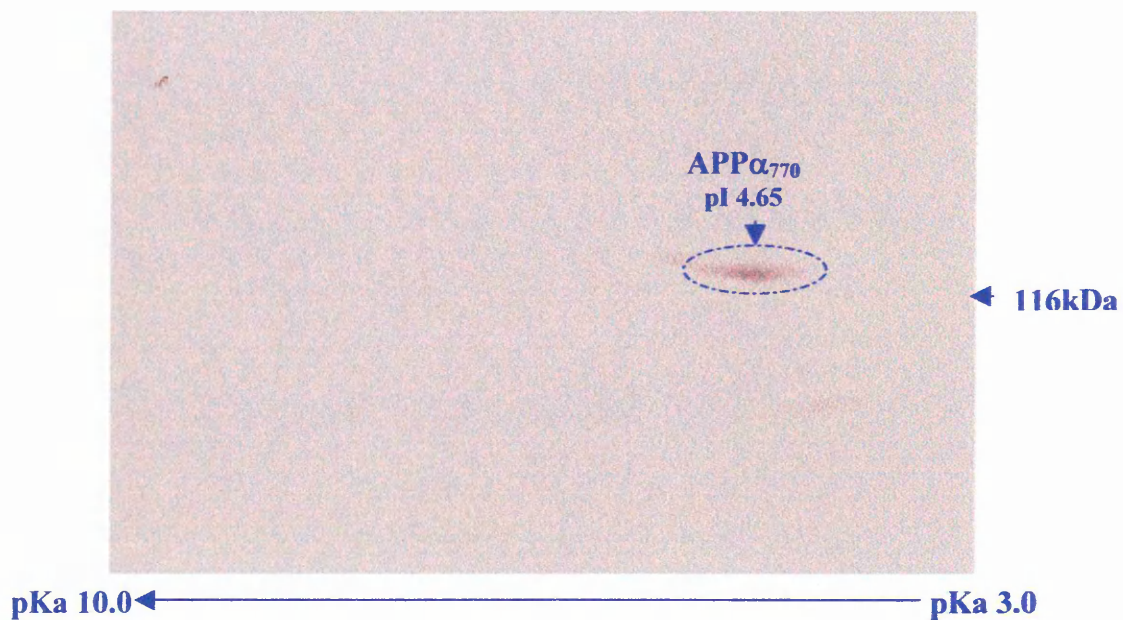


Figure 41. Western blot using 1151 of a two-dimensional gel of APP α_{770} isolated from CHO 770 cells identical to the one shown in figure 40.

The two-dimensional gel of APP α_{770} (figure 40) does not show any obvious signs of the isoform even though the concentration of isolated APP α_{770} loaded is similar to

that loaded upon the one-dimensional gels. The nature of two-dimensional analysis, however, means that sample losses can occur generally but also the removal of any co-eluting species in the first dimension may also reduce staining in the areas observed. Although the isoform cannot be seen on the gel (figure 40) the discrete sensitivity of the antibodies used in Western blotting allows detection of very low-level proteins and visualisation of APP α_{770} (figure 41). Identical gels were run and the Western analysis acted as a template for the excision of the APP α_{770} from the gel.

3.1223 Two-dimensional gel electrophoresis of alpha secretase cleaved amyloid precursor protein (APP α).

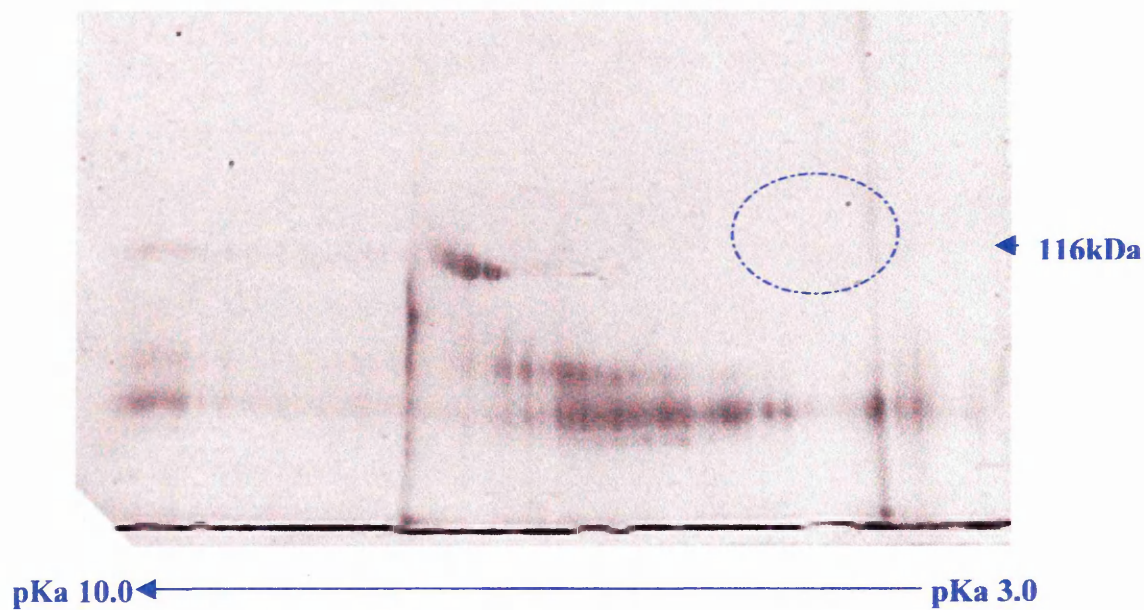


Figure 42. Two-dimensional analysis of APP α extracted from Ntera 2 cells. The circle predicts the area in which APP isoforms can be expected.

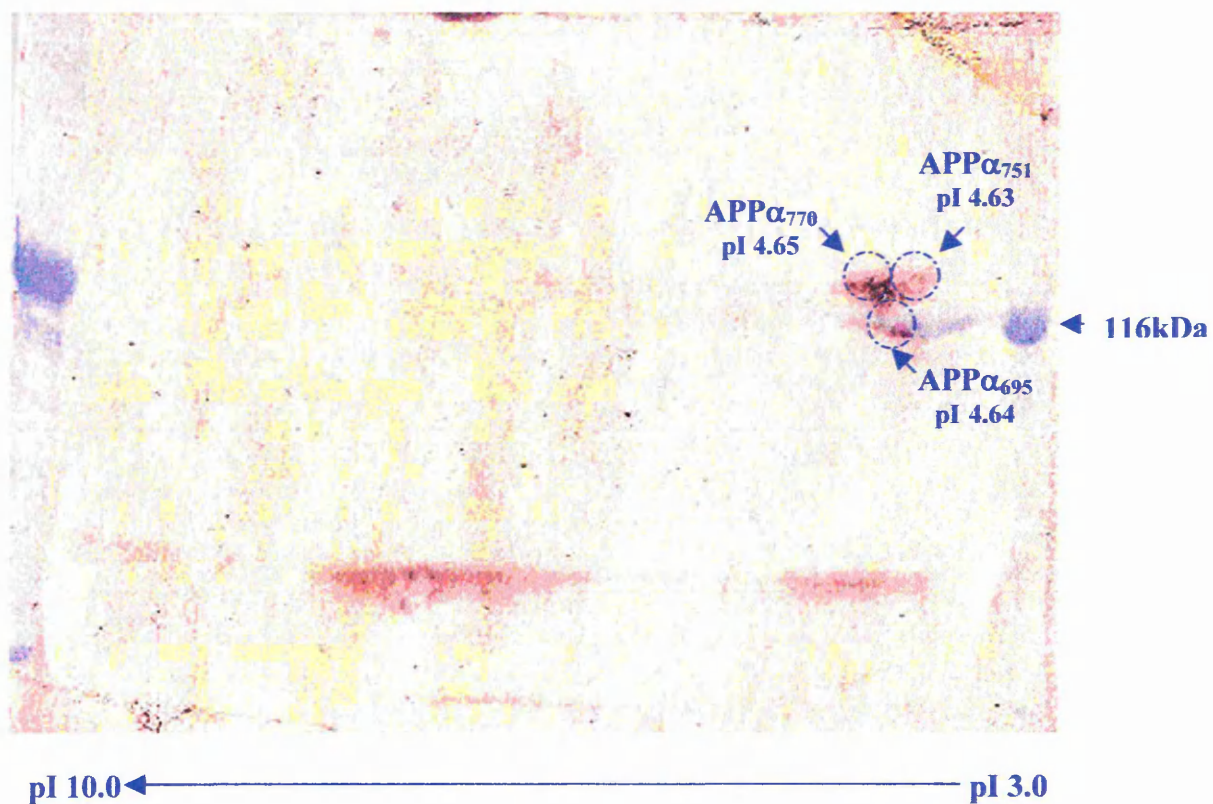


Figure 43. Western blot using 1151 of a two-dimensional gel of APP α identical to figure 42.

Again the two-dimensional gel of APP α (figure 42) does not show any sign of the isoforms even though the concentration loaded is similar to that loaded upon the one-dimensional gels. The use of Western analysis, however, helps to combat this showing clearly the presence of all three isoforms (figure 43) in this sample as well as acting as a template for gel excision.

The concluding remarks from this section must be the ability of two-dimensional gel electrophoresis to resolve all three APP isoforms (figure 43) compared to one-dimensional electrophoresis (figure 34), which is unable to resolve APP α_{770} from APP α_{751} due to closeness of molecular weights. The first dimension separation by isoelectric focusing point (pI) shows a vague separation between APP α_{770} at pI 4.65 and APP α_{751} at pI 4.63. The pI of APP α_{695} is in between at 4.64 and separation in this dimension may prove difficult but the difference in molecular weight of APP α_{695} allows a clear separation in the second dimension SDS-PAGE step. The two-dimensional gels shown here have all been performed using pH 3.0-10.0 drystrips and 7cm gels. To improve separation in the first dimension the use of drystrips with a more optimal pH range could be used such as pH 4.0-7.0 and improvements in the second dimension could be achieved by using larger gels. The disadvantage of two-dimensional electrophoresis, however, is the reduction of sample concentration making visualisation of low-level proteins difficult and the sensitivity of the staining technique being the limiting step. Improvements in this area, however, will help circumvent such problems.

3.2 Examination of intact bovine serum albumin (BSA) and amyloid precursor protein (APP).

3.21 MALDI-MS and nanospray analysis of intact BSA.

3.211 MALDI-MS of intact BSA

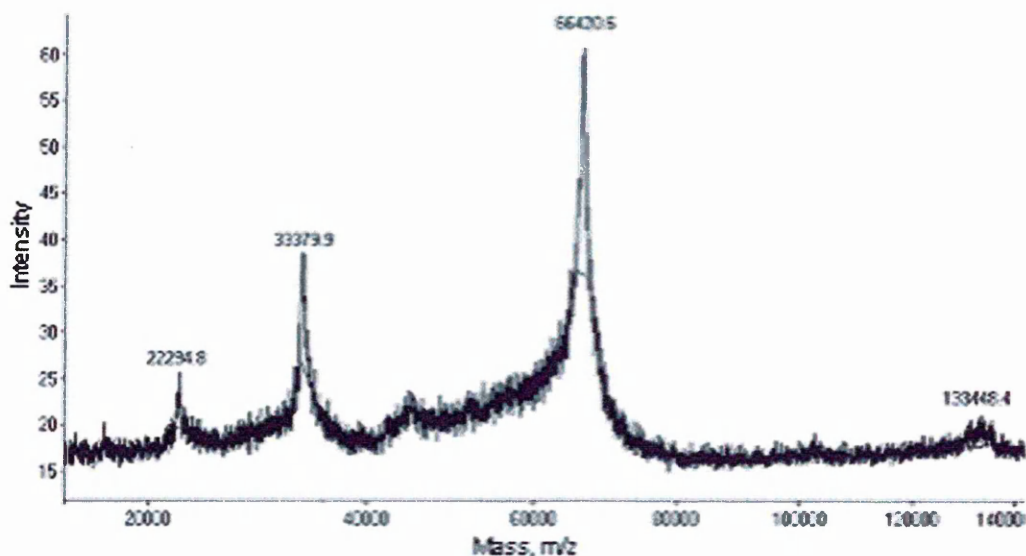


Figure 44. MALDI-MS spectrum of intact BSA, m/z 66,420 and its dimer at 132,448. The triply and doubly charged ions are also seen at 22,294 and 33,379 respectively.

3.212 Nanospray of intact BSA.

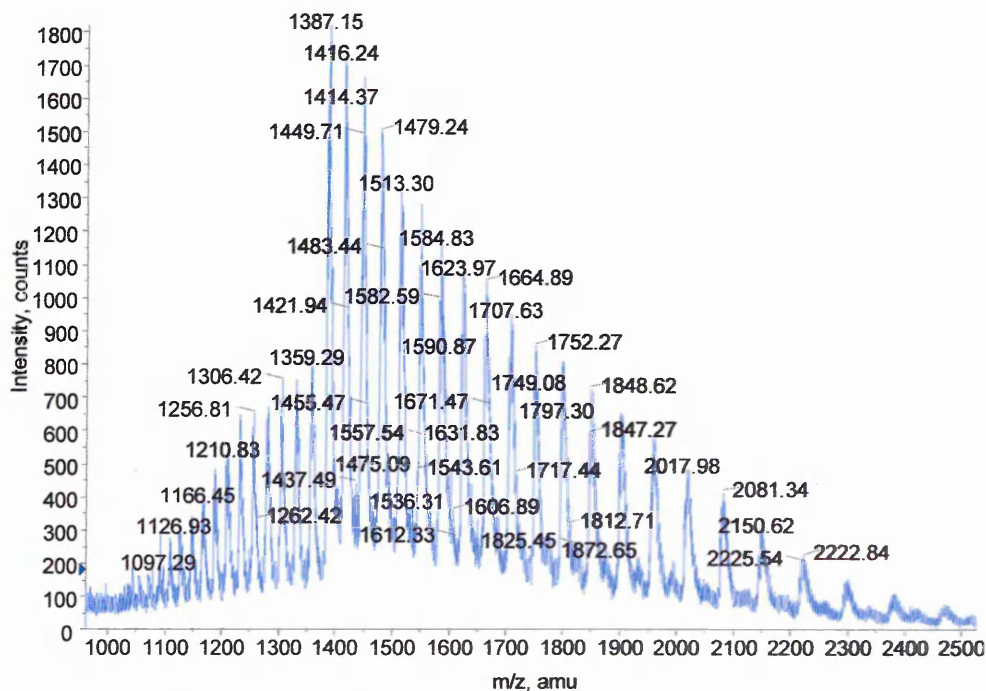


Figure 45. Nanospray analysis of intact BSA.

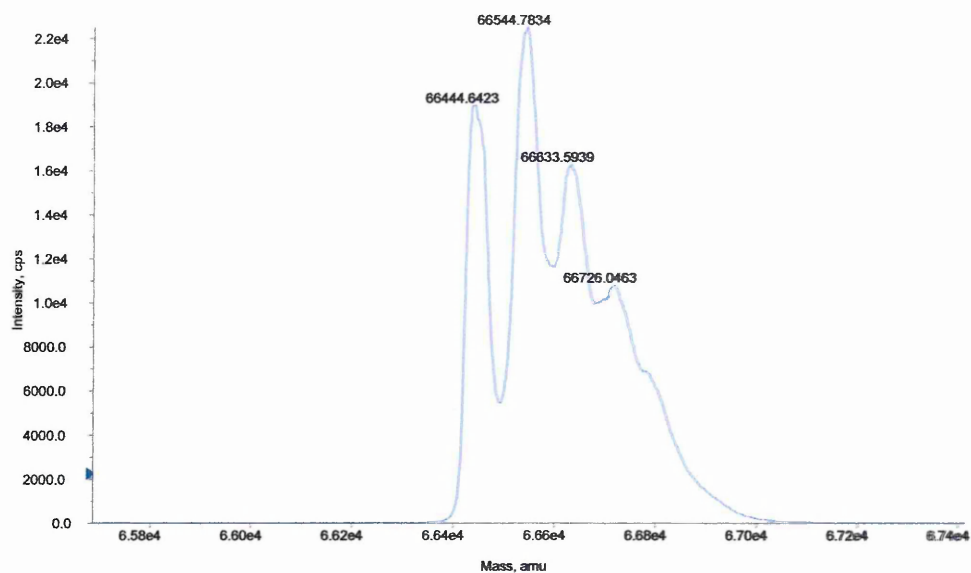


Figure 46. Bayesian reconstruction of intact BSA from figure 45, highlighting the presence of BSA isoforms.

The MALDI-MS spectrum for intact BSA (figure 44) gives a clean singly charged ion peak at m/z 66420.6 and although MALDI-MS gives predominantly singly charged ion species, in the analysis of large molecules, such as proteins multiple charging can be seen due to the presence of ionisable groups on the molecule. This is apparent with the peaks at m/z 's 33,779 and 22,294 representing the doubly and triply charged BSA molecules. The BSA dimer is also present at m/z 132,448. The Nanospray spectrum (figure 45) shows a nicely resolved envelope for BSA, the deconvoluted spectrum showing the presence of BSA isoforms (figure 46).

3.22 MALDI-MS and nanospray analysis of intact alpha secretase cleaved amyloid precursor protein standard, isoform 695 (APP α_{695}).

3.221 MALDI-MS of intact standard APP α_{695}

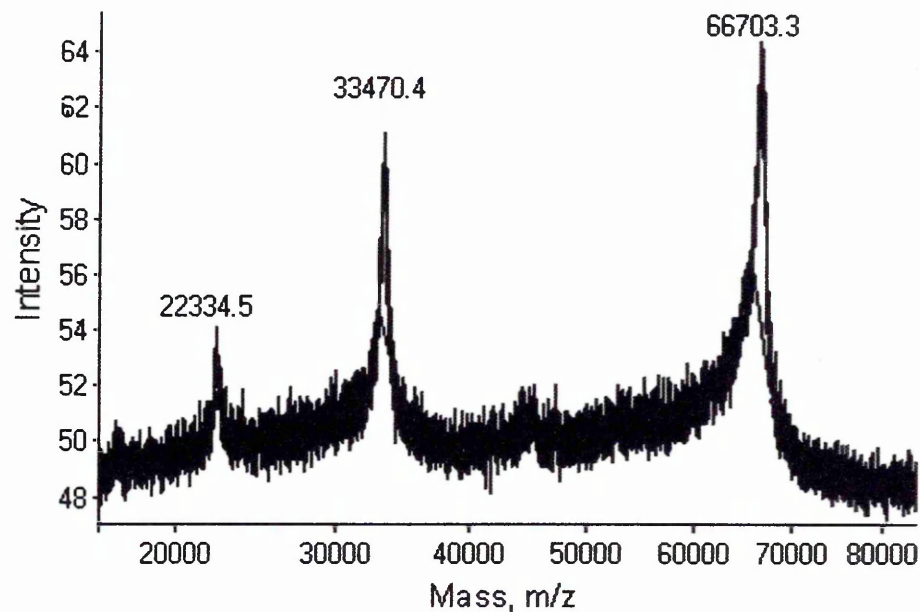


Figure 47. MALDI-MS spectrum of intact standard APP α_{695} , 67708.02MW. The single, double and triply charged ions are present at m/z's 66703.3, 33470.4 and 22334.5 respectively.

3.222 Nanospray of intact standard APP α_{695}

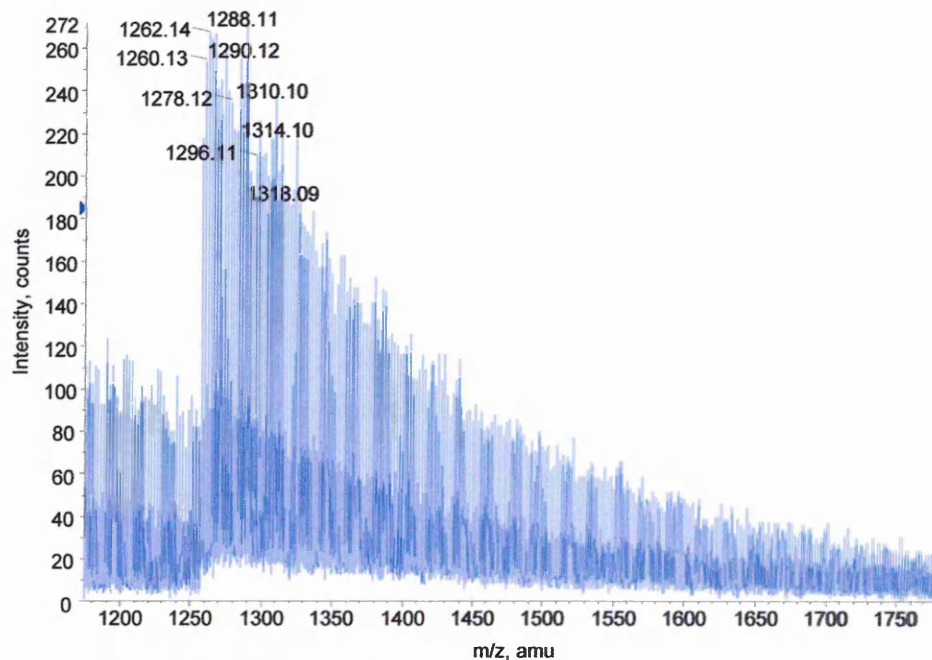


Figure 48. Nanospray analysis of intact standard APP α_{695} .

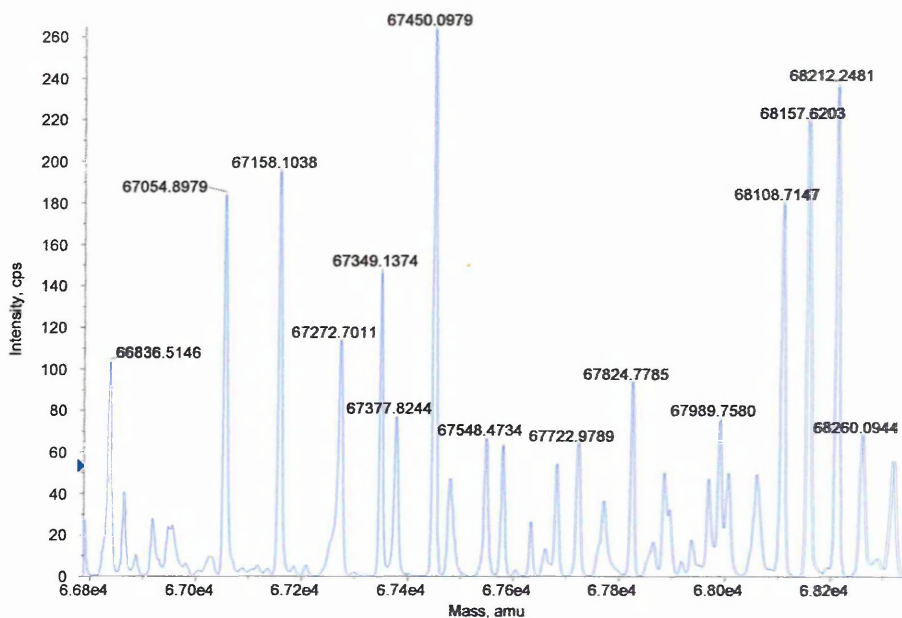


Figure 49. Bayesian reconstruction of intact standard APP α_{695} from figure 48.

The MALDI-MS spectrum of intact APP α_{695} (figure 47) displays resolved peaks for the singly charged species at m/z 66,703.3 as well as the doubly and triply charged molecules at 33,470.4 and 22,334.5 respectively. The nanospray data (figure 48) is less impressive, however, giving no clear indication of the intact APP α_{695} molecule and deconvolution of the area of interest (figure 49) again shows no obvious results.

3.23 MALDI-MS and nanospray analysis of intact alpha secretase cleaved amyloid precursor protein, isoform 770 (APP α_{770}).

3.231 MALDI-MS of intact APP α_{770}

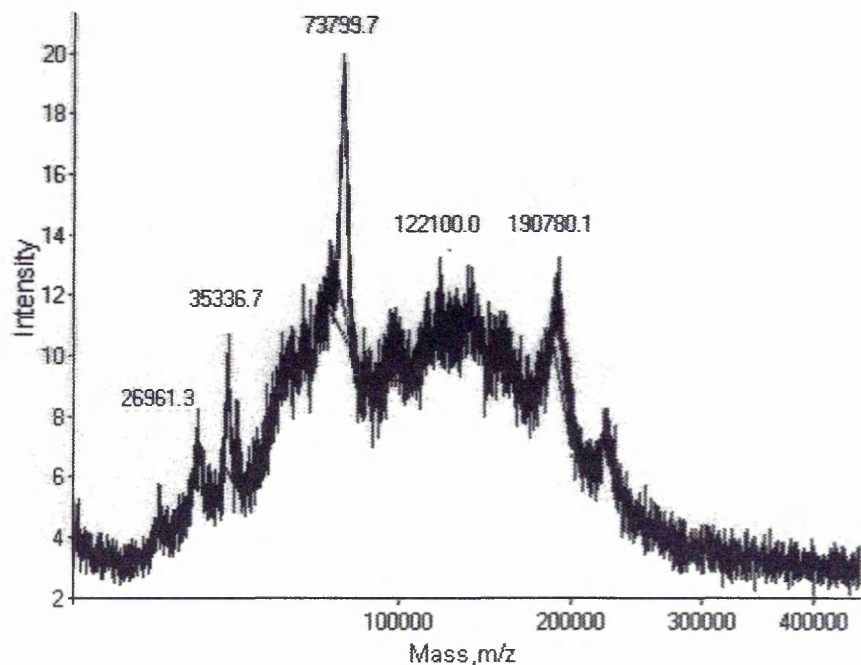


Figure 50. MALDI-MS spectrum of intact APP α_{770} , 75998.34 MW.

3.232 Nanospray of intact APP α_{770}

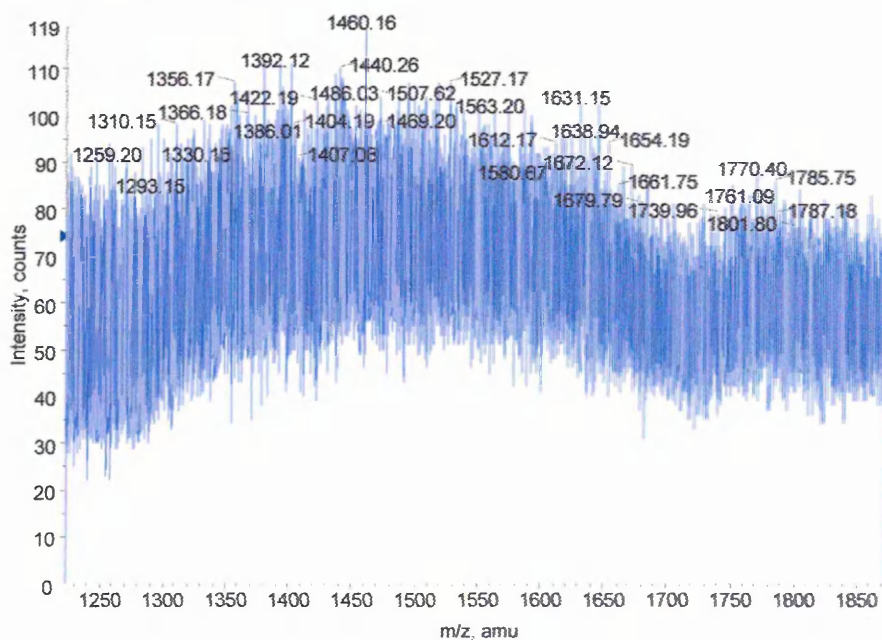


Figure 51. Nanospray analysis of intact APP α_{770} .

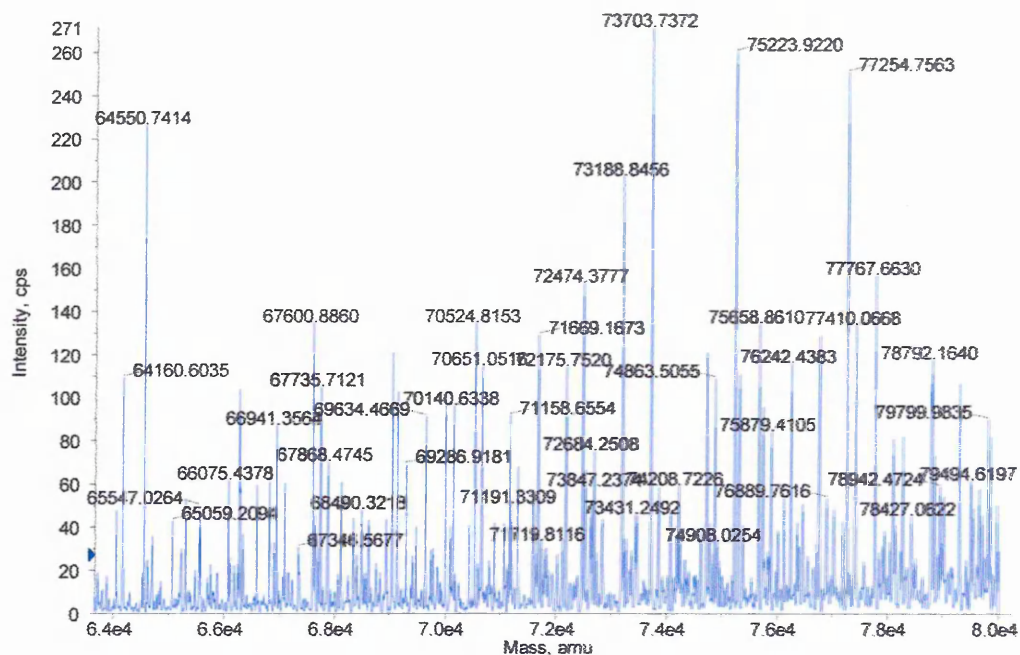


Figure 52. Bayesian reconstruction of intact APP α 770 from figure 51.

The MALDI-MS spectra of intact APP α 770 (figure 50) shows a strong peak at m/z 73,799.7 believed to be APP α 770, MW 75,940.3. Although the mass accuracy of this peak at 2.8% seems poor the size of the protein and calibration of the instrument play a large part. Nanospray (figure 51) gave no convincing data for APP α 770 and the Bayesian reconstruction (figure 52) compounded this showing no specific peaks.

3.24 MALDI-MS and nanospray analysis of intact alpha secretase cleaved amyloid precursor protein (APP α).

3.241 MALDI-MS of intact APP α .

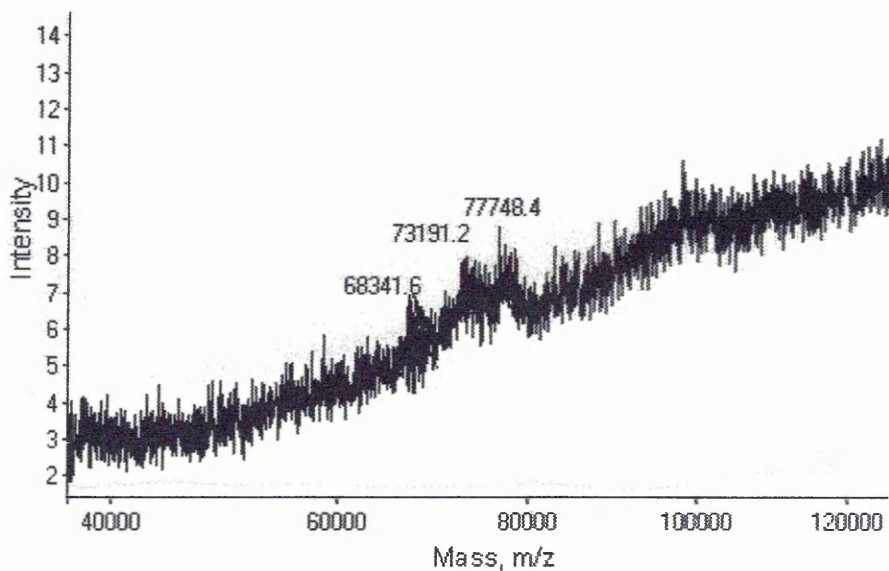


Figure 53. MALDI-MS spectra of intact APP α , containing the isoforms, APP695, APP751 and APP770. The average theoretical molecular weights of 67,708.02, 73,863.85 and 75,988.34 respectively corresponding to the observed m/z values.

3.242 Nanospray of intact APP α .

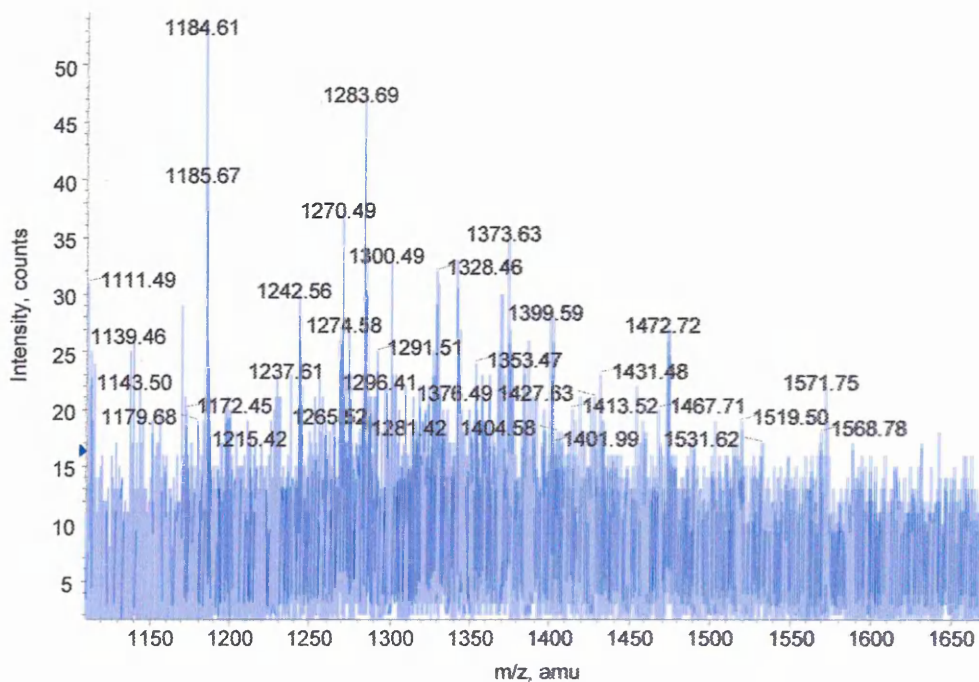


Figure 54. Nanospray analysis of intact APP α .

The MALDI-MS spectrum of intact APP α (figure 53) showed a spectral pattern, which could potentially be the resolution of the three isoforms present within this sample. The mass accuracy of each peak is poor and inconsistency is seen between the isoforms. Explanations for this could be instrument calibration and manual peak picking not achieving a true centroid for each peak. The nanospray results were unsuccessful (figure 54) and the area of interest did not provide any reconstructed data.

The concluding remarks from the data shown in this chapter must be the utility for MALDI-MS towards the analysis of high molecular weight making it the obvious choice for intact protein molecules, as well as its sensitivity and tolerance of contaminants compared to nanospray.

3.3 In-silico digestion of APP isoforms

Alternative splicing of the amyloid precursor protein (APP) gene transcript gives rise to nine named isoforms. With regards to Alzheimer's disease (AD) research, however, only three of these isoforms appear to be significant; APP₆₉₅, APP₇₅₁ and APP₇₇₀ all arising from exon variation. APP₇₇₀, known as full length APP has a full series of exons, APP₇₅₁, lacks exon 8, which codes for the OX2-homology domain, APP₆₉₅ lacks both exon 8 and 7. Exon 7 codes for the Kunitz-type inhibitor domain, present in both APP₇₇₀ and APP₇₅₁, designating them APP_{KPI} isoforms. Differences between the isoform domains not only give rise to functional variations but also alter the primary amino acid sequences (figure 55). One of the research areas looking at AD pathology is isoform variation in AD and non-AD brains. The original hypothesis was that APP₆₉₅ was the only isoform, which may be causative of AD as it was present only within brain cells, whereas APP₇₅₁ and APP₇₇₀ both existed within the periphery. Several studies, however, have since shown that this may not be the case, by revealing a predominance of the APP_{KPI} isoforms in disease states. If the pathology of AD does involve isoform peculiarity then rapid identification of the isoforms within disease states would be extremely advantageous. Proteomics could hold the key to this problem, utilising the inherent sensitivity of MS-fingerprinting. Neither one-dimensional nor two-dimensional SDS-PAGE have the ability to separate out all three isoforms sufficiently. In one-dimensional SDS-PAGE, APP₆₉₅ is resolved but APP₇₅₁ and APP₇₇₀ run together. This problem could be overcome by two-dimensional SDS-PAGE utilising the resolving power of isoelectric focusing, however, although there is variation within the pI values of the two APP_{KPI} isoforms (APP₇₅₁= 4.63 and APP₇₇₀= 4.65) resolution is not always repeatable due to

10	20	30	40	50	60
MLPGLALLLL	AAWTARALEV	PTDGNAGLLA	EPQIAMFCGR	LNMHMNVQNG	KWSDSPSGTK
70	80	90	100	110	120
TCIDTKEGIL	QYCQEVYPEL	QITNVVEANQ	PVTIQNWCKR	GRKQCKTHPH	FVIPYRCLVG
	140	150	160	170	180
130EFVSDALLVP	DKCKFLHQER	MDVCETHLHW	HTVAKETCSE	KSTNLHDYGM	LLPCGIDKFR
190	200	210	220	230	240
GVEFVCCPLA	EESDNVDSAD	AEEDDSDVWW	GGADTDYADG	SEDKVVEVAE	EEEVAEVEEE
250	260	270	280	290	300
EADDDDEDDED	GDEVEEEAEE	PYEEATERTT	SIATTTTTTT	ESVEEVVRE ^V	<u>CSEQAETGPC</u>
310	320	330	340	350	360
<u>RAMISRWYFD</u>	<u>VTEGKCAPFF</u>	<u>YGGCGGNRRN</u>	<u>FDTEEYCMVA</u>	<u>CGSAM^SQSLL</u>	<u>KTTOEPLARD</u>
370	380	390	400	410	420
<u>PVKL</u> PTTAAAS	PTDAVDKYLE	TPGDENEHAH	FQKAKERLEA	KHRERMSQVM	REWEEAERQA
430	440	450	460	470	480
JNLPKADKKA	VIQQHFQEKVE	SLEQEAANER	QQLVETHMAR	VEAMLNDRRR	LALenyITAL
490	500	510	520	530	540
QAVPPRPRHV	FNMLKKYVRA	EQKDRQHTLK	HFEHV ^R MVDP	KKAAQIRSQV	MTHLRVIYER
550	560	570	580	590	600
MNQSLSLLYN	VPAVAEEIQD	EVDELLQKEQ	NYSDDVLANM	ISEPRISYGN	DALMPSLTET
610	620	630	640	650	660
KTTVELLPVN	GEFSLDDLQP	WHSFGAADSVP	ANTENEVEPV	DARPAADRGL	TTRPGSGLTN
670	680	690	700	710	720
IKTEEISEVK	MDAEFRHDSG	YEVHHQKLVF	FAEDVGSNKG	AIIGLMVGGV	VIATVIVITL
730	740	750	760	770	
VMKKKQYTS	IHHGVVEVDA	AVTPEERHLS	KMQQNGYENP	TYKFFEQM ^Q N	

Figure 55. SWISS-PROT amino acid sequence entry for membrane bound, full length APP₇₇₀ splice isoform, highlighting the differences in both APP₆₉₅ and APP₇₅₁. **E** = V in APP₆₉₅; **M** = I in APP₇₅₁; **blue font** missing in APP₆₉₅ and **underlined blue font** missing in APP₇₅₁.

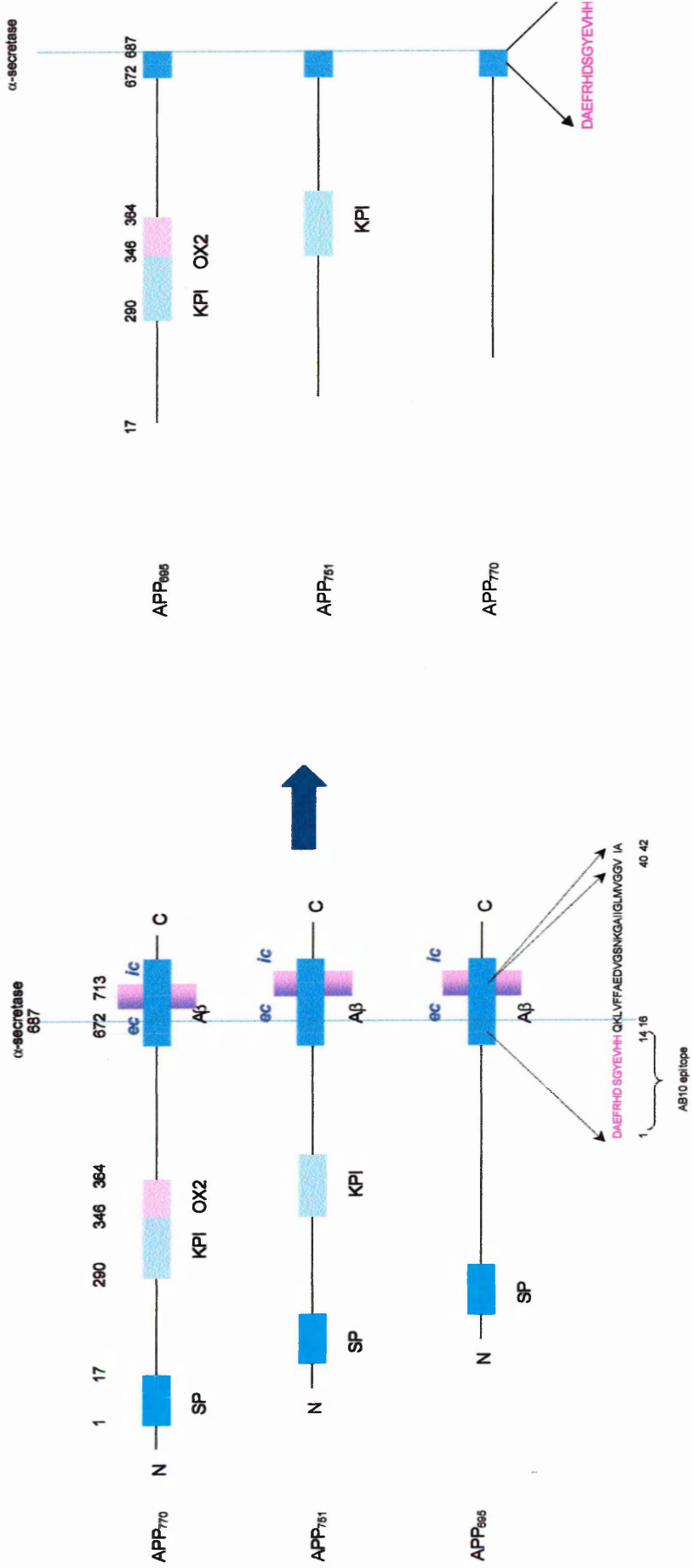
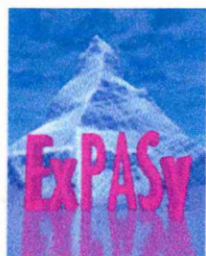


Figure 56. Schematic diagram of APP isoforms of interest before and after α -secretase cleavage with the AB10 primary antibody epitope highlighted in red. The secreted APP isoforms illustrating the loss of the signal peptide and remains of the A β peptide sequence after α -secretase cleavage, resulting in isoforms of amino acid lengths 670, 651 and 595 for APP₇₇₀, APP₇₅₁ and APP₆₉₅ respectively.



Peptide Mass

[Documentation](#) is available.

The entered sequence is:

```

MLPGLALLLLAAWNTARALEVPTDGNAGLLAEPQIAMFCGRLLNMHMNVQNG KWDSDPSTGK
TCIDTKEGILQYCEVYPELQITNVVEANQPVTIQNWCKRGRKQCKTHPHFVIPYRCLVGEFVSDALLVP
DKCKFLHQERMDVCETHLHWHTVAKETCSEKSTNLHDYGMLLPCGIDKFRGVEFVCCPLAEESDNVDS
ADAEEDSDVWVGGADTDYADGSEDKVVEVAEEEEVAEVEEEEADDEDEDGDEVEEEAEPEYEEA
TERTTSIATTTTTTTSVEEVVREVCSEQAETGPCRAMISRWFYFDVTEGKCAPFFYGGCGGNRNNFDTE
EYCMAVCGSAMSQSLLKTTQEPLARDPVKLPPTAASTPDAVDKYLETPGDENEHAHFQKAKERLEAKHR
ERMSQVMREWEAERQAKNLPKADKKAVIQHFQEKVESLEQEAANERQQLVETHMARVEAMLNDRRR
LALENYITALQAVPPRPRHVFNMLKKYVRAEQKDRQHTLKHFEHVVMVDPKAAQIRSQVMTHLRVIYE
RMNQSLSLLYNVPAAVEEIQDEVDLQKEQNYSDVLANM ISEPRISYGNALMPSLTET
KTTVELLPVN GEFSLDDLQP WHSFGADSV ANTENEVEPV DARPAADRGL TTRPGSGLTN
IKTEEISEVK MDAEFRHDSG YEVHHQKLVF FAEDVGSNKG AIIGLMVGGV VIATVIVITL
VMLKKKQYTS IHHGWEVDA AVTPEERHLS KMQQNGYENP TYKFFEQMQN
    
```

The selected enzyme is: Trypsin

Maximum number of missed cleavages (MC): 2

All cysteines have been treated with Iodoacetic acid to form carboxymethyl-cysteine (Cys_CM).

Methionines have been oxidized to form methionine sulfoxide (MSO).

Displaying peptides with a mass bigger than 500 Dalton.

Using monoisotopic masses of the occurring amino acid residues and giving peptide masses as $[M+H]^+$.

Figure 57. Web page from ExPASy's Peptide Mass site, which performs theoretical digests upon user supplied sequences creating insilico digest lists of peptide values.

experimental variation and low protein concentration. It is possible that MS-fingerprinting could resolve the isoforms by means of the specific cleavage sites of reagents. It is a fair assumption, due to the amino acid differences between the isoforms that any cleavage occurring within the areas of difference may result in peptides of varying lengths from each isoform. This, however, needs to be clarified by carrying out an *insilico* digest, utilising database facilities such as MS-Digest and ExPASy's Peptide Mass, allowing user supplied sequences to be entered and theoretically digested. The antibody used in the immunoprecipitation procedure utilised in this study, namely AB10 raised to amino acids 1-17 of the β amyloid peptide sequence, thus the nature of the APP examined is secreted α -secretase cleaved (figure 56) and it is these isoform sequences that were entered into the database. Using ExPASy's Peptide Mass site (figure 57) the isoform sequences, cleavage reagents and type of modifications present were entered, from which a list of theoretical digest peptides were generated (appendix F). Examination of these lists highlighted several unique digest peptides (table 9) for both the trypsin and Asp-N digests highlighted in figure 58.

Monoisotopic M+H⁺ of the Predicted Isoform Specific Peptides

Digest reagent	APP α_{695}	APP α_{751}	APP α_{770}
Trypsin	1372.6954	3121.3434	2541.0764 1386.7111 915.4894
Asp-N	1327.7216	1872.8176	2150.9589 1297.6998
Formic acid	1327.7216	1872.8176	2150.9589 1297.6998

Table 9. Summarising the theoretical isoform specific peptides generated from the ExPASy's peptide mass database.

LEVPTDGNAG LLAEPQIAMF CGRLNMHMNV QNGKWSDPS GTKTCIDTKE GILQYCQEVY
 PELQITNVVE ANQPVTIQNW CKRGRKQCKT HPHFVIYRC LVGEFVSDAL LVPDKCKFLH
 QERMDVCETH LHWHTVAKET CSEKSTNLHD YGMLLPCGID KFRGVEFVCC PLAEESDNVD
 SADAEEEDSD VWWGGADTDY ADGSEDKVVE VAEVEEVAEV EEEEADDDDED DEDGDEVEEEE
 AEEPVEEATE RTTSIATTTT TTTESVVEEV RVPTTAASTP DAVDKYLETP GDENEHAHFQ
 KAKERLEAKH RERMSQVMRE WEEAERQAKN LPKADKKAVI QHFQEKVESL EQEAAERQQ
 LVETHMARVE AMLNDRRRLA LENYITALQA VPPRPRHVFN MLKKYVRAEQ KDRQHTLKH
 EHVVMVDPK AAQIRSQVMT HLRVIYERMN QSLSLLYNVP AVAEEIQDEV DELLQKEQNY
 SDDVLANMIS EPRISYGNDA LMPSLTETKT TVELLPVNGE FSLDDLQPDWH SFGADSVPAN
 TENEVEPVDA RPAADRGLTT RPSGLTNIK TEEISEVKMD AEFRHDSGYE VHHQK

APP α ₆₉₅

LEVPTDGNAG LLAEPQIAMF CGRLNMHMNV QNGKWSDPS GTKTCIDTKE GILQYCQEVY
 PELQITNVVE ANQPVTIQNW CKRGRKQCKT HPHFVIYRC LVGEFVSDAL LVPDKCKFLH
 QERMDVCETH LHWHTVAKET CSEKSTNLHD YGMLLPCGID KFRGVEFVCC PLAEESDNVD
 SADAEEEDSD VWWGGADTDY ADGSEDKVVE VAEVEEVAEV EEEEADDDDED DEDGDEVEEEE
 AEEPVEEATE RTTSIATTTT TTTESVVEEV REVCSEQAET GPCRAMISRW YFDVTEGKCA
 PFFYGGCGGN RNNFDTEEYC MAVCGSAIPT TAASTPDAVD KYLETPGDEN EHAHFQKAKE
 RLEAKHRERM SQVMREWEEA ERQAKNLPKA DKKAVIQHFQ EKVESLEQEA ANERQQLVET
 HMARVEAMLN DRRRLALENY ITALQAVPPR PRHVFNMLKK YVRAEQKDRQ HTLKHFEHVR
 MVDPKKAAQI RSQVMTHLRV IYERMNQSLS LLYNVPVAE EIQDEVDELL QKEQNYSDDV
 LANMISEPRI SYGNDALMPS LTETKTVEL LPVNGEFLD DLQPDWH SFGA DSVANTENE
 VEPVDARPA DRGLTTRPGS GLTNIKTEEI SEVKMDAEFR HDSGYEVHHQ K

APP α ₇₅₁

LEVPTDGNAG LLAEPQIAMF CGRLNMHMNV QNGKWSDPS GTKTCIDTKE GILQYCQEVY
 PELQITNVVE ANQPVTIQNW CKRGRKQCKT HPHFVIYRC LVGEFVSDAL LVPDKCKFLH
 QERMDVCETH LHWHTVAKET CSEKSTNLHD YGMLLPCGID KFRGVEFVCC PLAEESDNVD
 SADAEEEDSD VWWGGADTDY ADGSEDKVVE VAEVEEVAEV EEEEADDDDED DEDGDEVEEEE
 AEEPVEEATE RTTSIATTTT TTTESVVEEV REVCSEQAET GPCRAMISRW YFDVTEGKCA
 PFFYGGCGGN RNNFDTEEYC MAVCGSAMSQ SLLKTQEPL ARDPVKLPTT AASTPDAVDK
 YLETPGDENE HAHFQKAKER LEAKHRERMS QVMREWEEAE RQAKNLPKAD KKAVIDQHFQE
 KVESLEQEA NERQQLVETH MARVEAMLND RRRRLALENYI TALQAVPPRP RHVFNMLKKY
 VRAEQKDRQH TLKHFEHVRM VDPKAAQIR SQVMTHLRVI YERMNQSLS LYNVPVAEAE
 IQDEVDELLQ KEQNYSDDV ANMISEPRIS YGNDALMPSL TETKTVELL PVNGEFLDD
 LQPDWH SFGAD SVANTENE EPVDARPAAD RGLTTRPGSG LTNIKTEEIS EVKMDAEFRH
 DSGYEVHHQK

APP α ₇₇₀

Figure 58. Amino acid sequences of soluble APP α -secretase cleaved isoforms of interest, highlighting peptides unique to each isoform for both trypsin (highlighted in blue) and Asp-N (underlined in red) digests.

Trypsin shows unique peptides for APP₆₉₅ at position 272-285, monoisotopic mass of 1371.5954; likewise for APP₇₅₁ at position 312-341, monoisotopic mass 3120.2434 and APP₇₇₀ exhibits three peptides at positions 312-334, monoisotopic mass 2539.9764, 347-360, monoisotopic mass 1385.6111 and 335-342, monoisotopic mass 914.3894. The Asp-N digest again produces unique peptides for APP₆₉₅ (position 268-280, monoisotopic mass 1326.6216) APP₇₅₁ (position 318-336, monoisotopic mass 1871.7176) and APP₇₇₀ (positions 318-337, monoisotopic mass 2149.8589 and 343-355, monoisotopic mass 1296.5998). The cleavage site of formic acid is the same as Asp-N and so specific peptides are identical. All three methods of digestion could, therefore in theory be used as diagnostic tests for the presence of each isoform. Viability of the test, however, would be highly dependent upon optimal protease activity in order to provide good sequence coverage and, therefore a full range of digest peptides.

3.4 Analysis by mass spectrometry of the in-gel digestions of bovine serum albumin (BSA) and amyloid precursor protein (APP).

This section of chapter three covers the analysis by mass spectrometry of in-gel digests of BSA and APP. APP encompasses all three samples utilised, namely the standard APP α_{695} , immunoprecipitated APP α_{770} and immunoprecipitated APP α . Comparison of the in-gel digests from both 1D and 2D gel electrophoresis is covered as well as the cleavage efficiency of the different digest reagents, trypsin Asp-N and formic acid. Mass spectroscopic analysis is performed firstly by MALDI-MS and then capillary LC/MS each method followed by subsequent MS/MS analysis.

The analysis by mass spectrometry (MALDI-MS followed by capillary LC/MS) of the 1D in-gel digests are covered first in sections 3.41, 3.42 and 3.43, looking at the different digest reagents, trypsin, Asp-N and formic acid respectively. Finally analysis by mass spectrometry (MALDI-MS followed by capillary LC/MS) of the 2D in-gel digest is shown in sections 3.44, 3.45 and 3.46 again corresponding to the different digest reagent utilised, namely trypsin, Asp-N and formic acid respectively. All the experiments performed in this chapter are shown in table 10 and results from these sections are briefly summarised in table 105 showing the percentage sequence coverage achieved and presence of isoform specific peptides for each analysis.

The full or partial sequences achieved by both MALDI-MS/MS and LC/MS/MS are annotated and numbered as follows; if the 'b' ion series predominates then the legend showing the sequence will read from left to right with regards to the amino acid sequence i.e. *N* to *C* terminus, however, if the 'y' series is dominant the legend will read from right to left.

Summary of Successful Isolation and Analyses Performed upon the Protein Samples, BSA, Standard APP α 695, Immunoprecipitated APP α 770 and Immunoprecipitated APP α .

Two-Dimensional Electrophoresis												
Digest Reagent	One-Dimensional Electrophoresis						Two-Dimensional Electrophoresis					
	Trypsin						Asp-N					
Sample	1D	MALDI		LC		2D	Western	MALDI		LC		MS/MS
		MS	MS/MS	MS	MS/MS			MS	MS/MS	MS	MS/MS	
BSA	x	x	x	x	xx	x	-	x	xx	x	xx	x
Standard APP α 695	x	x	x	x	xx	x	x	x	xx	x	xx	x
IP APP α 770	x	x	x	x	xx	x	x	x	xx	x	xx	x
IP APP α	x	x	x	x	xx	x	x	x	xx	x	xx	x
Sample	1D	MALDI		LC \times		2D	Western	MALDI		LC		MS/MS
		MS	MS/MS	MS	MS/MS			MS	MS/MS	MS	MS/MS	
BSA	x	x	xx	x	xx	x	-	x	--	x	--	x
Standard APP α 695	x	x	xx	x	x-	x	x	x	xx	x	xx	x
IP APP α 770	x	x	--	x	xx	x	x	x	--	x	--	x
IP APP α	x	x	--	x	x-	x	x	x	--	x	--	x
Sample	1D	MALDI		LC		2D	Western	MALDI		LC		MS/MS
		MS	MS/MS	MS	MS/MS			MS	MS/MS	MS	MS/MS	
BSA	x	x	--	x	--	x	-	x	--	x	--	x
Standard APP α 695	x	x	--	x	--	x	x	x	--	x	--	x
IP APP α 770	x	x	--	x	--	x	x	x	--	x	--	x
IP APP α	x	x	--	x	--	x	x	x	--	x	--	x

Table 10. Shown are all the successful experiments present in chapter 3. Experiments for which data was achieved = x. Experiments that were unsuccessful = -. IP = immunoprecipitated. Western analysis was used as a primary detection for the low-level immunoprecipitated proteins and as such was not necessary for BSA. This table clearly highlights the lack of MS/MS data for the formic acid digests both from one-dimensional and two-dimensional gels.

3.41 One-dimensional in-gel tryptic digestion of BSA and APP.

3.411 MALDI-MS analysis of a one-dimensional in-gel tryptic digestion of BSA.

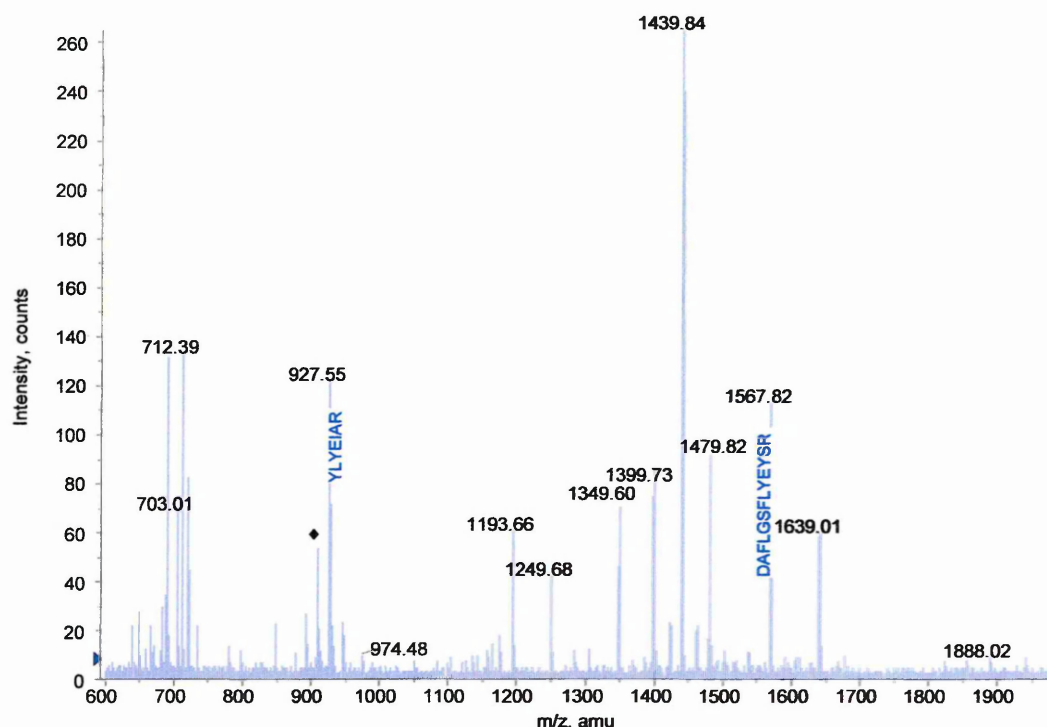


Figure 59. MALDI-MS spectrum of a one-dimensional in-gel tryptic digest of BSA. The annotated peaks at m/z 927.55 and 1567.82 gave the best results when subjected to MS/MS analysis (figures 60 and 61). Calculation of the peptide sequences takes into account the molecular weight similarities between the isomers leucine (L) and isoleucine (I). Keratin contamination highlighted by the black diamond.

mass ($M+H^+$)	mass (experimental)	position	missed cleavages	peptide sequence
703.41	703.01	212-218	0	VLISSAR
712.37	712.39	29-34	0	SEIAHR
927.49	927.55	161-167	0	YLYEIAR
974.46	974.48	37-44	0	DLGEEHFK
1193.60	1193.66	25-34	1	DTHKSEIAHR
1249.62	1249.68	35-44	1	FKDLGEEHFK
1349.55	1349.60	76-88	0	TCVADESHAGCEK
1399.69	1399.73	569-580	0	TVMENFVAFVDK
1439.81	1439.84	360-371	1	RHPEYAVSVLLR
1479.80	1479.82	421-433	0	LGEYGFQNALIVR
1567.74	1567.82	347-359	0	DAFLGSFLYEYSR
1639.94	1639.01	437-451	1	KVPQVSTPTLVEVSR
1888.92	1888.02	169-183	0	HPYFYAPPELLYYANK

Table 11. Mascot search results from the one-dimensional in-gel tryptic digest of BSA (figure 59), showing 18% sequence coverage. The peaks subjected to MS/MS analysis highlighted in blue.

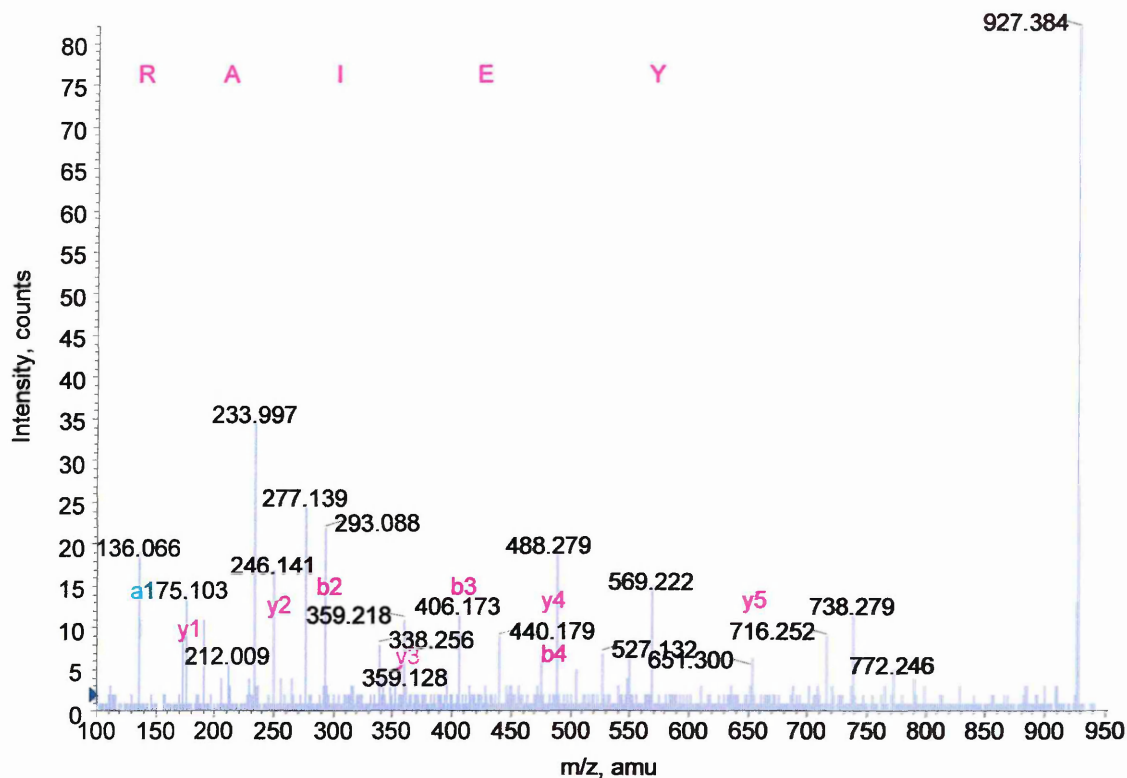


Figure 60. MALDI-MS/MS of peak at m/z 927.55 from the one-dimensional in-gel tryptic digest of BSA seen in figure 59. The uncovered ‘y’ ion sequence tag YEIAR corresponds to the peptide YLYEIAR, 926.48 MW.

Amino acid		Ion type ($M+H^+$)						
residue	mass/Da	immonium	a	a-NH ₃	b	b-NH ₃	y	y-NH ₃
Y, Tyr	163.06		136.07	119.04	164.07	147.04	651.34	634.31
E, Glu	129.04	102.05	265.11	248.09	293.11	276.08	488.28	471.25
I, Ile	113.08	86.04	378.20	361.17	406.19	389.17	359.24	342.21
A, Ala	71.03	44.04	449.23	432.21	477.23	460.20	246.15	229.12
R, Arg	156.10	129.11	605.34	588.31	633.33	616.30	175.11	158.09

Table 12. BioAnalyst software results from the MALDI-MS/MS one-dimensional in-gel tryptic digest of BSA seen in figure 60. Shown is the ‘a’, ‘b’ and ‘y’ product ions available for the sequence YEIAR, highlighting the ions present.

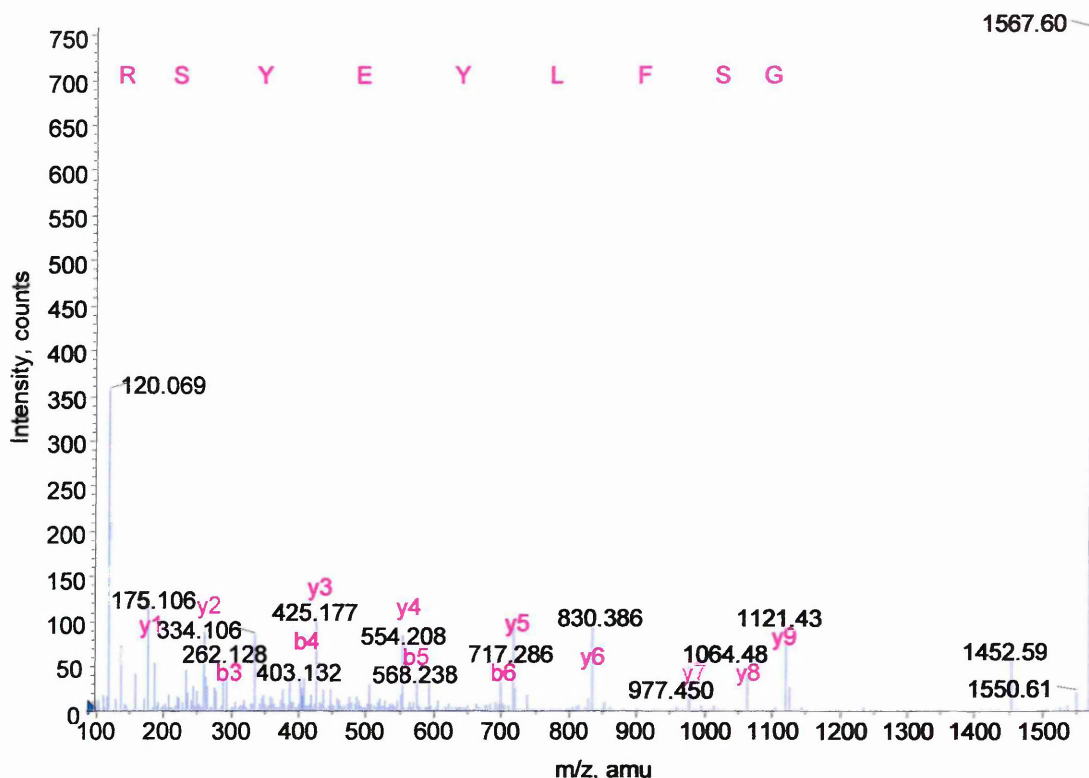


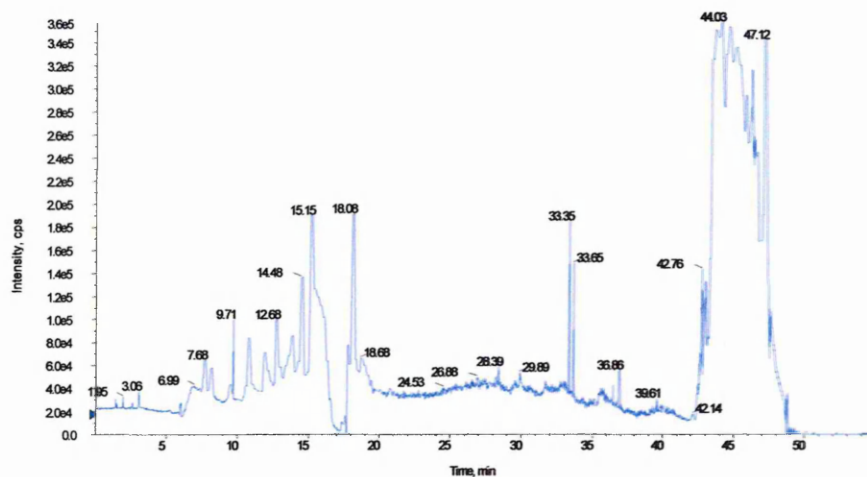
Figure 61. MALDI-MS/MS spectrum of the peak m/z 1567.82 from the one-dimensional in-gel tryptic digest of BSA seen in figure 59. This peak corresponds to the BSA tryptic peptide DAFLGSFLYEYSR, verified by the sequence tag GSFLYEYSR. Immonium as well as ‘b’ and ‘y’ product ions can be seen.

Amino acid		Ion type ($M+H^+$)						
residue	mass/Da	immonium	a	a-NH ₃	b	b-NH ₃	y	y-NH ₃
G, Gly	57.02	30.03	30.03	13.00	58.02	41.00	1121.52	1104.49
S, Ser	87.03	60.04	117.06	100.03	145.06	128.03	1064.50	1047.47
F, Phe	147.06	120.06	264.13	247.10	292.12	275.10	977.47	960.44
L, Leu	113.08	86.09	377.21	360.19	405.21	388.18	830.40	813.37
Y, Tyr	163.06	136.07	540.28	523.25	568.27	551.25	717.32	700.29
E, Glu	129.04	102.05	669.32	652.29	697.31	680.29	554.25	537.23
Y, Tyr	163.03	136.07	832.38	815.36	860.38	843.35	425.21	408.18
S, Ser	87.03	60.04	919.41	902.39	947.41	930.38	262.15	245.12
R, Arg	156.10	129.11	1075.52	1058.49	1103.55	1086.48	175.11	158.09

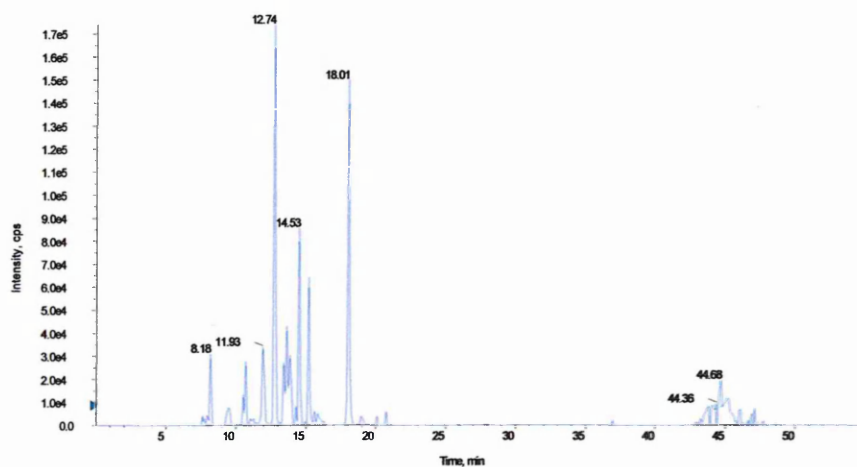
Table 13. BioAnalyst results from the MALDI-MS/MS spectrum of the peak m/z 1567.82 from the one-dimensional in-gel tryptic digest of BSA seen in figure 61, showing the possible and highlighting the actual ‘a’, ‘b’ and ‘y’ product ions for the sequence GSFLYEYSR.

3.412 Capillary LC/MS analysis of a one-dimensional in-gel tryptic digestion of BSA.

(a)



(b)



(c)

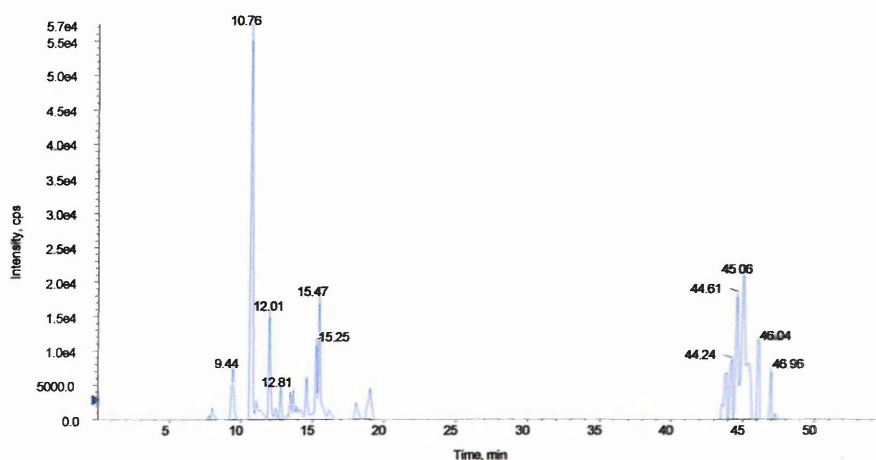


Figure 62. Capillary LC/MS run of a BSA one-dimensional in-gel tryptic digest performed using information dependant acquisition (IDA) software. For experimental conditions see chapter 2.92, page 92. (a) Shows the survey scan or total ion chromatogram (TIC). (b) Shows the TIC for the product ion scan of the most intense peak in the normal mass spectrum. (c) Shows the TIC for the product ion intensities generated by product ion scan of the second most intense peak in the normal mass spectrum. The peak lists generated from traces (b) and (c) were sorted according to predefined parameters (chapter 2.92, page 93) and a selection of the most intense peaks automatically sent for MS/MS (figures 63 and 64).

mass observed	mass (experimental)	position	missed cleavages	peptide sequence
395.23	788.45	257-263	0	LVTDLTK
461.79	921.39	249-256	0	AEFVEVTK
464.24	926.47	161-167	0	YL YEI AR
501.78	1001.55	598-607	0	LVVSTQTALA
507.80	1013.59	549-557	0	QTALVELLK
582.30	1162.59	66-75	0	LVNELTEFAK
653.34	1304.67	402-412	0	HLVDEPQNLIK
700.33	1398.65	569-580	0	TVMENFVAFVDK
480.60	1438.78	360-371	1	RHPEYAVSVLLR
493.93	1478.77	421-433	0	LGEYGFQNALIVR
740.39	1478.77	421-433	0	LGEYGFQNALIVR
756.41	1510.80	438-451	0	VPQVSTPTLVEVSR
523.24	1566.71	347-359	0	DAFLGSFLYEYSR
784.36	1566.71	347-359	0	DAFLGSFLYEYSR
547.31	1638.91	437-451	1	VPQVSTPTLVEVSR
630.30	1887.87	169-183	0	HPYFYAPELLYYANK
652.60	1954.90	319-336	0	DAIPENLPPLTADFAEDK
978.46	1954.92	319-336	0	DAIPENLPPLTADFAEDK
682.32	2043.95	168-183	1	RHPYFYAPELLYYANK
820.70	2459.08	319-340	1	DAIPENLPPLTADFAEDKDVCK

Table 14. BioAnalyst automatic data analysis (using Matrix Science software) of the chromatograms shown in figure 62 of a one-dimensional in-gel tryptic digest of BSA gave 27% sequence coverage. The data highlights the presence of both doubly and triply charged species seen with ESI-MS as opposed to the singly charged ions seen with MALDI-MS. The sequences highlighted in blue gave the best results when subjected to MS/MS (figures 63 and 64). Calculation of the peptide sequences takes into account the molecular weight similarities between the amino acids lysine (K) and glutamine (Q) and isomers isoleucine (I) and leucine (L).

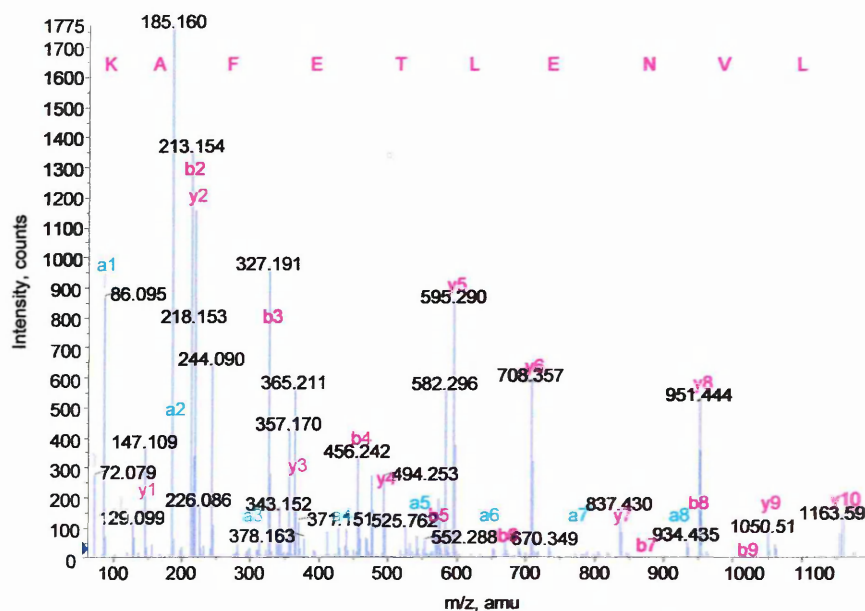


Figure 63. Capillary LC/MS/MS run of the doubly charged product ion at m/z 582.30, retention time 12.7 minutes from the LC/MS run of a one-dimensional in-gel tryptic digest of BSA (figure 62b). This product is consistent with the BSA tryptic peptide, LVNELTEFAK and the full sequence coverage verifies this.

Amino acid		Ion type (M+H ⁺)						
residue	mass/Da	Immonium	a	a-NH ₃	b	b-NH ₃	y	y-NH ₃
L, Leu	113.08		86.09	69.06	114.09	97.06	1163.60	1146.58
V, Val	99.06		185.16	168.13	213.15	196.13	1050.52	1033.47
N, Asn	114.04	87.05	299.20	282.18	327.20	310.17	951.45	934.42
E, Glu	129.04		428.25	411.22	456.24	439.21	837.41	820.38
L, Leu	113.08		541.33	524.30	569.32	552.30	708.36	691.34
T, Thr	101.04	74.06	642.38	625.35	670.37	653.35	595.28	578.25
E, Glu	129.04		771.42	754.39	799.41	782.39	494.23	477.21
F, Phe	147.06		918.49	901.46	946.48	929.46	365.19	348.16
A, Ala	71.03	44.04	989.53	972.50	1017.51	1000.49	218.12	201.10
K, Lys	128.09	101.10	1117.62	1100.59	1145.62	1128.59	147.08	130.06

Table 15. BioAnalyst results of the capillary LC/MS/MS spectrum of the product at m/z 582.30 from the one-dimensional in-gel tryptic digest of BSA shown in figure 63. The possible and actual product ions for the peptide LVNELTEFAK are shown highlighting good sequence coverage in 'a', 'b' and 'y' ions, as well as several immonium ions.

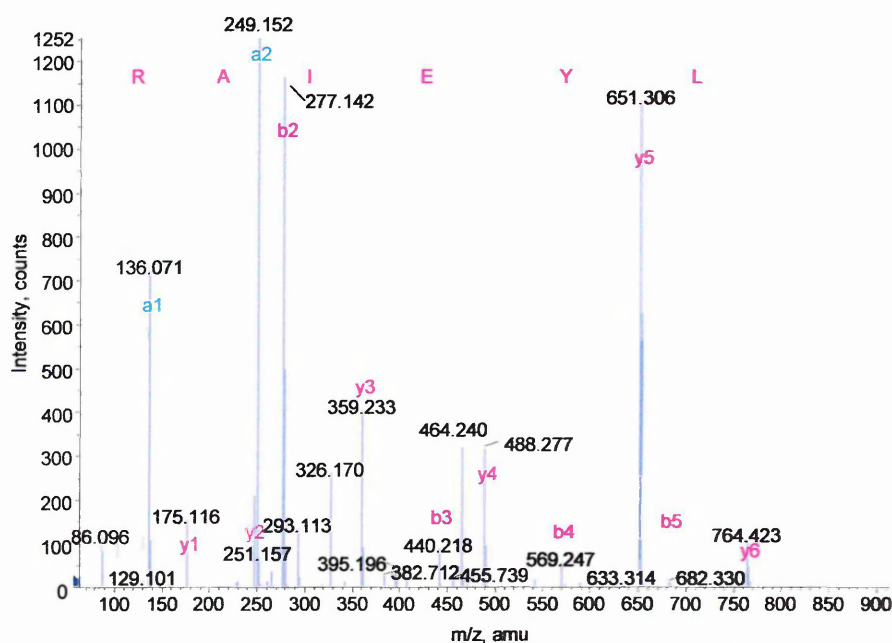


Figure 64. Capillary LC/MS/MS run of the doubly charged product ion at m/z 464.24, retention time 12.0 minutes from the LC/MS run of a one-dimensional in-gel tryptic digest of BSA (figure 62c). This product is consistent with the BSA tryptic peptide, YLYEIAR, 926.47 monoisotopic mass and the MS/MS results showing the sequence tag establish the validity of the peptide.

Amino acid		Ion type (M+H ⁺)						
residue	mass/Da	immonium	a	a-NH ₃	b	b-NH ₃	y	y-NH ₃
L, Leu	113.08		249.15	232.13	277.15	260.12	764.41	747.38
Y, Tyr	163.06		412.22	395.19	440.21	423.19	651.32	634.30
E, Glu	129.04	102.05	541.26	524.23	569.26	552.23	488.26	471.24
I, Ile	113.08		654.34	637.32	682.34	665.31	359.22	342.19
A, Ala	71.03	44.04	725.38	708.36	753.38	736.35	246.13	229.11
R, Arg	156.10		881.48	864.46	909.48	892.45	175.10	158.07

Table 16. BioAnalyst results of the capillary LC/MS/MS spectrum of the product at m/z 424.24 from the one-dimensional in-gel tryptic digest of BSA shown in figure 64. Showing the possible and actual (highlighted) 'a', 'b' and 'y' product ions for the sequence LYEIAR.

Bovine serum albumin (BSA, 66,432.96 MW) was used as a standard due to its availability, similarity in molecular weight to the amyloid precursor protein isoforms (APP α_{695} , MW 67,708.02, APP α_{751} , MW 73,863.85, APP α_{770} , MW 75,988.34) and knowledge of the expected digests^{195,196}.

The MALDI-MS analysis of the one-dimensional in-gel tryptic digest of BSA (figure 59) resulted in 13 tryptic peptides covering 18% of the protein. LC-MS analysis (figure 62) of the same sample revealed 17 tryptic peptides for BSA, which covered 27% of the protein sequence. MS/MS analysis of peaks from both MALDI-MS (figures 60 and 61) and LC/MS (figures 63 and 64) allowed automatic identification of BSA via the BioAnalyst software. The LC/MS/MS data gave one full amino acid sequence and a generous sequence tag for the chosen peptides and MALDI-MS/MS gave two sequence tags. The sequence coverage achieved for the BSA tryptic digestions (MALDI 18%, LC-MS 27%) are poor in comparison to literature references of up to 70% sequence coverage from tryptic in-gel digestions¹⁹⁷.

3.413 MALDI-MS analysis of a one-dimensional in-gel tryptic digestion of alpha secretase cleaved amyloid precursor protein standard, isoform 695 (APP α_{695}).

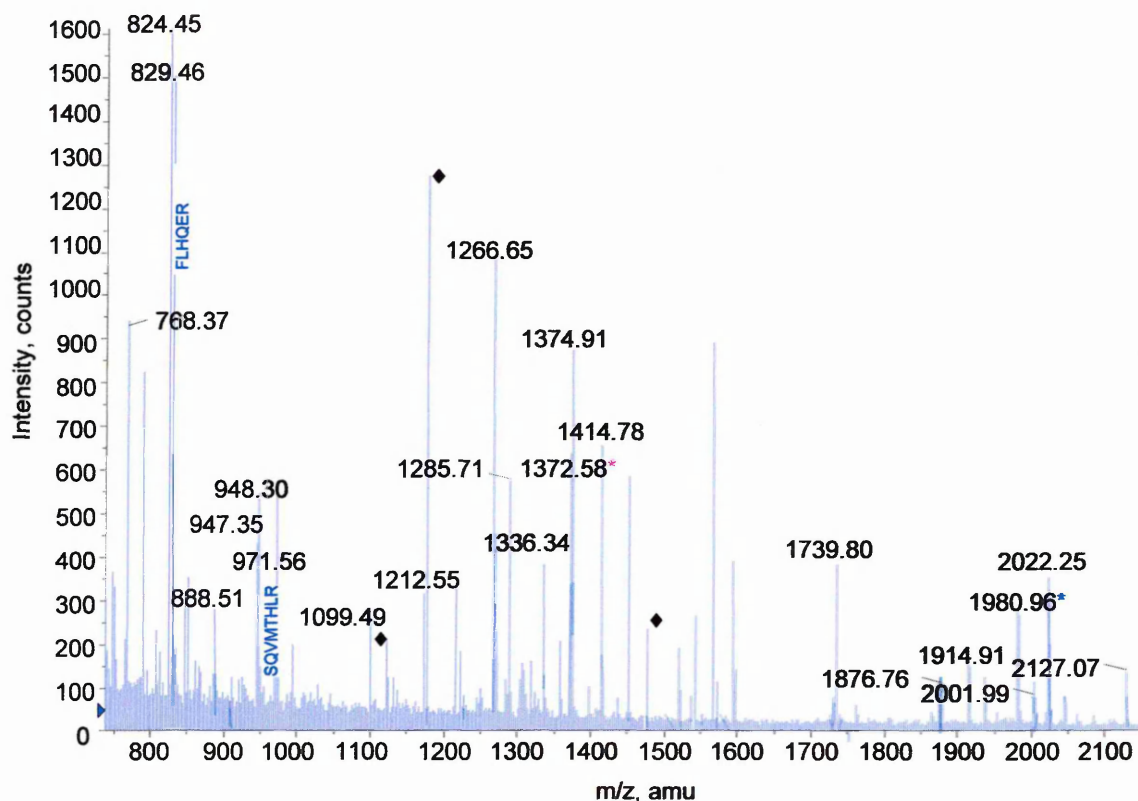


Figure 65. MALDI-MS spectrum of a one-dimensional in-gel tryptic digest of standard APP α_{695} . The annotated peaks at m/z 829.46 and 971.56 gave the best results when subjected to MS/MS analysis the results of which are shown in figures 66 and 67. The peak at 1372.58 MW, marked by a red asterisk is specific to APP α_{695} , MS/MS analysis, however, was unsuccessful. The peak at m/z 1980.96 marked by the blue asterisk is present in all three isoforms of interest and is noted as a peptide with a possible *N*-glycosylation site. Further investigation of the unlabelled peaks prominent within the spectrum was needed, however, time restrictions did not allow this. The peaks annotated with a black diamond are thought to be keratin contamination.

mass ($M+H^+$)	mass (experimental)	position (APP α_{695} numbering)	missed cleavages	peptide sequence
768.33	768.37	579-584	0	MDAEFR
824.42	824.45	419-424	0	HFEHVR
829.43	829.46	118-123	0	FLHQER
888.48	888.51	397-403	0	HVFNMLK
947.46	947.35	369-376	0	VEAMLNDR
948.41	948.30	320-326	0	EWEEAER
971.51	971.56	436-443	0	SQVMTHLR
1099.59	1099.49	338-346	0	AVIQHFQEK
1212.62	1212.55	359-368	0	QLLVETHMAR
1266.67	1266.65	90-99	0	THPHFVIPYR
1285.61	1285.71	24-34	0	LNMHMNVQNGK
1336.60	1336.34	585-595	0	HDSGYEVHHQK

1372.70	1372.58	272-285	0	VPTTAASTPDAVDK*
1374.65	1374.91	347-358	0	VESLEQEAAANER
1414.80	1414.78	557-570	0	GLTTRPGSGLTNIK
1739.85	1739.80	494-509	0	ISYGN DALMPSLTETK
1876.89	1876.76	145-161	0	STNLHDYGM L L P C G I D K
1914.86	1914.91	286-301	0	YLETPGDENEHAHFQK
1980.90	1980.96	477-493	0	EQNYSDDVLANMISEPR*
2002.04	2001.99	414-429	2	QHTLKHFEHV R M V D P K
2022.15	2022.25	379-396	0	LALENYITALQAVPP R P R
2127.07	2127.07	252-271	0	TTSIATTTTTTTESVEEV R

Table 17. Mascot search results from the MALDI-MS of the one-dimensional in-gel tryptic digest of APP α_{695} shown (figure 65) covering 33% of the peptide sequence. The peptides analysed by MS/MS highlighted in blue.

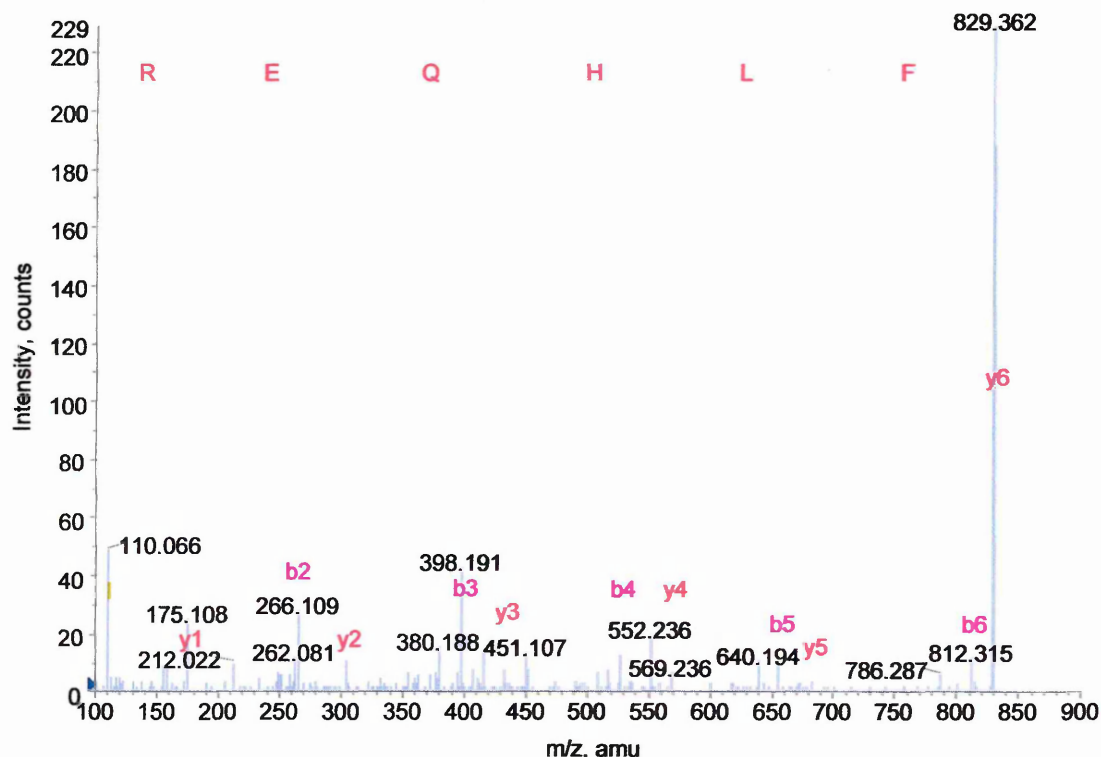


Figure 66. MALDI-MS/MS spectrum of peak at m/z 829.46 from the one-dimensional in-gel tryptic digest of standard APP α_{695} in figure 65. This peak corresponds to the APP α_{695} tryptic peptide FLHQER, MW 828.33 and the MS/MS analysis results validate this by giving the full peptide sequence.

Amino acid		Ion type (M+H ⁺)						
residue	mass/Da	immonium	a	a-NH ₃	b	b-NH ₃	y	y-NH ₃
F,Phe	147.068	120.080	120.080	103.054	148.075	131.049	829.431	812.405
L,Leu	113.084	86.096	233.164	216.138	261.159	244.133	682.363	665.336
H,His	137.058	110.071	370.223	353.197	398.218	381.192	569.279	552.252
Q,Gln	128.058	101.070	498.282	481.255	526.277	509.250	432.220	415.193
E,Glu	129.042	102.055	627.324	610.298	655.319	638.293	304.161	287.135
R,Arg	156.101	129.113	783.426	766.399	811.420	794.394	175.119	158.092

Table 18. BioAnalyst software results from the MALDI-MS/MS one-dimensional in-gel tryptic digest of APP α_{695} shown in figure 66. Listed are all the possible 'a', 'b' and 'y' product ions for the peptide FLHQER, highlighting the products ions present.

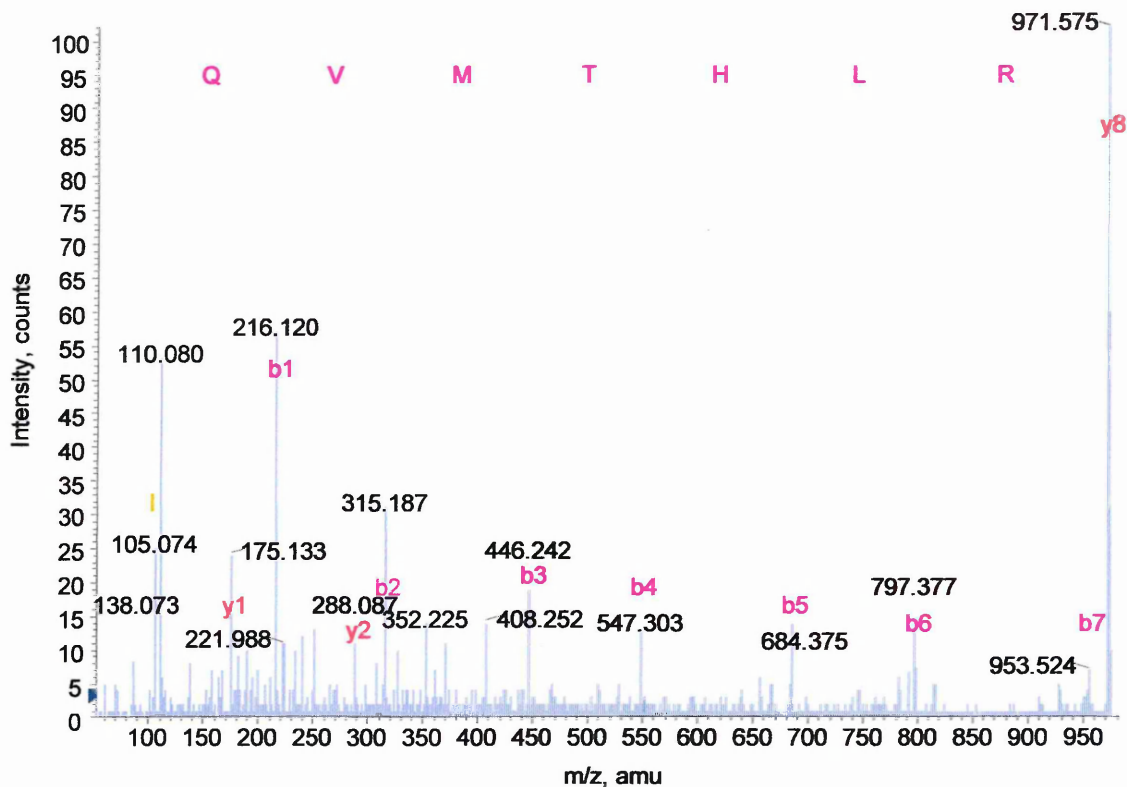


Figure 67. MALDI-MS/MS spectrum of peak at m/z 971.56 peak from the one-dimensional in-gel tryptic digest of APP α_{695} in figure 65. This peak corresponds to the APP α_{695} tryptic peptide SQVMTHLR, MW 971.51 and the resulting ‘b’ ion sequence tag, QVMTHLR authenticates the peak.

Amino acid		Ion type ($M+H^+$)						
residue	mass/ Da	immonium	a	a-NH ₃	b	b-NH ₃	y	y-NH ₃
Q, Gln	128.05	101.07	188.10	171.07	216.09	199.07	884.54	867.52
V, Val	99.06	72.08	287.17	270.14	315.16	298.13	756.48	739.46
M, Met	131.04	104.05	418.21	401.18	446.20	429.18	657.42	640.39
T, Thr	101.04	74.06	519.25	502.23	547.25	530.22	526.38	509.35
H, His	137.05	110.07	656.31	639.29	684.31	667.28	425.33	408.30
L, Leu	113.08	86.09	769.40	752.37	797.39	780.37	288.27	271.24
R, Arg	156.10	129.11	925.50	908.47	953.49	936.47	175.19	158.16

Table 19. BioAnalyst software results from the MALDI-MS/MS one-dimensional in-gel tryptic digest of APP α_{695} shown in figure 67. Listed are all the possible ‘a’, ‘b’ and ‘y’ product ions for the sequence QVMTHLR, highlighting the products ions present.

3.414 Capillary LC/MS analysis of a one-dimensional in-gel tryptic digestion of standard APP α_{695} .

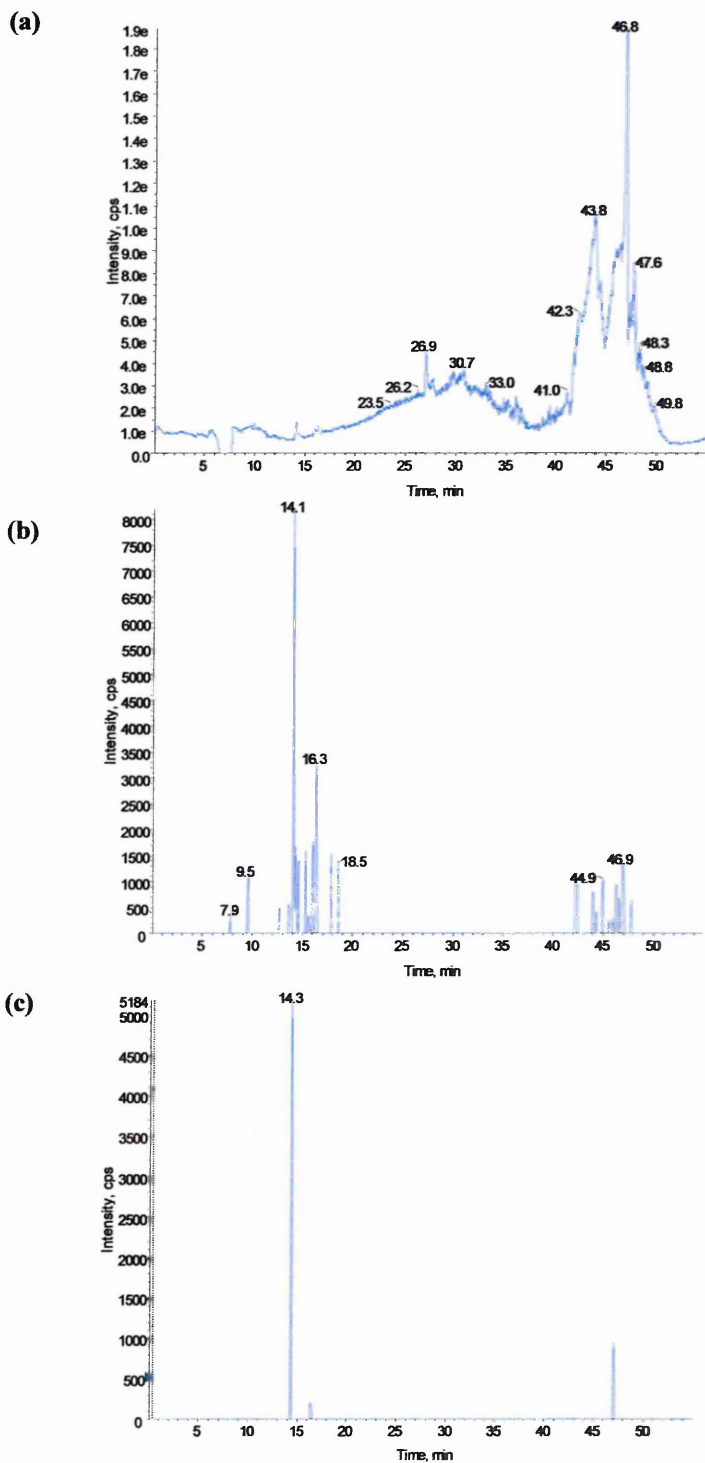


Figure 68. Capillary LC/MS run of an APP α_{695} one-dimensional in-gel tryptic digest performed using information dependant acquisition (IDA) software. For experimental conditions see chapter 2.92, page 92. (a) Shows the survey scan or total ion chromatogram (TIC). (b) Shows the TIC for the product ion intensities generated by product ion scan of the most intense peak in the normal mass spectrum. (c) Shows the TIC for the product ion intensities generated by product ion scan of the second most intense peak in the normal mass spectrum. The peak lists generated from traces (b) and (c) were sorted according to predefined parameters (chapter 2.92, page 93) and a selection of the most intense peaks automatically sent for MS/MS (figures 69 and 70).

mass observed	mass (experimental)	Position (APP α_{695} numbering)	missed cleavages	peptide sequence
686.84	1371.66	272-285	0	VPTTAASTPDAVDK*
687.81	1373.61	347-358	0	VESLEQEAAANER
870.42	1738.83	494-509	0	ISYGN DALMPSLTETK
660.97	1979.87	477-493	0	EQNYSDDVLANMISEPR*
990.94	1979.86	477-493	0	EQNYSDDVLANMISEPR*
674.71	2021.12	379-396	0	LALENYITALQAVPPRPR
709.68	2126.02	252-271	0	TTSIATTTTTTTTESVEEVVR
1064.01	2126.00	252-271	0	TTSIATTTTTTTTESVEEVVR

Table 20. BioAnalyst automatic data analysis (using Matrix Science software) of the chromatograms seen in figure 68 of a one-dimensional in-gel tryptic digest of standard APP α_{695} gave 16% sequence coverage. The data highlights the presence of both doubly and triply charged species seen with ESI-MS as opposed to the singly charged ions seen with MALDI-MS. The sequences highlighted in blue were subjected to MS/MS analysis, the isoform specific peptide sequence VPTTAASTPDAVDK (marked by a red asterisk) analysed in order to prove the sample to be APP α_{695} .

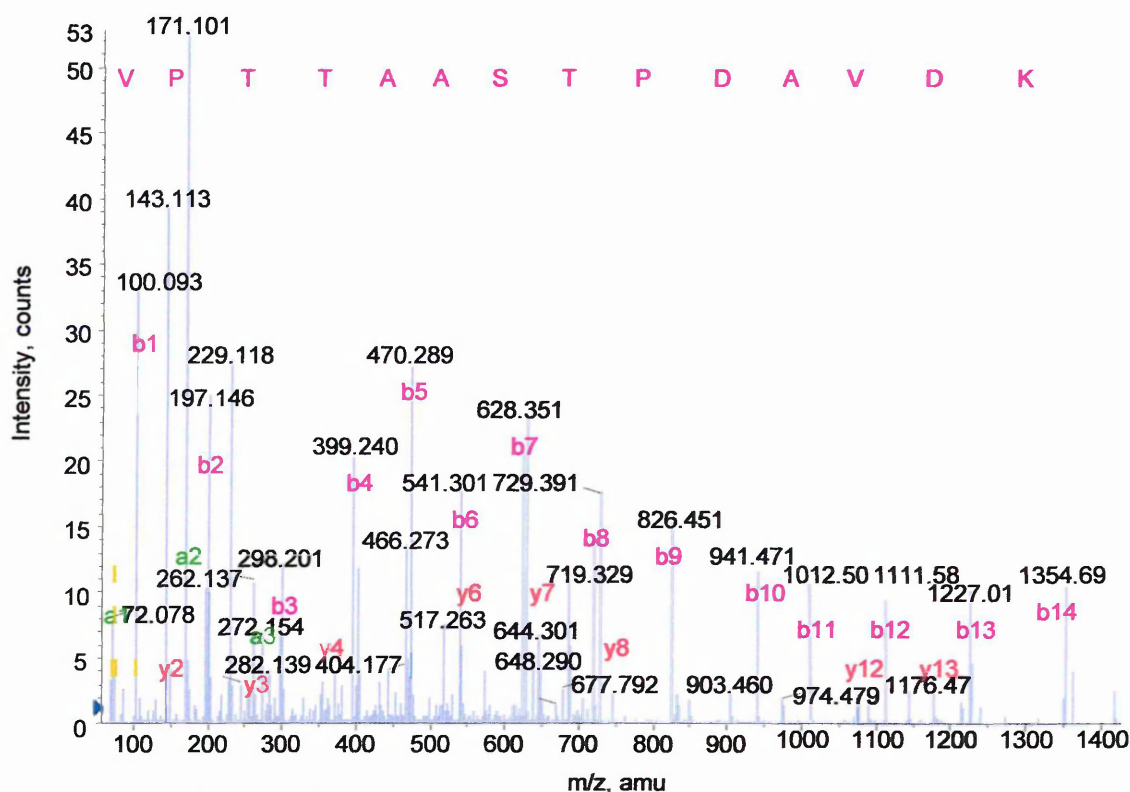


Figure 69. Capillary LC/MS/MS run of the doubly charged product ion at m/z 686.84, retention time 7.9 minutes from the LC/MS run of a one-dimensional in-gel tryptic digest of standard APP α_{695} (figure 68b). This product is consistent with the APP α_{695} tryptic peptide, VPTTAASTPDAVDK, MW 1371.66, a peptide specific to the APP α_{695} isoform, validated by full sequence coverage in 'b' ions.

Amino acid			Ion type (M+H ⁺)					
residue	mass/Da	immonium	a	a-NH ₃	b	b-NH ₃	y	y-NH ₃
V, Val	99.06	72.08	72.08	55.05	100.07	83.04	1372.60	1355.58
P, Pro	97.05	70.06	169.13	152.10	197.12	180.10	1273.53	1256.51
T, Thr	101.04	74.06	270.18	253.15	298.17	281.14	1176.48	1159.45

T, Thr	101.04	74.06	371.22	354.20	399.22	382.19	1075.43	1058.41
A, Ala	71.03	44.04	442.26	425.23	470.26	453.23	974.39	957.36
A, Ala	71.03	44.04	513.30	496.27	541.29	524.27	903.35	886.32
S, Ser	87.03	60.04	600.33	583.30	628.33	611.30	832.31	815.28
T, Thr	101.04	74.06	701.38	684.35	729.37	712.35	745.28	728.25
P, Pro	97.05	70.06	798.43	781.40	826.43	809.40	644.23	627.21
D, Asp	115.02	88.03	913.46	896.43	941.45	924.43	547.18	530.15
A, Ala	71.03	44.04	984.49	967.47	1012.49	995.46	432.15	415.13
V, Val	99.08	72.08	1083.56	1066.55	1111.56	1094.53	361.12	344.09
D, Asp	115.02	88.03	1198.59	1181.56	1226.58	1209.56	262.05	245.02
K, Lys	128.09	101.10	1326.69	1309.66	1354.68	1337.65	147.02	129.99

Table 21. BioAnalyst software results of the capillary LC/MS/MS spectrum of the doubly charged product at m/z 686.84 from the one-dimensional in-gel tryptic digest of standard APP α_{695} shown in figure 69.

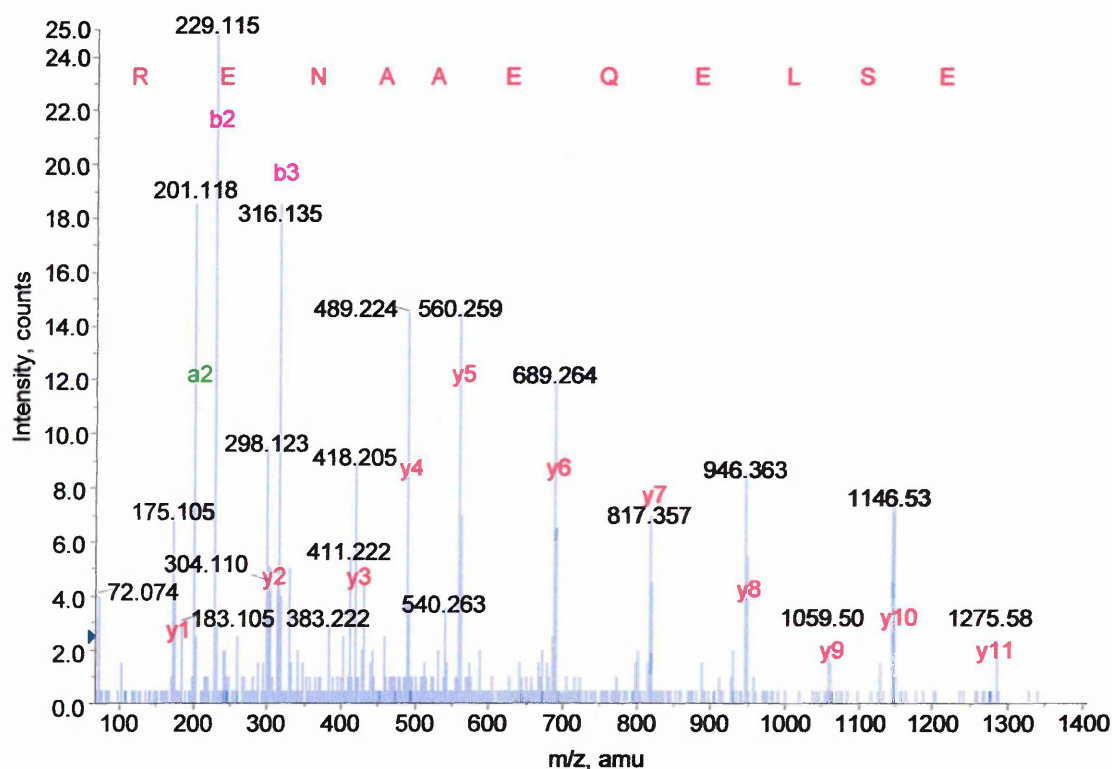


Figure 70. Capillary LC/MS/MS run of the doubly charged product ion at m/z 687.81, retention time 9.4 minutes from the LC/MS run of a one-dimensional in-gel tryptic digest of standard APP α_{695} (figure 68b). This product is consistent with the APP α_{695} tryptic peptide, VESLEQEAANER, MW 1373.61 and the sequence tag ESLEQEAANER, verifies this.

Amino acid		Ion type (M+H ⁺)						
residue	mass/Da	immonium	a	a-NH ₃	b	b-NH ₃	y	y-NH ₃
E, Glu	129.04	102.05	201.12	184.09	229.11	212.09	1275.53	1258.51
S, Ser	87.03	60.04	288.15	271.12	316.15	299.12	1146.49	1129.47
L, Leu	113.08	86.09	401.23	384.21	429.23	412.20	1059.46	1042.47
E, Glu	129.04	102.05	530.28	513.25	558.27	541.25	946.38	929.35
Q, Gln	128.05	101.07	658.34	641.31	686.33	669.30	817.33	800.31

E, Glu	129.04	102.05	787.38	770.35	815.37	798.35	689.27	672.25
A, Ala	71.03	44.04	858.42	841.39	886.41	869.38	560.23	543.20
A, Ala	71.03	44.04	929.45	912.43	957.45	940.42	489.19	472.17
N, Asn	114.04	87.05	1043.50	1026.47	1071.49	1054.46	418.16	401.13
E, Glu	129.04	102.05	1172.54	1155.51	1200.53	1183.51	304.11	287.09
R, Arg	156.10	129.11	1328.64	1311.61	1356.63	1339.61	175.07	158.05

Table 22. BioAnalyst software results of the capillary LC/MS/MS spectrum of the doubly charged product at m/z 687.81 from the one-dimensional in-gel tryptic digest of standard APP α_{695} shown in figure 70.

Amyloid precursor protein standard was purchased from Sigma for use as a direct comparison. The standard was the alpha secretase cleaved APP α_{695} isoform (APP α_{695}) from E.coli origin.

The MALDI-MS examination of the one-dimensional in-gel tryptic digestion of APP α_{695} (figure 65) gave amino acid sequence coverage of 33% of the APP α_{695} molecule from 22 tryptic peptides. The sequence coverage achieved from the LC/MS (figure 68) analysis was poorer giving 16% of the protein sequence from 6 peptides. The inferior LC/MS results in this instance could be due to the variations in manual and automatic peak retrieval. Due to the automation of LC/MS data it is possible that peaks of interest may be overlooked. MS/MS examination of both MALDI-MS (figures 66 and 67) and LC/MS (figures 69 and 70) showed excellent results, providing full peptide sequences for both methods. The unique tryptic peptide exhibited by APP α_{695} (position 272-285, monoisotopic mass 1378.6882, amino acid sequence VPTTAASTPDAVDK) was present in both the MALDI-MS and LC/MS data. Observed as the peak at m/z 1372.58 in the MALDI-MS spectrum (figure 65) and its presence within the LC/MS chromatograms were highlighted both in the BioAnalyst search results (table 20) as well as analysis by LC/MS/MS (figure 69) giving a full peptide sequence. Another peptide of interest,

EQNYSDDVLANMISEPR, position 477-493 (APP α_{695} numbering) seen in the MALDI-MS spectrum (figure 65) at m/z 1980.96, highlighted with a blue asterisk also present in the LC/MS data (table 20) in both double (m/z 990.94) and triply (m/z 660.97) charged species is thought to have a possible *N*-glycosylation site at position 479. If glycosylation does occur at this point the mass of the peptide would increase and the species at 1980 and 1979 for MALDI-MS and LC/MS respectively would not be seen. The bacterial nature of the standard APP α_{695} , however, means that glycosylation does not occur and as such the 1980 and 1979 ion species are visible. Contamination peaks visible within the MALDI-MS spectra needed further investigation by MS/MS to establish their identity, however, time limitations did not allow this. The peaks believed to be from keratin digestion (appendix 2, table 2) are highlighted.

3.415 MALDI-MS analysis of a one-dimensional in-gel tryptic digestion of immunoprecipitated alpha secretase cleaved amyloid precursor protein, isoform 770 (APP α_{770}).

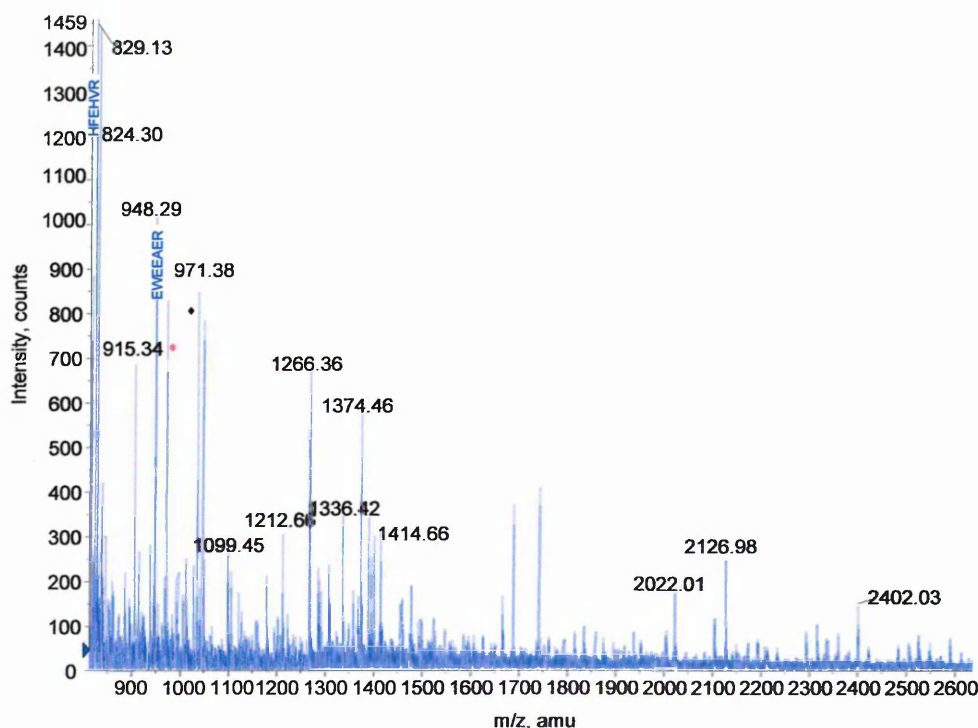


Figure 71. MALDI-MS spectrum of an in-gel tryptic digest of APP α_{770} from a one-dimensional gel. Annotated are the peptides upon which MS/MS analysis was performed (figures 72 and 73). Note the peak at m/z 915.34, specific to the APP α_{770} isoform. Keratin contamination marked with a black diamond.

mass (M+H ⁺)	mass (experimental)	position (sAPP ₇₇₀ numbering)	missed cleavages	peptide sequence
824.42	824.30	494-499	0	HFEHVR
829.43	829.13	118-123	0	FLHQER
915.49	915.34	335-342	0	TTQPELAR*
948.41	948.29	395-401	0	EWEEAER
971.51	971.38	511-518	0	SQVMTHLR
1099.59	1099.45	413-421	0	AVIQHFQEK
1212.62	1212.66	434-443	0	QLLVETHMAR
1266.67	1266.36	90-99	0	THPHFVIPYR
1336.60	1336.42	660-670	0	HDSGYEVHHQK
1374.65	1374.46	422-433	0	VESLEQEANER
1414.80	1414.66	632-645	0	GLTTRPGSGLTNIK
2022.15	2022.01	454-471	0	LALenyITALQAVPPRPR
2127.07	2126.98	252-271	0	TTSIATTTTTTTSVEEVVR
2402.18	2402.03	1-23	0	LEVPTDGNAGLLAEPQIAMFCR

Table 23. Mascot search results from the MALDI-MS mass fingerprint of the one-dimensional in-gel tryptic digest (figure 71) yielding 19% sequence coverage. The sequences highlighted in blue gave the best results when subjected to MS/MS analysis. The red asterisk marks the tryptic peptide TTQPELAR specific to APP α_{770} , however MS/MS analysis of this peak did not give any comprehensive results.

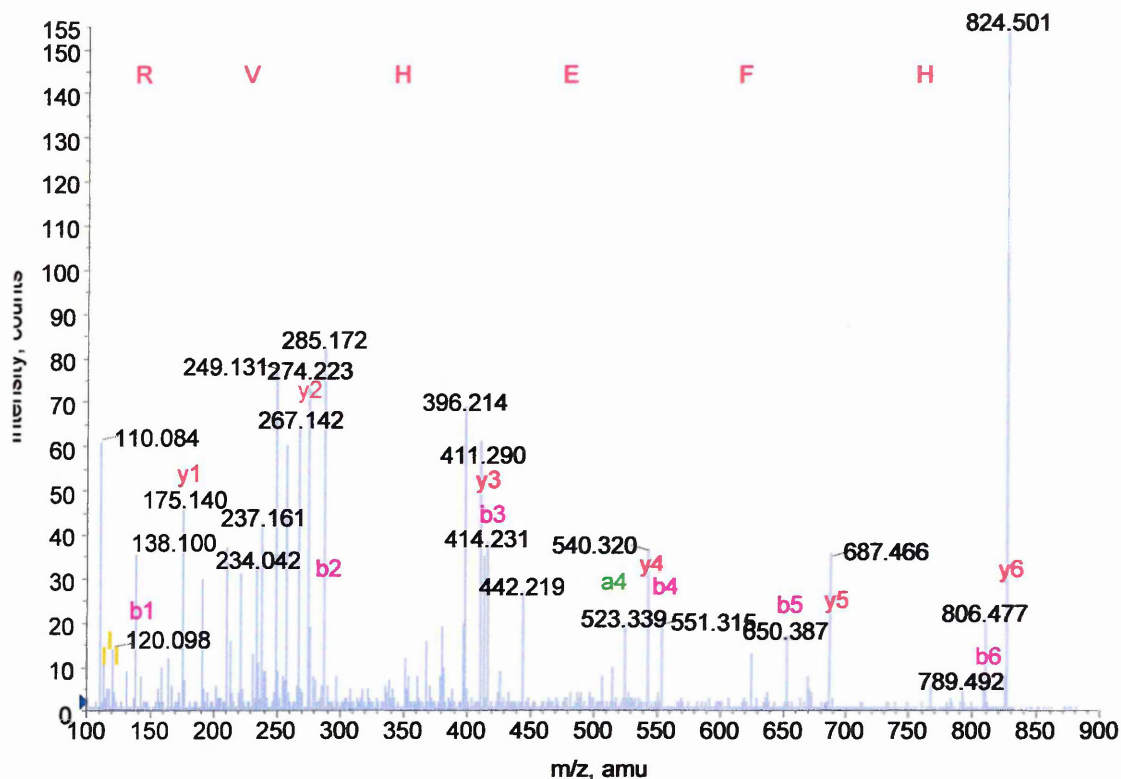


Figure 72. MALDI-MS/MS spectrum of peak at m/z 824.30 from the one dimensional in-gel digest of APP α_{770} (figure 71) corresponding to the APP α_{770} tryptic peptide HFEHVR. MS/MS analysis assigned the full sequence in ‘b’ and ‘y’ ions.

Amino acid		Ion type ($M+H^+$)						
residue	mass/Da	immonium	a	a-NH ₃	b	b-NH ₃	y	y-NH ₃
H, His	137.05	110.07	110.07	93.04	138.06	121.03	824.41	807.38
F, Phe	147.06	120.08	257.13	240.11	285.13	268.10	687.35	670.33
E, Glu	129.04	102.05	386.18	369.15	414.17	397.15	540.28	523.26
H, His	137.05	110.07	523.24	506.21	551.23	534.20	411.24	394.21
V, Val	99.06	72.08	622.30	605.28	650.30	633.27	274.18	257.16
R, Arg	156.10	129.11	778.41	761.38	806.40	789.37	175.11	158.09

Table 24. BioAnalyst software results from the MALDI-MS/MS one-dimensional in-gel tryptic digest of APP α_{770} spectrum in figure 72. Shown is the list of ‘a’, ‘b’ and ‘y’ product ions available for the peptide HFEHVR, highlighting the ions present.

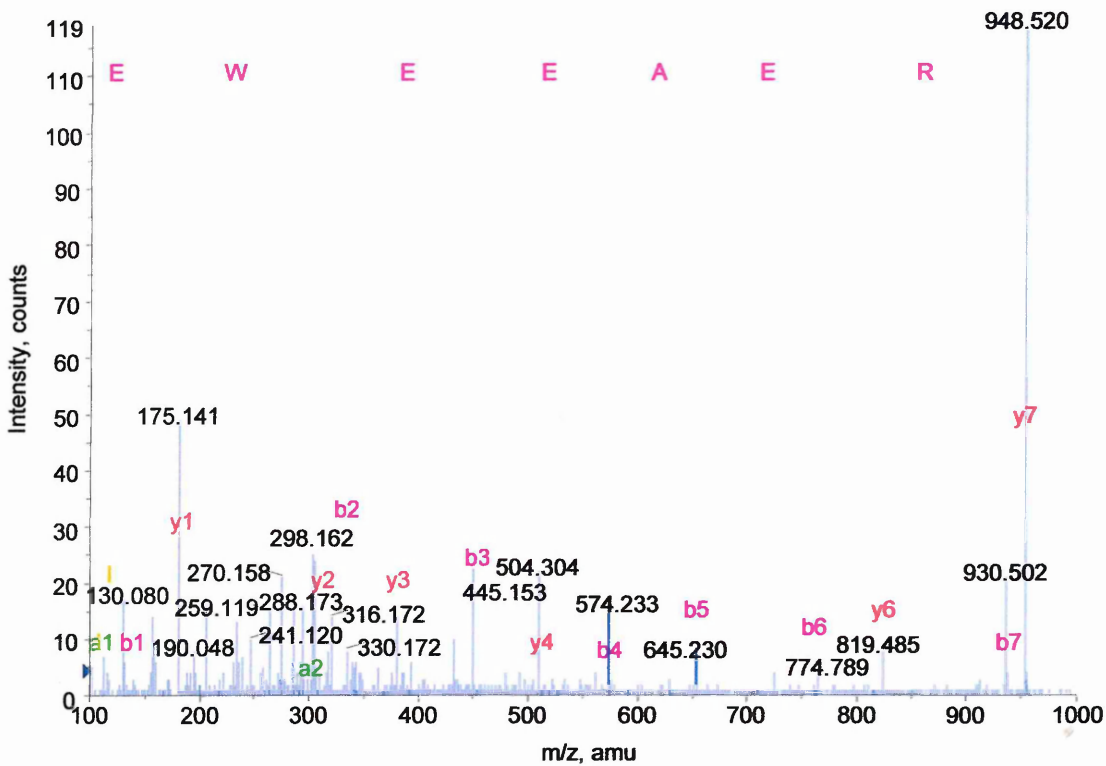


Figure 73. MALDI-MS/MS spectrum of peak at m/z 948.29 from the one-dimensional in-gel tryptic digest of APP α_{770} (figure 71). This peak corresponds to the APP α_{770} tryptic peptide EWEEAER, 947.31 monoisotopic MW. Full sequence coverage of ‘b’ product ions substantiates the peak.

Amino acid		Ion type ($M+H^+$)						
residue	mass/Da	immonium	a	a-NH ₃	b	b-NH ₃	y	y-NH ₃
E, Glu	129.04	102.05	102.05	85.02	130.04	113.02	948.40	931.37
W, Trp	186.07	159.09	288.13	271.10	316.12	299.10	819.36	802.33
E, Glu	129.04	102.05	417.17	400.15	445.17	428.14	633.28	616.25
E, Glu	129.04	102.05	546.21	529.19	574.21	557.18	504.24	487.21
A, Ala	71.03	44.04	617.25	600.23	645.25	628.22	375.19	358.17
E, Glu	129.04	102.05	746.29	729.27	774.29	757.26	304.16	287.13
R, Arg	156.10	129.11	902.40	885.37	930.39	913.36	175.11	158.09

Table 25. BioAnalyst results from the MALDI-MS/MS one-dimensional in-gel tryptic digest of APP α_{770} seen in figure 73, showing the possible ‘a’, ‘b’ and ‘y’ product ions and highlighting the ions present for the peptide EWEEAER.

3.416 Capillary LC/MS analysis of a one-dimensional in-gel tryptic digest of immunoprecipitated APP α_{770} .

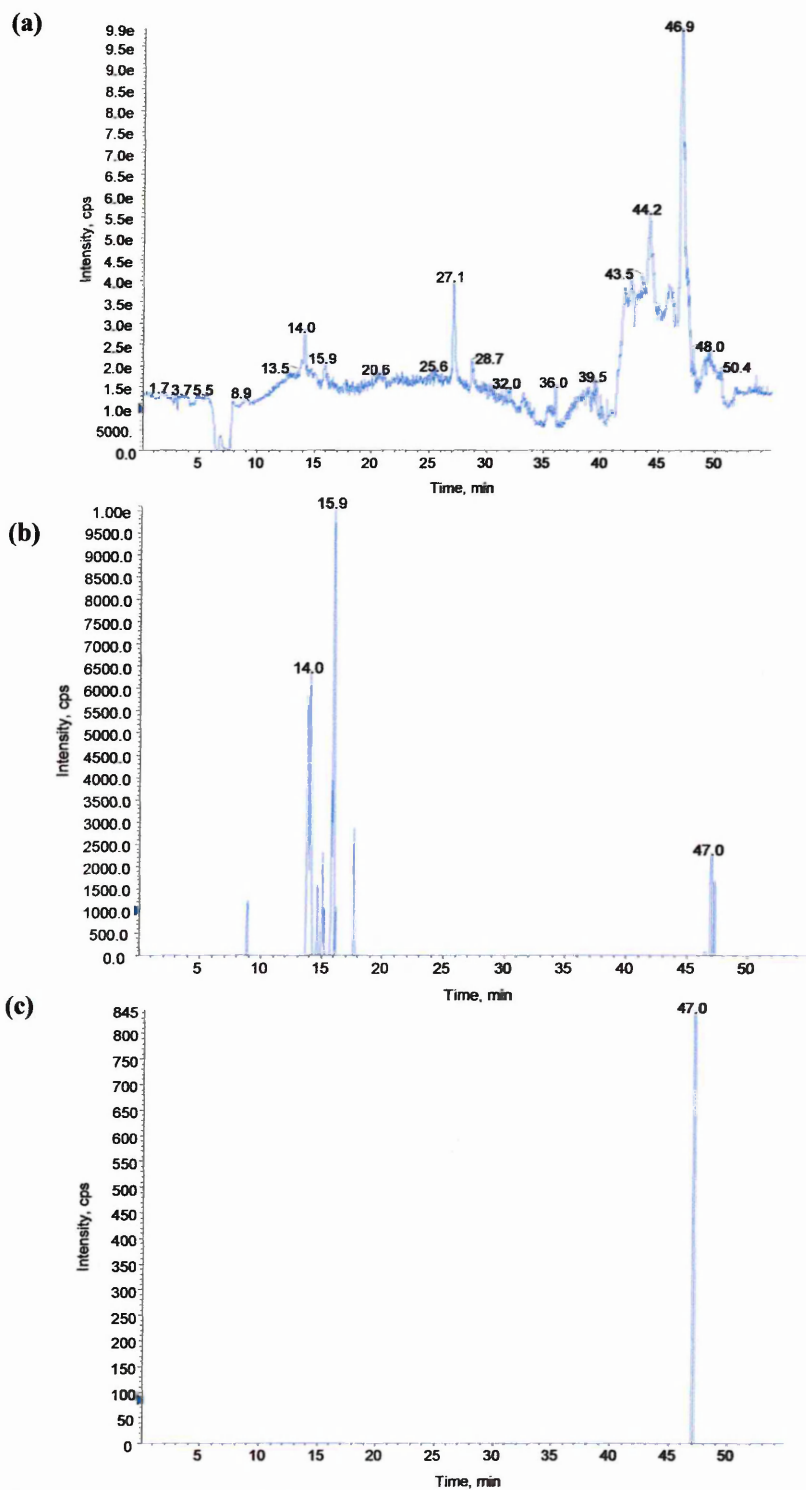


Figure 74. Capillary LC/MS run of an APP α_{770} one-dimensional in-gel tryptic digest performed using information dependant acquisition (IDA) software. For experimental conditions see chapter 2.92, page 92. (a) Shows the survey scan or total ion chromatogram (TIC). (b) Shows the TIC for the product ion intensities generated by product ion scan of the most intense peak in the normal mass spectrum. (c) Shows the TIC for the product ion intensities generated by product ion scan of the second most intense peak in the normal mass spectrum. The peak lists generated from trace (b) was sorted according to predefined parameters (chapter 2.92, page 93) and a selection of the most intense peaks automatically sent for MS/MS (figures 75 and 76).

mass observed	mass (experimental)	position	missed cleavages	peptide sequence
404.87	1211.60	434-433	0	QQLVETHMAR
687.83	1373.64	420-431	0	VESLEQEAAANER
580.61	1738.82	567-582	0	ISYGN DALMP SLTETK
870.42	1738.82	567-582	0	ISYGN DALMP SLTETK
674.72	2021.13	454-471	0	LALENYITALQAVPPRPR
709.69	2126.03	252-271	0	TTSIATTTTTT TESV EEVVR

Table 26. BioAnalyst automatic data analysis (using Matrix Science software) of the chromatograms seen in figure 74 of a one-dimensional in-gel tryptic digest of APP α_{770} gave 11% sequence coverage. The data highlights the presence of both doubly and triply charged species seen with ESI-MS as opposed to the singly charged ions seen with MALDI-MS. The sequences that gave the best MS/MS results are highlighted in blue.

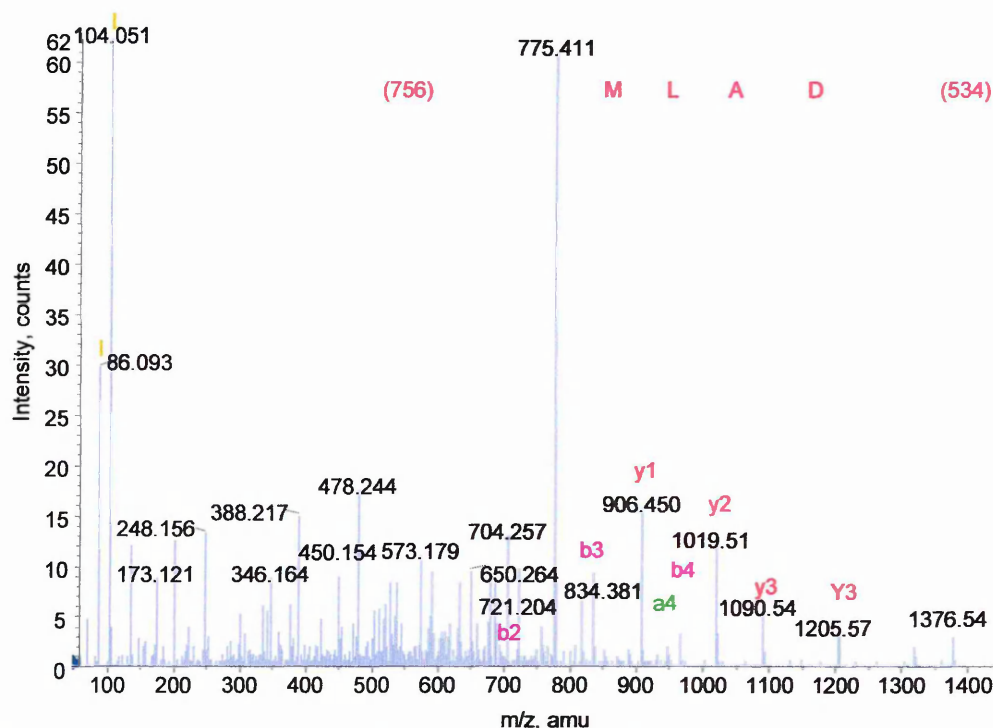


Figure 75. Capillary LC/MS/MS run of the doubly charged product ion at m/z 870.42, retention time 14.0 minutes from the LC/MS run of a one-dimensional in-gel tryptic digest of APP α_{770} (figure 74b). This product is consistent with the APP α_{770} tryptic peptide ISYGN DALMP SLTETK, 1738.83 MW and the sequence tag DALM seen in 'y' ions verify this.

Amino acid			Ion type (M+H ⁺)					
residue	mass/Da	immonium	a	a-NH ₃	b	b-NH ₃	y	y-NH ₃
(534.23)	534.23	n/a	507.24	490.22	535.24	518.21	1739.80	1722.78
D, Asp	115.02	88.03	622.26	605.23	650.25	633.23	1205.58	1188.55
A, Ala	71.03	44.04	693.30	676.27	721.29	704.26	1090.55	1073.52
L, Leu	113.08	86.09	806.38	789.35	834.38	817.35	1019.51	1002.49
M, Met	131.04	104.05	937.42	920.39	965.42	948.39	906.43	889.40
(756.36)	756.36	n/a	1693.80	1676.77	1721.79	1704.77	1662.28	1645.76

Table 27. BioAnalyst automated searching of the capillary LC/MS/MS spectrum of the doubly charged product at m/z 870.42 from the one-dimensional in-gel tryptic digest of APP α_{770} shown in figure 75, shows the product ions from the sequence tag DALM as well as the amino acid residues upstream and downstream from this sequence, which make up the full amino acid sequence.

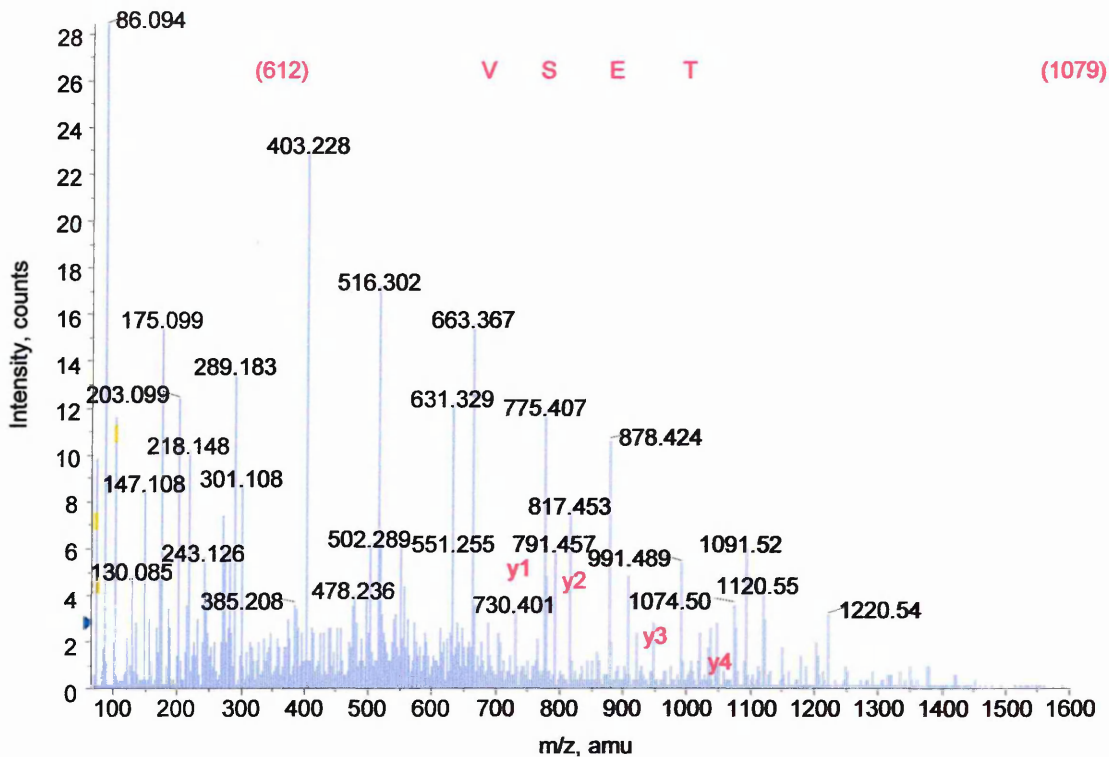


Figure 76. Capillary LC/MS/MS analysis of the triply charged product ion at m/z 709.69, retention time 13.9 minutes from the LC/MS run of a one-dimensional in-gel tryptic digest of APP α_{770} (figure 74b). This product is consistent with the APP α_{770} tryptic peptide TTSIATTTTTTTSVEEVVR, 2126.03 MW and the sequence tag VSET expands this.

Amino acid		Ion type ($M+H^+$)						
residue	mass/Da	immonium	a	a-NH ₃	b	b-NH ₃	y	y-NH ₃
(1079.48)	1079.48	n/a	1052.49	1035.47	1080.49	1063.46	2127.00	2109.98
T, Thr	101.04	74.06	1153.54	1136.52	1181.54	1164.51	1047.52	1030.49
E, Glu	129.04	102.05	1282.58	1265.56	1310.58	1293.55	946.47	929.44
S, Ser	87.03	60.04	1369.62	1352.59	1397.61	1380.59	817.43	800.40
V, Val	99.06	72.08	1468.69	1451.66	1496.68	1479.65	730.39	713.37
(612.31)	612.31	n/a	2081.00	2063.97	2108.99	2091.97	1342.70	1325.68

Table 28. BioAnalyst automated searching of the capillary LC/MS/MS spectrum from the one-dimensional in-gel tryptic digest of APP α_{770} shown in figure 76, highlights the product ions from the sequence tag TESV.

The alpha secretase cleaved amyloid precursor protein, isoform 770 (APP α_{770}) was immunoprecipitated from CHO 770 cell secretions.

The MALDI-MS examination of the one-dimensional in-gel tryptic digestion of APP α_{770} (figure 71) gave amino acid sequence coverage of 19% of the APP α_{770}

molecule from 14 tryptic peptides. The sequence coverage achieved from the LC/MS (figure 74) analysis was poorer giving 11% of the protein sequence from 5 peptides. The low sequence coverage achieved was to be expected considering the low initial concentration of *in vivo* APP. Again the inferior LC/MS results could be due to the variations in manual and automatic peak retrieval as the information dependant acquisition software functionality (IDA) allows automatic searching of LC/MS peak lists, whereas the MALDI-MS peak lists were edited and searched manually. As the LC/MS data is processed without human intervention it is possible that peaks of interest may be overlooked. MALDI-MS/MS examination of two tryptic peptides produced full sequence coverage in both cases (figures 72 and 73), whereas the results from the LC/MS/MS (figures 75 and 76) were less notable generating only sequence tags. This was, however, sufficient to achieve positive results from the automated search engine. APP α_{770} produces three unique tryptic peptides; position 312-334, monoisotopic mass 2540.076; position 347-360, monoisotopic mass 1385.6111; position 335-342, monoisotopic mass 914.3894, the latter is present in the MALDI-MS spectrum (figure 71) at m/z 915.34 marked by a red asterisk. None of the other unique peptides were resolved and attempts at assigning the sequence for the 915.34 peptide were insufficient for protein identification. Identification of the contaminating species present in the MALDI-MS spectra (figure 71) was not performed due to time limitations.

3.417 MALDI-MS analysis of a one-dimensional in-gel tryptic digestion of immunoprecipitated alpha secretase cleaved amyloid precursor protein (APP α).

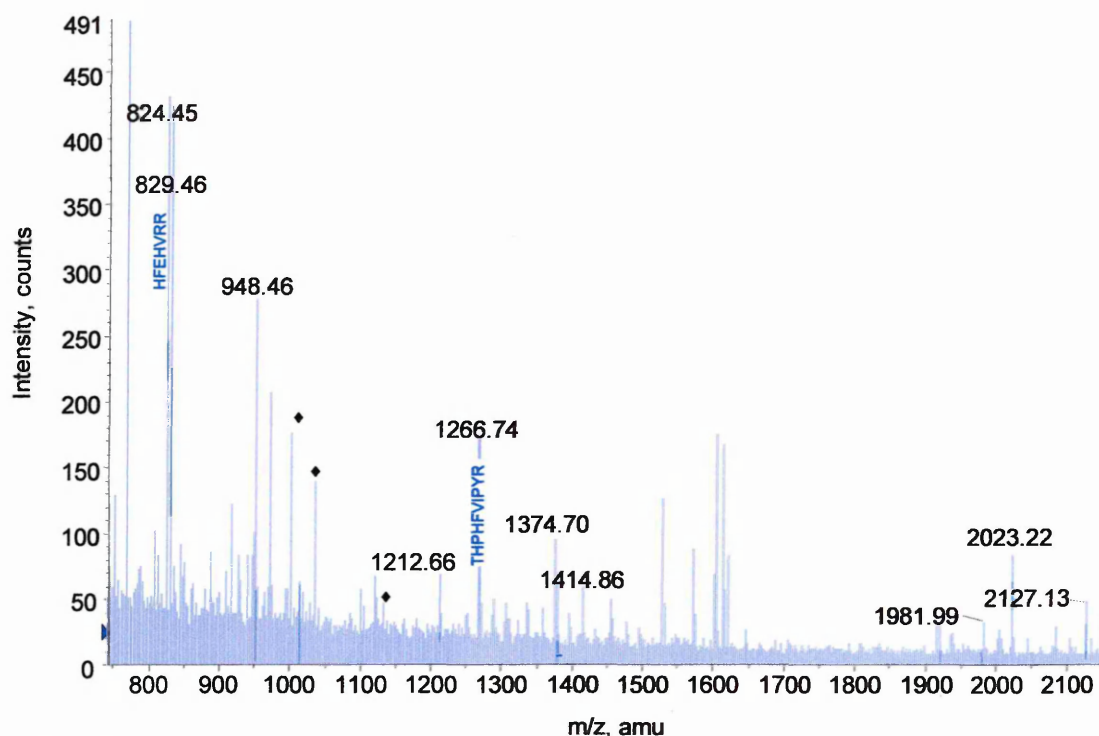


Figure 77. MALDI-MS spectrum of an in-gel tryptic digest of APP α from a one-dimensional gel. Annotated are the peaks upon which MS/MS analysis was performed (figures 78 and 79). Keratin contamination peaks highlighted by the black diamond.

mass (M+H ⁺)	mass (experimental)	Position sAPP ₇₇₀ numbering	missed cleavages	peptide sequence
824.42	824.45	494-499	0	HFEHVR
829.43	829.46	118-123	0	FLHQER
948.41	948.46	395-401	0	EWEEAER
1212.62	1212.66	434-443	0	QQLVETHMAR
1266.67	1266.74	90-99	0	THPHFVIPYR
1374.65	1374.70	422-433	0	VESLEQEANER
1414.80	1414.86	632-645	0	GLTTRPGSGLTNIK
1980.90	1981.99	552-568	0	EQNYSDDVLANMISEPR
2022.15	2022.22	454-471	0	LALENYITALQAVPPRPR
2127.07	2127.13	252-271	0	TTSIATTTTTTTESVEEVVR

Table 29. Mascot search results from the MALDI-MS mass fingerprint of the one-dimensional in-gel tryptic digest of APP α (figure 77), containing the three isoforms of interest (695, 751 and 770), giving coverage of 17% of the peptide sequence although no specific isoforms are seen. The sequences highlighted in blue gave the best MS/MS results (figures 78 and 79).

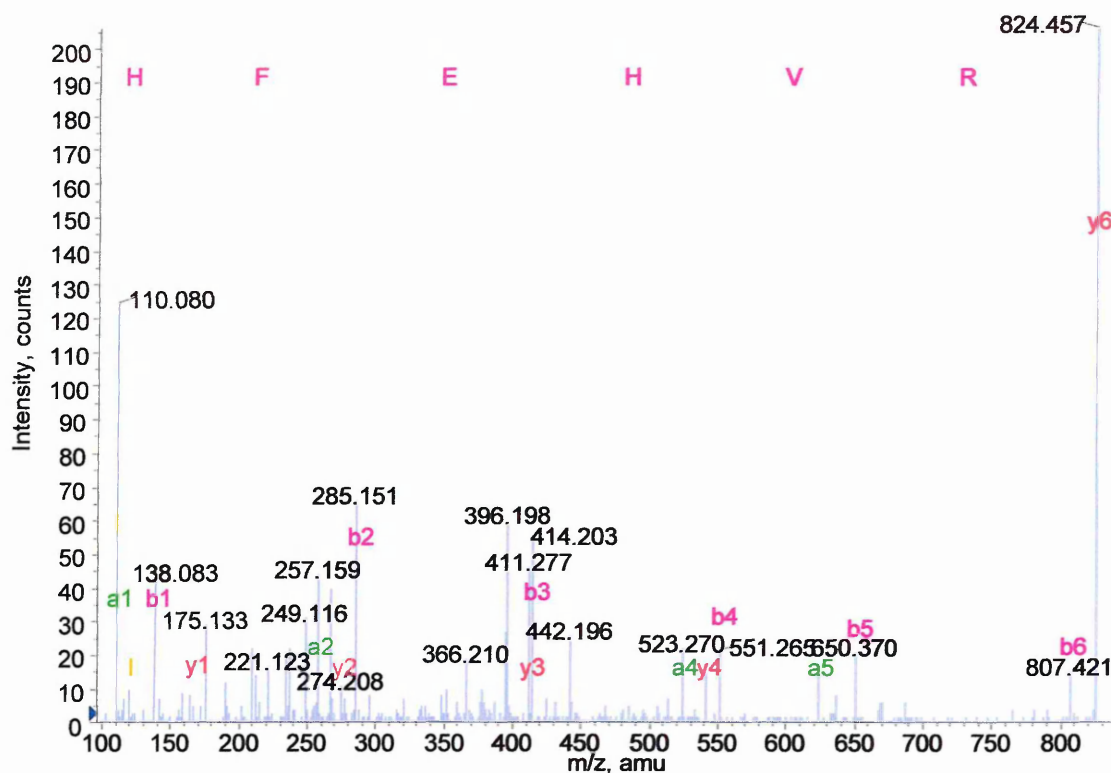


Figure 78. MALDI-MS/MS spectrum of peak at m/z 824.45 from the one dimensional in-gel digest of APP α (figure 77) corresponding to the APP α tryptic peptide HFEHVR, 824.42 MW. MS-MS analysis assigned the full sequence in ‘b’ and ‘y’ ions.

Amino acid		Ion type ($M+H^+$)						
residue	mass/Da	immonium	a	a-NH ₃	b	b-NH ₃	y	y-NH ₃
H, His	137.05	110.07	110.07	93.04	138.06	121.03	824.41	807.38
F, Phe	147.06	120.08	257.13	240.11	285.13	268.10	687.35	670.33
E, Glu	129.04	102.05	386.18	369.15	414.17	397.15	540.28	523.26
H, His	137.05	110.07	523.24	506.21	551.23	534.20	411.24	394.21
V, Val	99.06	72.08	622.30	605.28	650.30	633.27	274.18	257.16
R, Arg	156.10	129.11	778.41	761.38	806.40	789.37	175.11	158.09

Table 30. BioAnalyst software results from the MALDI-MS/MS one-dimensional in-gel tryptic digest of APP α spectrum in figure 78. Shown is the list of ‘a’, ‘b’ and ‘y’ product ions available for the peptide HFEHVR, emphasizing the ions present.

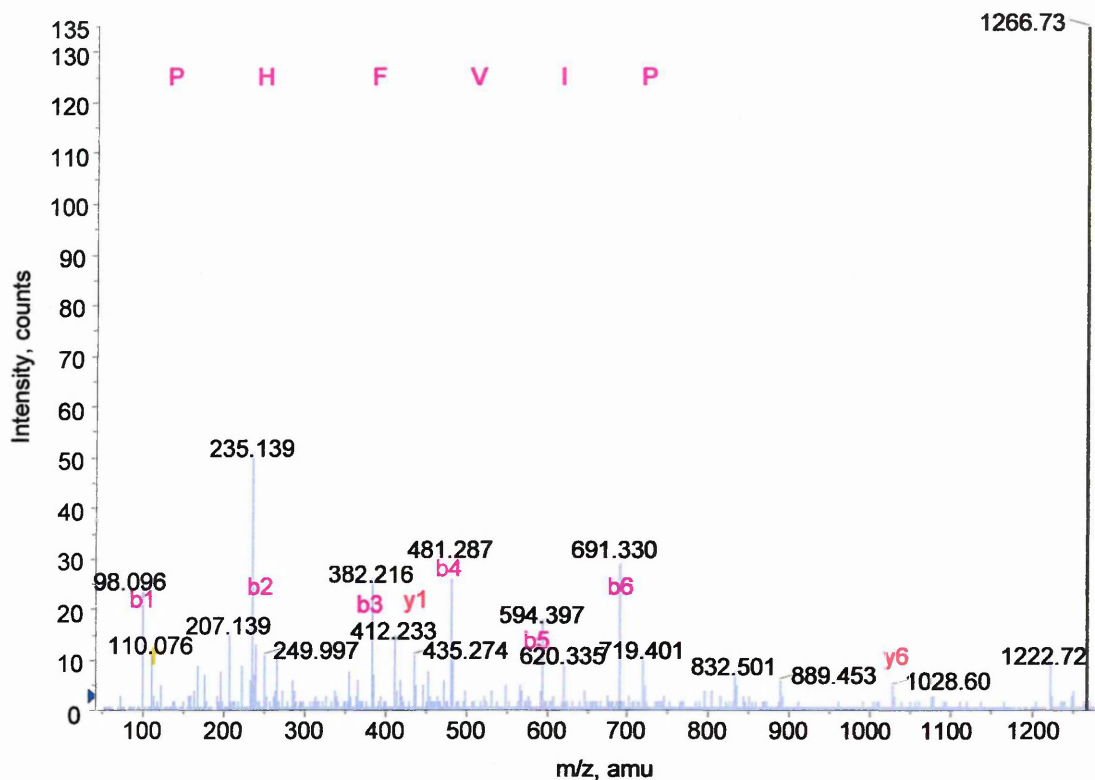


Figure 79. MALDI-MS/MS spectrum of peak at m/z 1266.74 from the one dimensional in-gel tryptic digest of APP α (figure 77) corresponding to the APP α tryptic peptide THPHFVIPYR 1265.67 monoisotopic mass. MS/MS analysis revealed the sequence tag PHFVIP in ‘b’ ions.

Amino acid		Ion type (M+H ⁺)						
residue	Mass /Da	immonium	a	a-NH ₃	b	b-NH ₃	y	y-NH ₃
P, Pro	97.05	70.06	110.07	93.04	98.06	81.04	1028.56	1011.53
H, His	137.05	110.07	207.12	190.09	235.11	218.09	931.51	914.48
F, Phe	147.06	120.08	354.19	337.16	382.18	365.16	794.45	777.42
V, Val	99.06	72.08	453.26	436.23	481.25	464.22	647.38	630.36
I, Ile	113.08	86.09	566.34	549.31	594.36	577.31	548.31	531.29
P, Pro	97.05	70.06	663.39	646.37	691.39	674.36	435.23	418.20

Table 31. BioAnalyst software results from the MALDI-MS/MS one-dimensional in-gel tryptic digest of APP α spectrum in figure 79. Shown is the list of ‘a’, ‘b’ and ‘y’ product ions available for the sequence PHFVIP, highlighting the ions present.

3.418 Capillary LC/MS analysis of a one-dimensional in-gel tryptic digestion of immunoprecipitated APP α .

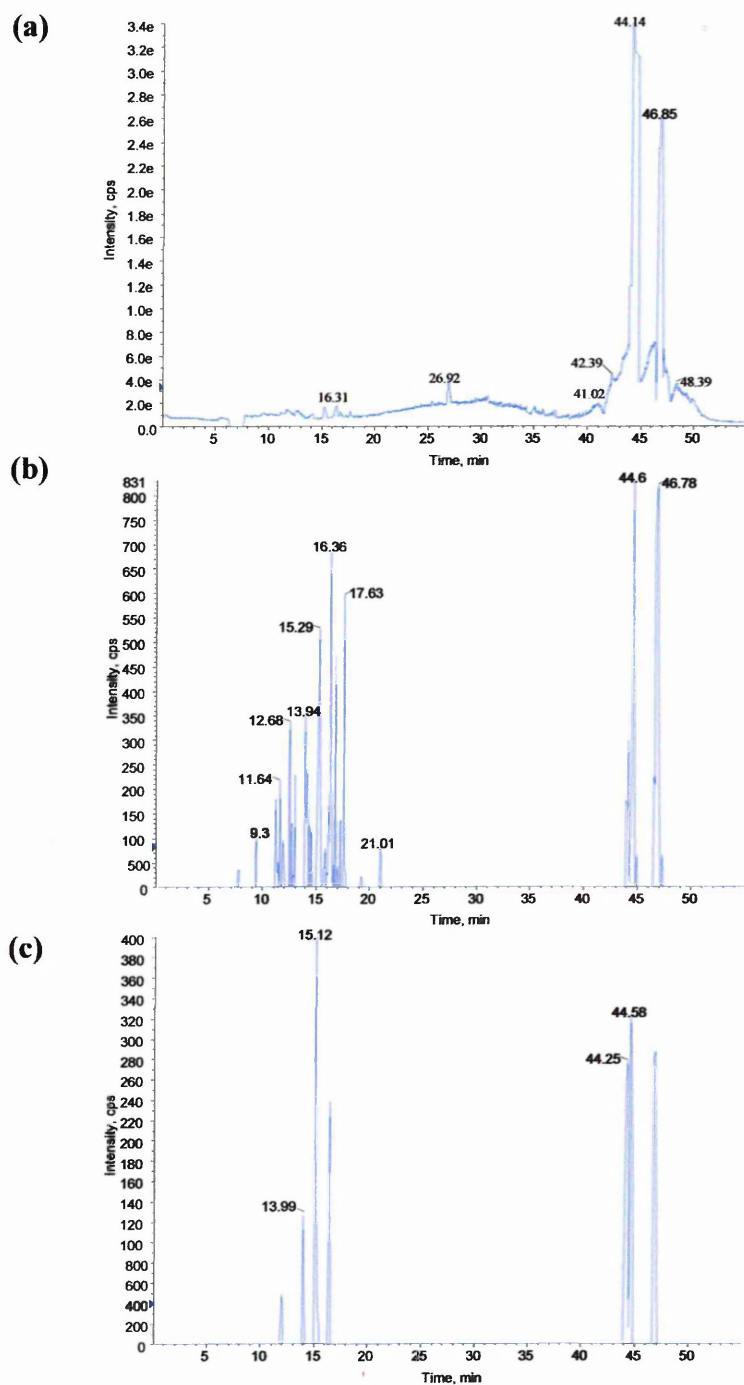


Figure 80. Capillary LC/MS run of an APP α one-dimensional in-gel tryptic digest performed using information dependant acquisition (IDA) software. For experimental conditions see chapter 2.92, page 92. (a) Shows the survey scan or total ion chromatogram (TIC). (b) Shows the TIC for the product ion intensities generated by product ion scan of the most intense peak in the normal mass spectrum. (c) Shows the TIC for the product ion intensities generated by product ion scan of the second most intense peak in the normal mass spectrum. The peak lists generated from traces (b) and (c) were sorted according to predefined parameters (chapter 2.92, page 93) and a selection of the most intense peaks automatically sent for MS/MS (figures 81 and 82).

mass observed	mass (experimental)	position (sAPP ₇₇₀ numbering)	missed cleavages	peptide sequence
687.83	1373.64	422-433	0	VESLEQEAAANER
709.69	2126.04	252-271	0	TTSIATTTTTTTSVEEVVR

Table 32. BioAnalyst automatic data analysis (using Matrix Science software) of the chromatograms seen in figure 80 of a one-dimensional in-gel tryptic digest of APP α gave sequence coverage of 4%. Both of the peptides were then subjected to MS/MS analysis (figure 81 and 82).

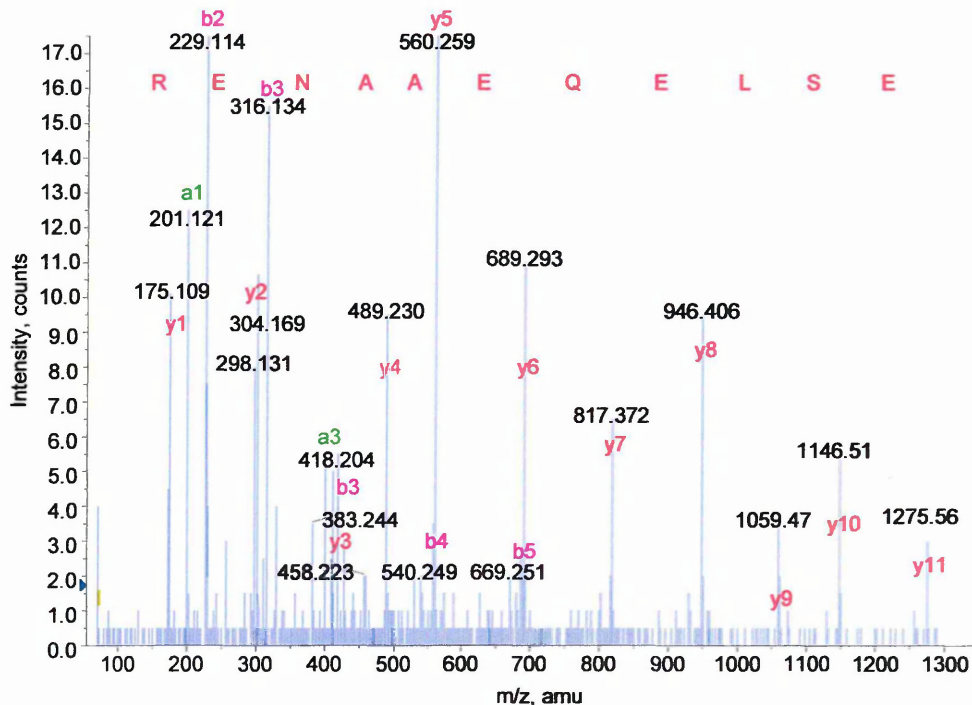


Figure 81. Capillary LC/MS/MS analysis of the doubly charged product ion at m/z 687.82, retention time 9.3 minutes from the LC/MS run of a one-dimensional in-gel tryptic digest of APP α (figure 80b). This product is consistent with the APP α tryptic peptide VESLEQEAAANER, 1373.63 monoisotopic mass and the sequence tag ESLEQEAAANER verifies this.

Amino acid		Ion type ($M+H^+$)						
residue	mass/Da	immonium	a	a-NH ₃	b	b-NH ₃	y	y-NH ₃
E, Glu	129.04	102.05	201.12	184.09	229.11	212.09	1275.53	1258.51
S, Ser	87.03	60.04	288.15	271.12	316.15	299.12	1146.49	1129.46
L, Leu	113.08	86.09	401.23	384.21	429.23	412.20	1059.46	1042.43
E, Glu	129.04	102.05	530.28	513.25	558.27	541.25	946.38	929.35
Q, Gln	128.05	101.07	658.34	641.31	686.33	669.30	817.33	800.31
E, Glu	129.04	102.05	787.38	770.35	815.37	798.35	689.27	672.25
A, Ala	71.03	44.04	858.42	841.39	886.41	869.38	560.23	543.20
A, Ala	71.03	44.04	929.45	912.43	957.45	940.42	489.19	472.17
N, Asn	114.04	87.05	1043.50	1026.43	1071.49	1054.46	418.16	401.13
E, Glu	129.04	102.05	1172.54	1155.51	1200.53	1183.51	304.11	287.09
R, Arg	156.10	129.11	1328.64	1311.61	1356.63	1339.61	175.07	158.05

Table 33. BioAnalyst automated searching of the capillary LC/MS/MS spectrum from the one-dimensional in-gel tryptic digest of APP α shown in figure 81, highlighting the product ions from the sequence tag ESLEQEAAANER.

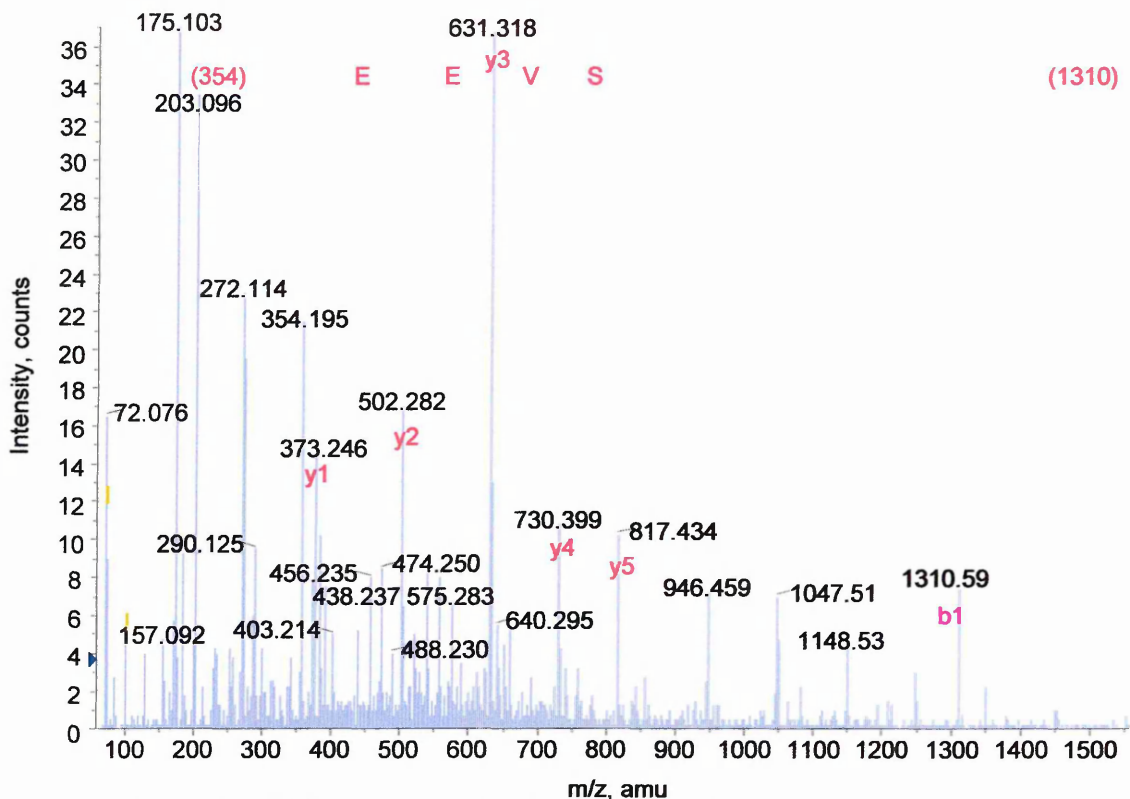


Figure 82. Capillary LC/MS/MS analysis of the triply charged product ion at m/z 709.69, retention time 13.9 minutes from the LC/MS run of a one-dimensional in-gel tryptic digest of APP α (figure 80c). This product is consistent with the APP α tryptic peptide TTSIATTTTTTESVEEVVR, 2126.05 MW and the sequence tag EEVS expands this.

Amino acid		Ion type ($M+H^+$)						
residue	mass/Da	immonium	a	a-NH ₃	b	b-NH ₃	Y	y-NH ₃
(1309.57)	1309.57	n/a	1282.58	1265.56	1310.58	1293.55	2127.00	2109.98
S, Ser	87.03	60.04	1369.61	1352.59	1397.61	1380.58	817.43	800.40
V, Val	99.06	72.08	1468.68	1451.66	1496.68	1479.65	730.40	713.37
E, Glu	129.04	102.05	1597.72	1580.70	1625.72	1608.69	631.33	614.30
E, Glu	129.04	102.05	1726.77	1709.74	1754.76	1737.74	502.28	485.26
(354.22)	354.22	n/a	2081.00	2063.97	2108.99	2091.97	373.24	356.22

Table 34. BioAnalyst automated searching of the capillary LC/MS/MS spectrum from the one-dimensional in-gel tryptic digest of APP α in figure 82, highlighting the product ions from the sequence tag EEVS.

The alpha secretase cleaved amyloid precursor protein (APP α) used was immunoprecipitated from Ntera 2 cell secretions. APP α encompasses all three isoforms of interest (APP α_{695} , APP α_{751} , APP α_{770}) and as such is a more plausible model of *in vivo* conditions.

The MALDI-MS results from the one-dimensional in-gel tryptic digestion of APP α (figure 77) gave amino acid sequence coverage of 17% of the APP α molecule from 10 tryptic peptides. The sequence coverage achieved from the LC/MS (figure 80) analysis was poorer giving 4% of the protein sequence from only 2 peptides. Sequence coverage for model proteins can range from 40-90%, low sequence coverage achieved from the immunoprecipitated APP α was expected due to low concentration of *in vivo* APP. The inferior LC/MS results in this instance could be due to the variations in manual and automatic peak retrieval. MALDI-MS/MS analysis of two tryptic peptides provided a sequence tag and a full peptide sequence (figures 78 and 79). LC/MS/MS (figures 81 and 82) gave two sequence tags. All the MS/MS data was adequate in protein verification. Disappointingly neither the MALDI-MS or LC/MS data showed any specific tryptic peptides, however, the peptide significant for its probable *N*-glycosylation site (EQNYSDDVLANMISEPR, position 552-568 APP α_{770} numbering) at position 554 may be present in the MALDI-MS data (figure 77) at *m/z* 1981.99, although attempts to validate the peptide by MALDI-MS/MS were unsuccessful. If this peptide is authentic there is a strong argument for presuming that the site may not be glycosylated. MS/MS identification of the prominent contaminating peaks visible in the MALDI-MS spectra (figure 77) was not performed due to time limitations and ideally should be investigated further. The peaks thought to be keratin contamination are highlighted and the remaining peaks may be due to antibodies remaining from the immunoprecipitation procedure.

3.42 One-dimensional in-gel Asp-N digestion of BSA and APP.

3.421 MALDI-MS analysis of a one-dimensional in-gel Asp-N digestion of BSA.

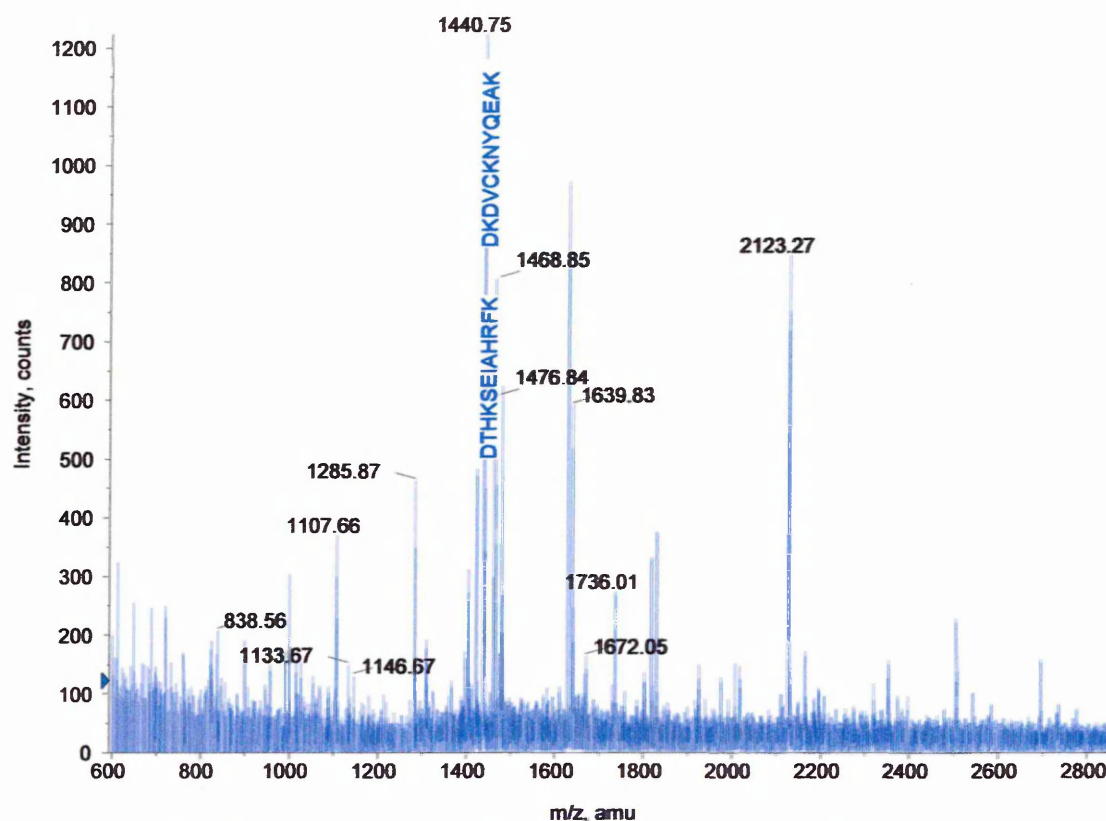


Figure 83. MALDI-MS spectrum of a one-dimensional in-gel Asp-N digest of BSA. The annotated peaks at m/z 1440.75 and 1468.85 and were chosen for MS/MS analysis due to their intensity, the results shown in figures 84 and 85.

mass ($M+H^+$)	mass (experimental)	position	missed cleavages	peptide sequence
838.48	838.56	62-68	0	EHVKLVN
1107.55	1107.66	526-534	1	DEKLFTFHA
1133.60	1133.67	96-105	1	DELCKVASLR
1146.58	1146.67	87-96	1	EKSLHTLFGD
1285.78	1285.87	543-553	0	EKQIKKQTALV
1440.68	1440.75	335-346	2	DKDVCKNYQEA
1468.77	1468.85	25-36	1	DTHKSEIAHRFK
1476.75	1476.84	153-163	1	DEKKFWGKYLY
1639.74	1639.83	278-291	3	DDRADLAKYICDNQ
1671.93	1672.05	474-487	0	DYLSLILNRLCVLH
1735.91	1736.01	315-330	3	EVEKDAIPENLPPLTA
2123.19	2123.27	554-571	2	ELKHKPKATEEQLKTVM

Table 35. Mascot search results from the one-dimensional in-gel Asp-N digest of BSA (figure 83), showing 20% sequence coverage. The sequences highlighted in blue subjected to MS/MS analysis (figures 84 and 85).

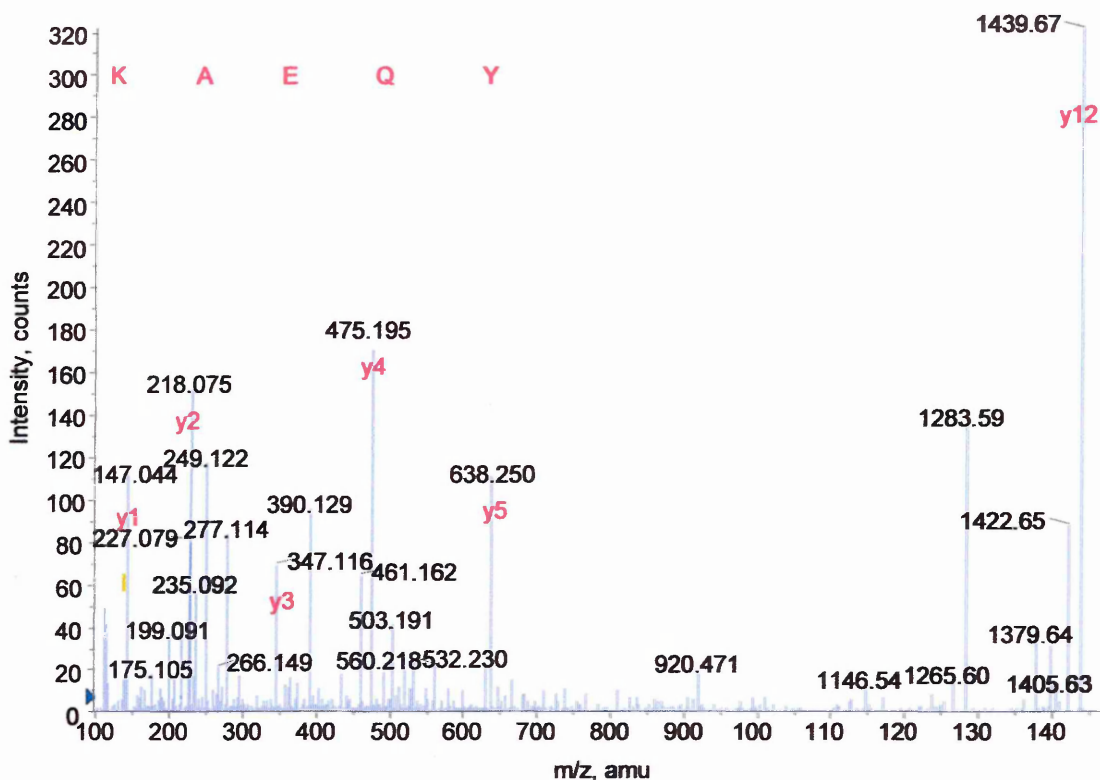


Figure 84. MALDI-MS/MS of peak at m/z 1440.75 from the one-dimensional in-gel Asp-N digest of BSA seen in figure 83. The uncovered 'y' ion sequence tag YQEAK corresponds to the peptide DKDVCKNYQEAK, 1439.58 MW.

Amino acid		Ion type ($M+H^+$)						
residue	mass/Da	immonium	a	a-NH ₃	b	b-NH ₃	y	y-NH ₃
Y, Tyr	163.06	136.07	136.07	119.04	164.07	147.04	638.31	621.28
Q, Gln	128.05	101.07	264.13	247.10	292.12	275.10	475.25	458.22
E, Glu	129.04	102.05	393.17	376.15	421.17	404.14	347.19	330.16
A, Ala	71.03	44.04	464.21	447.18	492.20	475.18	218.14	201.12
K, Lys	128.09	101.10	592.30	575.28	620.30	603.27	147.11	130.08

Table 36. BioAnalyst software results from the MALDI-MS/MS one-dimensional in-gel Asp-N digest of BSA seen in figure 84. Showing the 'a', 'b' and 'y' product ions available for the sequence YQEAK, highlighting the 'y' product ions present.

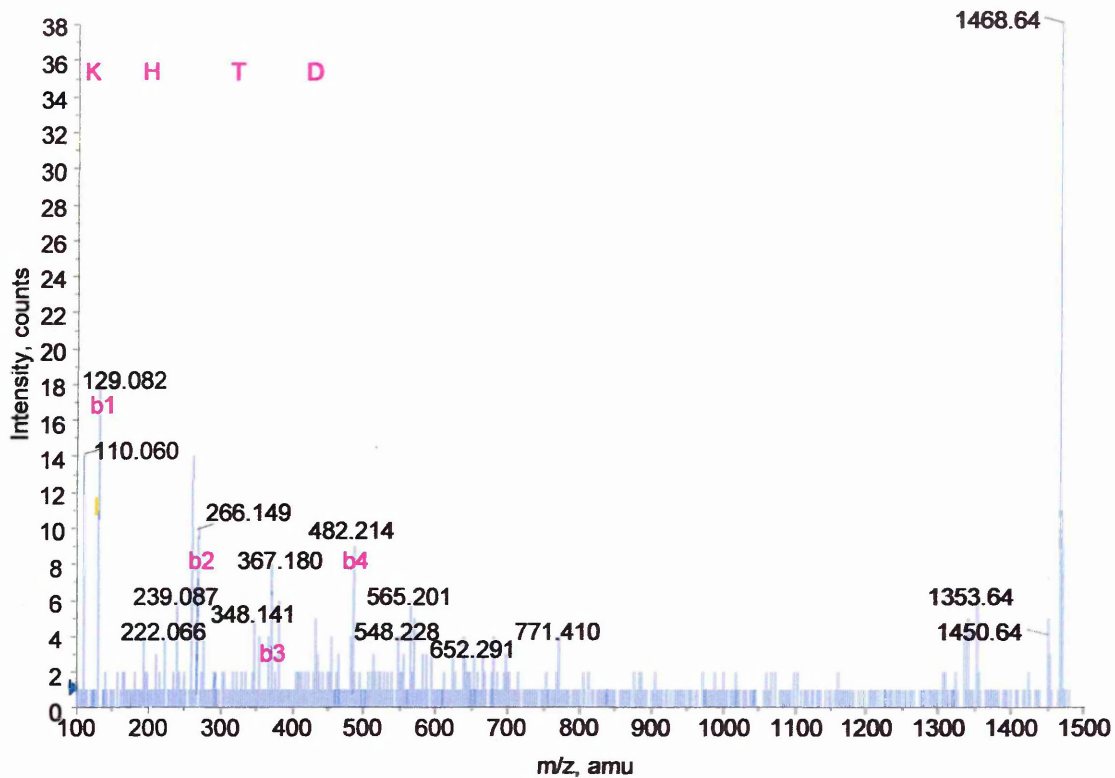


Figure 85. MALDI-MS/MS of peak at m/z 1468.85 from the one-dimensional in-gel Asp-N digest of BSA seen in figure 83. The uncovered 'b' ion sequence tag KHTD corresponds to the peptide DTHKSEIAHRFK, 1467.67 MW.

Amino acid		Ion type ($M+H^+$)						
residue	mass/Da	immonium	a	a-NH ₃	b	b-NH ₃	y	y-NH ₃
K, Lys	128.09	101.10	101.10	84.08	129.10	112.07	500.24	483.21
H, His	137.05	110.07	238.16	221.13	266.16	249.13	372.15	355.12
T, Thr	101.04	74.06	339.21	322.18	367.20	350.18	235.09	218.06
D, Asp	115.02	88.03	454.24	437.21	482.23	465.20	134.04	117.01

Table 37. BioAnalyst software results from the MALDI-MS/MS one-dimensional in-gel Asp-N digest of BSA seen in figure 85. The 'b' product ions for the sequence KHTD highlighted.

3.422 Capillary LC/MS analysis of a one-dimensional in-gel Asp-N digestion of BSA.

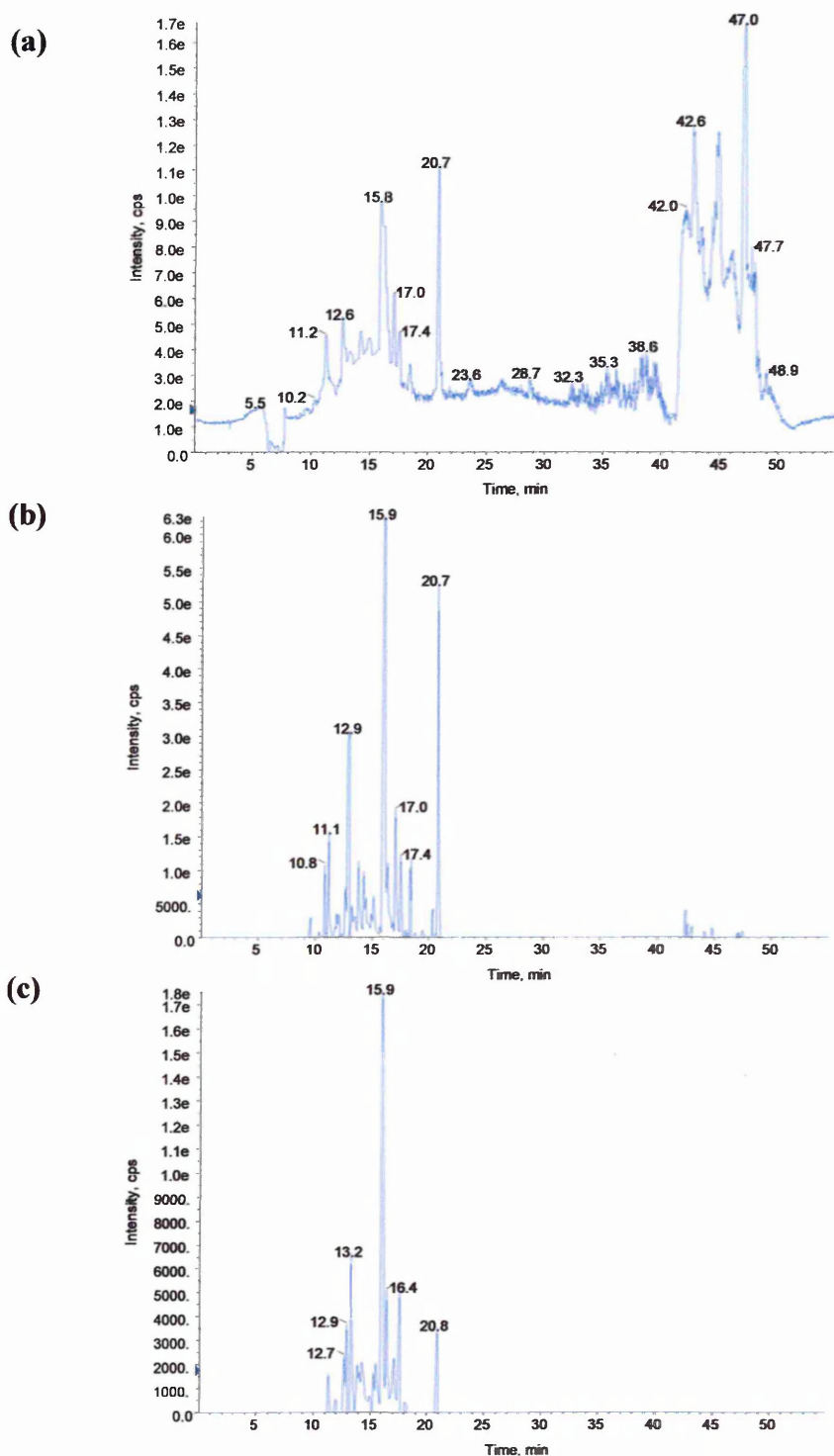


Figure 86. Capillary LC/MS run of a BSA one-dimensional in-gel Asp-N digest performed using information dependant acquisition (IDA) software. For experimental conditions see chapter 2.92, page 92. (a) Shows the survey scan or total ion chromatogram (TIC). (b) Shows the TIC for the product ion intensities generated by product ion scan of the most intense peak in the normal mass spectrum. (c) Shows the TIC for the product ion intensities generated by product ion scan of the second most intense peak in the normal mass spectrum. The peak lists generated from traces (b) and (c) were sorted according to predefined parameters (chapter 2.92, page 93) and a selection of the most intense peaks automatically sent for MS/MS (figures 87 and 88).

mass observed	mass (experimental)	position	missed cleavages	peptide sequence
405.75	809.49	136-142	0	LPKPKPD
535.26	1068.50	518-526	0	DETYVPKAF
554.26	1106.51	527-535	0	DEKLFTFHA
555.31	1108.61	133-142	1	SPDLPKPKPD
625.85	1249.68	320-331	0	AIPENLPPLTAD
856.91	1711.80	320-335	1	AIPENLPPLTADFAED
652.66	1954.95	320-337	2	AIPENLPPLTADFAEDKD
978.48	1954.95	320-337	2	AIPENLPPLTADFAEDKD

Table 38. BioAnalyst automatic data analysis (using Matrix Science software) of the chromatograms shown in figure 86 of a one-dimensional in-gel Asp-N digest of BSA gave 7% sequence coverage. The data highlights the presence of both doubly and triply charged species seen with ESI-MS as opposed to the singly charged ions seen with MALDI-MS. Successful MS/MS analysis was performed on the blue highlighted sequences (figures 87 and 88).

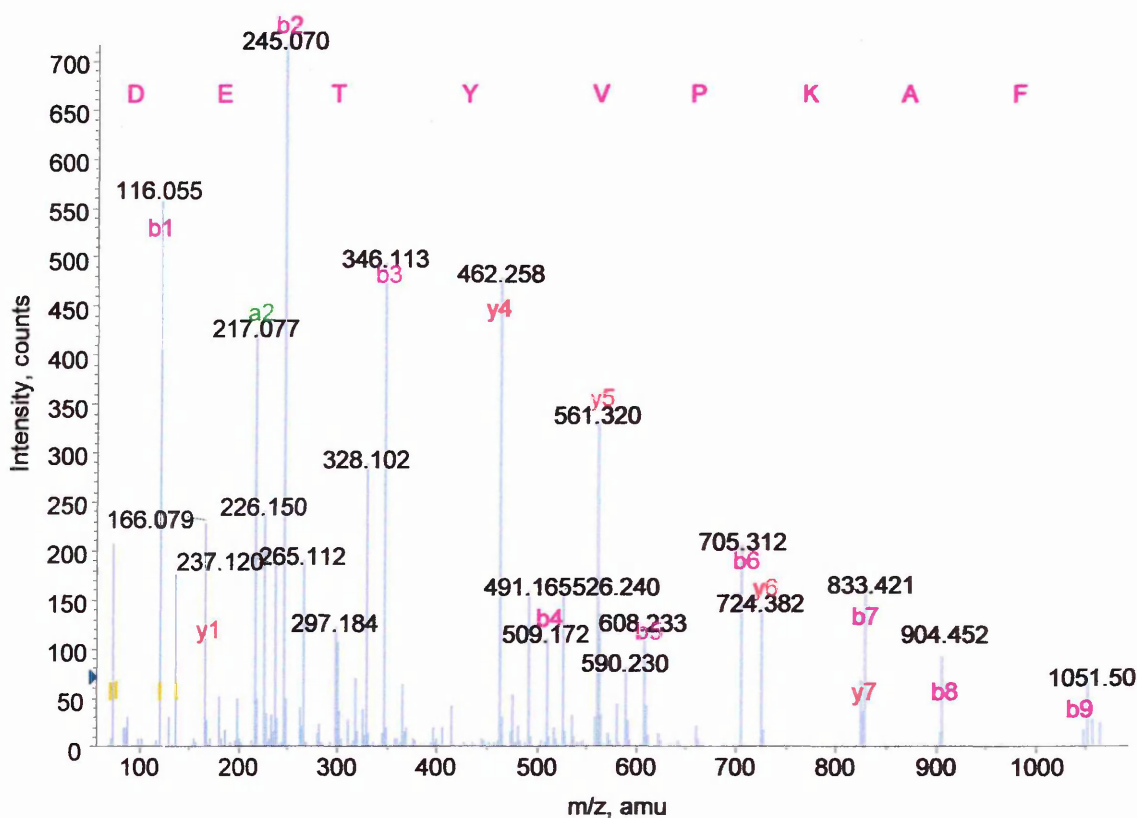


Figure 87. Capillary LC/MS/MS run of the doubly charged product ion at m/z 535.26, retention time 12.8 minutes from the LC/MS run of a one-dimensional in-gel Asp-N digest of BSA (figure 86b). This ion is consistent with the peptide DETYVPKAF, 1069.52 MW and LC/MS/MS analysis uncovering the full peptide sequence verifies this.

Amino acid		Ion type (M+H ⁺)						
residue	mass/Da	immonium	a	a-NH ₃	b	b-NH ₃	y	y-NH ₃
D, Asp	115.02	88.03	88.03	71.01	116.03	99.00	1069.49	1052.47
E, Glu	129.04	102.05	217.08	200.05	245.07	228.05	954.47	937.44
T, Thr	101.04	74.06	318.12	301.10	346.12	329.09	825.42	808.40

Y, Tyr	163.06	136.07	481.19	464.16	509.18	492.16	724.38	707.35
V, Val	99.06	72.08	580.26	563.23	608.25	591.22	561.31	544.29
P, Pro	97.05	70.06	677.31	660.28	705.30	688.28	462.24	445.22
K, Lys	128.09	101.13	805.40	788.35	833.40	816.37	365.19	348.16
A, Ala	71.03	44.04	876.44	859.41	904.44	887.41	237.10	220.07
F, Phe	147.08	120.08	1023.51	1006.48	1051.50	1034.48	166.06	149.03

Table 39. BioAnalyst results of the capillary LC/MS/MS spectrum of the product at m/z 535.26 from the one-dimensional in-gel Asp-N digest of BSA shown in figure 87. The possible and actual 'a', 'b' and 'y' product ions for the peptide DETYVPKAF are shown.

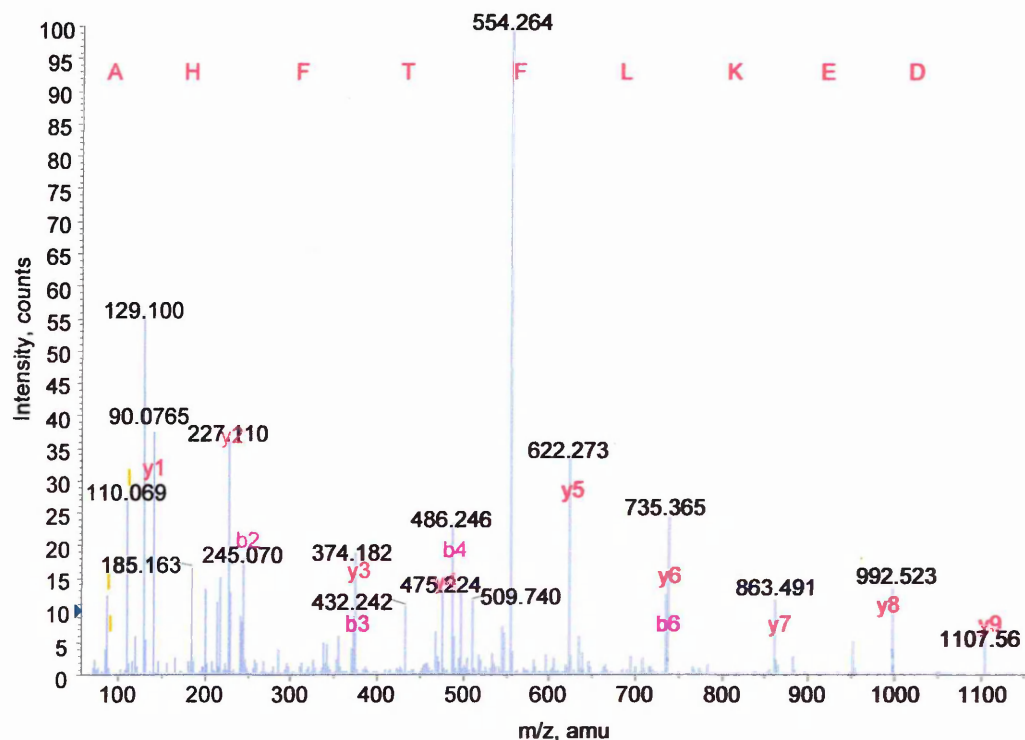


Figure 88. Capillary LC/MS/MS run of the doubly charged product ion at m/z 554.26, retention time 13.2 minutes from the LC/MS run of a one-dimensional in-gel Asp-N digest of BSA (figure 86c). This product is consistent with the BSA Asp-N peptide DEKLFTFHA, 1106.51 MW and the MS/MS analysis giving the full sequence corresponds with this.

Amino acid		Ion type (M+H ⁺)						
residue	Mass/Da	immonium	a	a-NH ₃	b	b-NH ₃	y	y-NH ₃
D, Asp	115.02	88.03	88.03	71.01	116.03	99.00	1107.54	1090.57
E, Glu	129.04	102.05	217.08	200.05	245.07	228.05	992.51	975.49
K, Lys	128.09	101.10	345.17	328.15	373.17	356.14	863.47	846.44
L, Leu	113.08	86.09	458.26	441.23	486.25	469.22	735.37	718.35
F, Phe	147.06	120.08	605.32	588.30	633.32	616.29	622.29	605.26
T, Thr	101.04	74.06	706.37	689.35	734.37	717.34	475.22	458.20
F, Phe	147.06	120.08	853.44	836.41	881.44	864.41	374.17	357.15
H, His	137.05	110.07	990.49	973.46	1018.49	1001.46	227.11	210.09
A, Ala	71.03	44.04	1061.52	1044.49	1089.52	1072.49	90.06	73.04

Table 40. BioAnalyst results of the capillary LC/MS/MS spectrum of the product at m/z 554.26 from the one-dimensional in-gel Asp-N digest of BSA shown in figure 88.

Bovine serum albumin (BSA, MW 66,432.96) was used as a standard due to its availability, similarity in molecular weight to the amyloid precursor protein isoforms (APP α_{695} , MW 67,708.02, APP α_{751} , MW 73,863.85, APP α_{770} , MW 75,988.34) and previous characterisation by in-gel digestion¹⁹⁷.

The MALDI-MS determination of the one-dimensional in-gel Asp-N digest of BSA (figure 83) resulted in 12 Asp-N peptides covering 20% of the protein. LC/MS analysis (figure 86) of the same sample revealed 7 Asp-N peptides for BSA, which covered 7% of the protein sequence. Noticeably both MALDI-MS (table 34) and LC/MS (table 37) showed a relatively higher presence of peptides with missed cleavage sites compared to the tryptic digests. Sequence coverage for a model protein such as BSA should be in the range of 40 to 60 %²⁰¹. The low sequence coverage proves the need to investigate experimental parameters such as protein loss, solubility and digest procedures. MS/MS analyses for both methods enabled automatic determination of BSA from the subsequent peptide sequences. MALDI-MS/MS resulted in two sequence tags (figures 84 and 85), whereas LC/MS/MS gave full peptide sequences (figures 87 and 88).

3.423 MALDI-MS analysis of a one-dimensional in-gel Asp-N digestion of alpha secretase cleaved amyloid precursor protein standard, isoform 695 (APP α_{695}).

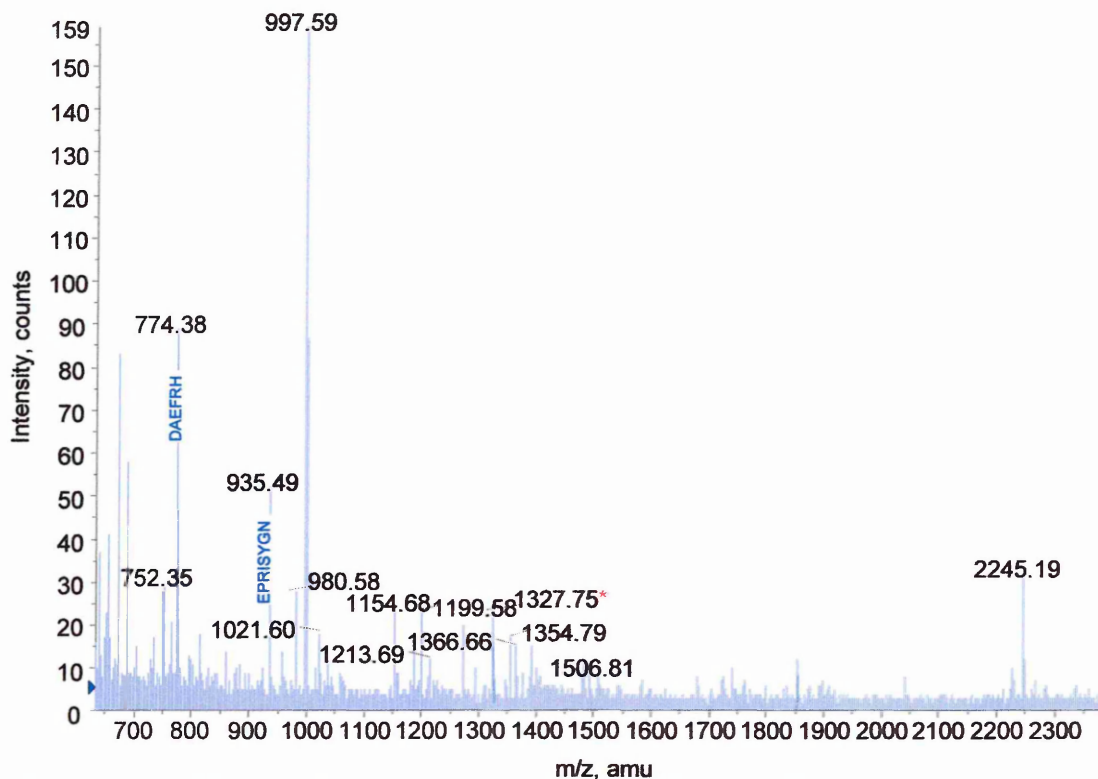


Figure 89. MALDI-MS spectrum of a one-dimensional in-gel Asp-N digest of standard APP α_{695} . The annotated peaks at m/zs 774.38 and 935.49 gave good results when subjected to MS/MS analysis (figures 90 and 91). The peak at m/z 1327.75, marked by a red asterisk is specific to APP α_{695} , MS/MS analysis of this peak, however, was unsuccessful.

mass (M+H ⁺)	mass (experimental)	position (APP α_{695} numbering)	missed cleavages	peptide sequence
752.31	752.35	122-127	1	ERMDVC
774.35	774.38	580-585	1	DAEFRH
935.46	935.49	491-498	0	EPRISYGN
997.40	997.59	166-173	0	EFVCCPLA(CM)
980.46	980.58	572-579	2	EEISEVKM(MSO)
1021.49	1021.60	573-581	2	EISEVKKMDA
1154.66	1154.68	325-334	0	ERQAKNLPKA
1199.54	1199.58	586-595	1	DSGYEVHHQK
1213.67	1213.69	335-344	0	DKKAVIQHFQ
1327.72	1327.75	268-280	1	EVVRVPTTAASTP*
1354.74	1354.79	323-334	1	EAERQAKNLPKA
1366.65	1366.66	472-482	2	ELLQKEQNYSD
1506.77	1506.81	499-512	1	DALMPSLTETKTTV
2245.18	2245.19	555-575	2	DRGLTTRPGSGLTNIKTEEIS

Table 41. Mascot search results from the MALDI-MS of the one-dimensional in-gel Asp-N digest of APP α_{695} shown (figure 89) covering 18% of the peptide sequence. The sequences highlighted in blue gave successful MS/MS data (figures 90 and 91)

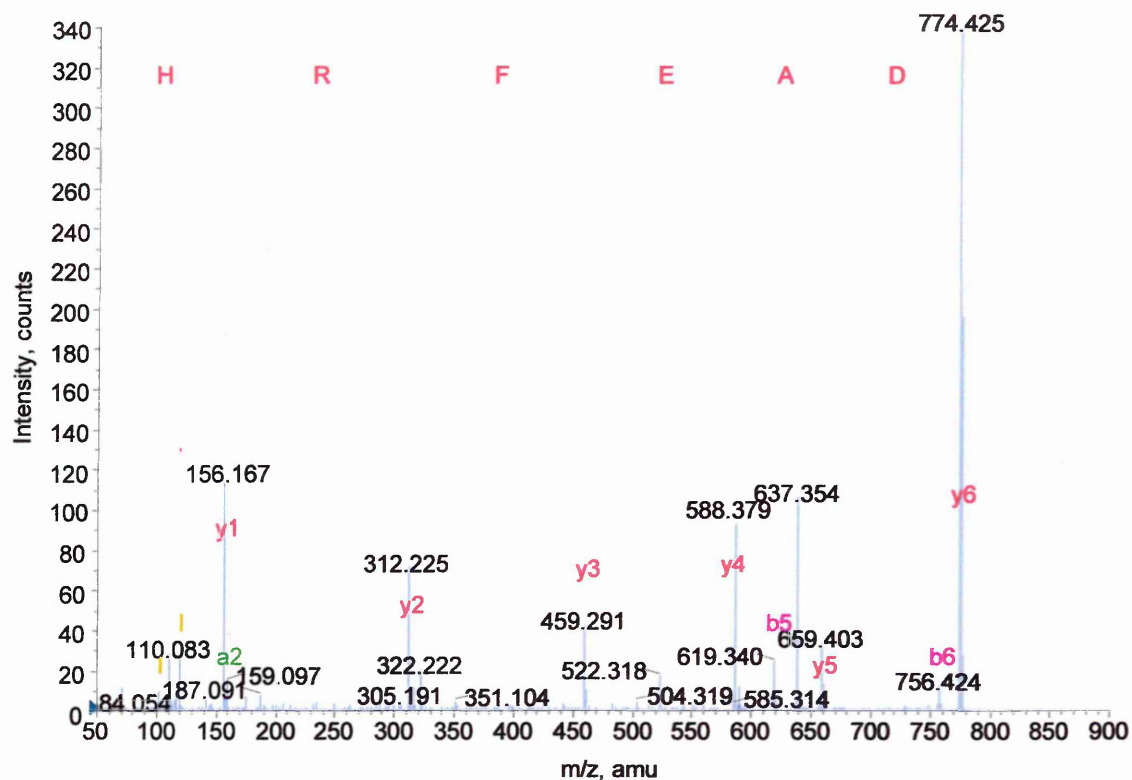


Figure 90. MALDI-MS/MS spectrum of peak at m/z 774.38 from the one-dimensional in-gel Asp-N digest of APP α_{695} in figure 89. This peak corresponds to the APP α_{695} tryptic peptide DAEFRH, 773.25 MW and the MS/MS results validate this by giving the full peptide sequence.

Amino acid		Ion type (M+H ⁺)						
residue	mass/Da	immonium	a	a-NH ₃	b	b-NH ₃	y	y-NH ₃
D, Asp	115.02	88.03	88.03	71.01	116.03	99.00	774.35	757.32
A, Ala	71.03	44.04	159.07	142.04	187.07	170.04	659.32	642.29
E, Glu	129.04	102.05	288.11	271.09	316.11	299.08	588.28	571.26
F, Phe	147.06	120.08	435.18	418.16	463.18	446.15	459.24	442.21
R, Arg	156.10	129.11	591.28	574.26	619.28	602.25	312.17	295.15
H, His	137.05	110.07	728.34	711.32	756.34	739.38	156.07	139.05

Table 42. BioAnalyst software results from the MALDI-MS/MS one-dimensional in-gel Asp-N digest of APP α_{695} shown in figure 90. Listed are all the possible 'a', 'b' and 'y' product ions for the peptide DAEFRH, highlighting the products ions present.

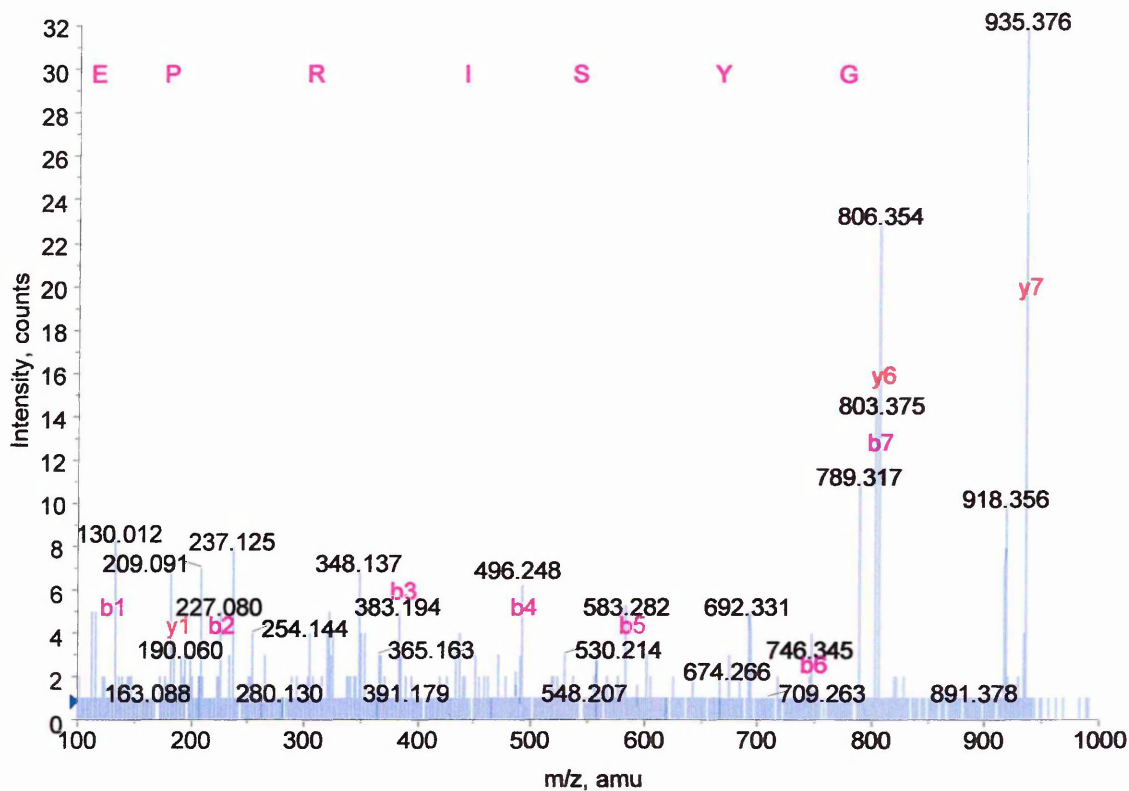


Figure 91. MALDI-MS/MS spectrum of peak at m/z 935.49 from the one-dimensional in-gel Asp-N digest of APP α_{695} in figure 89. This peak corresponds to the APP α_{695} Asp-N peptide EPRISYGN, 934.36 MW and the resulting 'b' ion sequence tag, authenticates the peak.

Amino acid		Ion type ($M+H^+$)						
residue	mass/Da	immonium	a	a-NH ₃	b	b-NH ₃	y	y-NH ₃
E, Glu	129.04	102.05	102.05	85.02	130.04	113.02	935.45	918.43
P, Pro	97.05	70.06	199.10	182.08	227.10	210.07	806.41	789.38
R, Arg	156.10	129.15	355.20	338.18	383.20	366.17	709.36	692.33
I, Ile	113.08	86.09	468.29	451.26	496.28	479.26	553.26	536.23
S, Ser	87.03	60.04	555.32	538.29	583.31	566.29	440.17	423.15
Y, Tyr	163.06	136.07	718.38	701.36	746.38	729.35	353.14	336.11
G, Gly	57.02	30.03	775.40	758.38	803.40	786.31	190.08	173.05

Table 43. BioAnalyst software results from the MALDI-MS/MS one-dimensional in-gel Asp-N digest of APP α_{695} shown in figure 91. Listed are all the possible 'a', 'b' and 'y' product ions for the sequence EPRISYG, highlighting the 'b' ions present.

3.424 Capillary LC/MS analysis of a one-dimensional in-gel Asp-N digestion of standard APP α_{695} .

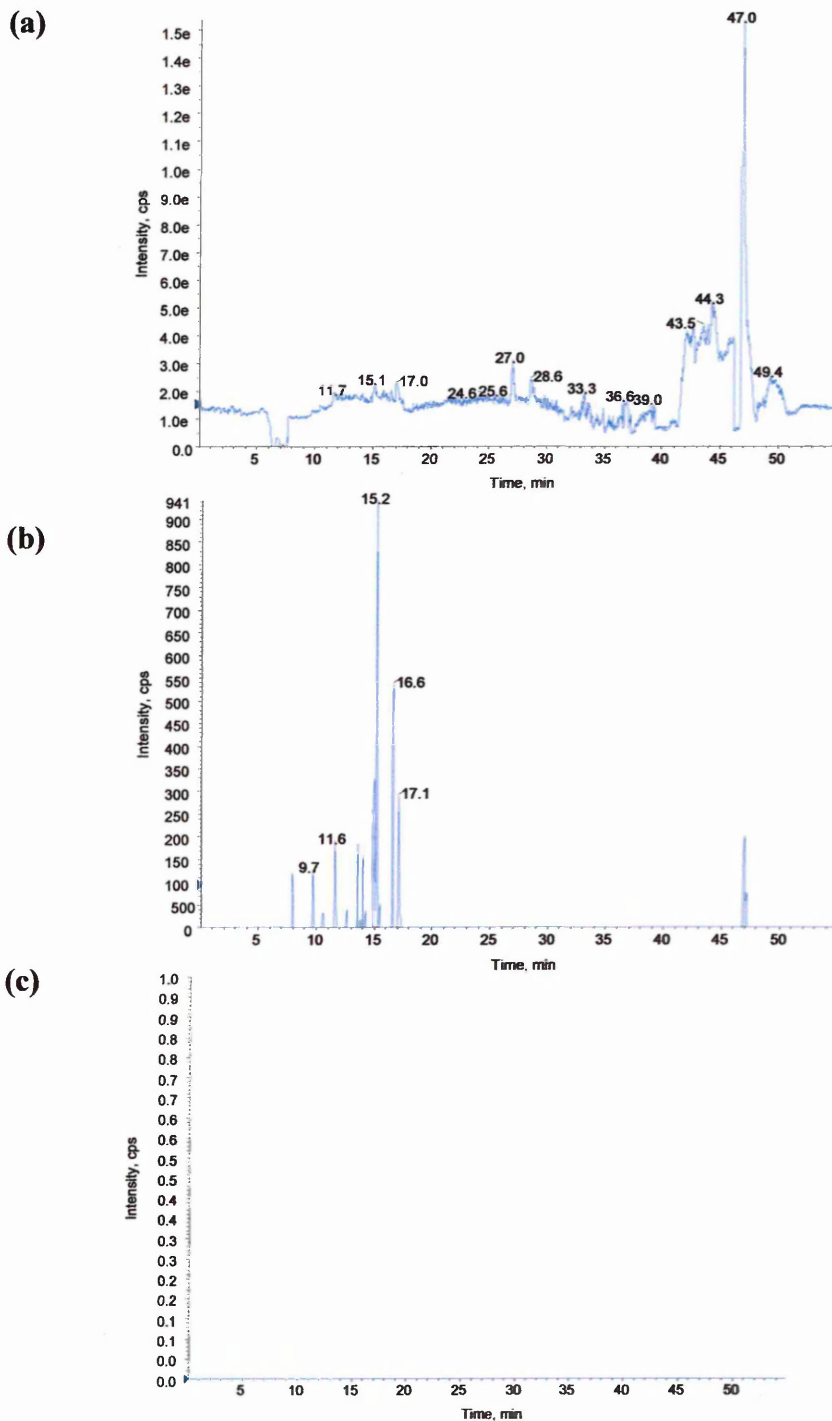


Figure 92. Capillary LC/MS run of an APP α_{695} one-dimensional in-gel Asp-N digest performed using information dependant acquisition (IDA) software. For experimental conditions see chapter 2.92, page 92. (a) Shows the survey scan or total ion chromatogram (TIC). (b) Shows the TIC for the product ion intensities generated by product ion scan of the most intense peak in the normal mass spectrum. (c) Should show the TIC for the product ion intensities generated by product ion scan of the second most intense peak in the normal mass spectrum, however, no data is seen due to the low intensity of the second most intense peak. The peak list generated from trace (b) was sorted according to predefined parameters (chapter 2.92, page 93) and a selection of the most intense peaks automatically sent for MS/MS (figures 93 and 94). (c) Gave no data showing that the intensity of the second most intense peak to be below the threshold of instrumental sensitivity.

mass observed	mass (experimental)	Position (APP α_{695} numbering)	missed cleavages	peptide sequence
424.20	846.40	499-506	0	DALMPSLT
461.73	921.44	284-291	1	DKYLEDPG
468.23	934.45	491-498	0	EPRISYGN
489.23	976.44	482-490	1	DDVLANMIS
579.27	1156.52	525-534	0	DLQPWHSFGA
636.78	1271.55	524-534	1	DDLQPWHSFGA
664.36	1326.71	268-280	0	EVVRVPTTAASTP*
669.76	1337.50	235-245	6	DEVEEEAEEPY
673.82	1345.63	345-356	3	EKVESLEQEAAN
683.70	1365.39	471-481	2	DELLQKEQNYS
750.34	1498.67	535-548	3	DSVPANTENEVEPV
753.89	1505.76	499-512	1	DALMSLTETKTTV

Table 44. BioAnalyst automatic data analysis (using Matrix Science software) of the chromatograms seen in figure 92 of a one-dimensional in-gel Asp-N digest of standard APP α_{695} gave 17% sequence coverage. The sequences highlighted in blue were subjected to MS/MS analysis. MS/MS characterisation of the doubly charged peptide EVVRVPTTAASTP, 1326.71 specific to the APP α_{695} isoform, however, was unsuccessful.

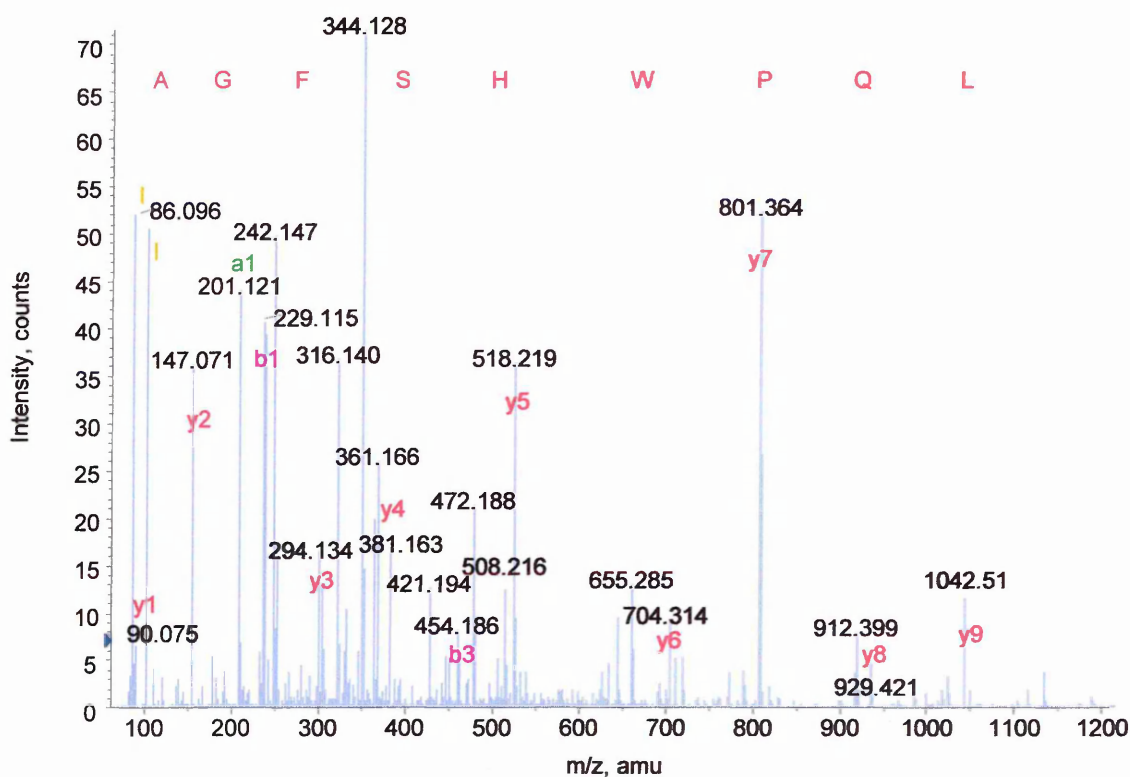


Figure 93. Capillary LC/MS/MS analysis of the doubly charged product ion at m/z 579.27, retention time 15.1 minutes from the LC/MS run of a one-dimensional in-gel Asp-N digest of standard APP α_{695} (figure 92b). This product is consistent with the APP α_{695} Asp-N peptide DLQPWHSFGA, 1156.52 MW.

Amino acid		Ion type (M+H ⁺)						
residue	mass/Da	immonium	a	a-NH ₃	b	b-NH ₃	y	y-NH ₃
L, Leu	113.08	86.09	201.12	184.09	229.11	212.09	1042.51	1025.48
Q, Gln	128.05	101.07	329.18	312.15	357.17	340.15	929.42	912.39
P, Pro	97.05	70.06	426.23	409.20	454.22	437.20	801.36	784.34
W, Trp	186.07	159.09	612.31	595.28	640.30	623.28	704.31	687.28
H, His	137.05	110.07	749.37	732.34	777.36	760.34	518.23	501.20
S, Ser	87.03	60.04	836.40	819.37	864.39	847.37	381.17	364.15
F, Phe	147.06	120.08	983.47	966.44	1011.46	994.44	294.14	277.11
G, Gly	57.02	30.03	1040.44	1023.46	1068.48	1051.46	147.07	130.04
A, Ala	71.03	44.04	1111.53	1094.50	1139.52	1122.50	90.05	73.02

Table 45. BioAnalyst software results of the capillary LC/MS/MS spectrum of the doubly charged product at 579.27 m/z from the one-dimensional in-gel Asp-N digest of standard APP α_{695} shown in figure 93.

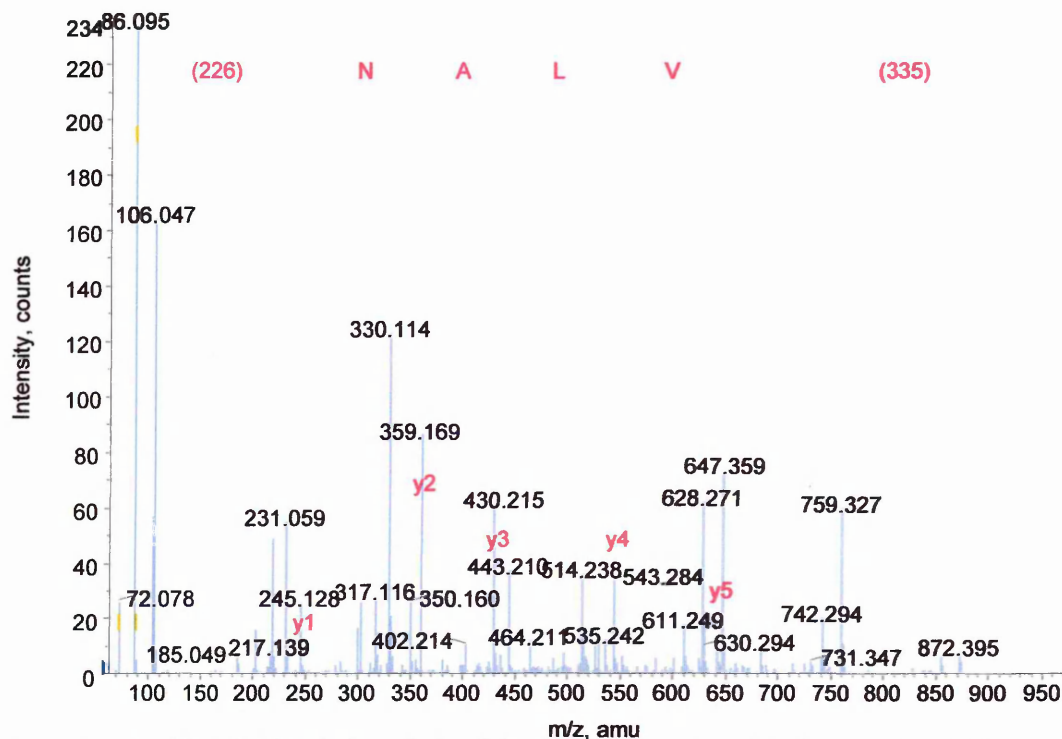


Figure 94. Capillary LC/MS/MS analysis of the doubly charged product ion at m/z 489.23, retention time 16.2 minutes from the LC/MS run of a one-dimensional in-gel Asp-N digest of standard APP α_{695} (figure 92b). This product is consistent with the APP α_{695} Asp-N peptide DDVLANMIS, 976.44 MW and the sequence tag VLAN, verifies this.

Amino acid		Ion type (M+H ⁺)						
residue	mass/Da	immonium	a	a-NH ₃	b	b-NH ₃	y	y-NH ₃
(335.11)	335.11	n/a	308.12	291.09	336.11	319.09	977.45	960.43
V, Val	99.06	72.08	407.19	390.16	435.18	418.16	642.34	625.31
L, Leu	113.08	86.09	520.27	503.24	548.27	531.24	543.27	526.25
A, Ala	71.03	44.04	591.31	574.28	619.30	602.28	430.19	413.16
N, Asn	114.04	87.05	705.35	688.32	733.35	716.32	359.15	342.13
(226.09)	226.09	n/a	931.45	914.42	959.44	942.42	245.11	228.08

Table 46. BioAnalyst software results of the capillary LC/MS/MS spectrum of the doubly charged product at m/z 489.23 from the one-dimensional in-gel Asp-N digest of standard APP α_{695} shown in figure 94.

Amyloid precursor protein standard was purchased from Sigma for use as a direct comparison. The standard was the alpha secretase cleaved APP₆₉₅ isoform (APP α ₆₉₅) from E.coli origin.

The MALDI-MS analysis of the one-dimensional in-gel Asp-N digestion of APP α ₆₉₅ (figure 89) gave amino acid sequence coverage of 18% of the APP α ₆₉₅ molecule from 14 Asp-N peptides. The sequence coverage achieved from the LC/MS (figure 92) was very similar covering 17% of the protein sequence from 12 peptides and both methods again showed missed cleavage peptides suggesting that Asp-N under the conditions applied is cleaving inefficiently and factors regarding the digest procedure may need to be adjusted. MS/MS data was available for both techniques giving conclusive evidence of the peptides authenticity. MALDI-MS/MS uncovered a full sequence (figure 90) and a generous sequence tag (figure 91) and the LC/MS/MS examination gave two sequence tags (figures 93 and 94). The unique Asp-N peptide exhibited by APP α ₆₉₅ (position 268-280, monoisotopic mass 1326.6216, amino acid sequence EVVPTTAASTP) was present in both the MALDI-MS and LC/MS data. Observed as the peak at m/z 1327.75 in the MALDI-MS spectrum (figure 89) and its presence within the LC/MS chromatograms was highlighted in the BioAnalyst search results (table 43). MS/MS confirmation of this peptide, however, was not achieved.

3.425 MALDI-MS analysis of a one-dimensional in-gel Asp-N digestion of immunoprecipitated alpha secretase cleaved amyloid precursor protein, isoform 770 (APP α_{770}).

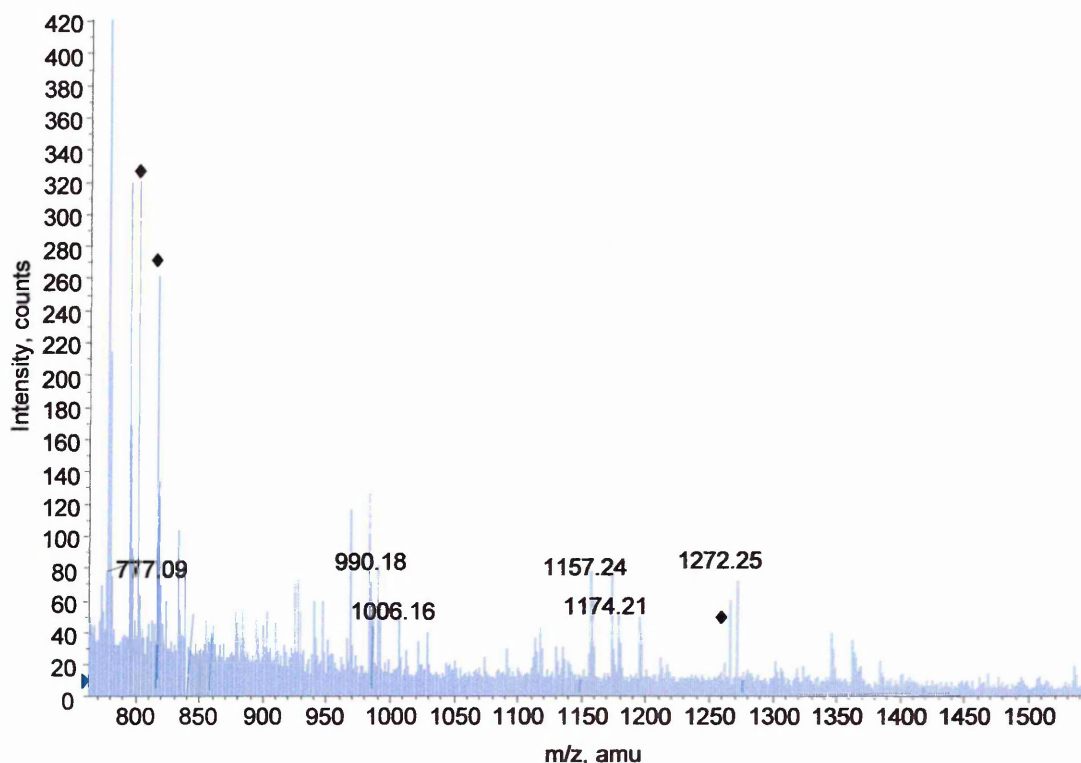


Figure 95. MALDI-MS spectrum of an in-gel Asp-N digest of APP α_{770} from a one-dimensional gel. The peaks believed to be due to keratin contamination are marked with a black diamond. Other unmarked peaks are of unknown origin.

mass (M+H ⁺)	mass (experimental)	position (APP α_{770} numbering)	missed cleavages	peptide sequence
777.40	777.09	665-670	0	EVHHQK
990.44	990.18	423-431	2	ESLEQEAAAN
1006.43	1006.16	190-198	1	DVWWGGADT
1157.54	1157.24	600-609	0	DLQPWHSFGA
1174.52	1174.21	610-620	2	DSVPANTENEV
1272.56	1272.25	599-609	1	DDLQPWHSFGA

Table 47. Mascot search results from the MALDI-MS mass fingerprint of the one-dimensional in-gel Asp-N digest (figure 95) yielding 6% sequence coverage. Although MS/MS analysis was attempted upon all the peaks present within the MALDI-MS spectrum (figure 95) none were successful.

3.426 Capillary LC/MS analysis of a one-dimensional in-gel Asp-N digestion of immunoprecipitated APP α_{770} .

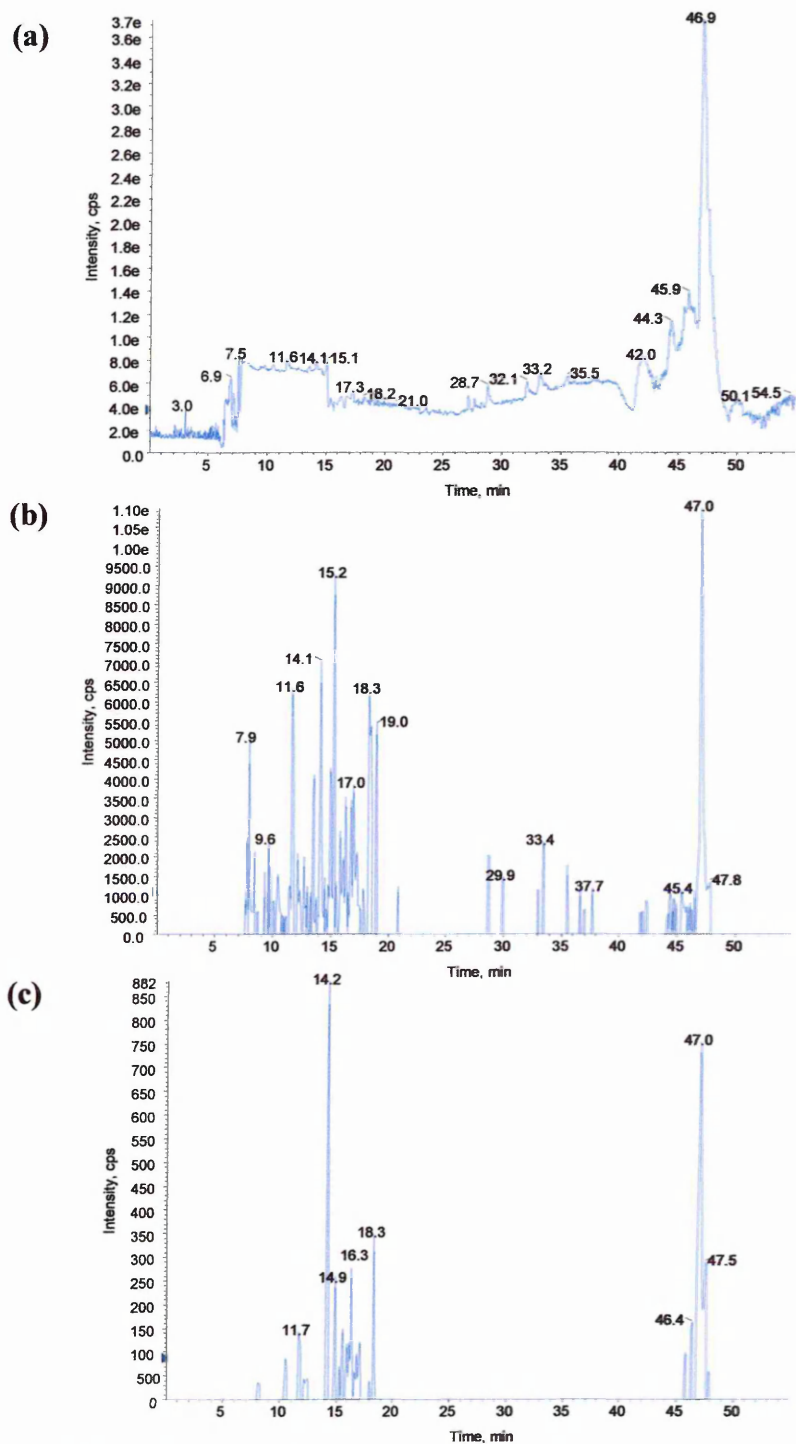


Figure 96. Capillary LC/MS run of an APP α_{770} one-dimensional in-gel Asp-N digest performed using information dependant acquisition (IDA) software. For experimental conditions see chapter 2.92, page 92. (a) Shows the survey scan or total ion chromatogram (TIC). (b) Shows the TIC for the product ion intensities generated by product ion scan of the most intense peak in the normal mass spectrum. (c) Shows the TIC for the product ion intensities generated by product ion scan of the second most intense peak in the normal mass spectrum. The peak lists generated from traces (b) and (c) were sorted according to predefined parameters (chapter 2.92, page 93) and a selection of the most intense peaks automatically sent for MS/MS (figures 97 and 98).

mass observed	mass (experimental)	position (APP α_{770} numbering)	missed cleavages	peptide sequence
636.78	1271.55	599-609	1	DDLQPWHSFGA
683.82	1365.62	546-556	2	DELLQKEQNYS

Table 48. BioAnalyst automatic data analysis (using Matrix Science software) of the chromatograms seen in figure 96 of a one-dimensional in-gel Asp-N digest of APP α_{770} gave 3% sequence coverage.

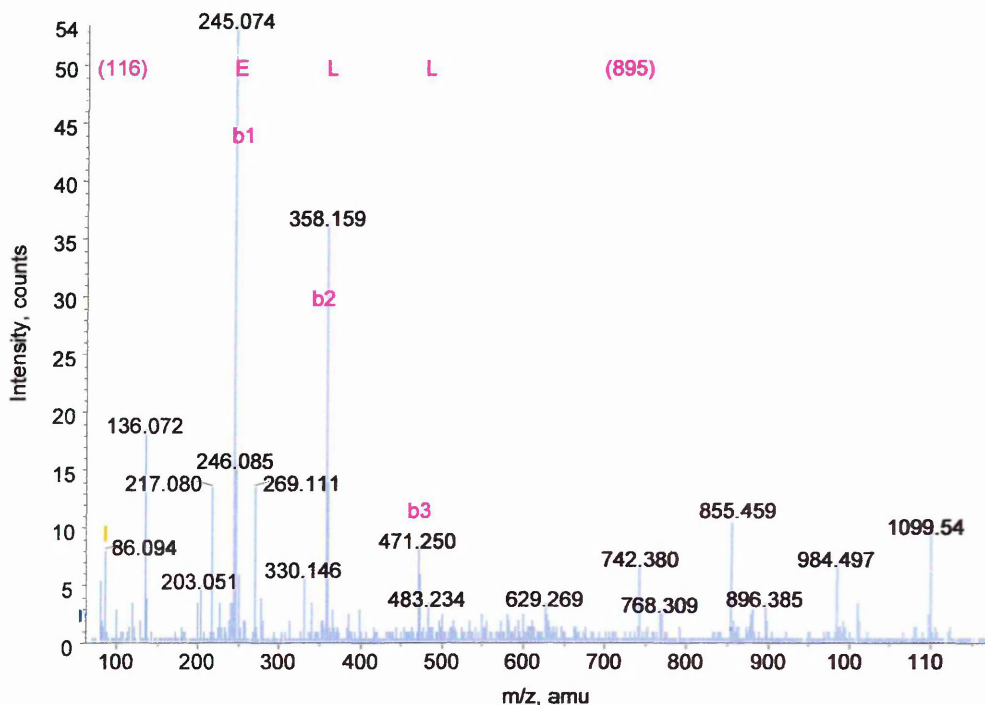


Figure 97. Capillary LC/MS/MS analysis of the doubly charged product ion at m/z 683.82, retention time 9.7 minutes from the LC/MS run of a one-dimensional in-gel Asp-N digest of APP α_{770} (figure 96b). This product is consistent with the APP α_{770} Asp-N peptide DELLQKEQNYS, 1365.62 MW and the sequence tag ELL verifies this.

Amino acid		Ion type ($M+H^+$)						
residue	mass/Da	immonium	a	a-NH ₃	b	b-NH ₃	y	y-NH ₃
(116.22)	115.02	n/a	88.03	71.01	116.03	99.00	1408.65	1391.63
E, Glu	129.04	102.05	217.08	200.05	245.07	228.05	1293.63	1276.60
L, Leu	113.08	86.09	330.16	313.13	358.16	341.13	1164.58	1147.56
L, Leu	113.08	86.09	443.25	426.22	471.24	454.21	1051.50	1034.47
(895.46)	895.46	n/a	1338.71	1321.68	1366.70	1349.67	1946.96	1929.93

Table 49. BioAnalyst automated searching of the capillary LC/MS/MS spectrum of the doubly charged product at m/z 683.82 from the one-dimensional in-gel Asp-N digest of APP α_{770} shown in figure 97, shows the 'a', 'b' and 'y' product ions from the sequence tag ELL.

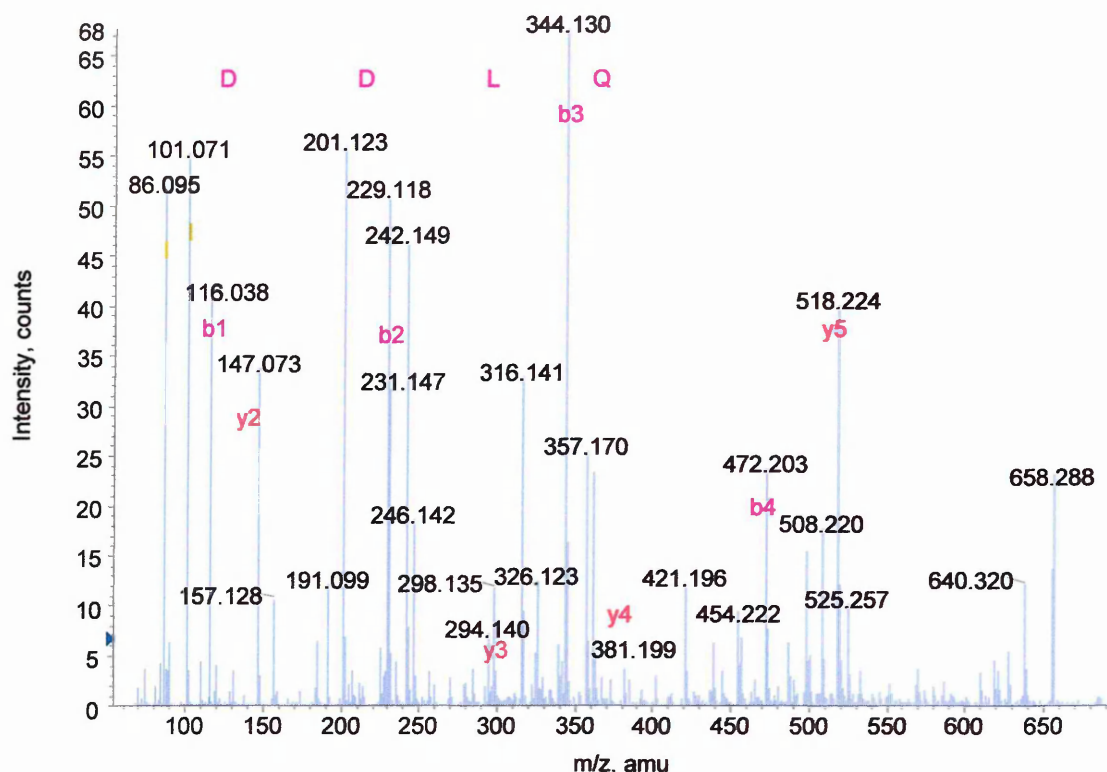


Figure 98. Capillary LC/MS/MS analysis of the doubly charged product ion at m/z 636.78, retention time 14.9 minutes from the LC/MS run of a one-dimensional in-gel Asp-N digest of APP α_{770} (figure 96c). This product is consistent with the APP α_{770} Asp-N peptide DDLQPWHSFGA, 1271.55 MW and the sequence tags DDLQ ('b' ions) and HSFG ('y' ions) expand this.

Amino acid		Ion type (M+H ⁺)						
residue	mass/Da	immonium	a	a-NH ₃	b	b-NH ₃	y	y-NH ₃
D, Asp	115.02	88.03	88.03	71.01	116.03	99.00	1272.56	1255.53
D, Asp	115.02	88.03	203.06	186.03	231.06	214.03	1157.53	1140.51
L, Leu	113.08	86.09	316.15	299.12	344.14	327.11	1042.51	1025.48
Q, Gln	128.05	101.07	444.20	427.18	472.20	455.17	929.42	912.39
P, Pro	97.05	70.06	541.26	524.23	569.25	552.23	801.36	784.34
W, Trp	186.07	159.09	727.34	710.31	755.33	738.30	704.31	687.28
H, His	137.05	110.07	864.39	847.37	892.39	875.36	518.23	501.20
S, Ser	87.03	60.04	951.43	934.40	979.42	962.40	381.17	364.15
F, Phe	147.06	120.00	1098.50	1081.47	1126.49	1109.46	294.14	277.11
G, Gly	57.02	30.03	1155.52	1138.49	1183.51	1166.49	147.07	130.04
A, Ala	71.03	44.04	1226.55	1209.53	1254.55	1237.52	90.05	73.02

Table 50. BioAnalyst automated searching of the capillary LC/MS/MS spectrum from the one-dimensional in-gel Asp-N digest of APP α_{770} shown in figure 98, shows the 'a', 'b' and 'y' product ions for the sequence DDLQPWHSFGA, highlighting the ions present.

The alpha secretase cleaved amyloid precursor protein, isoform 770 (APP α_{770}) was immunoprecipitated from CHO 770 cell secretions.

The MALDI-MS examination of the one-dimensional in-gel Asp-N digestion of APP α_{770} (figure 95) gave amino acid sequence coverage of 6% of the APP α_{770} molecule from 6 Asp-N peptides. The sequence coverage achieved from the LC/MS (figure 96) analysis was poorer giving 3% of the protein sequence from 2 peptides. The poor sequence coverage may possibly be due to low protein concentration and insufficient digestion by Asp-N. The inferior LC/MS data may be a result of variations in manual and automatic peak retrieval. As the LC/MS data is processed without human intervention it is possible that peaks of interest may be overlooked, however, with low-level digests, such as these, although peptides may be visible within the MALDI-MS spectra the low concentrations make it such that MS/MS analysis is unattainable. LC/MS/MS analysis was more successful resulting in two sequence tags (figures 97 and 98) sufficient to achieve positive results from the automated search engine. APP α_{770} produces two unique Asp-N peptides (position 318-337, MW 2149.8589 and position 343-355, MW 1296.5998) regrettably neither of these peptides was detected by either technique.

3.427 MALDI-MS analysis of a one-dimensional in-gel Asp-N digestion of immunoprecipitated alpha secretase cleaved amyloid precursor protein (APP α).

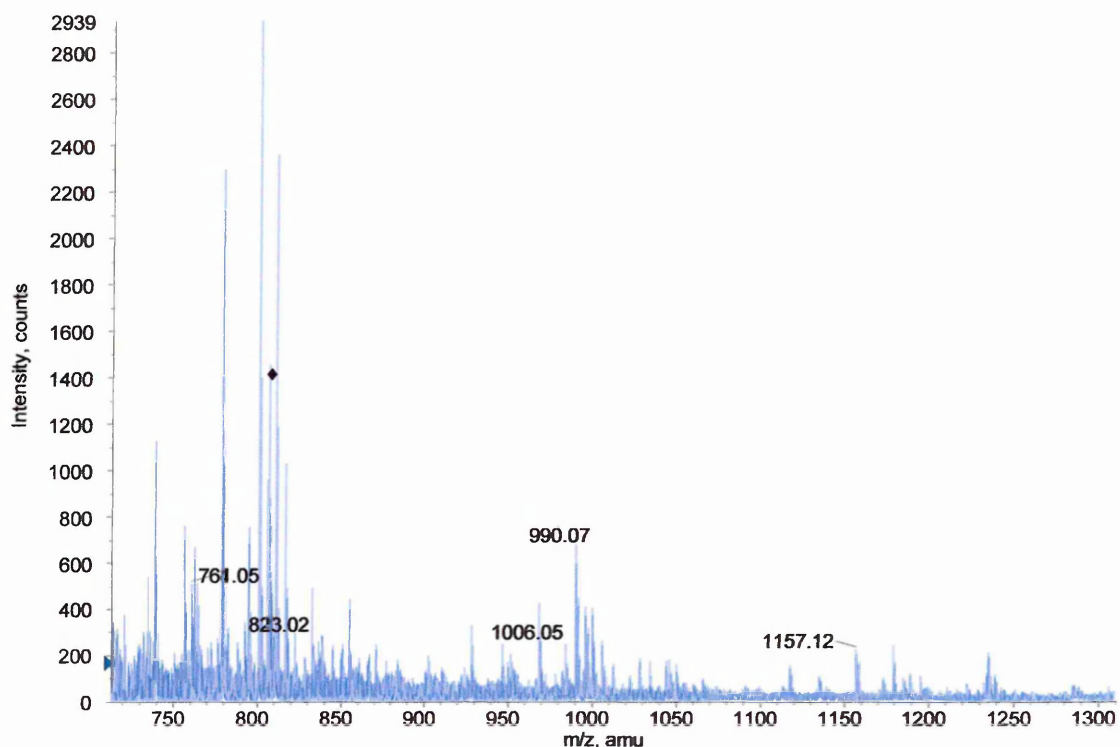


Figure 99. MALDI-MS spectrum of an in-gel Asp-N digest of APP α from a one-dimensional gel. The overwhelming presence of contaminating species within this spectrum needs further investigation, which in turn may help reveal why the Asp-N digests are not achieving adequate sequence coverage.

mass (M+H ⁺)	mass (experimental)	position	missed cleavages	peptide sequence
761.29	761.05	363-369	2	ETPGDEN
823.42	823.02	356-362	1	DAVDKYL
990.44	990.07	423-431	2	ESLEQEAAN
1006.43	1006.05	190-198	1	DVWWGGADT
1157.54	1157.12	600-609	0	DLQPWHSFGA

Table 51. Mascot search results from the MALDI-MS mass fingerprint of the one-dimensional in-gel Asp-N digest of APP α (figure 99), containing the three isoforms of interest (695, 751 and 770), giving possible sequence coverage of 5% of the peptide sequence although no specific isoforms are seen and MS/MS analysis was unsuccessful.

3.428 Capillary LC/MS analysis of a one-dimensional in-gel Asp-N digestion of immunoprecipitated APP α .

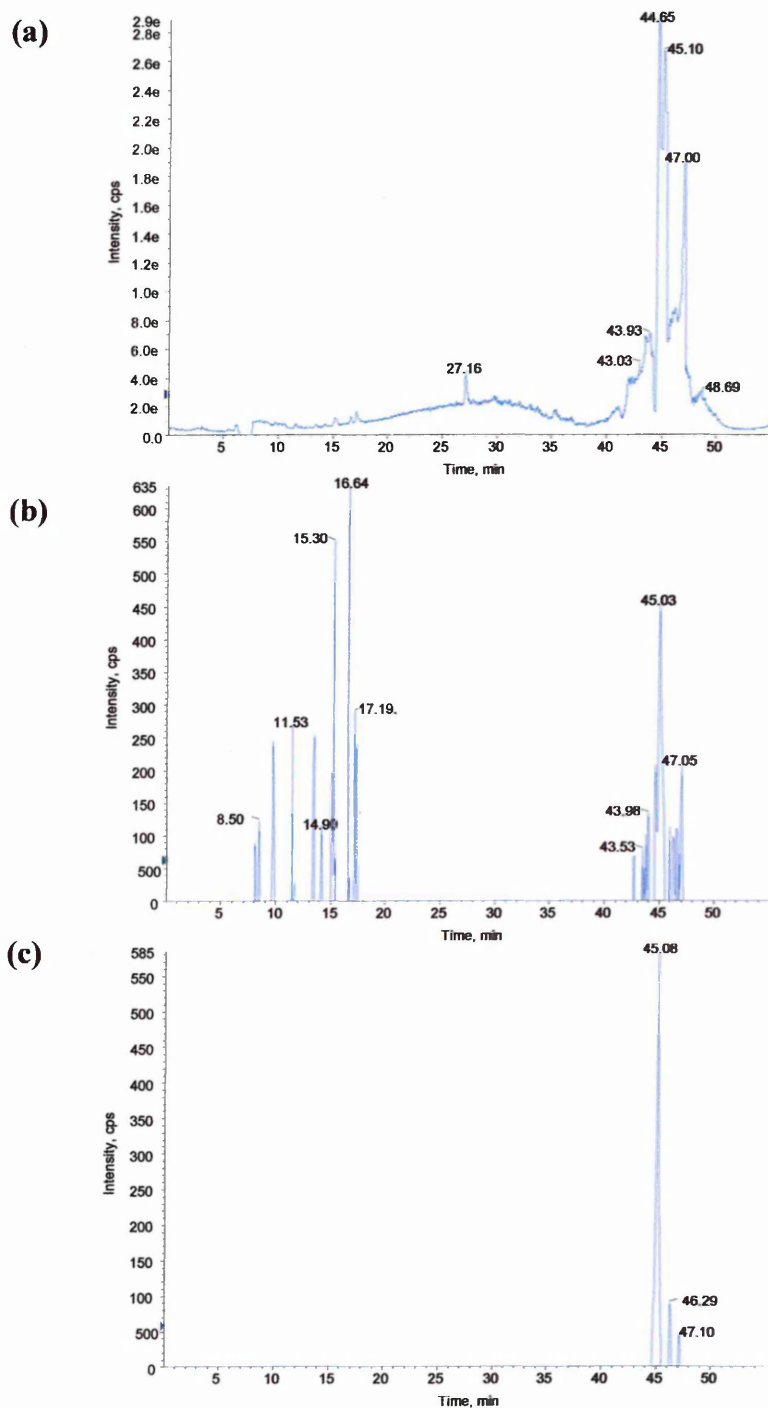


Figure 100. Capillary LC/MS run of an APP α one-dimensional in-gel Asp-N digest performed using information dependant acquisition (IDA) software. For experimental conditions see chapter 2.92, page 92. (a) Shows the survey scan or total ion chromatogram (TIC). (b) Shows the TIC for the product ion intensities generated by product ion scan of the most intense peak in the normal mass spectrum. (c) Shows the TIC for the product ion intensities generated by product ion scan of the second most intense peak in the normal mass spectrum. The peak list generated from trace (b) was sorted according to predefined parameters (chapter 2.92, page 93) and a selection of the most intense peaks automatically sent for MS/MS (figure 101).

mass observed	mass (experimental)	position (sAPP ₇₇₀ numbering)	missed cleavages	peptide sequence
489.23	976.44	556-565	1	DDVLANMIS
636.80	1271.59	599-609	1	DDLQPWHSFGA

Table 52. BioAnalyst automatic data analysis (using Matrix Science software) of the chromatograms seen in figure 100 of a one-dimensional in-gel Asp-N digest of APP α gave sequence coverage of 2%. The sequence highlighted in blue was the only peptide that gave useful MS/MS data.

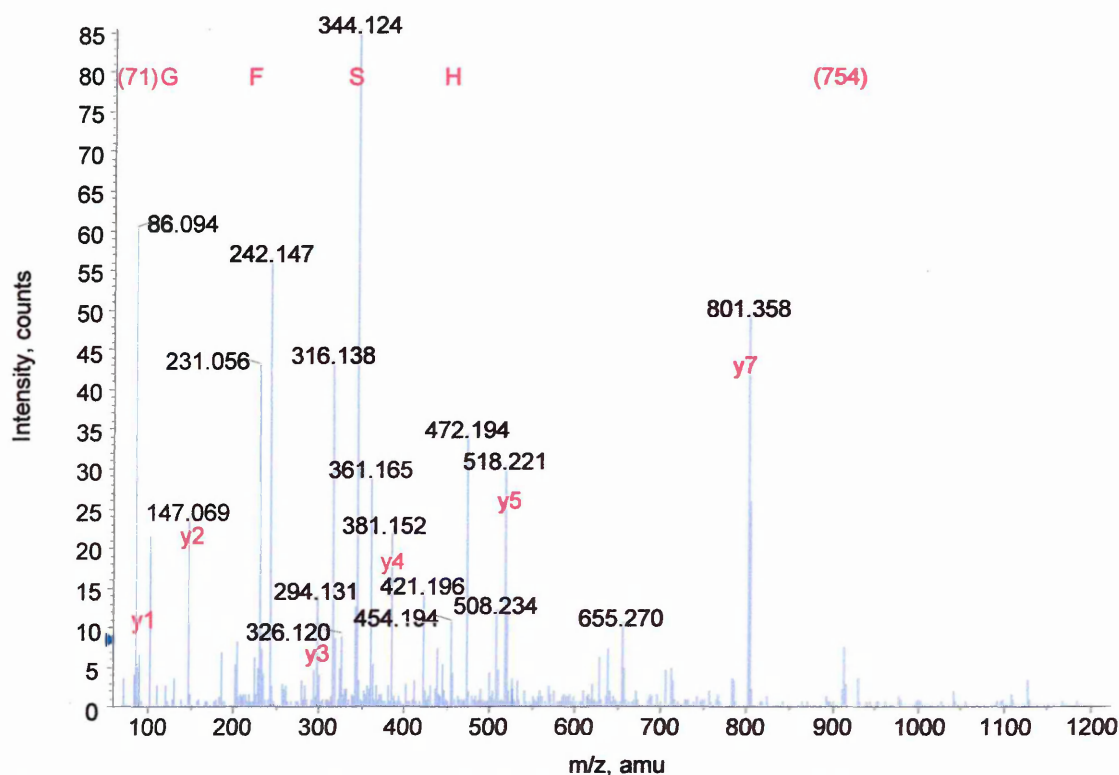


Figure 101. Capillary LC/MS/MS analysis of the doubly charged product ion at 636.80 m/z, retention time 14.8 minutes from the LC/MS run of a one-dimensional in-gel Asp-N digest of APP α (figure 100b). This product is consistent with the APP α Asp-N peptide DDLQPWHSFGA, 1271.59 MW and the sequence tag HSFSG verifies this.

Amino acid		Ion type (M+H ⁺)						
residue	mass/Da	immonium	a	a-NH ₃	b	b-NH ₃	y	y-NH ₃
(754.28)	754.28	n/a	727.29	710.26	755.28	738.26	1272.50	1255.48
H, His	137.05	110.07	864.35	847.32	892.34	875.32	518.22	501.19
S, Ser	87.03	60.04	951.38	934.35	979.38	962.35	381.15	364.13
F, Phe	147.06	120.08	1098.45	1081.42	1126.44	1109.42	294.13	277.10
G, Gly	57.02	30.03	1155.47	1138.44	1183.47	1166.44	147.06	130.03
(71.02)	71.02	n/a	1226.50	1209.47	1254.49	1237.47	90.04	73.01

Table 53. BioAnalyst automated searching of the capillary LC/MS/MS spectrum from the one-dimensional in-gel Asp-N digest of APP α shown in figure 101, shows the product ions from the sequence tag HSFSG.

The alpha secretase cleaved amyloid precursor protein (APP α) was immunoprecipitated from Ntera 2 cell secretions. APP α encompasses all three isoforms of interest (APP α_{695} , APP α_{751} , APP α_{770}) and as such is a more plausible model of *in vivo* conditions.

The MALDI-MS results from the one-dimensional in-gel Asp-N digestion of APP α (figure 99) gave amino acid sequence coverage of 5% of the APP α molecule from 5 Asp-N peptides. The sequence coverage achieved from the LC/MS (figure 100) analysis was poorer giving 2% of the protein sequence from only 2 peptides. The Asp-N digestion methodology needs to be investigated in order to establish a possible cause for the low sequence coverage. Again the inferior LC/MS results in this instance could be due to the variations in manual and automatic peak retrieval. Although MALDI-MS/MS analysis was insufficient for protein verification the LC/MS/MS data gave one sequence tag (figure 101) from the two peptides revealed allowing protein identification using the online search engine. APP α encompasses all three isoforms of interest (APP α_{695} , APP α_{751} and APP α_{770}) all of which exhibit specific Asp-N peptides, disappointingly none of these were detected.

3.43 One-dimensional in-gel formic acid digestion of BSA and APP.

3.431 MALDI-MS analysis of a one-dimensional in-gel formic acid digestion of BSA.

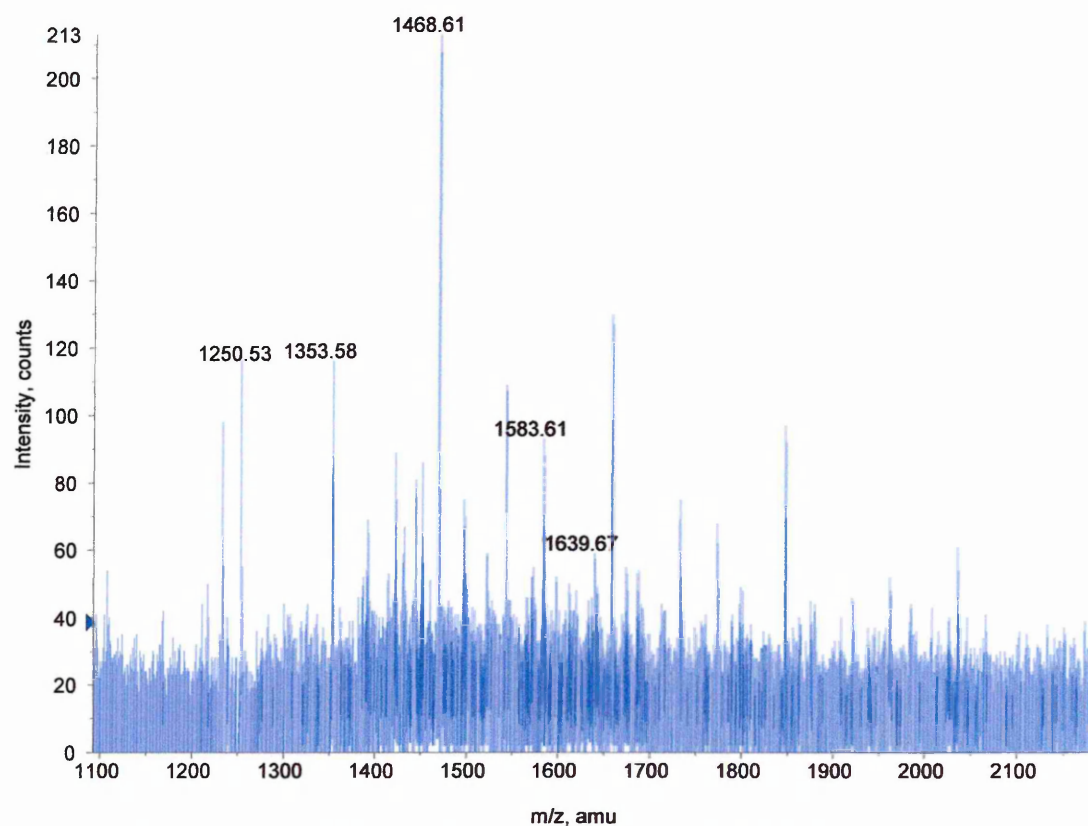


Figure 102. MALDI-MS spectrum of a one-dimensional in-gel formic acid digest of BSA dominated by the presence of noise and contamination that may be caused by the formic acid digestion being too harsh cleaving areas within the protein other than the specified bonds (*N* and *C* termini of aspartic acid) or perhaps the presence of intermediates present within the cleavage pathway.

mass ($M+H^+$)	mass (experimental)	position	missed cleavages	peptide sequence
1250.66	1250.53	319-330	1	DAIPENLPPLTA
1353.72	1353.58	303-314	1	DKPLLEKSHCIA
1468.77	1468.61	25-36	1	DTHKSEIAHRFK
1583.80	1583.61	319-333	2	DAIPENLPPLTADFA
1639.74	1639.67	278-291	3	DDRADLAKYICDNQ

Table 54. Mascot search results from the one-dimensional in-gel formic acid digest of BSA (figure 102), showing 5% sequence coverage. MS/MS analysis of the peptide sequences shown was unsuccessful.

3.432 Capillary LC/MS analysis of a one-dimensional in-gel formic acid digestion of BSA.

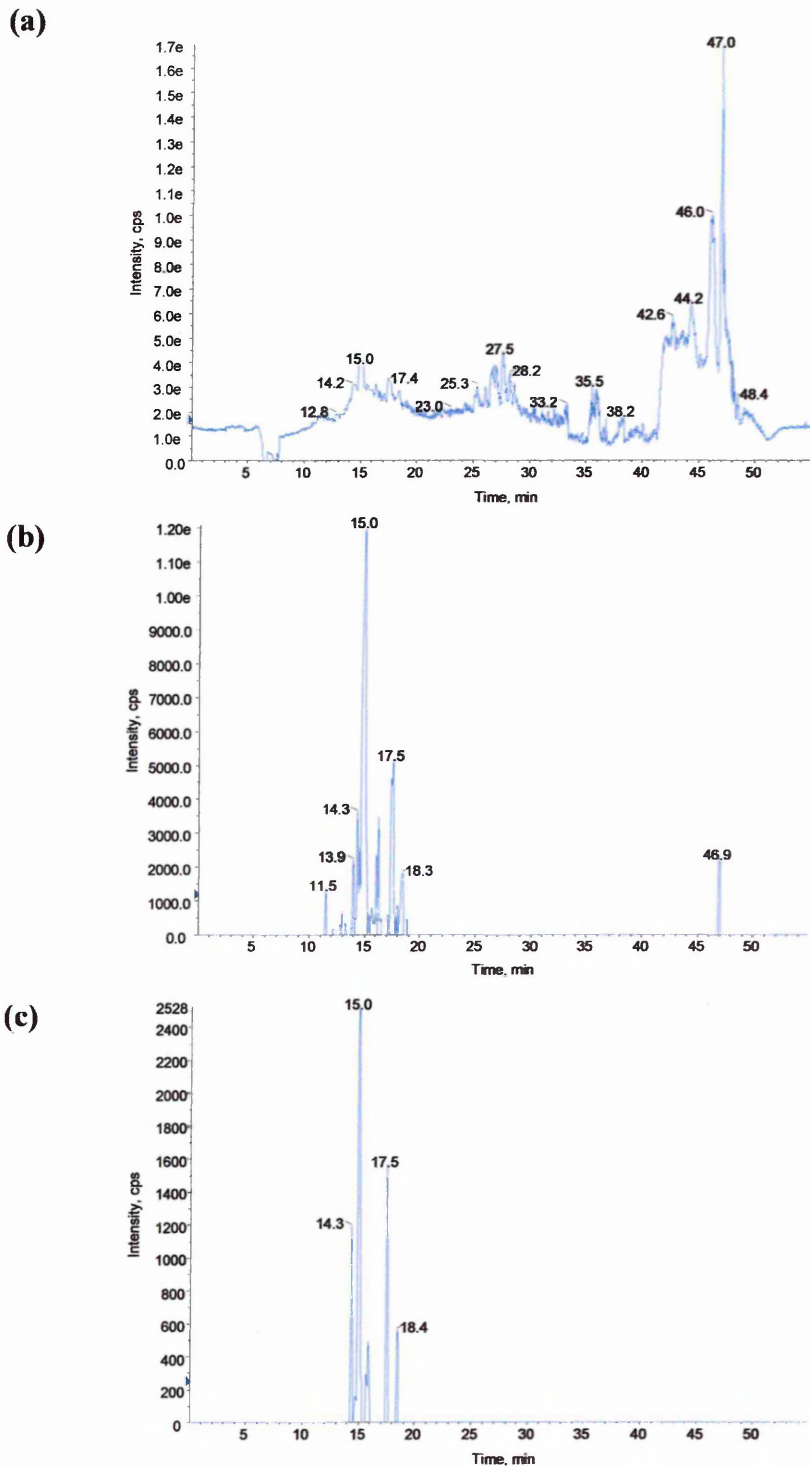


Figure 103. Capillary LC/MS run of a BSA one-dimensional in-gel formic acid digest performed using information dependant acquisition (IDA) software. For experimental conditions see chapter 2.92, page 92. (a) Shows the survey scan or total ion chromatogram (TIC). (b) Shows the TIC for the product ion intensities generated by product ion scan of the most intense peak in the normal mass spectrum. (c) Shows the TIC for the product ion intensities generated by product ion scan of the second most intense peak in the normal mass spectrum. The peak lists generated from traces (b) and (c) were sorted according to predefined parameters (chapter 2.92, page 93) and a selection of the most intense peaks automatically sent for MS/MS, unfortunately no data was achieved.

mass observed	mass (experimental)	position	missed cleavages	peptide sequence
856.91	1711.80	320-335	1	AIPENLPPLTADFAED
652.65	1954.94	319-336	4	DAIPENLPPLTADFAEDK

Table 55. BioAnalyst automatic data analysis (using Matrix Science software) of the chromatograms shown in figure 103 of a one-dimensional in-gel formic acid digest of BSA gave 3% sequence coverage.

Bovine serum albumin (BSA, MW 66,432.96) was used as a standard due to its availability and similarity in molecular weight to the amyloid precursor protein isoforms (APP α_{695} , MW 67,708.02, APP α_{751} , MW 73,863.85, APP α_{770} , MW 75,988.34).

The MALDI-MS analysis of the one-dimensional in-gel formic acid digest of BSA (figure 102) resulted in 5 formic acid peptides covering 5% of the protein. LC/MS analysis (figure 103) of the same sample revealed 2 formic acid peptides for BSA, which covered 3% of the protein sequence. Neither MALDI-MS/MS nor LC/MS/MS analysis of the peaks revealed failed to uncover any of the sequences placing a question mark over the actual authenticity of the data achieved.

3.433 MALDI-MS analysis of a one-dimensional in-gel formic acid digestion of alpha secretase cleaved amyloid precursor protein standard, isoform 695 (APP α_{695}).

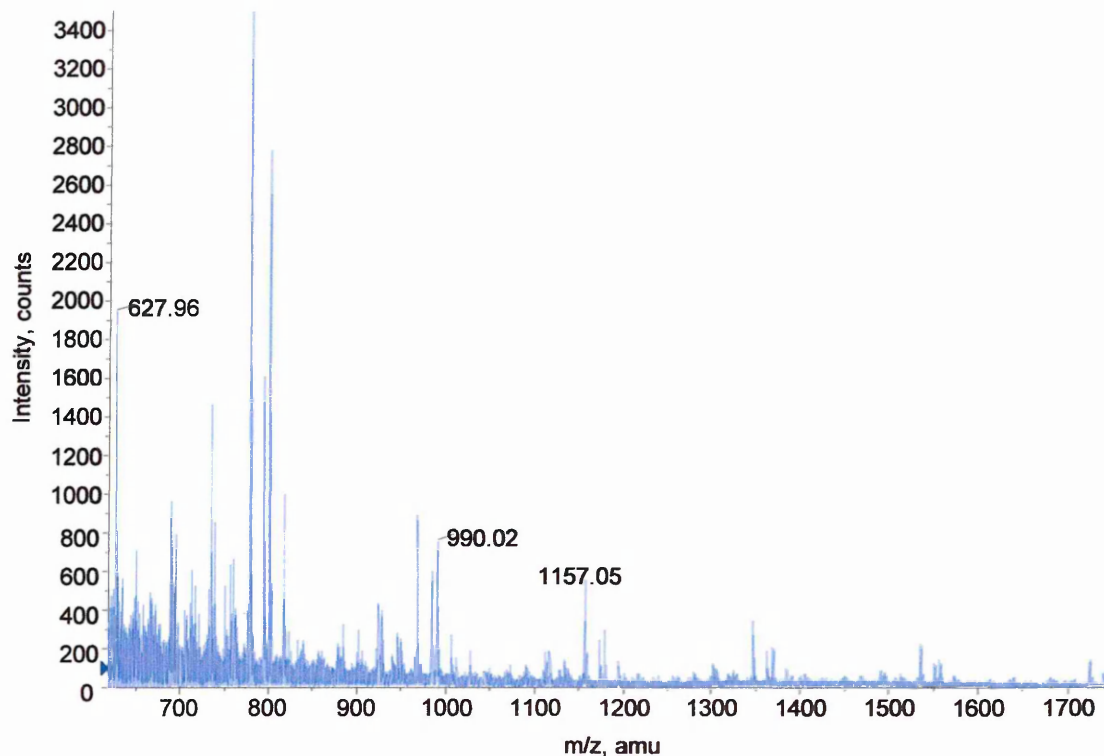


Figure 104. MALDI-MS spectrum of a one-dimensional in-gel formic acid digest of standard APP α_{695} . The principal peaks shown here are possibly due to the presence of adduct formation or contamination as a result of the formic acid cleavage pathway.

mass (M+H ⁺)	mass (experimental)	position (APP α_{770} numbering)	missed cleavages	peptide sequence
627.37	627.96	108-113	0	DALLVP
990.44	990.02	423-431	2	ESLEQEAAN
1157.54	1157.05	600-609	0	DLQPWHSFGA

Table 56. Mascot search results from the MALDI-MS of the one-dimensional in-gel formic acid digest of APP α_{695} (figure 104) covering 2% of the peptide sequence although lack of any MS/MS data to support these peptides places uncertainty over their authenticity.

3.434 Capillary LC/MS analysis of a one-dimensional in-gel formic acid digestion of standard APP α_{695} .

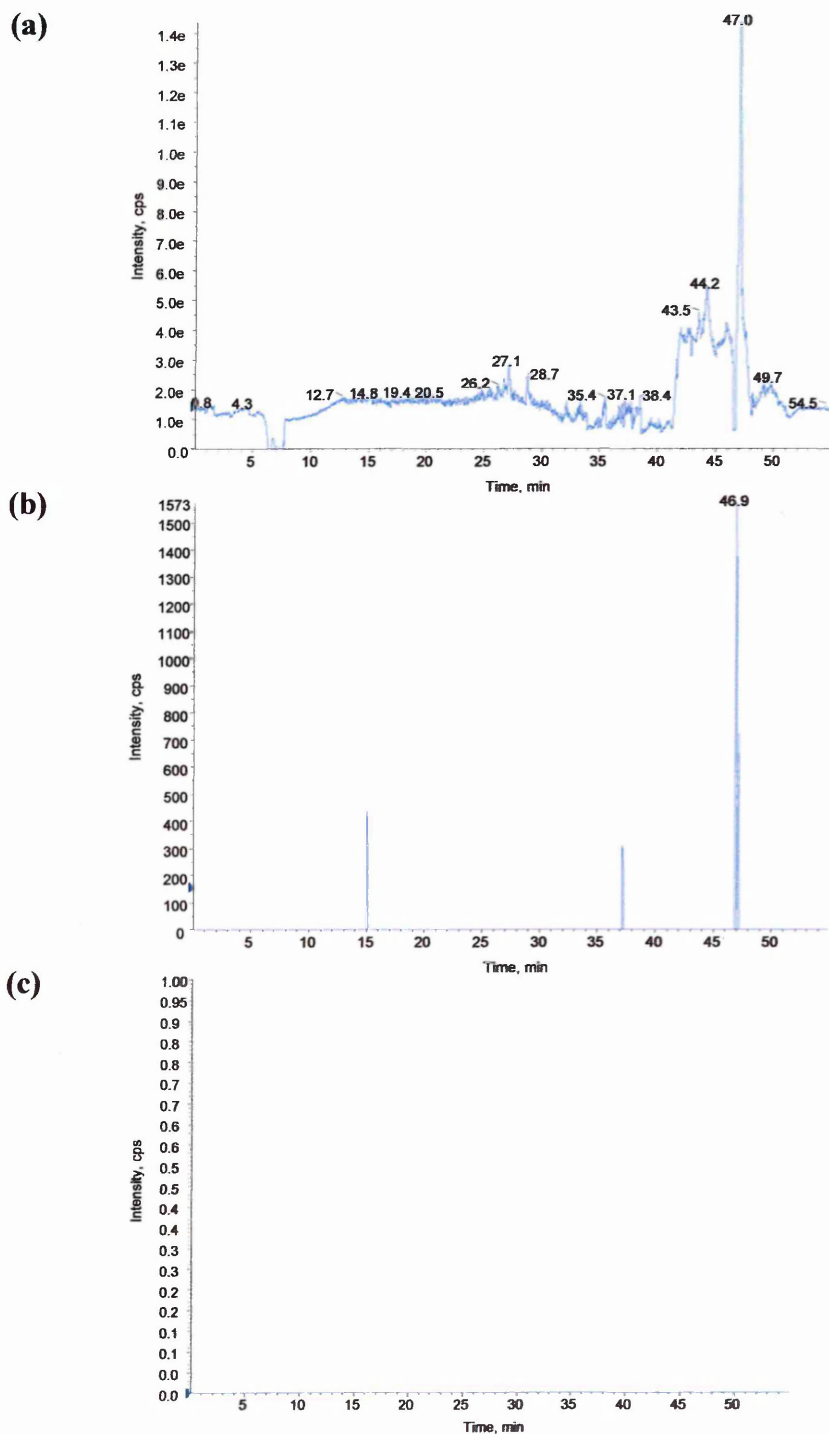


Figure 105. Capillary LC/MS run of an APP α_{695} one-dimensional in-gel formic acid digest performed using information dependant acquisition (IDA) software. For experimental conditions see chapter 2.92, page 92. (a) Shows the survey scan or total ion chromatogram (TIC). (b) Shows the TIC for the product ion intensities generated by product ion scan of the most intense peak in the normal mass spectrum. (c) Should show the TIC for the product ion intensities generated by product ion scan of the second most intense peak in the normal mass spectrum.

Amyloid precursor protein standard was purchased from Sigma for use as a direct comparison. The standard was the alpha secretase cleaved APP isoform 695 (APP α_{695}) from E.coli origin.

The MALDI-MS examination of the one-dimensional in-gel formic acid digestion of APP α_{695} (figure 104) gave amino acid sequence coverage of 2% of the APP α_{695} molecule from 3 formic acid peptides, however, MS/MS analysis of these peaks did not reveal any peptide sequences. The LC/MS analysis (figure 105) did not reveal any formic acid peptides for APP α_{695} and as such no LC/MS/MS data was achieved. The appearance of both the MALDI-MS spectrum and LC/MS chromatograph as well as the lack of MS/MS data places uncertainty over the results achieved. It is possible that the formic acid digest procedure is either hydrolysing at more positions within the peptide than stated or an incomplete reaction has occurred creating intermediates of the reaction pathway.

3.435 MALDI-MS analysis of a one-dimensional in-gel formic acid digestion of immunoprecipitated alpha secretase cleaved amyloid precursor protein, isoform 770 (APP α_{770}).

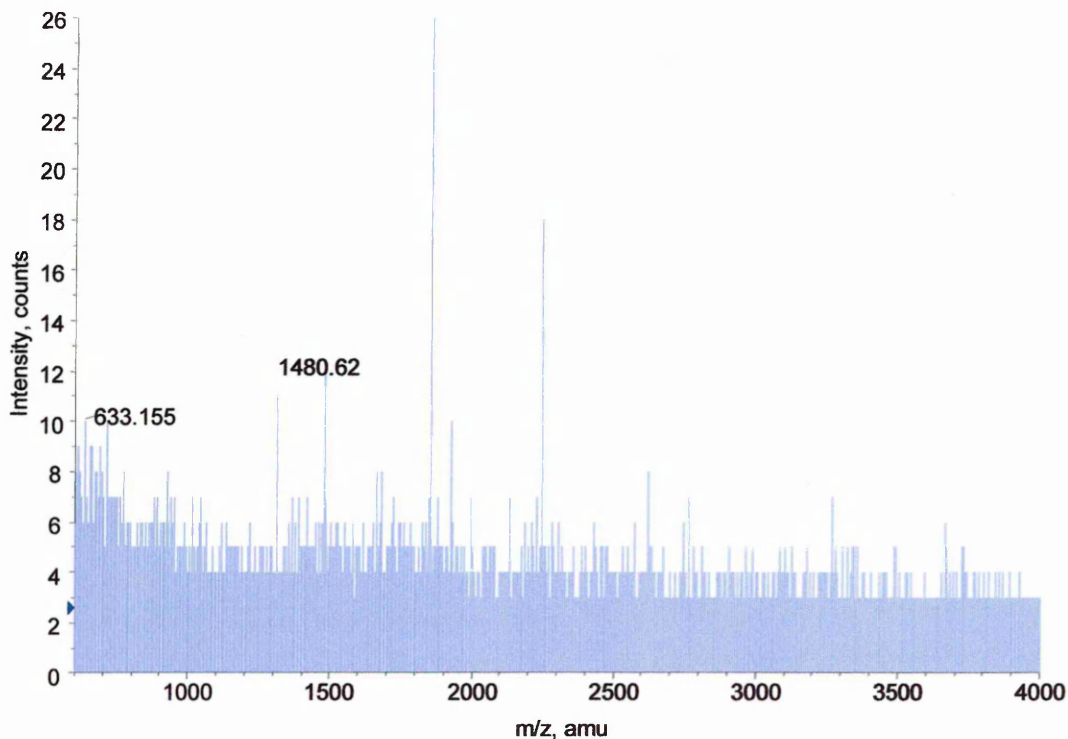


Figure 106. MALDI-MS spectrum of an in-gel formic acid digest of APP α_{770} from a one-dimensional gel. Very poor spectra overwhelmed by noise puts forward the strong possibility that the annotated peaks may not be real.

mass (M+H ⁺)	mass (experimental)	position (APP α_{695} numbering)	missed cleavages	peptide sequence
633.27	633.16	520-524	2	EEIQD
1480.67	1480.62	368-378	2	ERMSQVMREWE

Table 57. Mascot search results from the MALDI-MS mass fingerprint of the one-dimensional in-gel formic acid digest (figure 106) yielding 2% sequence coverage. Low sequence coverage, lack of MS/MS data and the appearance of the MALDI-MS spectrum (figure 106) places ambiguity over these results.

3.436 Capillary LC/MS analysis of a one-dimensional in-gel formic acid digestion of immunoprecipitated APP α_{770} .

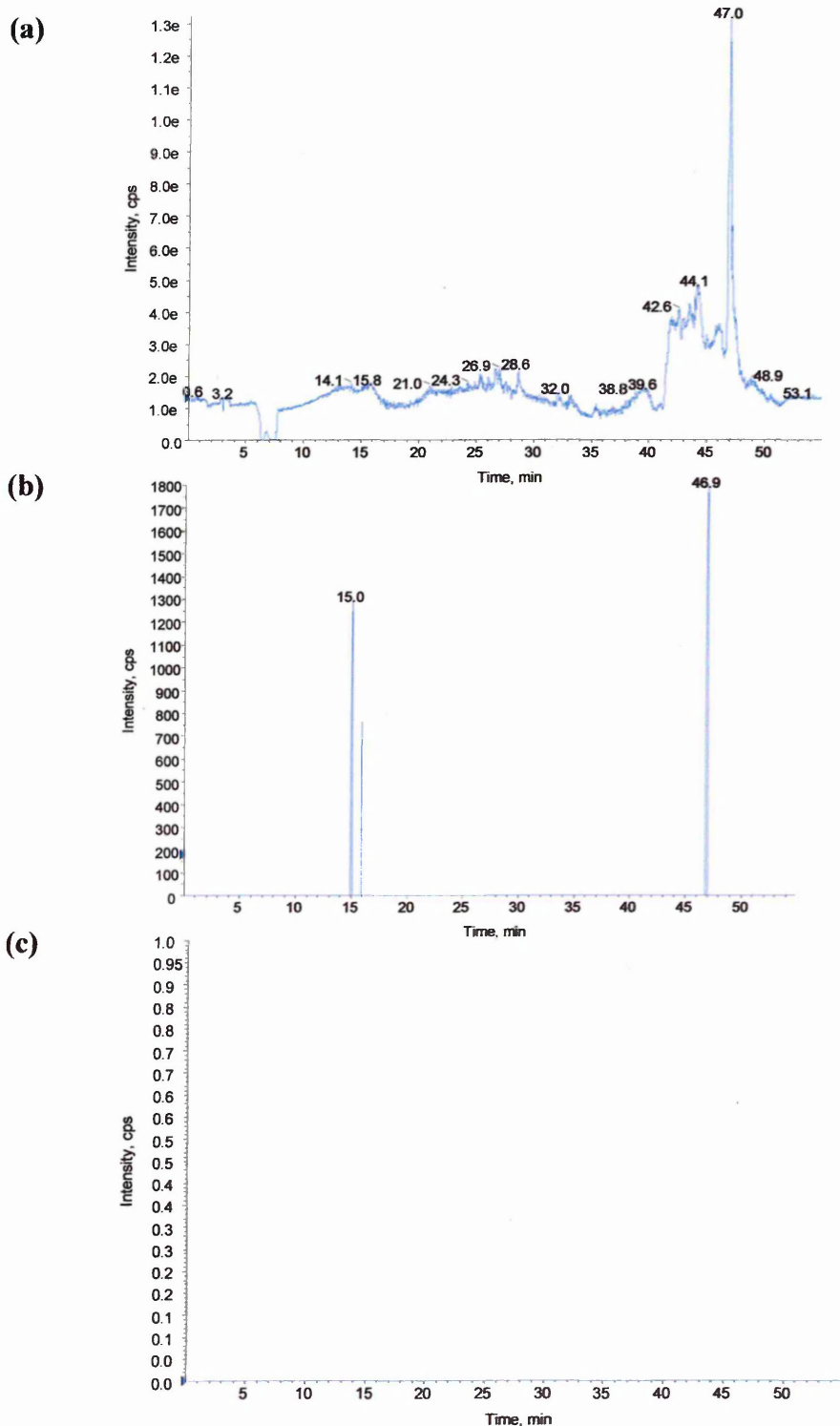


Figure 107. Capillary LC/MS run of an APP α_{770} one-dimensional in-gel formic acid digest performed using information dependant acquisition (IDA) software. For experimental conditions see chapter 2.92, page 92. (a) Shows the survey scan or total ion chromatogram (TIC). (b) Shows the TIC for the product ion intensities generated by product ion scan of the most intense peak in the normal mass spectrum. (c) Should show the TIC for the product ion intensities generated by product ion scan of the second most intense peak in the normal mass spectrum, however, lack of data shows the poor quality of the sample.

The alpha secretase cleaved amyloid precursor protein, isoform 770 ($APP_{\alpha 770}$) was immunoprecipitated from CHO 770 cell secretions.

The MALDI-MS examination of the one-dimensional in-gel formic acid digestion of $APP_{\alpha 770}$ (figure 106) gave amino acid sequence coverage of 2% of the $APP_{\alpha 770}$ molecule from 2 formic acid peptides, however the appearance of the peaks, background 'noise' and lack of MS/MS data discredit the validity of the peaks. LC/MS analysis again failed to reveal any data and as such no MS/MS data was achieved. The overall lack of results proves the inadequate quality of the sample. As all the digests performed within this work were carried out in parallel keeping all steps constant the sample clarity or lack of can only be due to the formic acid digestion procedure. Reasons for this are unknown, although it is not a widely used method successful digestions yielding sequence coverage of up to 43% have been reported¹⁹⁸.

3.437 MALDI-MS analysis of a one-dimensional in-gel formic acid digestion of immunoprecipitated alpha secretase cleaved amyloid precursor protein (APP α).

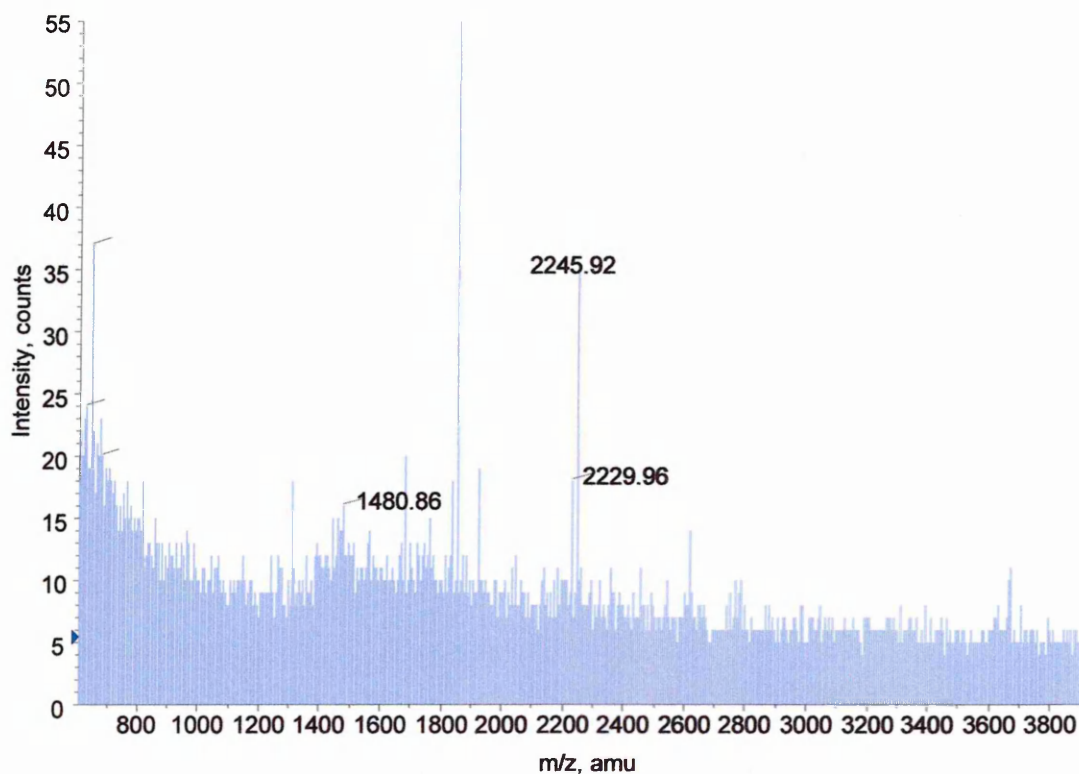


Figure 108. MALDI-MS spectrum of an in-gel formic acid digest of APP α from a one-dimensional gel. Appearance of spectra poor dominated by noise.

mass (M+H ⁺)	mass (experimental)	position	missed cleavages	peptide sequence
1480.67	1480.86	387-397	2	ERMSQVMREWE
2245.18	2245.92	630-650	2	DRGLTTRPGSGLTNIKTEEEIS
2229.17	2229.96	574-594	2	DALMPSLTETKTTVELLPVNG

Table 58. Mascot search results from the MALDI-MS mass fingerprint of the one-dimensional in-gel formic acid digest of APP α (figure 108), containing the three isoforms of interest (695, 751 and 770), giving coverage of 4%, although these results are spurious due to the unconvincing MALDI-MS data (figure 108).

3.438 Capillary LC/MS analysis of a one-dimensional in-gel formic acid digestion of immunoprecipitated APP α .

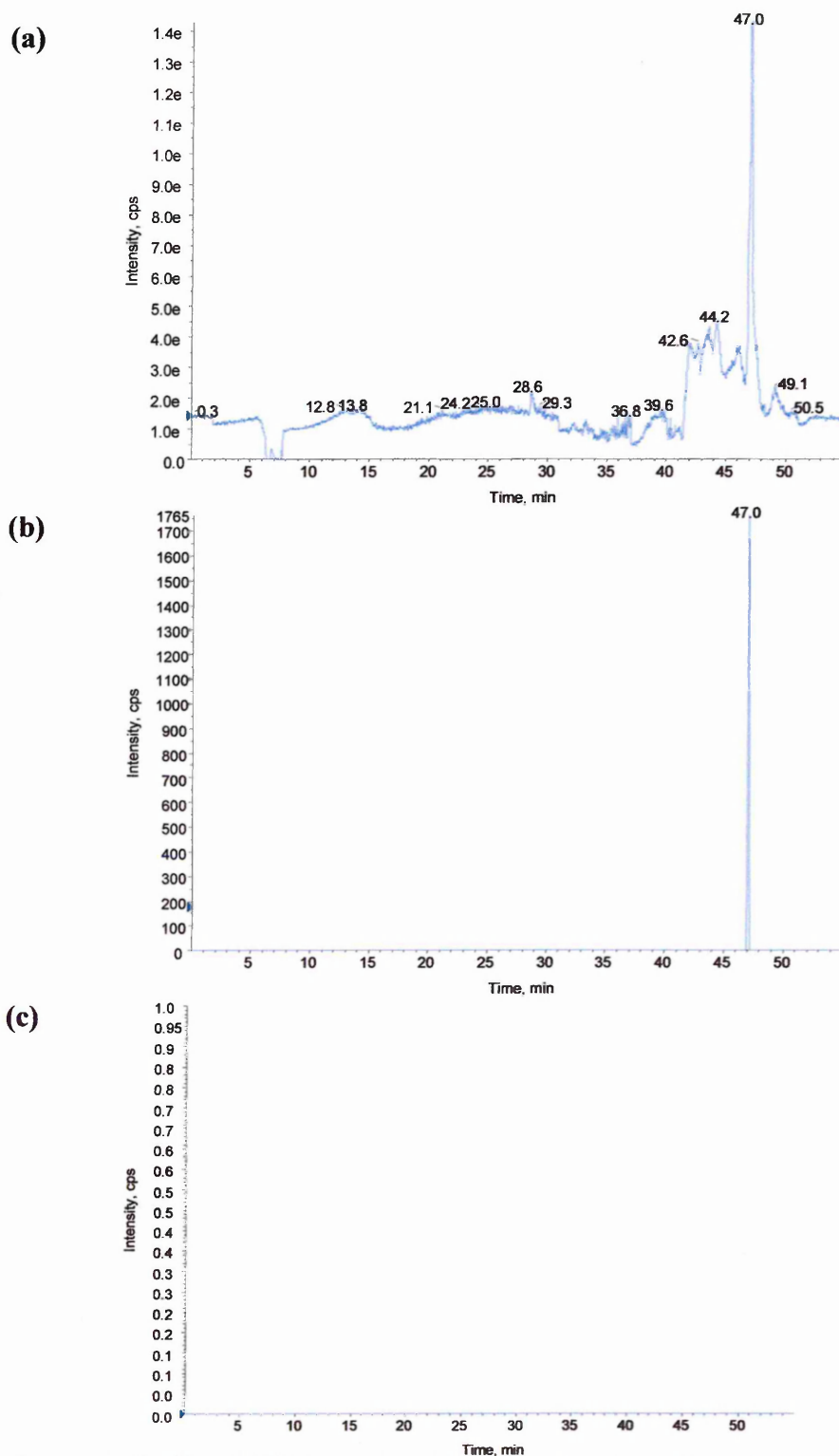


Figure 109. Capillary LC/MS run of an APP α one-dimensional in-gel formic acid digest performed using information dependant acquisition (IDA) software. For experimental conditions see chapter 2.92, page 92. (a) Shows the survey scan or total ion chromatogram (TIC). (b) Shows the TIC for the product ion intensities generated by product ion scan of the most intense peak in the normal mass spectrum. (c) Should show the TIC for the product ion intensities generated by product ion scan of the second most intense peak in the normal mass spectrum, however, lack of data is due to low quality sample.

The alpha secretase cleaved amyloid precursor protein (APP α) used was immunoprecipitated from Ntera 2 cell secretions. APP α encompasses all three isoforms of interest (APP α_{695} , APP α_{751} , APP α_{770}) and as such is a more plausible model of *in vivo* conditions.

The MALDI-MS results from the one-dimensional in-gel formic acid digestion of APP α (figure 108) gave amino acid sequence coverage of 4% of the APP α molecule from three formic acid peptides. LC/MS did not provide any formic acid peptides. Again the appearance of the MALDI-MS spectra, lack of LC/MS data and MS/MS data allows a question mark to hang over the MALDI-MS results attained. This can only be due to sample quality. As mentioned earlier all the digests were performed in parallel keeping all steps constant except the digest reagent and as successful digest results have been reported earlier¹⁹⁸ further investigation of this digest method is needed.

3.44 Two-dimensional in-gel tryptic digestion of BSA and APP.

3.441 MALDI-MS analysis of a two-dimensional in-gel tryptic digestion of BSA.

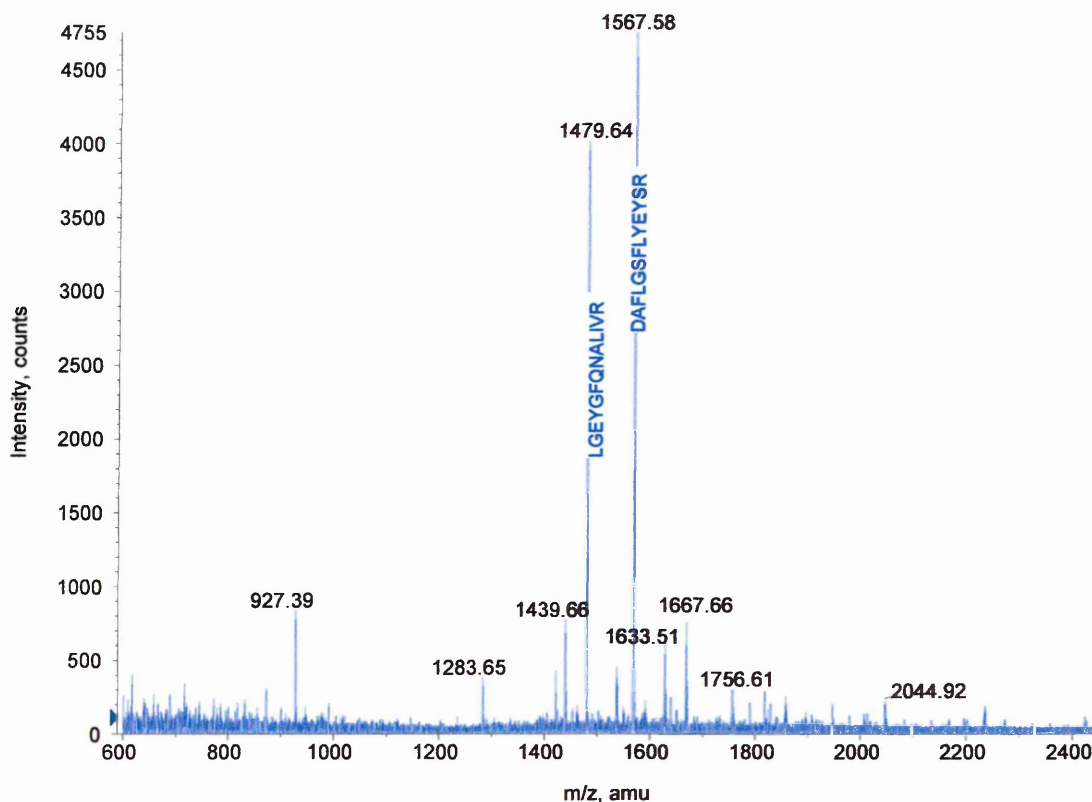


Figure 110. MALDI-MS spectrum of a two-dimensional in-gel tryptic digest of BSA. The annotated peaks at m/z s 1479.64 and 1567.58 subjected to MS/MS analysis, the results of which are shown in figures 111 and 112.

mass ($M+H^+$)	mass (experimental)	position	missed cleavages	peptide sequence
927.49	927.39	161-167	0	YLYEIAR
1283.71	1283.65	361-371	0	HPEYAVSVLLR
1439.81	1439.66	360-371	1	RHPEYAVSVLLR
1479.80	1479.64	421-433	0	LGEYGFQNALIVR
1567.74	1567.58	347-359	0	DAFLGSFLYEYSR
1633.66	1633.51	184-197	0	YNGVFQECCQAEDK
1667.81	1667.66	469-482	0	MPCTEDYSLILNR
1756.73	1756.61	581-597	1	CCAADDKEACFAVEGPK
2045.03	2044.92	168-183	1	RHPYFYAPELLYYANK

Table 59. Mascot search results from the two-dimensional in-gel tryptic digest shown in figure 110 covering 17% of the protein sequence. The sequences highlighted in blue were chosen for MS/MS analysis due to their intensity within the MALDI-MS spectrum (figure 110).

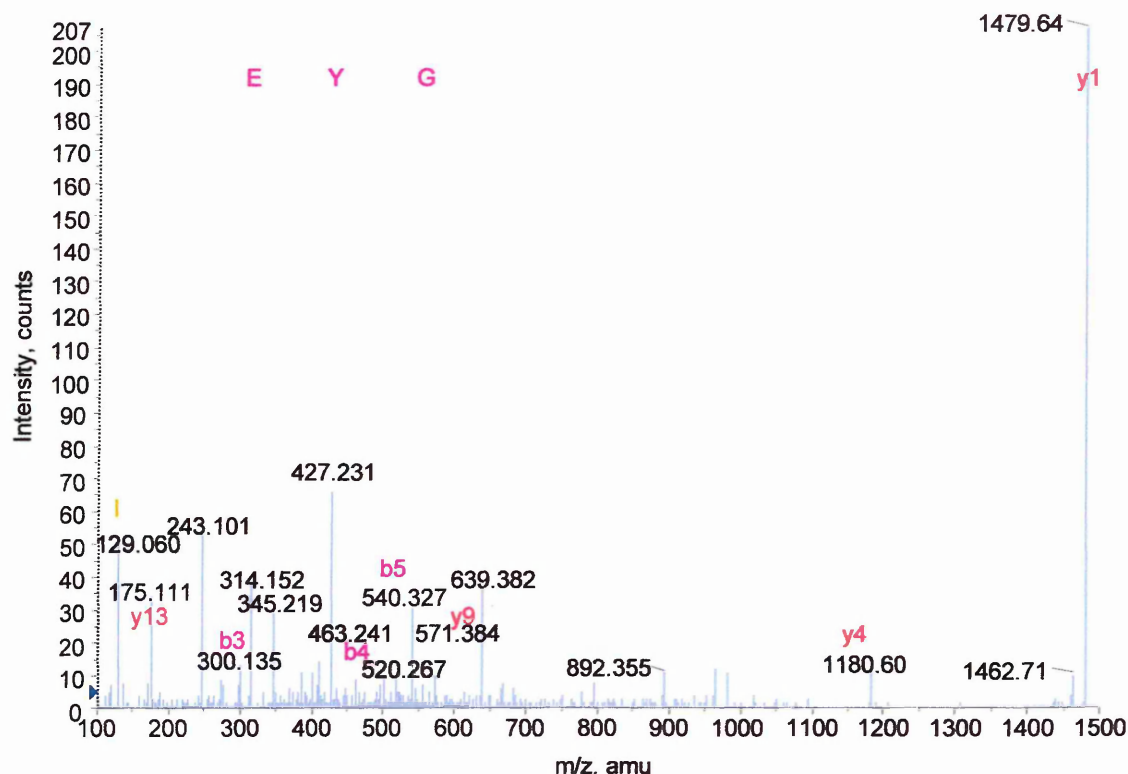


Figure 111. MALDI-MS/MS spectrum of the peak at m/z 1479.64 from the two-dimensional in-gel tryptic digest of BSA seen in figure 110. The ‘b’ product ion sequence tag EYG corresponds to the peptide LGEYGFQNALIVR, MW 1478.70 and allowed automatic determination via the BioAnalyst software.

Amino acid		Ion type ($M+H^+$)						
residue	mass/Da	immonium	a	a-NH ₃	b	b-NH ₃	y	y-NH ₃
L, Leu	113.08	86.09	86.09	69.06	114.09	97.06	1479.79	1462.76
G, Gly	57.02	30.03	143.11	126.09	171.11	154.08	1366.71	1349.68
E, Glu	129.04	102.05	272.16	255.13	300.15	283.12	1309.68	1292.66
Y, Tyr	163.06	136.07	435.22	418.19	463.21	446.19	1180.64	1163.68
G, Gly	57.02	30.03	492.24	475.21	520.24	503.21	1017.58	1000.54
F, Phe	147.06	120.08	639.31	622.28	667.30	650.28	960.56	943.53
Q, Gln	128.05	101.07	767.37	750.34	795.36	778.34	813.49	796.46
N, Asn	114.04	87.05	881.41	864.38	909.41	892.38	685.43	668.40
A, Ala	71.03	44.04	952.45	935.42	980.44	963.42	571.39	554.36
L, Leu	113.08	86.09	1065.53	1048.50	1093.53	1076.50	500.35	483.32
I, Ile	113.08	86.09	1178.62	1161.59	1206.61	1189.58	387.27	370.24
V, Val	99.06	72.08	1277.68	1260.66	1305.68	1288.65	274.18	257.16
R, Arg	156.10	129.11	1433.79	1416.76	1461.78	1444.75	175.11	158.09

Table 60. BioAnalyst software results from the MALDI-MS/MS two-dimensional in-gel tryptic digest of BSA seen in figure 111. The ‘a’, ‘b’ and ‘y’ product ions for the peptide LGEYGFQNALIVR are shown highlighting the ions present.

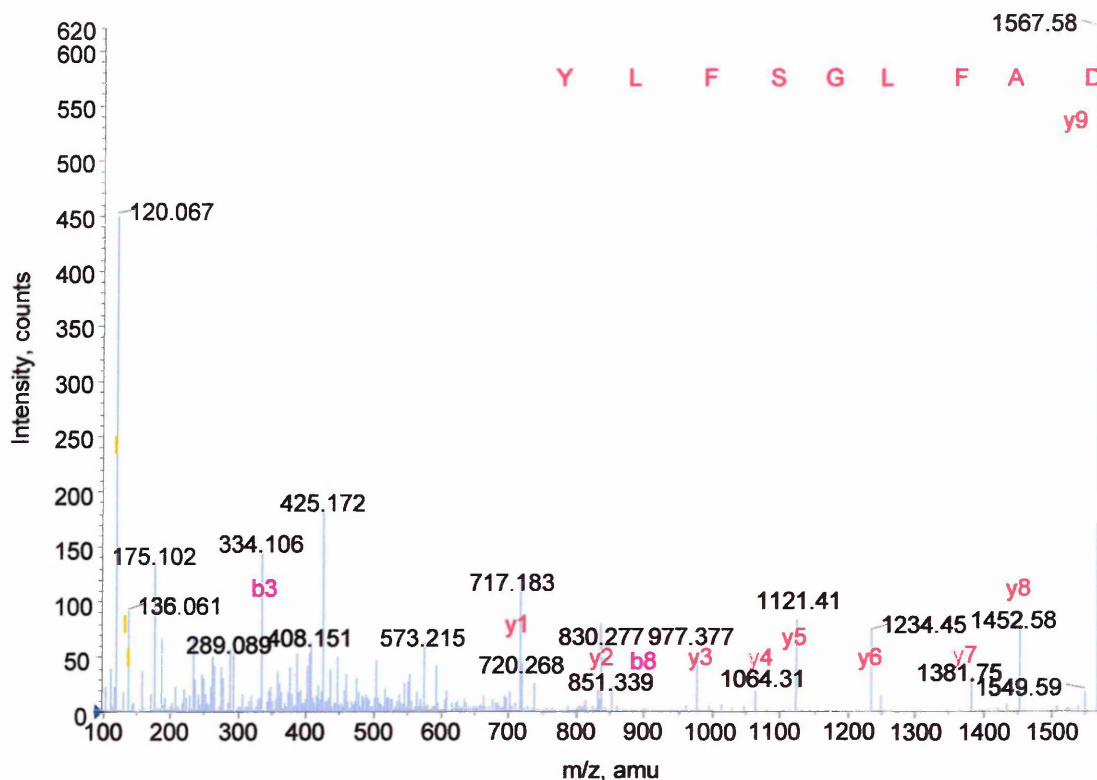


Figure 112. MALDI-MS/MS spectrum of the peak at m/z 1567.58 from the two-dimensional in-gel tryptic digest of BSA seen in figure 110. This peak corresponds to the BSA tryptic peptide DAFLGSFLYEYSR, MW 1566.64, which is verified by the 'y' ion sequence tag DAFLGSFLY.

Amino acid		Ion type ($M+H^+$)						
residue	mass/Da	immonium	a	a-NH ₃	b	b-NH ₃	y	y-NH ₃
D, Asp	115.02	88.03	88.03	71.01	116.03	99.00	1567.59	1550.56
A, Ala	71.03	44.04	159.07	142.04	187.07	170.04	1452.56	1435.53
F, Phe	147.06	120.08	306.14	289.11	334.13	317.11	1381.52	1364.50
L, Leu	113.08	86.09	419.22	402.20	447.22	430.19	1234.46	1217.43
G, Gly	57.02	30.03	476.25	459.22	504.24	487.21	1121.37	1104.34
S, Ser	87.03	60.04	563.28	546.25	591.27	574.25	1064.35	1047.32
F, Phe	147.06	120.08	710.35	693.32	738.34	721.31	977.32	960.29
L, Leu	113.08	86.09	823.43	806.40	851.42	834.40	830.25	813.22
Y, Tyr	163.06	136.07	986.49	969.47	1014.41	997.46	717.17	700.14

Table 61. BioAnalyst software results from the MALDI-MS/MS two-dimensional in-gel tryptic digest of BSA seen in figure 112. Shown are the 'a', 'b' and 'y' product ions possible for the peptide sequence DAFLGSFLY, highlighting the ones present.

3.442 Capillary LC/MS analysis of a two-dimensional in-gel tryptic digestion of BSA.

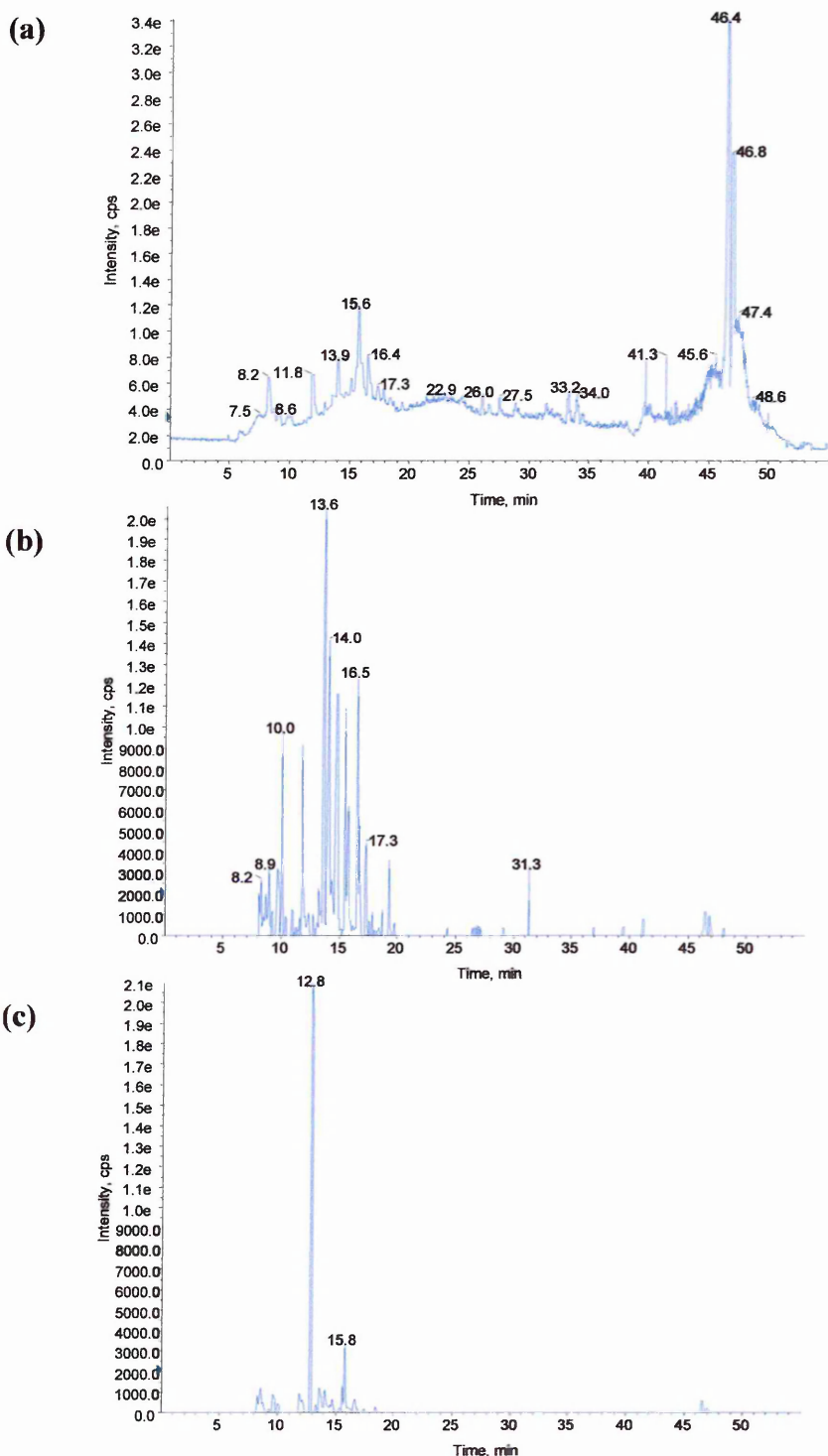


Figure 113. Capillary LC/MS run of a BSA two-dimensional in-gel tryptic digest performed using information dependant acquisition (IDA) software. For experimental conditions see chapter 2.92, page 92. (a) Shows the survey scan or total ion chromatogram (TIC). (b) Shows the TIC for the product ion intensities generated by product ion scan of the most intense peak in the normal mass spectrum. (c) Shows the TIC for the product ion intensities generated by product ion scan of the second most intense peak in the normal mass spectrum. The peak lists generated from traces (b) and (c) were sorted according to predefined parameters (chapter 2.92, page 93) and a selection of the most intense peaks automatically sent for MS/MS (figures 114 and 115).

mass observed	mass (experimental)	position	missed cleavages	peptide sequence
461.76	921.50	249-256	0	AEFVEVTK
464.26	926.50	161-167	0	YLYEIAR
501.80	1001.60	598-607	0	LVVSTQTALA
507.82	1013.63	549-557	0	QTALVELLK
582.33	1162.65	66-75	0	LVNELTEFAK
435.92	1304.74	402-412	0	HLVDEPQNLIK
708.35	1414.69	569-580	0	TVMENFVAFVDK
480.62	1438.84	360-371	1	RHPEYAVSVLLR
740.41	1478.81	421-433	0	LGEYGFQNALIVR
504.63	1510.86	438-451	0	VPQVSTPTLVEVSR
756.44	1510.87	438-451	0	VPQVSTPTLVEVSR
784.39	1566.76	347-359	0	DAFLGSFLYEYSR
547.40	1639.18	437-451	1	VPQVSTPTLVEVSR
652.67	1955.00	319-336	0	DAIPENLPPLTADFAEDK

Table 62. BioAnalyst automatic data analysis (using Matrix Science software) of the chromatograms seen in figure 113 of a two-dimensional in-gel tryptic digest of BSA gave 22% sequence coverage. The data highlights the presence of both doubly and triply charged species seen with ESI-MS as opposed to the singly charged ions seen with MALDI-MS. The sequences highlighted in blue produced good results when subjected to MS/MS analysis (figures 114 and 115).

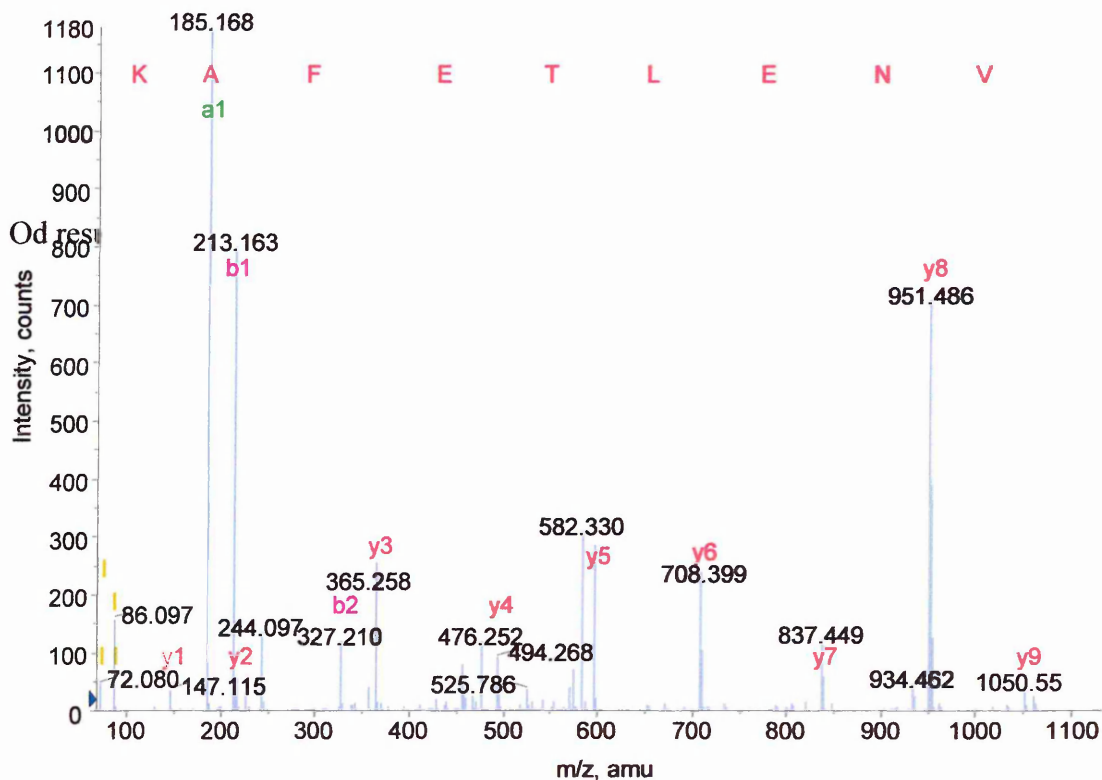


Figure 114. Capillary LC/MS/MS run of the doubly charged product ion at m/z 582.33, retention time 12.5 minutes from the LC/MS run of a two-dimensional in-gel tryptic digest of BSA (figure 113b). This product is consistent with the BSA tryptic peptide, LVNELTEFAK, MW 1162.65 and the sequence tag VNELTEFAK, verifies this.

Amino acid		Ion type (M+H ⁺)						
residue	mass/Da	immonium	a	a-NH ₃	b	b-NH ₃	y	y-NH ₃
V, Val	99.06	72.08	185.16	168.13	213.15	196.13	1050.57	1033.54
N, Asn	114.04	87.05	299.20	282.18	327.20	310.17	951.50	934.47
E, Glu	129.04	102.05	428.25	411.22	456.24	439.21	837.46	820.43
L, Leu	113.08	86.09	541.33	524.30	569.32	552.30	708.41	691.39
T, Thr	101.04	74.06	642.38	625.35	670.37	653.35	595.33	578.30
E, Glu	129.04	102.05	771.42	754.39	799.41	782.39	494.28	477.26
F, Phe	147.06	120.08	918.49	901.46	946.48	929.46	365.24	348.21
A, Ala	71.03	44.04	989.53	972.50	1017.51	1000.49	218.17	201.15
K, Lys	128.09	101.10	1117.62	1100.59	1145.62	1128.59	147.13	130.11

Table 63. BioAnalyst results of the capillary LC/MS/MS spectrum of the product at m/z 582.30 from the two-dimensional in-gel tryptic digest of BSA shown in figure 114. The possible and actual 'a', 'b' and 'y' product ions for the sequence VNELTEFAK are shown, highlighting the sequence coverage in 'a', 'b' and 'y' ions, as well as several immonium ions.

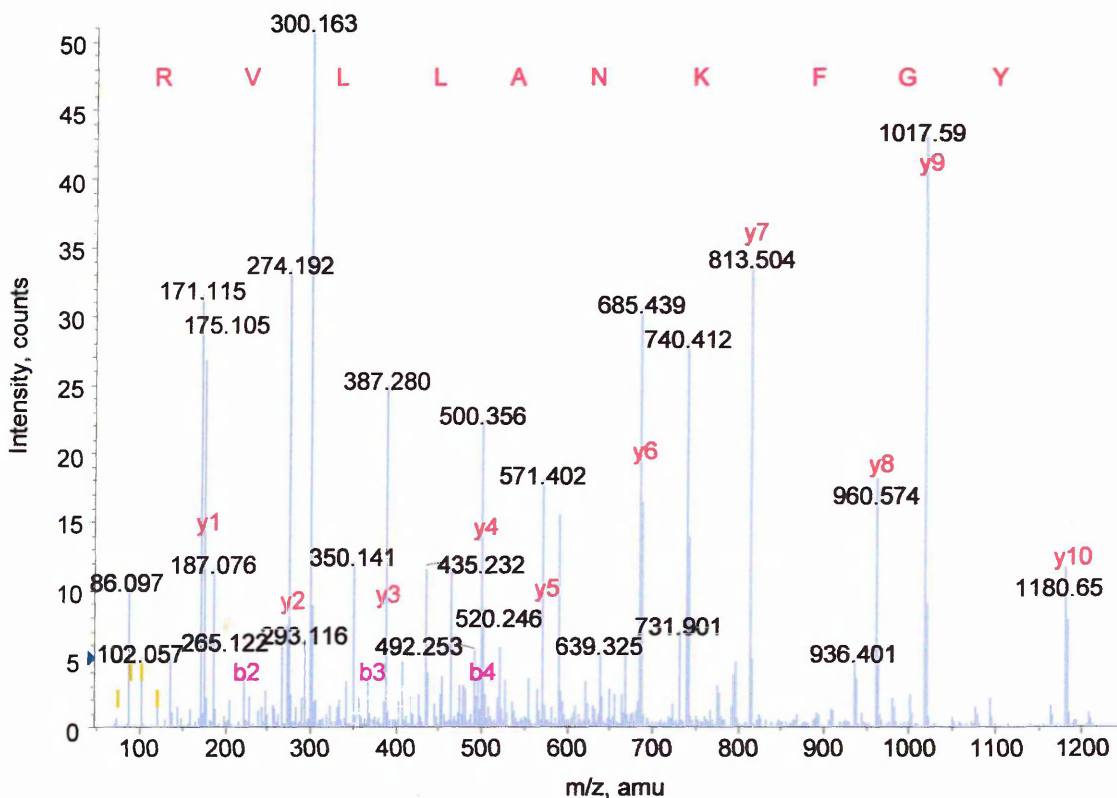


Figure 115. Capillary LC/MS/MS analysis of the doubly charged peak at m/z 740.41, retention time 12.9 minutes from the LC/MS run of a two-dimensional in-gel tryptic digest of BSA (figure 113c). This product is consistent with the peptide LGEYGFQNALIVR, 1478.81 MW. Note that the annotation upon the spectrum substitutes a lysine (K) for glutamine (Q) and a leucine (L) for isoleucine (I), due to similarities in molecular weight.

Amino acid		Ion type (M+H ⁺)						
residue	mass/Da	immonium	a	a-NH ₃	b	b-NH ₃	y	y-NH ₃
Y, Tyr	163.06	136.07	136.07	119.04	164.07	147.04	1180.65	1163.63
G, Gly	57.02	30.03	193.09	176.07	221.09	204.06	1017.59	1000.59

F, Phe	147.06	120.08	340.16	323.13	368.16	351.13	960.57	943.54
Q, Gln	128.09	101.10	468.26	451.23	496.25	479.22	813.50	796.47
N, Asn	114.04	87.05	582.30	565.27	610.29	593.27	685.41	668.38
A, Ala	71.03	44.04	653.34	636.31	681.33	664.30	571.36	554.34
L, Leu	113.08	86.09	766.42	749.39	794.41	777.39	500.33	483.30
I, Ile	113.08	86.09	879.50	862.48	907.50	890.47	387.24	370.22
V, Val	99.06	72.08	978.57	961.55	1006.52	989.54	274.16	257.13
R, Arg	156.10	129.11	1134.67	1117.65	1162.67	1145.64	175.09	158.06

Table 64. BioAnalyst automated results of the capillary LC/MS/MS spectrum of the product at m/z 740.41 from the two-dimensional in-gel tryptic digest of BSA shown in figure 115. The possible 'a', 'b' and 'y' product ions for the sequence YGFQNALIVR are shown highlighting the ones pre

Bovine serum albumin (BSA, 66,432.96 MW) was used as a standard due to its availability and similarity in molecular weight to the amyloid precursor protein isoforms (APP α_{695} , MW 67,708.02, APP α_{751} , MW 73,863.85, APP α_{770} , MW 75,988.34).

The MALDI-MS analysis of the two-dimensional in-gel tryptic digest of BSA (figure 110) resulted in 9 tryptic peptides covering 17% of the protein. LC/MS analysis (figure 113) of the same sample revealed 14 tryptic peptides covering 22% of the protein sequence. The sequence coverage achieved for the BSA tryptic digestions is poor compared to usual 40-60% within the literature¹⁹⁷. This should be investigated further with regards to optimising protein coverage for both standards and samples. MS/MS analysis of peaks from both MALDI-MS (figures 111 and 112) and LC/MS (figures 114 and 115) created long sequence tags, which allowed automatic identification of BSA via the BioAnalyst software.

3.443 MALDI-MS analysis of a two-dimensional in-gel tryptic digestion of alpha secretase cleaved amyloid precursor protein standard, isoform 695 (APP α_{695}).

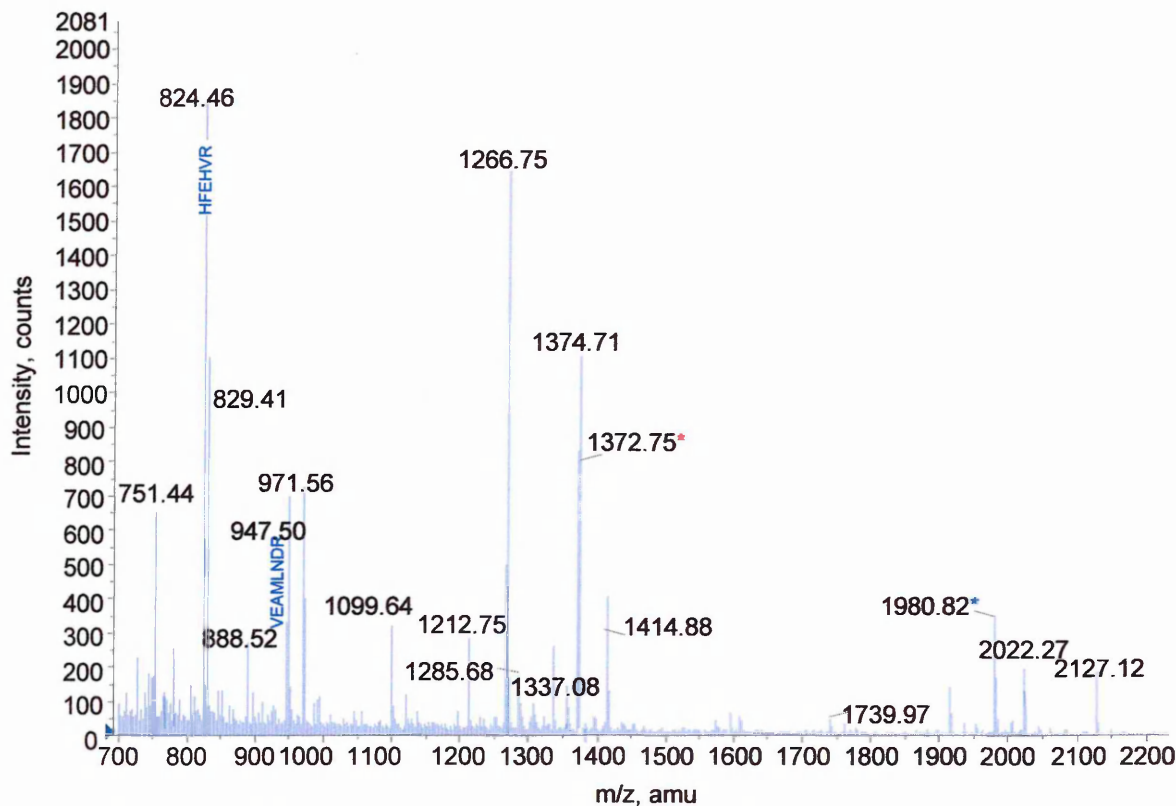


Figure 116. MALDI-MS spectrum of a two-dimensional in-gel tryptic digest of standard APP α_{695} . The annotated peaks at m/z 824.46 and 947.50 were subjected to MS/MS analysis the results of which are shown in figures 117 and 118. The peak at m/z 1372.75 marked by a red asterisk is specific to APP α_{695} and the peak at 1980.82 marked by the blue asterisk, has a site of probable glycosylation. Attempts to sequence these important peptides, however, were unsuccessful.

mass (M+H ⁺)	mass (experimental)	position (<i>s</i> APP ₆₉₅ numbering)	missed cleavages	peptide sequence
751.36	751.44	314-319	0	MSQVMR
824.42	824.46	419-424	0	HFEHVR
829.43	829.41	118-123	0	FLHQER
888.47	888.52	397-403	0	HVFNMLK
947.46	947.50	369-376	0	VEAMLNDR
971.51	971.56	436-443	0	SQVMTHLR
1099.59	1099.64	338-346	0	AVIQHFQEK
1212.62	1212.75	359-368	0	QLLVETHMAR
1266.67	1266.75	90-99	0	THPHFVIPYR
1285.62	1285.68	24-34	0	LNMHMNVQNGK
1336.60	1337.08	585-595	0	HDSGYEVHHQK
1372.70	1372.75	272-285	0	VPTTAASTPDAVDK*
1374.65	1374.91	347-358	0	VESLEQEAANER
1414.80	1414.88	557-570	0	GLTTRPGSGLTNIK
1739.85	1739.97	494-509	0	ISYGNDALMPSLTETK

1980.90	1980.80	477-493	0	EQNYSDDVLANMISEPR*
2022.15	2022.25	379-396	0	LALENYITALQAVPPRPR
2127.07	2127.12	252-271	0	TTSIATTTTTTTESVVEEVVR

Table 65. Mascot mass fingerprint analysis of the MALDI-MS of the two-dimensional in-gel tryptic digest of APP α_{695} shown in figure 116 gave 29% sequence coverage using the Mascot search engine. The peak at m/z 1372.75, amino acid sequence VPTTAASTPDAVDK being specific to APP α_{695} although MS/MS data was not achieved for this peptide. The sequences highlighted in blue, however, did give good MS/MS results (figures 117 and 118).

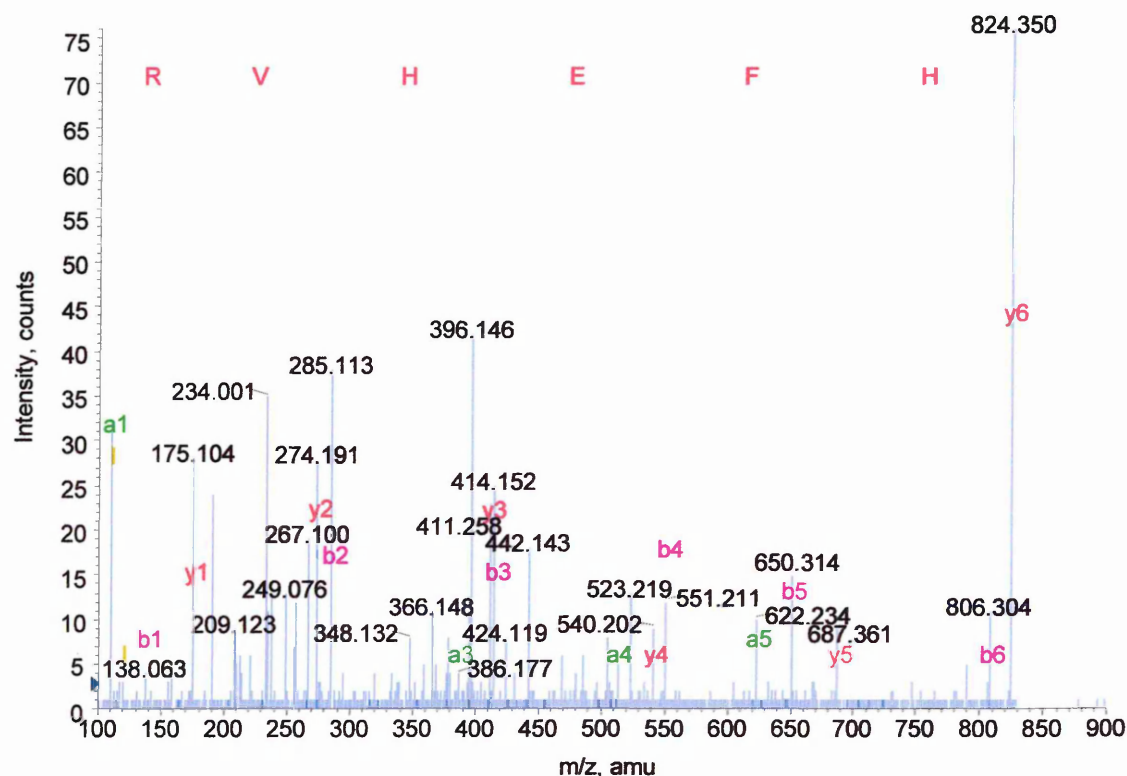


Figure 117. MALDI-MS/MS spectrum of peak at m/z 824.46 from the two-dimensional in-gel tryptic digest of APP α_{695} in figure 116. This peak corresponds to the APP α_{695} tryptic peptide HFEHVR, 823.41 monoisotopic mass and the MS/MS analysis results validate this by giving the full peptide sequence in both 'b' and 'y' product ions.

Amino acid		Ion type (M+H ⁺)						
residue	mass/Da	immonium	a	a-NH ₃	b	b-NH ₃	y	y-NH ₃
H, His	137.05	110.07	110.07	93.04	138.06	121.03	824.41	807.38
F, Phe	147.06	126.08	257.13	240.11	285.13	268.10	687.35	670.33
E, Glu	129.04	102.05	386.18	369.15	414.17	397.15	540.28	523.26
H, His	137.05	110.07	523.24	506.21	551.23	534.20	411.24	394.21
V, Val	99.06	72.08	622.30	605.28	650.30	633.27	274.18	257.16
R, Arg	156.10	129.11	778.41	761.38	806.40	789.37	175.11	158.09

Table 66. BioAnalyst software results from the MALDI-MS/MS two-dimensional in-gel tryptic digest of APP α_{695} shown in figure 117. Listed are all the possible 'a', 'b' and 'y' product ions for the peptide HFEHVR, highlighting the products ions present.

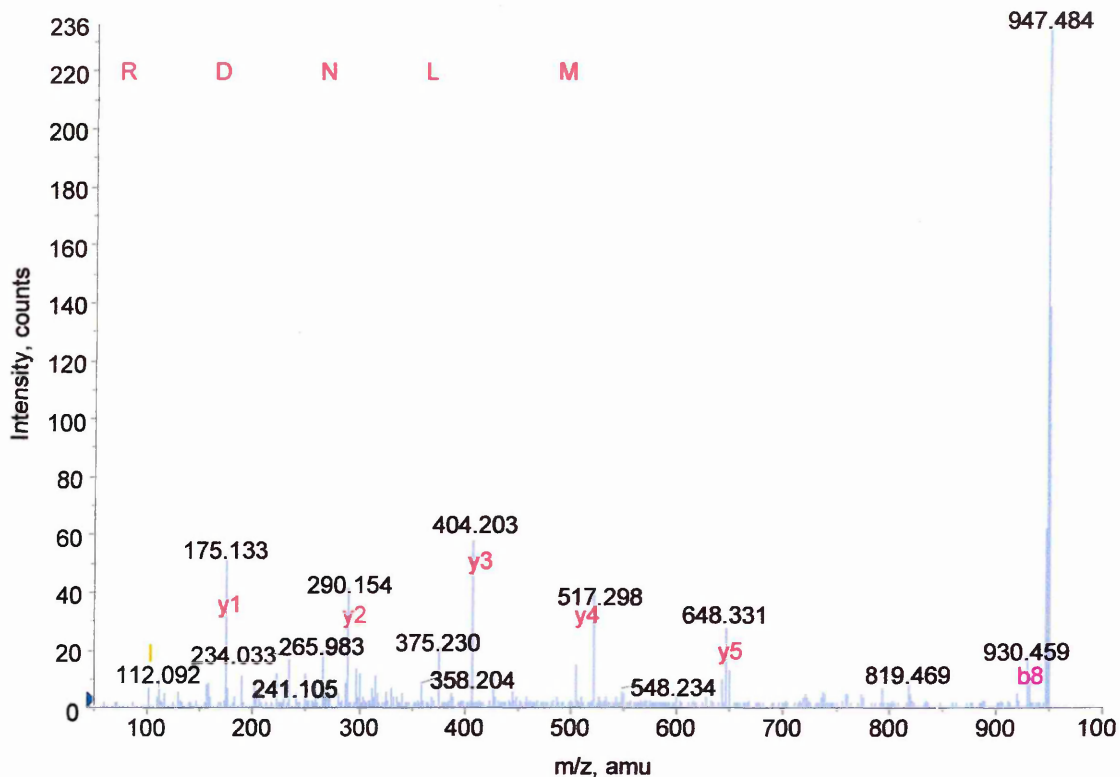


Figure 118. MALDI-MS/MS analysis of peak at m/z 947.50 from the two-dimensional in-gel tryptic digest of APP α_{695} in figure 116. This peak corresponds to the peptide VEAMLNDR, 946.45 monoisotopic mass and the sequence tag shown here confirms this.

Amino acid		Ion type (M+H ⁺)						
residue	mass/Da	immonium	a	a-NH ₃	b	b-NH ₃	y	y-NH ₃
M, Met	131.04	104.05	403.20	386.17	431.19	414.16	648.31	631.28
L, Leu	113.08	86.09	516.28	499.25	544.27	527.25	517.27	500.24
N, Asn	114.02	87.05	630.32	613.30	658.32	641.29	404.18	387.16
D, Asp	115.02	88.03	745.35	728.32	773.34	756.32	290.14	273.11
R, Arg	156.10	129.11	901.45	884.42	929.45	912.42	175.11	158.09

Table 67. BioAnalyst software results from the MALDI-MS/MS two-dimensional in-gel tryptic digest of APP α_{695} shown in figure 118. Listed are all the possible 'a', 'b' and 'y' product ions for the sequence MLNDR, highlighting the products ions present.

3.444 Capillary LC/MS analysis of a two-dimensional in-gel tryptic digestion of standard APP α_{695} .

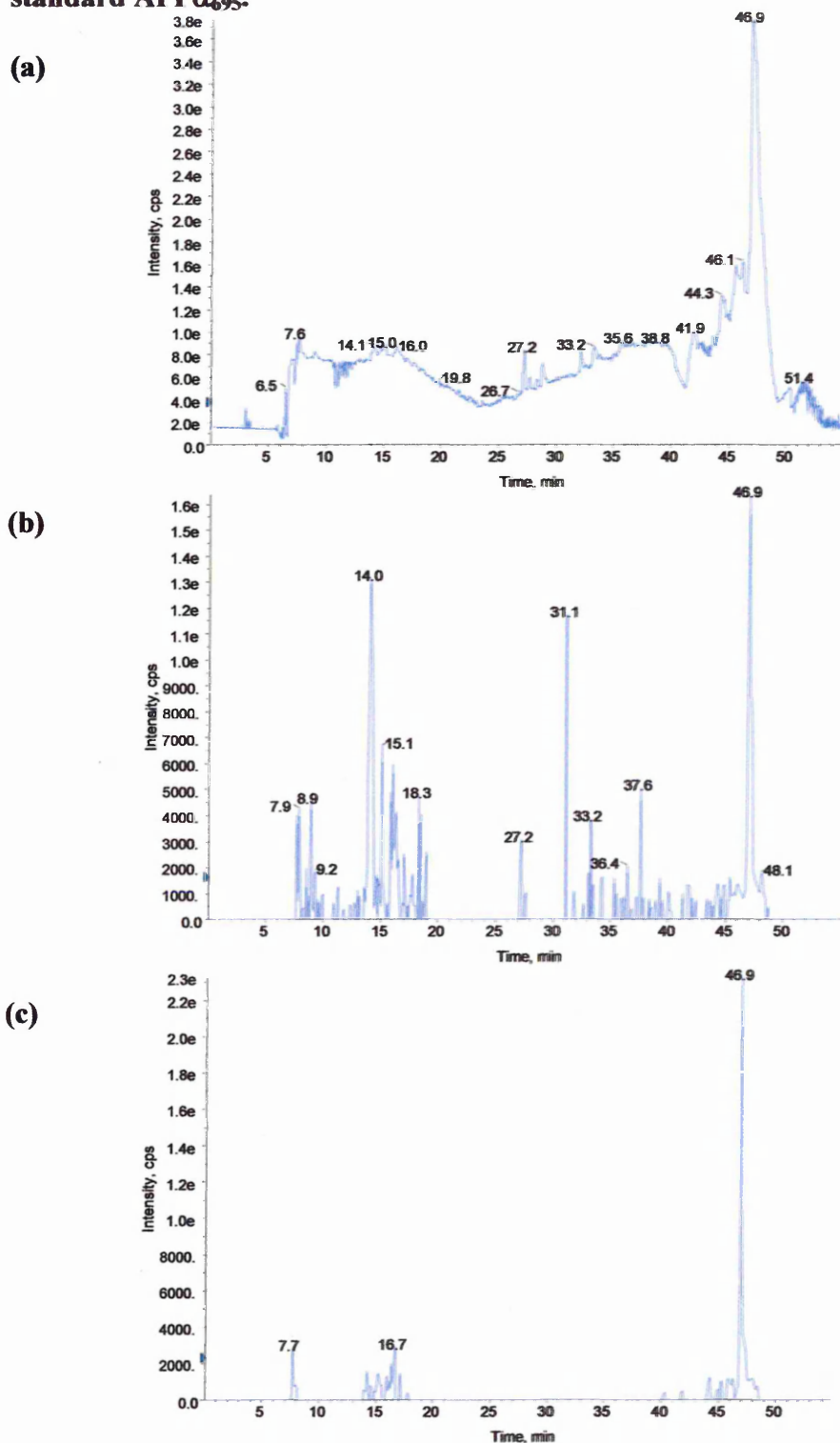


Figure 119. Capillary LC/MS run of an APP α_{695} two-dimensional in-gel tryptic digest performed using information dependant acquisition (IDA) software. For experimental conditions see chapter 2.92, page 92. (a) Shows the survey scan or total ion chromatogram (TIC). (b) Shows the TIC for the product ion intensities generated by product ion scan of the most intense peak in the normal mass spectrum. (c) Shows the TIC for the product ion intensities generated by product ion scan of the second most intense peak in the normal mass spectrum. The peak lists generated from traces (b) and (c) were sorted according to predefined parameters (chapter 2.92, page 93) and a selection of the most intense peaks automatically sent for MS/MS (figures 120 and 121).

mass observed	mass (experimental)	position (sAPP ₆₉₅ numbering)	missed cleavages	peptide sequence
404.87	1211.60	359-368	0	QQLVETHMAR
686.84	1371.66	272-285	0	VPTTAASTPDAVDK*
687.83	1373.64	347-358	0	VESLEQEAANER
870.42	1738.83	494-509	0	ISYGN DALMPSLTETK
878.42	1754.83	494-509	0	ISYGN DALMPSLTETK (MSO)
660.97	1979.88	477-493	0	EQNYSDDVLANMISEPR*
990.95	1979.88	477-493	0	EQNYSDDVLANMISEPR*

Table 68. BioAnalyst automatic data analysis (using Matrix Science software) of the chromatograms seen in figure 119 of a two-dimensional in-gel tryptic digest of standard APP_{α695} gave sequence coverage of 10%. The data highlights the presence of both doubly and triply charged species seen with ESI-MS as opposed to the singly charged ions seen with MALDI-MS. The presence of the peptide sequence VPTTAASTPDAVDK (marked by a red asterisk) proves the sample to be APP_{α695} as it is isoform specific.

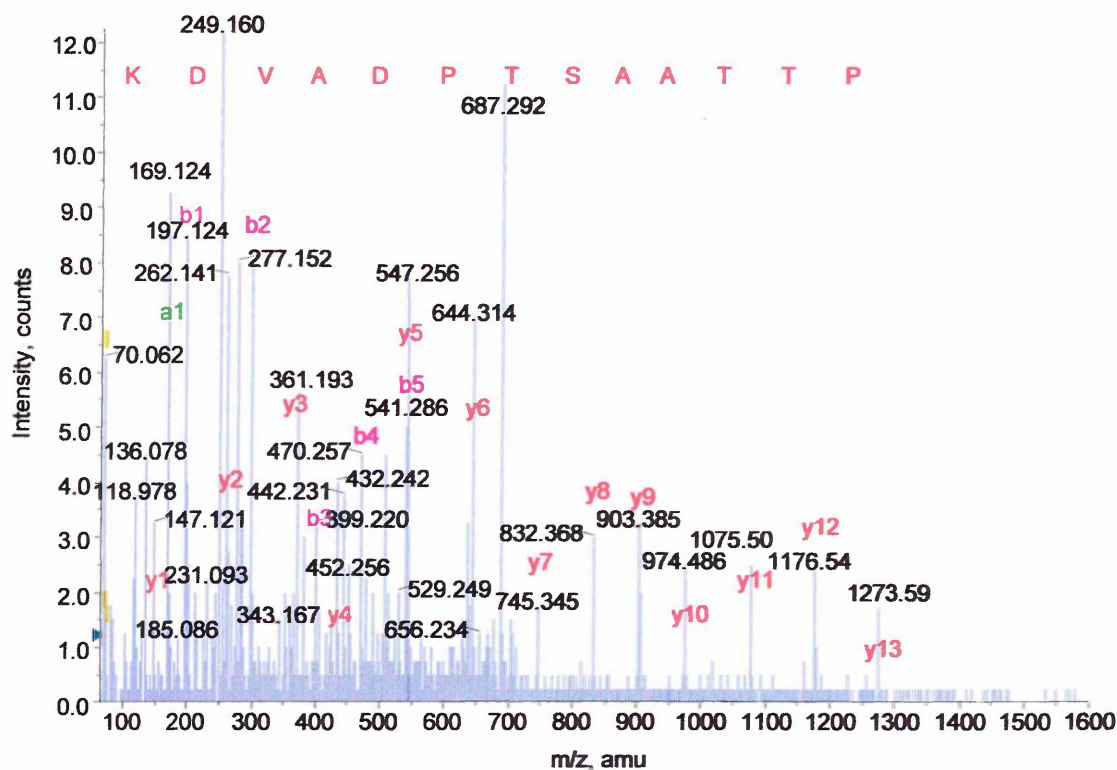


Figure 120. Capillary LC/MS/MS run of the doubly charged product ion at m/z 686.84, retention time 7.9 minutes from the LC/MS run of a two-dimensional in-gel tryptic digest of standard APP_{α695} (figure 119b). This product is consistent with the APP_{α695} tryptic peptide, VPTTAASTPDAVDK, MW 1371.66 and the sequence tag, PTTAASTPDAVDK verifies this.

Amino acid		Ion type (M+H ⁺)						
residue	mass/Da	immonium	a	a-NH ₃	b	b-NH ₃	y	y-NH ₃
P, Pro	97.05	70.06	169.13	152.10	197.12	180.10	1273.59	1256.57
T, Thr	101.04	74.06	270.18	253.15	298.17	281.14	1176.54	1159.51
T, Thr	101.04	74.06	371.22	354.20	399.22	382.19	1075.49	1058.47
A, Ala	71.03	44.04	442.26	425.23	470.26	453.23	974.45	957.42
A, Ala	71.03	44.04	513.30	496.27	541.29	524.27	903.41	886.38
S, Ser	87.03	60.04	600.33	583.30	628.33	611.30	832.37	815.35
T, Thr	101.04	74.06	701.38	684.35	729.37	712.35	745.34	728.31
P, Pro	97.05	70.06	798.43	781.40	826.43	809.40	644.29	627.27
D, Asp	115.02	88.03	913.46	896.43	941.45	924.43	547.24	530.21
A, Ala	71.03	44.04	984.49	967.47	1012.49	995.46	432.21	415.19
V, Val	99.06	72.08	1083.56	1066.54	1111.56	1094.53	361.18	344.15
D, Asp	115.02	88.03	1198.59	1181.56	1226.58	1209.56	262.11	245.08
K, Lys	128.09	101.10	1326.69	1309.66	1354.68	1337.65	147.08	130.05

Table 69. BioAnalyst software results of the capillary LC/MS/MS spectrum of the doubly charged product at m/z 686.84 from the two-dimensional in-gel tryptic digest of standard APP α_{695} shown in figure 120. Shown is the 'a', 'b' and 'y' product ions possible for the sequence PTTAASTPDAVDK highlighting in red the 'y' product ion present within the spectrum.

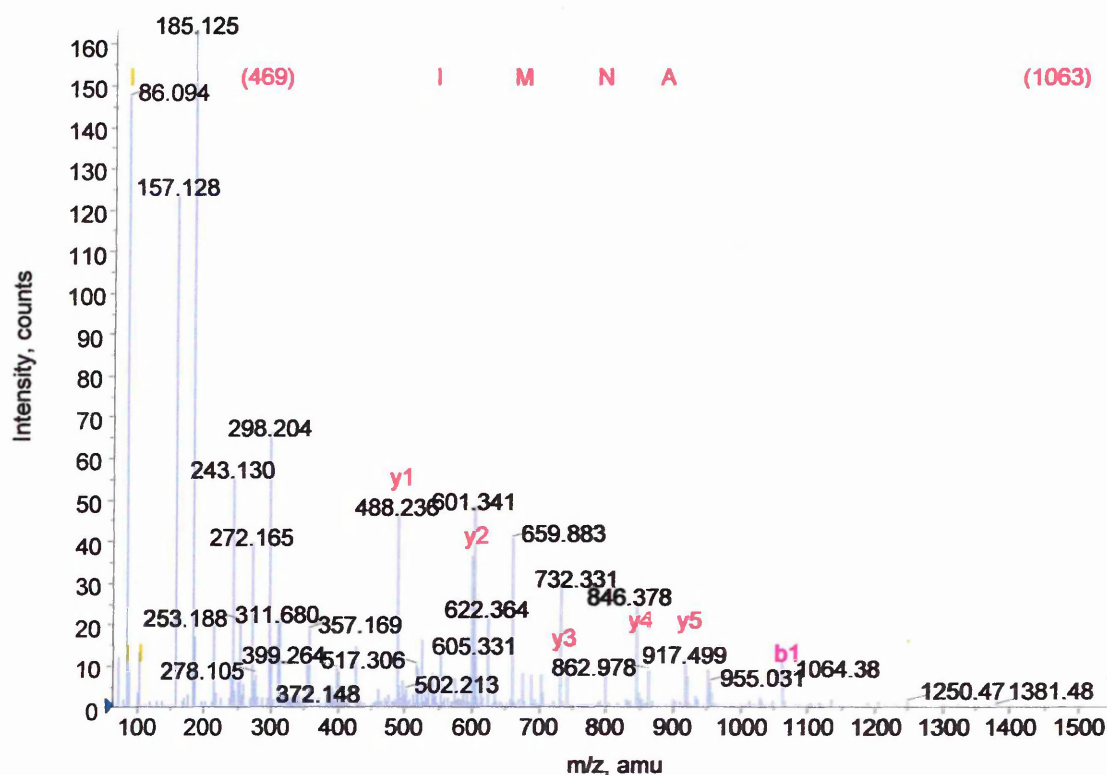


Figure 121. Capillary LC/MS/MS analysis of the triply charged product ion at m/z 660.97, retention time 16.7 minutes from the LC/MS run of a two-dimensional in-gel tryptic digest of APP α_{695} (figure 119c). This product is consistent with the APP α_{695} tryptic peptide EQNYSDDVLANMISEPR, 1979.88 monoisotopic mass and the sequence tag ANMI expands this.

Amino acid		Ion type (M+H ⁺)						
residue	mass/Da	immonium	a	a-NH ₃	b	b-NH ₃	y	y-NH ₃
(1063.47)	1063.47	n/a	1036.48	1019.46	1064.48	1047.45	1980.90	1963.88
A, Ala	71.03	44.04	1107.52	1090.50	1135.52	1118.49	917.42	900.40
N, Asn	114.04	87.05	1221.56	1204.54	1249.56	1232.53	846.39	829.36
M, Met	131.04	104.05	1352.61	1335.58	1380.60	1363.57	732.34	715.32
I, Ile	113.08	86.09	1465.69	1448.66	1493.68	1476.66	601.30	584.28
(469.20)	469.20	n/a	1934.90	1917.87	1962.89	1945.87	488.22	471.19

Table 70. BioAnalyst automated searching of the capillary LC/MS/MS spectrum from the two-dimensional in-gel tryptic digest of APP α_{695} shown in figure 121, shows the product ions from the sequence tag ANMI.

Amyloid precursor protein standard was purchased from Sigma for use as a direct comparison. The standard was the alpha secretase cleaved APP, isoform 695 (APP α_{695}) from E.coli origin.

The MALDI-MS examination of the two-dimensional in-gel tryptic digestion of APP α_{695} (figure 116) gave amino acid sequence coverage of 29% of the APP α_{695} molecule from 18 tryptic peptides. The sequence coverage achieved from the LC/MS (figure 119) analysis uncovered 10% of the protein sequence from 6 peptides. MS/MS examination of both MALDI-MS (figures 117 and 118) and LC/MS (figures 120 and 121) peaks provided one full peptide sequence (figure 117) and generous sequence tags. The unique tryptic peptide exhibited by APP α_{695} (position 272-285, monoisotopic mass 1372.6954, amino acid sequence VPTTAASTPDAVDK) was present in both the MALDI-MS and LC/MS data. Observed as the peak at m/z 1372.75 in the MALDI-MS spectrum (figure 116) highlighted in the BioAnalyst search results of the LC/MS data (table 67) and analysis by LC/MS/MS (figure 126). Another peptide of interest, EQNYSDVLANMISEPR, position 477-493 (APP α_{695} numbering) was seen in the MALDI-MS spectrum (figure 116) at m/z 1980.96. The LC/MS data (table 67) also showed its presence in both doubly (m/z 990.95) and

triply (m/z 660.97) charged species as well as LC/MS/MS analysis (figure 121) giving a sequence tag. The significance of this peptide is the possible *N*-glycosylation site at position 479. If glycosylation does occur at this point the mass of the peptide would be increased and the species at $1980 M+H^+$ for MALDI and $660 M+3H^+$ and $990 M+2H^+$ for LC/MS would not be seen. The bacterial nature of the standard APP α_{695} , however, means that glycosylation does not occur and as such the peptide may be present.

3.445 MALDI-MS analysis of a two-dimensional in-gel tryptic digestion of immunoprecipitated alpha secretase cleaved amyloid precursor protein, isoform 770 (APP α_{770}).

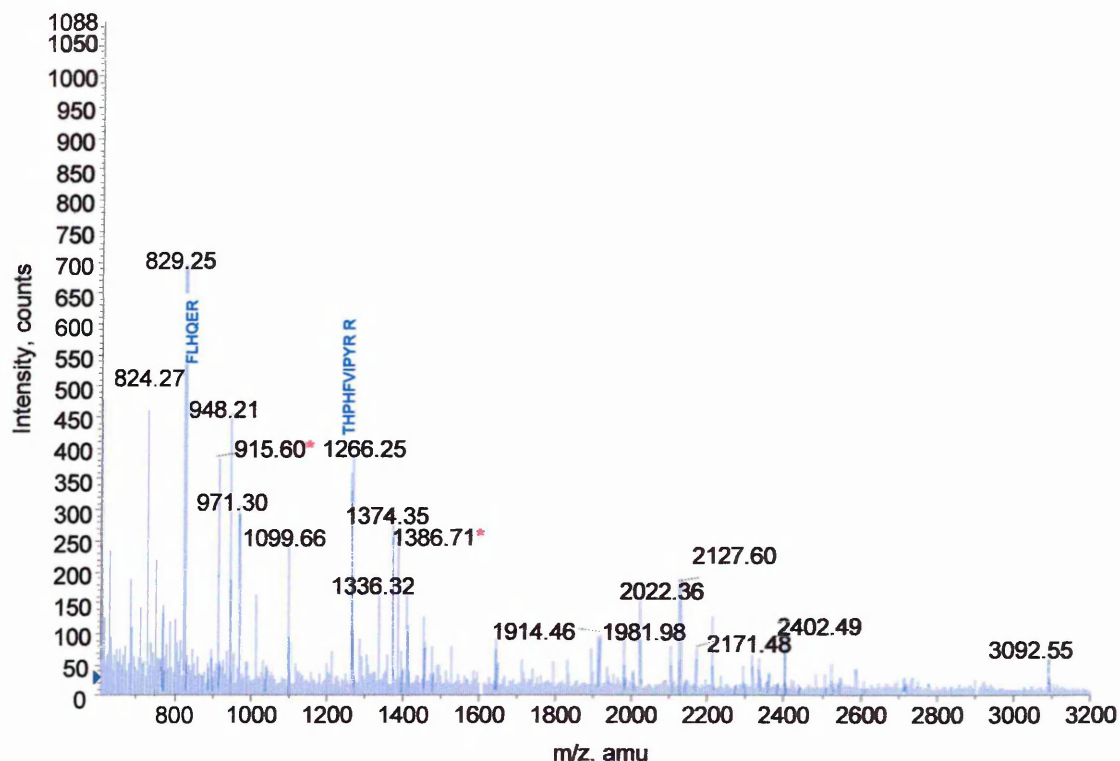


Figure 122. MALDI-MS spectrum of an in-gel tryptic digest of APP α_{770} from a two-dimensional gel. Annotated are the peptides upon which MS/MS analysis was performed (figures 123 and 124). Note the peaks at m/zs 915.60 and 1386.71 (marked with a red asterisk) specific to the APP α_{770} isoform.

mass (M+H ⁺)	mass (experimental)	position (APP α_{770} numbering)	missed cleavages	peptide sequence
824.42	824.27	494-499	0	HFEHVR
829.43	829.47	118-123	0	FLHGER
915.49	915.60	335-342	0	TTQEPLAR*
948.41	948.21	395-401	0	EWEEAER
971.51	971.30	511-518	0	SQVMTHLR
1099.59	1099.66	413-421	0	AVIQHFQEK
1266.67	1266.25	90-99	0	THPHFVIPYR
1336.60	1336.32	660-670	0	HDSGYEVHHQK
1374.65	1374.35	422-433	0	VESLEQEAAER
1386.71	1386.41	347-360	0	LPTTAASTPDAVDK*
1914.86	1914.46	286-301	0	YLETPGDENEHAHFQK
1980.90	1981.98	552-568	0	EQNYSDDVLANMISEPR
2022.15	2022.36	454-471	0	LALenyITALQAVVPPRPR
2127.07	2127.60	252-271	0	TTSIATTTTTTTESVEEVVR
2171.19	2171.48	506-523	2	AAQIRSQVMTHLRVIYER

2402.18	2402.49	1-23	0	LEVPTDGNAGLLAEPQIAMFCGR
3092.39	3092.55	272-298	2	EVCSEAETGPCRAMISRWYFDVTEGK

Table 71. Mascot search results from the MALDI-MS mass fingerprint of the two-dimensional in-gel tryptic digest of APP α_{770} (figure 122) showing 21% sequence coverage. The red asterisks marking the tryptic peptides TTQPELAR, m/z 915.60 and LPTTAASTPDAVDK, 1385.61 monoisotopic mass specific to APP α_{770} , attempts to sequence these peptides, however, failed.

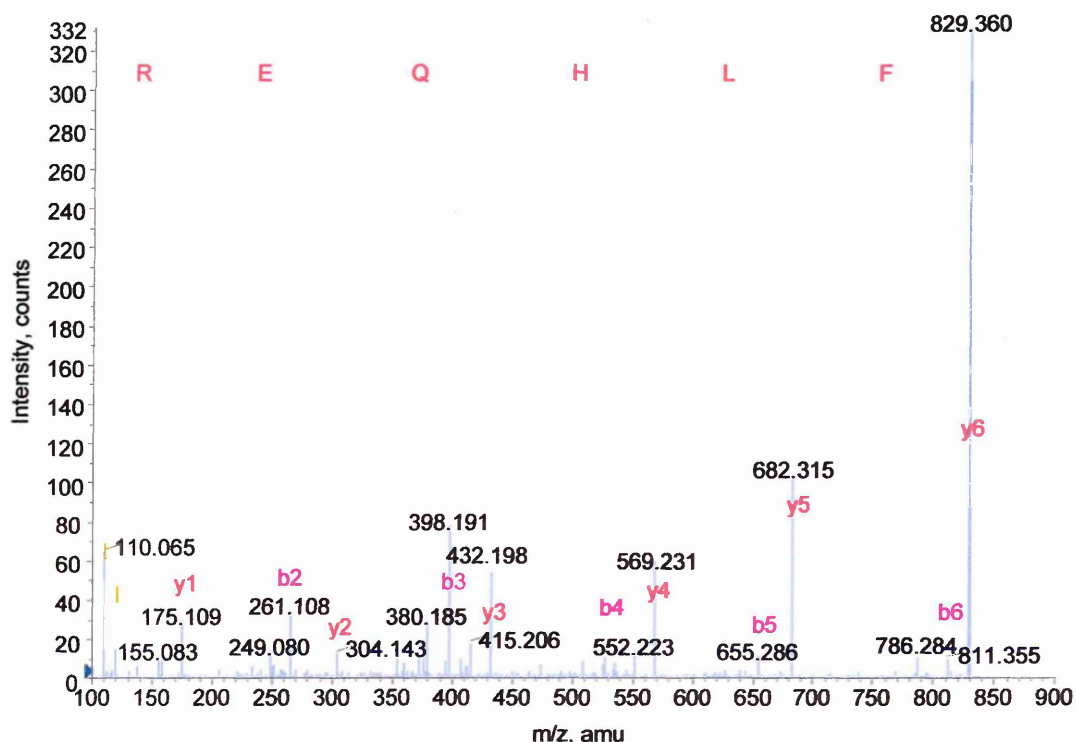


Figure 123. MALDI-MS/MS spectrum of peak at m/z 829.25 from the two-dimensional in-gel digest of APP α_{770} (figure 122) corresponding to the APP α_{770} tryptic peptide FLHQER, 828.33 monoisotopic mass. MS/MS analysis assigned the full sequence in ‘y’ ions.

Amino acid		Ion type (M+H ⁺)						
residue	mass/Da	immonium	a	a-NH ₃	b	b-NH ₃	y	y-NH ₃
F, Phe	147.06	120.08	120.08	103.05	148.07	131.04	829.43	812.40
L, Leu	113.08	86.09	233.16	216.13	261.15	244.13	682.36	665.33
H, His	137.05	110.07	370.22	353.19	398.21	381.19	569.27	552.25
Q, Gln	128.05	101.07	498.28	481.25	526.27	509.25	432.22	415.19
E, Glu	129.04	102.05	627.32	610.29	655.31	638.29	304.16	287.13
R, Arg	156.10	129.11	783.42	766.39	811.42	794.39	175.11	158.09

Table 72. BioAnalyst software results from the MALDI-MS/MS two-dimensional in-gel tryptic digest of APP α_{770} spectrum in figure 123. Shown is the list of ‘a’, ‘b’ and ‘y’ product ions available for the peptide FLHQER, highlighting the ions present.

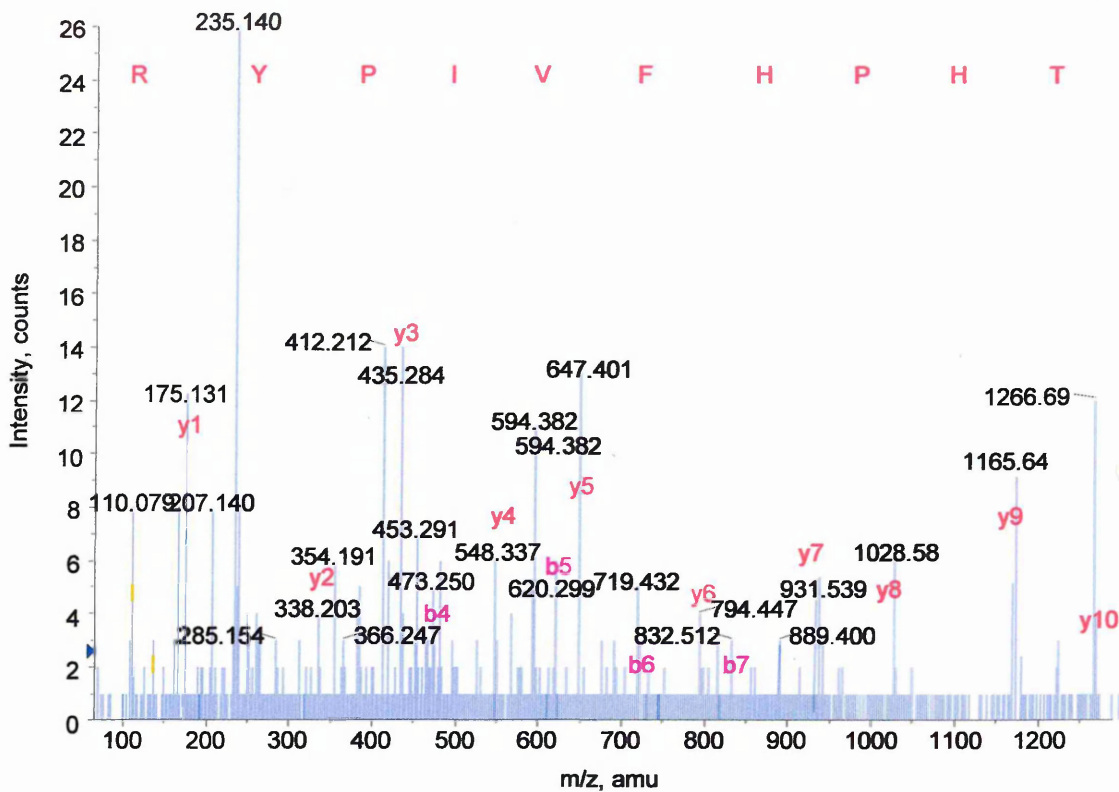


Figure 124. MALDI-MS/MS analysis of the peak at m/z 1266.25 (figure 122). Shown is the full sequence coverage for the peptide THPHFVIPYR.

Amino acid		Ion type (M+H ⁺)						
residue	mass/Da	immonium	a	a-NH ₃	b	b-NH ₃	y	y-NH ₃
T, Thr	101.04	74.06	74.06	57.03	102.05	85.02	1266.67	1249.64
H, His	137.05	110.07	211.11	194.09	239.11	222.08	1165.62	1148.60
P, Pro	97.05	70.06	308.17	291.14	336.16	319.14	1028.56	1011.54
H, His	137.05	110.07	445.23	428.20	473.22	456.19	931.51	914.48
F, Phe	147.06	120.08	592.29	575.27	620.29	603.26	794.45	777.42
V, Val	99.06	72.08	691.36	674.34	719.36	702.33	647.38	630.36
I, Ile	113.08	86.09	804.45	787.42	832.44	815.41	548.31	531.29
P, Pro	97.05	70.06	901.50	884.47	929.49	912.47	435.23	418.20
Y, Tyr	163.06	136.07	1064.56	1047.54	1092.56	1075.53	338.18	321.15
R, Arg	156.10	129.11	1220.66	1203.64	1248.66	1231.63	175.11	158.09

Table 73. BioAnalyst results from figure 124 showing the possible and actual 'a', 'b' and 'y' MS/MS products available for the peptide THPHFVIPYR.

3.446 Capillary LC/MS analysis of a two-dimensional in-gel tryptic digestion of immunoprecipitated APP α_{770} .

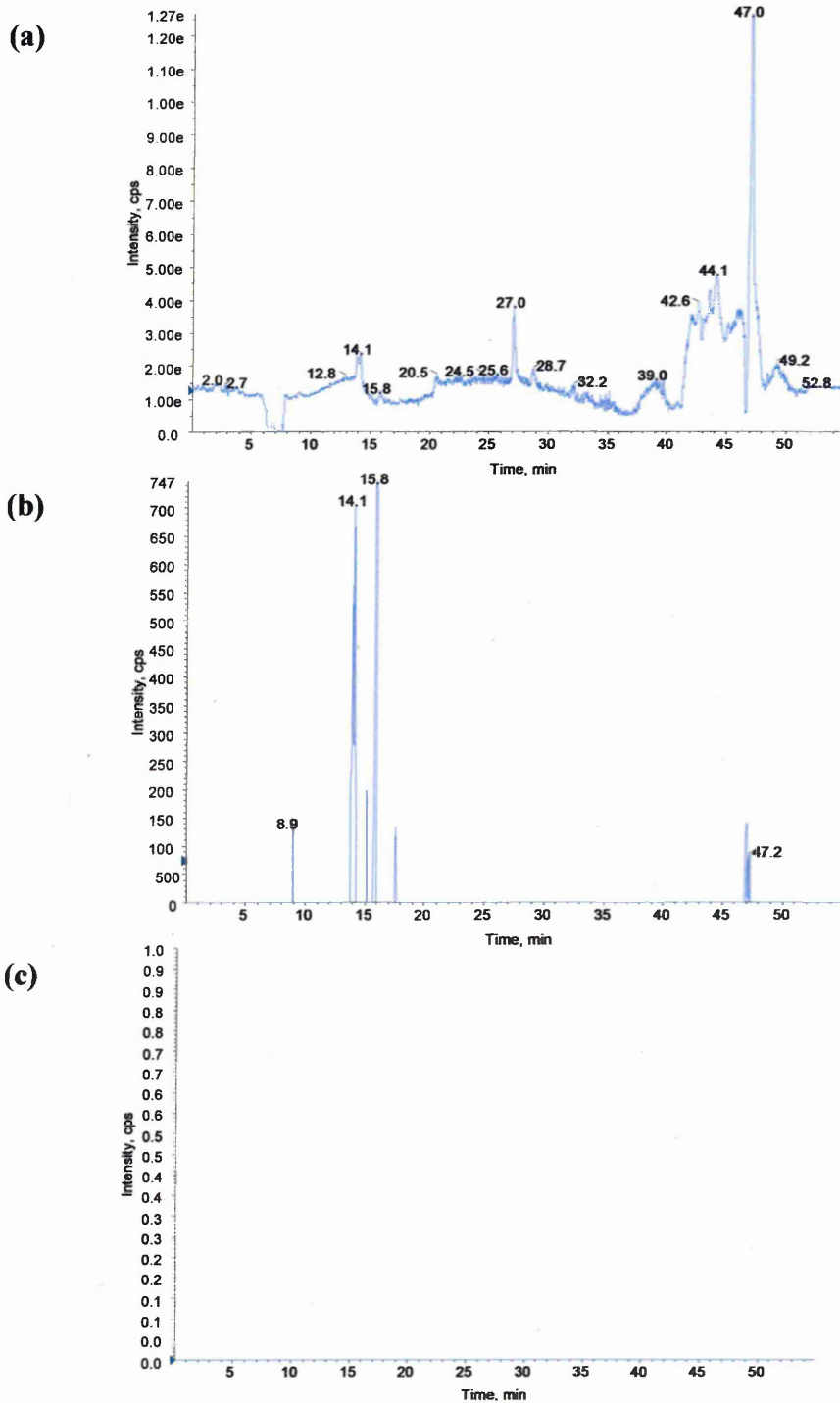


Figure 125. Capillary LC/MS run of an APP α_{770} two-dimensional in-gel tryptic digest performed using information dependant acquisition (IDA) software. For experimental conditions see chapter 2.92, page 92. (a) Shows the survey scan or total ion chromatogram (TIC). (b) Shows the TIC for the product ion intensities generated by product ion scan of the most intense peak in the normal mass spectrum. (c) Should show the TIC for the product ion intensities generated by product ion scan of the second most intense peak in the normal mass spectrum, however, no data is seen due to the poor quality of the sample. The peak lists generated from trace (b) was sorted according to predefined parameters (chapter 2.92, page 93) and a selection of the most intense peaks automatically sent for MS/MS (figures 126 and 127).

mass observed	mass (experimental)	position (sAPP770 numbering)	missed cleavages	peptide sequence
458.25	914.47	335-342	0	TTQEPLAR*
474.23	946.45	444-451	0	VEAMLNDR
404.87	1211.60	434-433	0	QQLVETHMAR
693.91	1385.61	347-360	0	LPTTAASTPDAVDK*
870.42	1738.83	569-584	0	ISYGN DALMPSLTETK
878.42	1754.83	569-584	0	ISYGN DALMPSLTETK(MSO)
674.72	2021.13	454-471	0	LALENYITALQAVPPRPR
709.69	2126.03	252-271	0	TTSIATTTTTTTESVEEVVR

Table 74. BioAnalyst automatic data analysis (using Matrix Science software) of the chromatograms seen in figure 125 of a two-dimensional in-gel tryptic digest of APP α_{770} gave 12% sequence coverage. The data highlights the presence of two APP α_{770} specific peptides unfortunately only one of these unique peptides was sequenced (highlighted in blue).

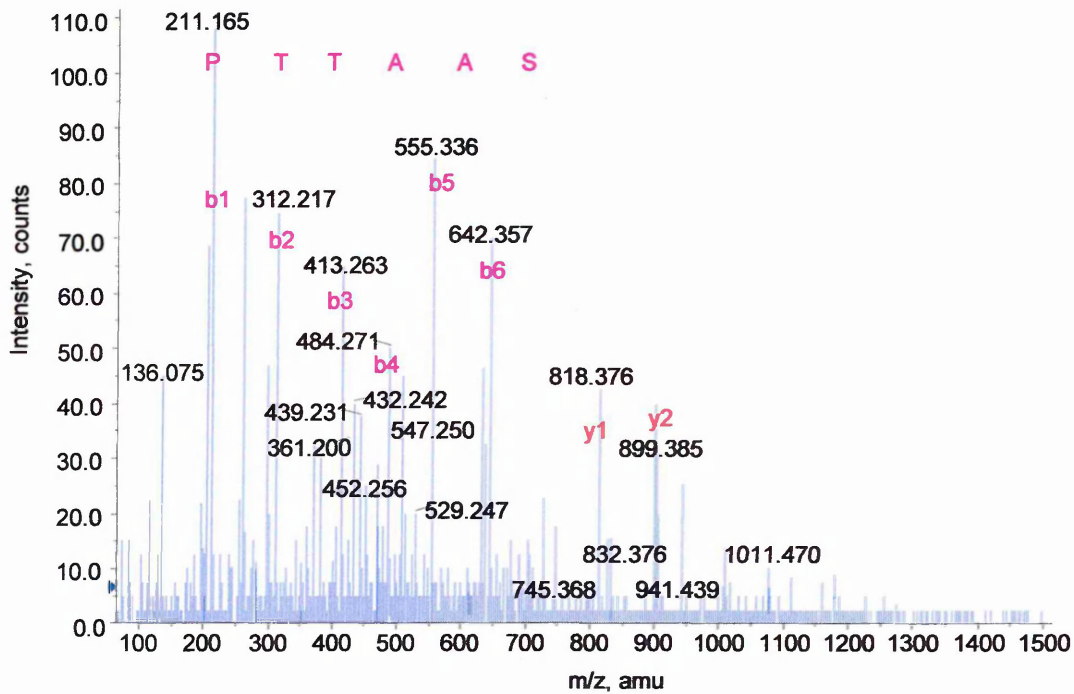


Figure 126. Capillary LC/MS/MS analysis of the doubly charged product ion at m/z 693.91, retention time 8.9 minutes from the LC/MS run of a two-dimensional in-gel tryptic digest of APP α_{770} (figure 125b). This product is consistent with the APP α_{770} tryptic peptide, LPTTAASTPDAVDK, MW 1385.61. This tryptic peptide is unique to the APP α_{770} isoform and the sequence tag PTTAAS uncovered validates its presence.

Amino acid		Ion type (M+H ⁺)						
residue	mass/Da	immonium	a	a-NH ₃	b	b-NH ₃	y	y-NH ₃
P, Pro	97.052	70.065	183.15	166.13	211.14	194.12	1259.57	1242.54
T, Thr	101.047	74.060	284.20	267.18	312.19	295.17	1162.52	1145.49

T, Thr	101.047	74.060	385.24	368.22	413.24	396.22	1061.47	1044.44
A, Ala	71.037	44.049	456.29	439.26	484.28	467.26	960.43	943.41
A, Ala	71.037	44.049	527.32	510.29	555.31	538.29	889.39	872.37
S, Ser	87.032	60.044	614.36	597.33	642.35	625.33	818.35	801.33

Table 75. BioAnalyst software results from the MALDI-MS/MS two-dimensional in-gel tryptic digest of APP α_{770} shown in figure 126. Listed are all the possible product ions for the sequence PTTAAS, highlighting the product ions present.

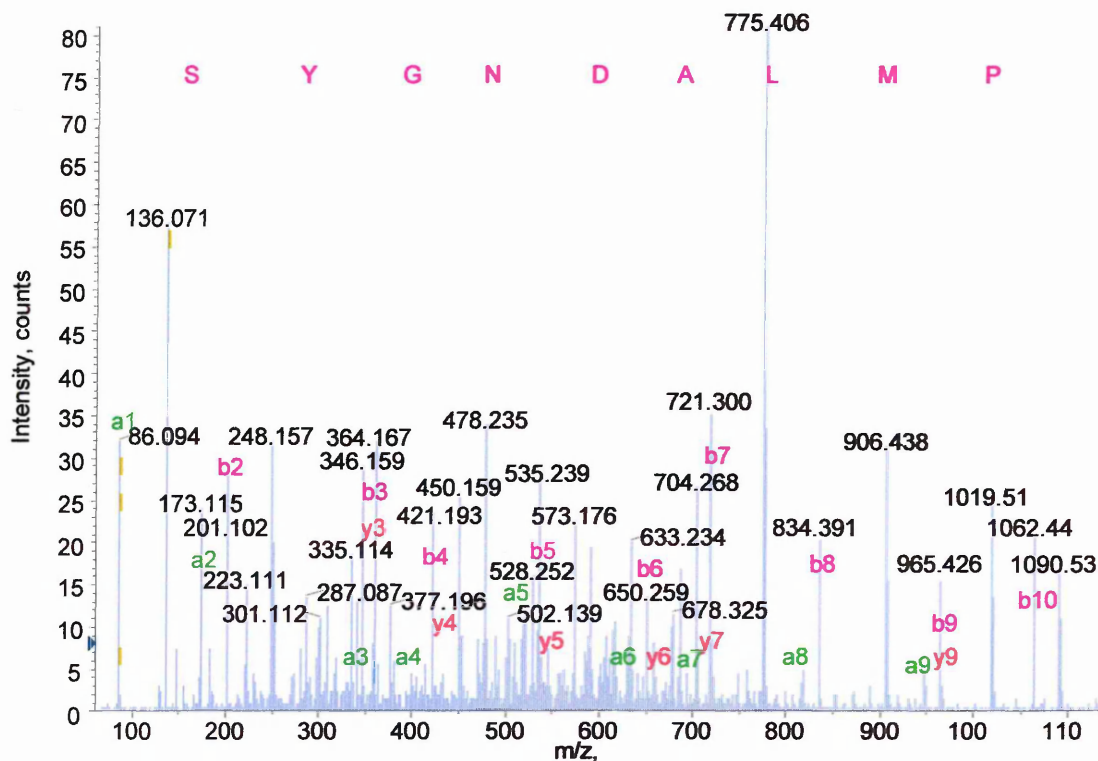


Figure 127. Capillary LC/MS/MS analysis of the doubly charged product ion at m/z 870.42, retention time 14.1 minutes from the LC/MS run of a two-dimensional in-gel tryptic digest of standard APP α_{770} (figure 125b). This product is consistent with the APP α_{770} tryptic peptide, ISYGN DALMPSLTETK, 1738.83 monoisotopic mass and the sequence tag, SYGN DALMP verifies this.

Amino acid		Ion type ($M+H^+$)						
residue	mass/Da	immonium	a	a-NH ₃	b	b-NH ₃	y	y-NH ₃
S, Ser	87.03	60.04	173.12	156.10	201.12	184.09	967.41	950.39
Y, Tyr	163.03	136.07	336.19	319.16	364.18	347.16	880.38	863.36
G, Gly	57.02	30.03	393.21	376.18	421.20	404.18	717.32	700.29
N, Asn	114.04	87.05	507.25	490.22	535.25	518.22	660.30	643.27
D, Asp	115.02	88.03	622.28	605.25	650.27	633.25	546.25	529.23
A, Ala	71.03	44.04	693.32	676.29	721.31	704.28	431.23	414.20
L, Leu	113.08	86.09	806.40	789.37	834.39	817.37	360.19	343.16
M, Met	131.04	104.05	937.44	920.41	965.43	948.41	247.11	230.08
P, Pro	97.05	70.06	1034.49	1017.47	1062.45	1045.46	116.0706	99.04

Table 76. BioAnalyst software results of the capillary LC/MS/MS spectrum in figure 127. The 'b' product ions highlighted show the presence of the sequence tag SYGN DALMP.

The alpha secretase cleaved amyloid precursor protein, isoform 770 (APP α_{770}) was immunoprecipitated from CHO 770 cell secretions.

MALDI-MS analysis of the two-dimensional in-gel tryptic digestion of APP α_{770} (figure 122) gave amino acid sequence coverage of 21% of the APP α_{770} molecule from 17 tryptic peptides. The sequence coverage achieved from the LC/MS (figure 125) analysis was inferior in comparison, uncovering 12% of the protein sequence from 7 peptides. Although the sequence coverage seem low compared to expected values the very low concentration of *in vivo* APP makes it a difficult molecule to isolate and investigate. MALDI-MS/MS examination of two tryptic peptides produced full sequence coverage in both cases (figures 123 and 124), whereas the results from the LC/MS/MS (figures 126 and 127) were less notable generating only sequence tags but they were sufficient to achieve positive results from automated searching. APP α_{770} produces three unique tryptic peptides; position 312-334, MW 2539.976; position 347-360, MW 1385.6111; position 335-342. MW 914.3894, the latter two are present in the both the MALDI-MS spectrum (figure 122) at m/zs 915.60 and 1386.71 marked by red asterisks and the LC/MS data (table 73) as the doubly charged species at m/zs 458.25 and 693.91 for the peptides 914.38 MW and 1385.61 MW respectively. Due to the relevance of these peptides verification by MS/MS analysis was attempted and although it was not achieved for 914.47, LC/MS/MS determination of 1385.61 MW was realised (figure 126). Presence of the possible *N*-glycosylated peptide in the MALDI-MS spectrum (figure 122) at m/z 1981.98 again suggests that glycosylation within this peptide does not occur, however, further investigation of this peptide would be necessary to prove its authenticity.

3.447 MALDI-MS analysis of a two-dimensional in-gel tryptic digestion of immunoprecipitated alpha secretase cleaved amyloid precursor protein (APP α).

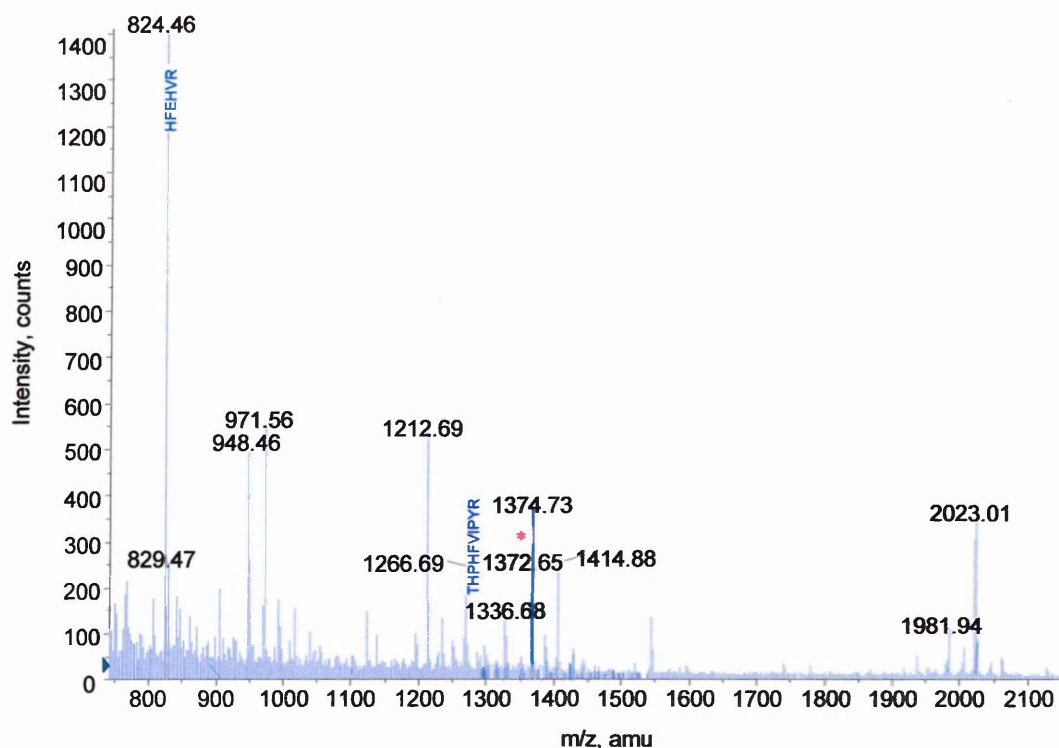


Figure 128. MALDI-MS spectrum of an in-gel tryptic digest of APP α from a two-dimensional gel. The peaks annotated were analysed by MS/MS (figures 129 and 130). The red asterisk marks the peak at m/z 1372.65 specific to the APP α_{695} isoform proving its presence within this sample. No other isoform specific peptides, however, were detected for either APP $_{751}$ or APP $_{770}$.

mass (M+H ⁺)	mass (experimental)	position (APP α_{770} numbering)	missed cleavages	peptide sequence
824.42	824.46	494-499	0	HFEHVR
829.43	829.47	118-123	0	FLHQER
948.41	948.46	395-401	0	EWEEAER
971.51	971.56	511-518	0	SQVMTHLR
1212.62	1212.69	434-443	0	QLLVETHMAR
1266.67	1266.69	90-99	0	THPHFVIPYR
1336.60	1336.68	660-670	0	HDSGYEVHHQK
1372.70	1372.65	272-285	0	VPTTAASTPDAVDK*
1374.65	1374.73	422-433	0	VESLEQEANER
1414.80	1414.88	632-635	0	GLTTRPGSGLTNIK
1980.90	1981.04	552-568	0	EQNYSDDVLANMISEPR
2022.15	2023.01	454-471	0	LALENYITALQAVPPRPR

Table 77. Mascot search results from the MALDI-MS mass fingerprint of the two-dimensional in-gel tryptic digest of APP α (figure 128), containing the three isoforms of interest (695, 751 and 770) and covering 19% of the sequence. The red asterisk marks the peptide specific to the APP α_{695} isoform and the position numbering in red is APP α_{695} numbering.

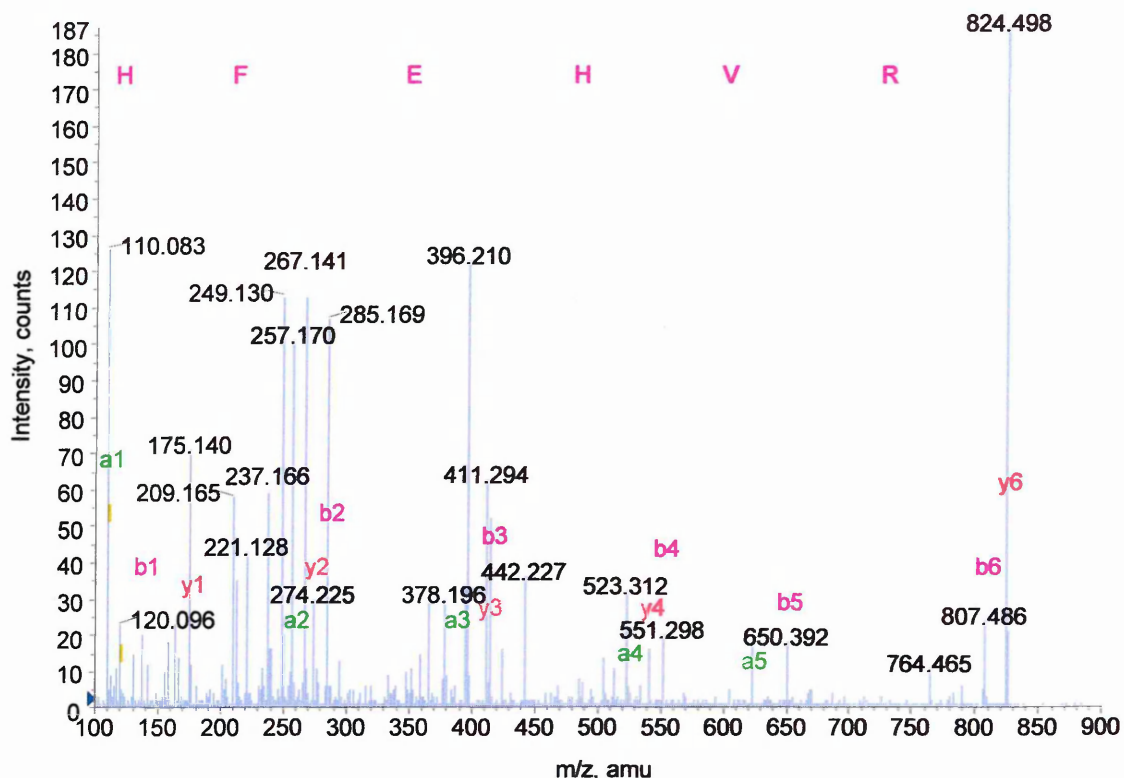


Figure 129. MALDI-MS/MS spectrum of peak at m/z 824.46 from the two-dimensional in-gel digest of APP α (figure 128) corresponding to the APP α tryptic peptide HFEHVR, 823.32 monoisotopic mass. MS/MS analysis assigned the full sequence in 'b' ions.

Amino acid		Ion type (M+H ⁺)						
residue	mass/Da	immonium	a	a-NH ₃	b	b-NH ₃	y	y-NH ₃
H, His	137.05	110.07	110.07	93.04	138.06	121.03	824.41	807.38
F, Phe	147.06	120.08	257.13	240.11	285.13	268.10	687.35	670.33
E, Glu	129.04	102.05	386.18	369.15	414.17	397.15	540.28	523.26
H, His	137.05	110.07	523.24	506.21	551.23	534.20	411.24	394.21
V, Val	99.06	72.08	622.30	605.28	650.30	633.27	274.18	257.16
R, Arg	156.10	129.11	778.41	761.38	806.40	789.37	175.11	158.09

Table 78. BioAnalyst software results from the MALDI-MS/MS two-dimensional in-gel tryptic digest of APP α spectrum in figure 129. Shown is the list of 'a', 'b' and 'y' product ions available for the peptide HFEHVR, emphasizing the ions present.

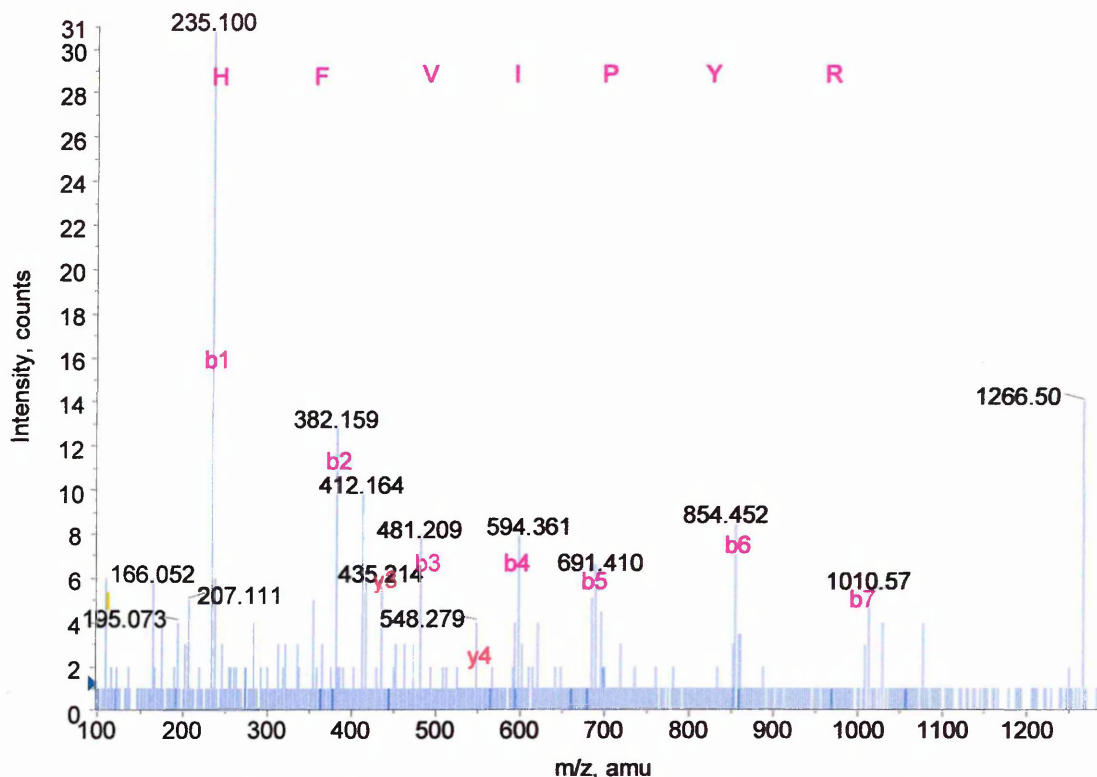


Figure 130. MALDI-MS/MS spectrum of peak at m/z 1266.65 from the two-dimensional in-gel digest of APP α (figure 128) corresponding to the APP α tryptic peptide THPHFVIPYR 1265.57 monoisotopic mass. MS/MS analysis revealed the sequence tag HFVIPYR in 'b' ions allowing automated searching to achieve a positive for APP.

Amino acid		Ion type ($M+H^+$)						
residue	mass/Da	immonium	a	a-NH ₃	b	b-NH ₃	y	y-NH ₃
H, His	137.05	110.07	207.12	190.09	235.11	218.09	931.51	914.48
F, Phe	147.06	120.08	354.19	337.16	382.18	365.16	794.45	777.42
V, Val	99.06	72.08	453.26	436.23	481.25	464.22	647.38	630.36
I, Ile	113.08	86.09	566.34	549.31	594.33	577.31	548.31	531.29
P, Pro	97.05	70.06	663.39	646.37	691.39	674.36	435.23	418.20
Y, Tyr	163.06	136.07	826.46	809.43	854.45	837.42	338.18	321.15
R, Arg	156.10	129.11	982.56	965.53	1010.55	993.53	175.11	158.09

Table 79. BioAnalyst software results from the MALDI-MS/MS two-dimensional in-gel tryptic digest of APP α spectrum in figure 130. Shown is the list of 'a', 'b' and 'y' product ions available for the sequence HFVIPYR, highlighting the ions present.

3.448 Capillary LC/MS analysis of a two-dimensional in-gel tryptic digestion of immunoprecipitated APP α .

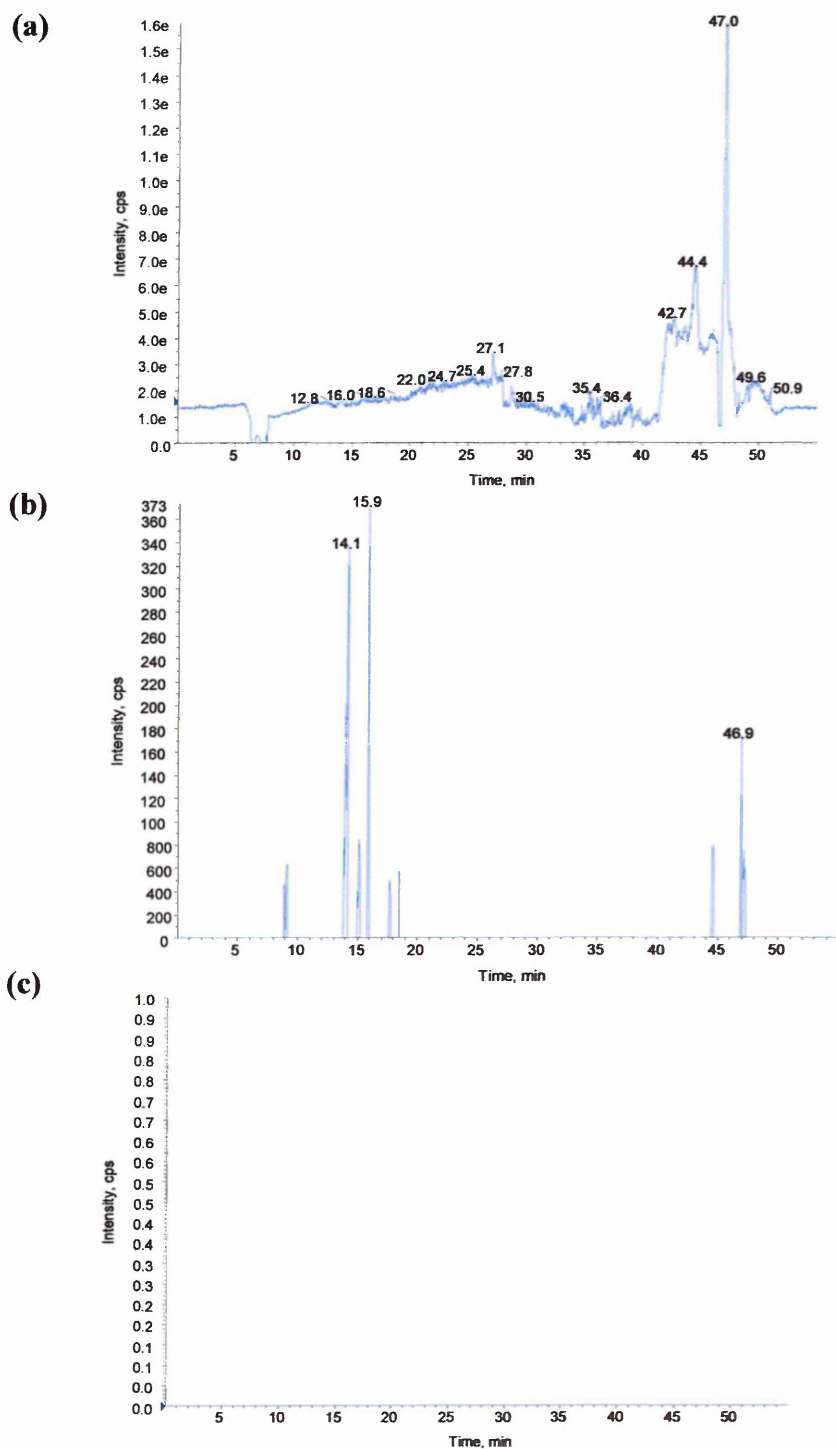


Figure 131. Capillary LC/MS run of an APP α two-dimensional in-gel tryptic digest performed using information dependant acquisition (IDA) software. For experimental conditions see chapter 2.92, page 92. (a) Shows the survey scan or total ion chromatogram (TIC). (b) Shows the TIC for the product ion intensities generated by product ion scan of the most intense peak in the normal mass spectrum. (c) Should shows the TIC for the product ion intensities generated by product ion scan of the second most intense peak in the normal mass spectrum. Lack of data however, may be due to low sample concentration. The peak list generated from trace (b) was sorted according to predefined parameters (chapter 2.92, page 93) and a selection of the most intense peaks automatically sent for MS/MS (figures 132 and 133).

mass observed	mass (experimental)	position (sAPP ₇₇₀ numbering)	missed cleavages	peptide sequence
687.82	1373.63	422-433	0	VESLEQEAAANER
870.40	1738.79	569-584	0	ISYGN DALMP SLTETK
674.71	2021.11	454-471	0	LALENYITALQAVPPRPR
709.69	2126.05	252-271	0	TTSIATTTTTTTSVEEVVR

Table 80. BioAnalyst automatic data analysis (using Matrix Science software) of the chromatograms seen in figure 131 of a two-dimensional in-gel tryptic digest of APP α giving 8% of the peptide sequence. The peptides sequences highlighted in blue were then subjected to MS/MS analysis (figures 132 and 133).

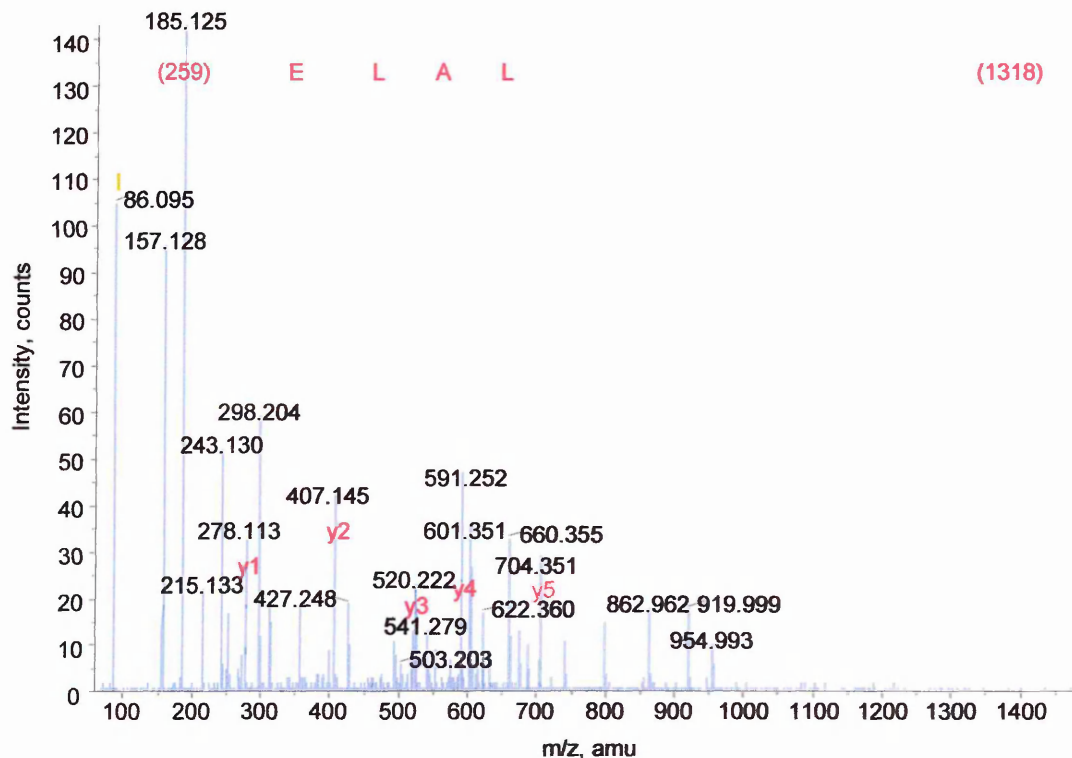


Figure 132. Capillary LC/MS/MS analysis of the triply charged product ion at m/z 674.71, retention time 16.0 minutes from the LC-MS run of a two-dimensional in-gel tryptic digest of APP α (figure 131b). This product is consistent with the APP α tryptic peptide LALENYITALQAVPPRPR, 2021.11 monoisotopic mass and the sequence tag LALE verifies this.

Amino acid		Ion type ($M+H^+$)						
residue	mass/Da	immonium	a	a-NH ₃	b	b-NH ₃	y	y-NH ₃
(1317.75)	1317.75	n/a	1290.76	1273.74	1318.76	1301.73	2022.10	2005.08
L, Leu	113.08	86.09	1403.85	1386.82	1431.84	1414.82	704.35	687.32
A, Ala	71.03	44.04	1474.89	1457.86	1502.88	1485.85	591.26	574.24
L, Leu	113.08	86.09	1587.97	1570.94	1615.96	1598.94	520.22	503.20
E, Glu	129.04	102.05	1717.01	1699.99	1745.01	1727.98	407.14	390.11
(259.08)	259.08	n/a	1976.10	1959.07	2004.09	1987.07	278.10	261.07

Table 81. BioAnalyst automated searching of the capillary LC/MS/MS spectrum from the two-dimensional in-gel tryptic digest of APP α shown in figure 132, shows the 'a', 'b' and 'y' product ions from the sequence tag LALE.

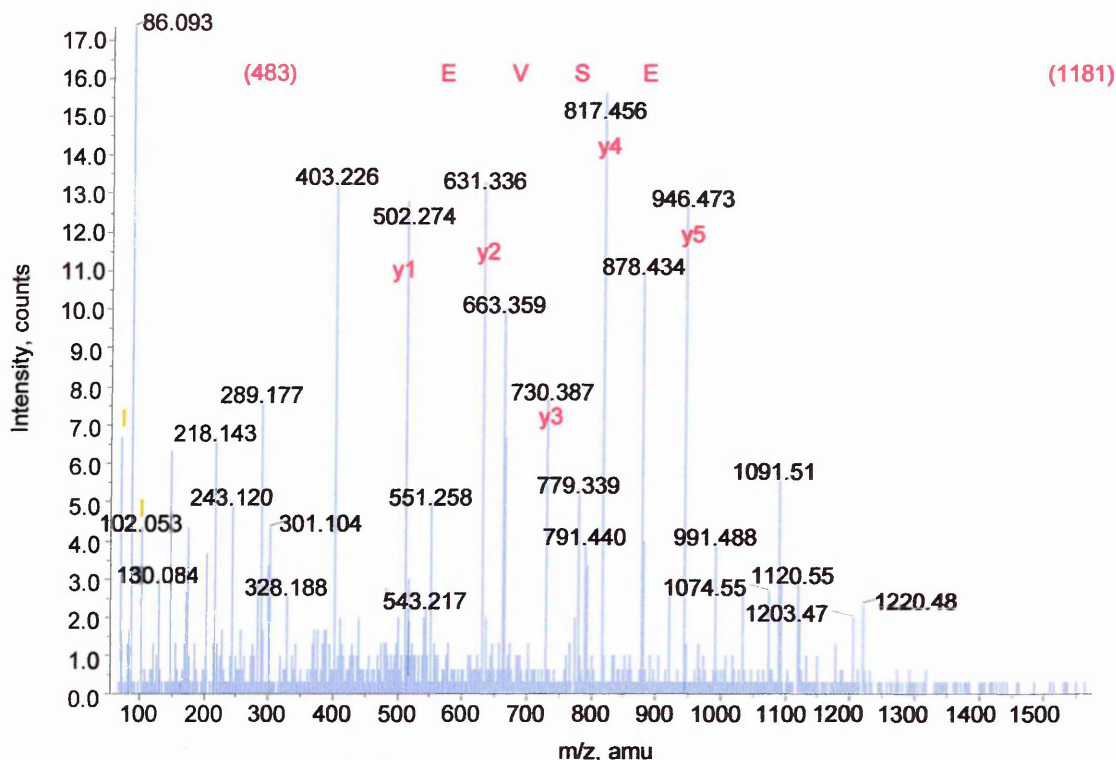


Figure 133. Capillary LC/MS/MS analysis of the triply charged product ion at m/z 709.69, retention time 14.0 minutes from the LC/MS run of a two-dimensional in-gel tryptic digest of APP α (figure 131b). This product is consistent with the APP α tryptic peptide TTSIATTTTTTTSVEEVVR, 2126.05 monoisotopic mass and the sequence tag ESVE expands this.

Amino acid		Ion type ($M+H^+$)						
residue	mass/Da	immonium	a	a-NH ₃	b	b-NH ₃	y	y-NH ₃
(1180.58)	1180.58	n/a	1153.59	1136.57	1181.59	1164.56	2127.04	2110.18
E, Glu	129.04	102.05	1282.63	1265.61	1310.63	1293.60	946.46	929.43
S, Ser	87.03	60.04	1369.67	1352.64	1397.66	1380.64	817.42	800.39
V, Val	99.06	72.08	1468.74	1451.71	1496.73	1479.70	730.38	713.36
E, Glu	129.06	102.05	1597.78	1580.75	1625.77	1608.75	631.32	614.29
(483.26)	483.26	n/a	2081.04	2064.01	2109.03	2092.01	502.27	485.25

Table 82. BioAnalyst automated searching of the capillary LC/MS/MS spectrum from the two-dimensional in-gel tryptic digest of APP α shown in figure 133, shows the 'a', 'b' and 'y' product ions from the sequence tag ESVE.

The alpha secretase cleaved amyloid precursor protein (APP α) used was immunoprecipitated from Ntera 2 cell secretions. APP α encompasses all three isoforms of interest (APP α_{695} , APP α_{751} , APP α_{770}) and as such is a more plausible model of *in vivo* conditions.

MALDI-MS results from the two-dimensional in-gel tryptic digestion of APP α (figure 128) uncovered 19% of the amino acid sequence in 12 peptides. The sequence coverage achieved from the LC/MS (figure 131) analysis was less impressive giving 8% of the protein sequence from only 4 peptides. Again the inferior LC/MS results are most likely due to differences in manual and automatic peak retrieval. MALDI-MS/MS analysis of two tryptic peptides provided a full sequence and a tag (figures 129 and 130). LC/MS/MS (figures 132 and 133) gave two sequence tags both of which were adequate in protein verification. The MALDI-MS data (figure 128) exhibited a specific tryptic peptide at m/z 1372.65, however, MALDI-MS/MS analysis was not achieved on this peak. The peptide significant for its probable *N*-glycosylation site (EQNYSDDVLANMISEPR, position 552-568 APP α_{770} numbering) at position 554 is present in the MALDI-MS data (figure 128) at m/z 1981.94, however, attempts to validate this by MALDI-MS/MS were unsuccessful. A final comment upon examination of all the MALDI-MS data seen here is the lack of contaminating species seen with the two-dimensional in-gel digests compared to the one-dimensional in-gel digests and although the sequence coverage of the standard proteins (BSA and APP α_{695}) is lower the coverage for immunoprecipitated samples is higher relative to the one-dimensional in-gel digests, thus showing the excellence of two-dimensional electrophoresis for resolving complex samples.

3.45 Two-dimensional in-gel Asp-N digestion of BSA and APP.

3.451 MALDI-MS analysis of a two-dimensional in-gel Asp-N digestion of BSA.

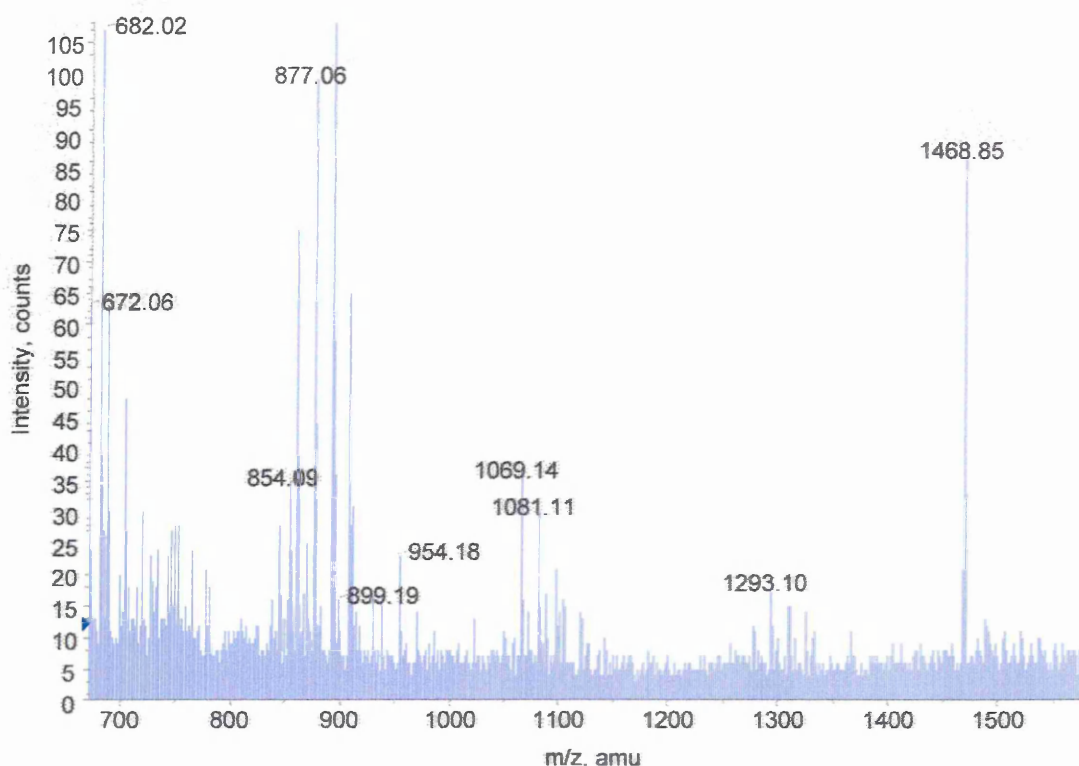


Figure 134. MALDI-MS spectrum of a two-dimensional in-gel Asp-N digest of BSA. The spectrum is dominated by contamination, the equidistant clusters signifying some form of polymer or adduct formation. None of the peaks present within this spectrum were able to provide convincing MS/MS data.

mass (M+H ⁺)	mass (experimental)	position	missed cleavages	peptide sequence
672.36	672.06	317-322	1	EKDAIP
682.25	682.02	190-195	1	ECCQAE
854.46	854.09	323-330	0	ENLPPLTA
877.40	877.06	535-542	1	DICTLPDT
900.50	899.19	30-36	0	EIAHRFK
954.49	954.18	518-525	0	ETYVPKAF
1069.52	1069.14	517-525	1	DETYVPKAF
1081.43	1081.11	465-473	2	ESERMPCTE
1293.75	1293.10	554-564	1	ELLKHKPKATE
1468.77	1468.85	25-36	1	DTHKSEIAHRFK

Table 83. Mascot search results from the two-dimensional in-gel Asp-N digest of BSA (figure 134), showing 10% sequence coverage although this is ambiguous due to the appearance of the MALDI-MS spectrum and lack of MS/MS data to substantiate any of the peaks listed.

3.452 Capillary LC/MS analysis of a two-dimensional in-gel Asp-N digestion of BSA.

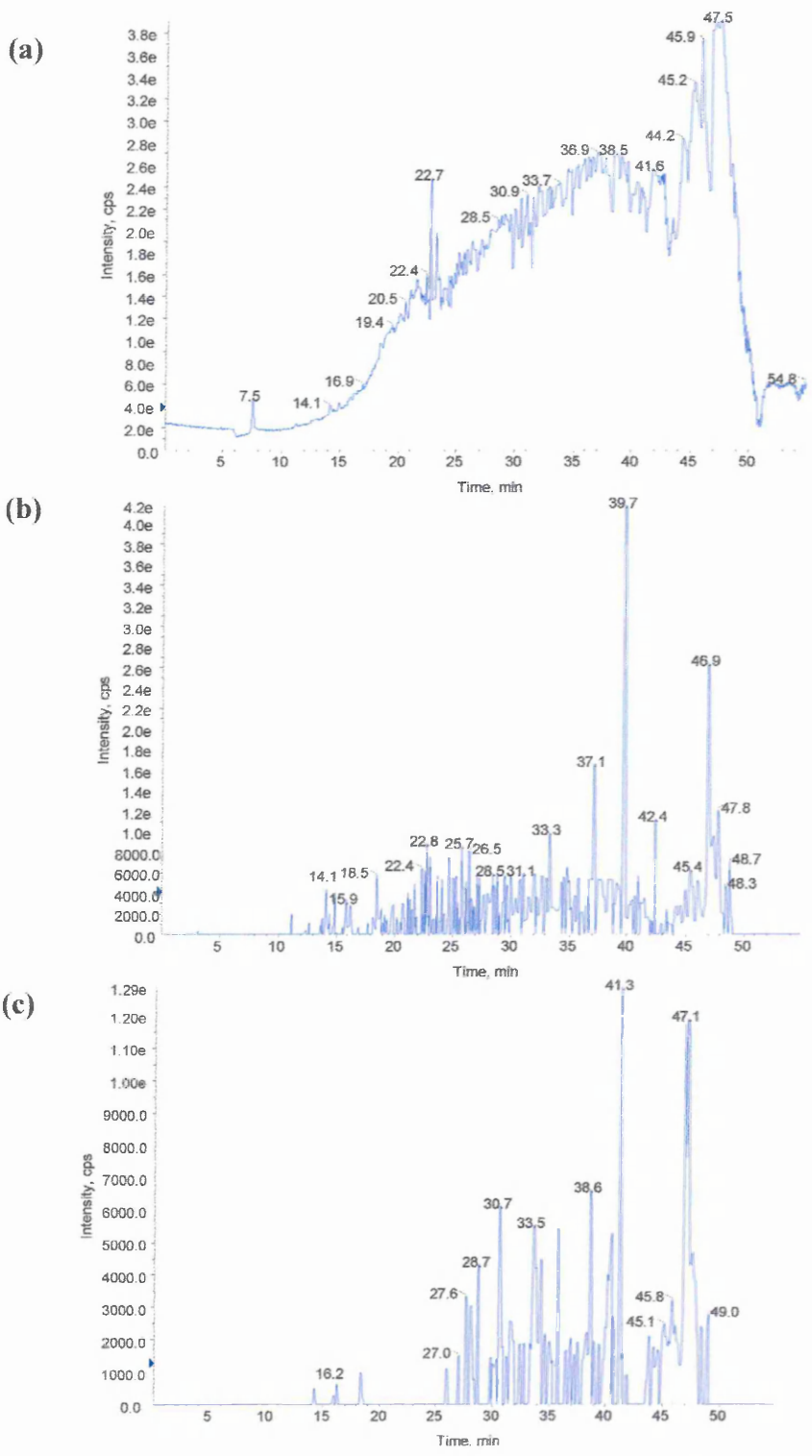


Figure 135. Capillary LC/MS run of a BSA two-dimensional in-gel Asp-N digest performed using information dependant acquisition (IDA) software. For experimental conditions see chapter 2.92, page 92. (a) Shows the survey scan or total ion chromatogram (TIC). (b) Shows the TIC for the product ion intensities generated by product ion scan of the most intense peak in the normal mass spectrum. (c) Shows the TIC for the product ion intensities generated by product ion scan of the second most intense peak in the normal mass spectrum. The peak lists generated from traces (b) and (c) were sorted according to predefined parameters (chapter 2.92, page 93) and a selection of the most intense peaks automatically sent for MS/MS (figure 136).

mass observed	mass (experimental)	position	missed cleavages	peptide sequence
625.82	1249.63	320-331	0	AIPENLPPLTAD
856.91	1711.80	320-335	1	AIPENLPPLTADFAED
978.45	1954.89	320-337	2	AIPENLPPLTADFAEDKD
790.30	2367.88	114-131	0	CCEKQEPERNECFLSHKD

Table 84. BioAnalyst automatic data analysis (using Matrix Science software) of the chromatograms shown in figure 135 of a two-dimensional in-gel Asp-N digest of BSA gave 5% sequence coverage. The sequence highlighted in blue was subjected to MS/MS analysis (figure 136).

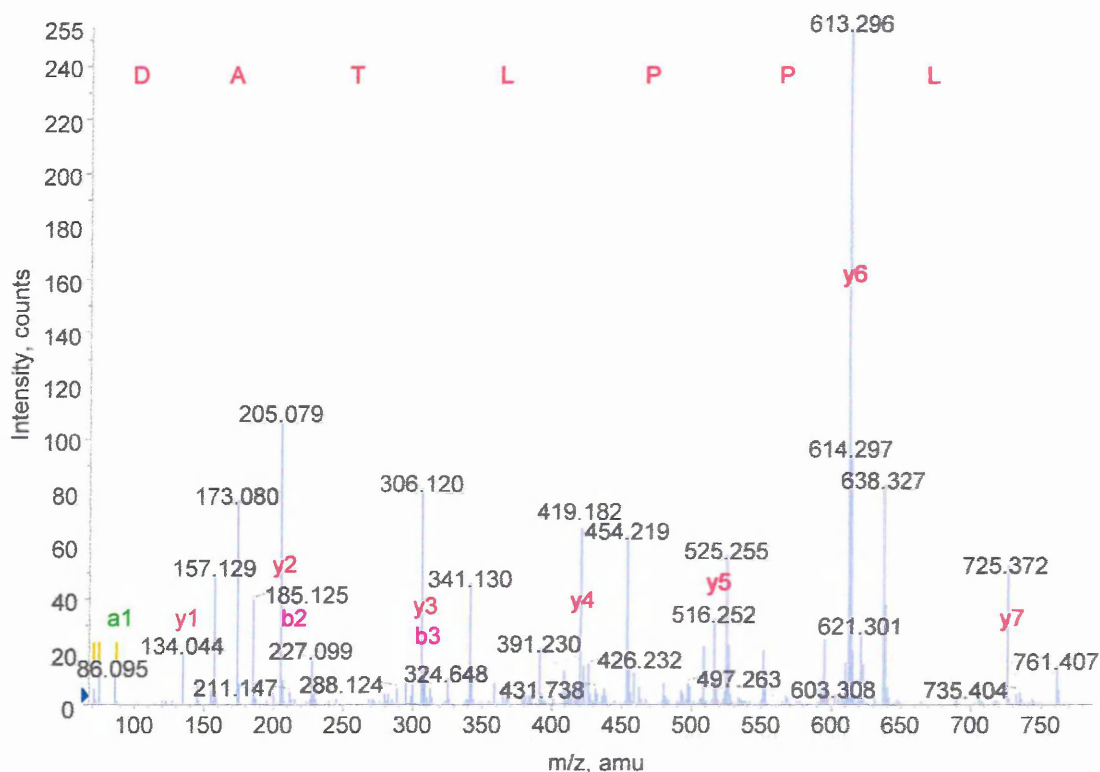


Figure 136. Capillary LC/MS/MS analysis of the doubly charged product ion at 625.82 m/z, retention time 16.1 minutes from the LC/MS run of a two-dimensional in-gel Asp-N digest of BSA (figure 135b). The sequence tag LPPLTAD is consistent with the BSA Asp-N peptide AIPENLPPLTAD, 1249.63 monoisotopic mass.

residue	mass/Da	Amino acid						
		immonium	a	a-NH ₃	b	b-NH ₃	y	y-NH ₃
L, Leu	113.08	86.09	86.09	69.06	114.09	97.06	726.42	709.39
P, Pro	97.05	70.06	183.14	166.12	211.14	194.11	613.34	596.31
P, Pro	97.05	70.06	280.20	263.17	308.19	291.17	516.28	499.26
L, Leu	113.08	86.09	393.28	376.25	421.28	404.25	419.23	402.20
T, Thr	101.04	74.06	494.33	477.30	522.32	505.31	306.15	289.12
A, Ala	71.03	44.04	565.37	548.34	593.36	576.33	205.10	188.07
D, Asp	115.02	88.03	680.39	663.37	708.39	691.31	134.06	117.03

Table 85. BioAnalyst results of the capillary LC/MS/MS spectrum of the product at 625.82 m/z from the two-dimensional in-gel Asp-N digest of BSA shown in figure 136. The possible and actual 'a', 'b' and 'y' product ions for the sequence LPPLTAD are shown.

Bovine serum albumin (BSA, MW 66,432.96) was used as a standard due to its availability and similarity in molecular weight to the amyloid precursor protein isoforms (APP α_{695} , MW 67,708.02, APP α_{751} , MW 73,863.85, APP α_{770} , MW 75,988.34).

The MALDI-MS analysis of the two-dimensional in-gel Asp-N digest of BSA (figure 134) resulted in 10 Asp-N peptides covering 10% of the protein. LC/MS analysis (figure 135) of the same sample revealed 4 Asp-N peptides for BSA, which covered 5% of the protein sequence. The protein sequence coverage of methods both was poor for a model protein such as BSA and needs further investigation to optimise the Asp-N digest procedure. The MALDI-MS spectrum (figure 34) was dominated by contamination that looked like some form of polymer or adducts. The difference between the peaks was approximately 16Da, which might suggest the addition of a NH₂ moiety. Further investigation of these peaks and experimental procedure is needed. Particularly prominent in the LC/MS results (table 83) are the presence of missed cleavages suggesting insufficient cleavage. None of the peaks present within MALDI-MS spectrum were able to provide convincing MS/MS data, however, LC/MS/MS gave one sequence tag (figure 136).

3.453 MALDI-MS analysis of a two-dimensional in-gel Asp-N digestion of alpha secretase cleaved amyloid precursor protein standard, isoform 695 (APP α_{695}).

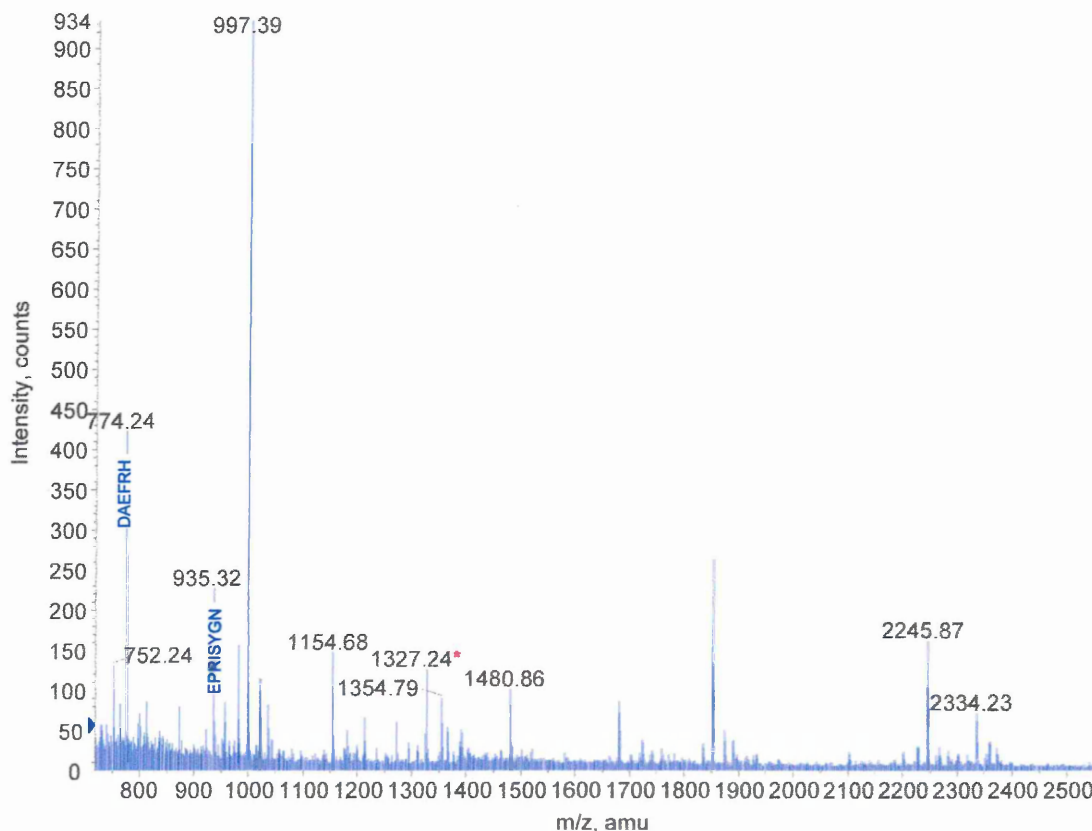


Figure 137. MALDI-MS spectrum of a two-dimensional in-gel Asp-N digest of standard APP α_{695} . The peak at m/z 1327.24, marked by a red asterisk is specific to APP α_{695} . The annotated peaks at m/zs 774.24 and 935.32 gave the best results when subjected to MS/MS analysis the results of which are shown in figures 138 and 139. The contaminating species present within the spectrum are unknown and further identification should ideally be carried out by MS/MS particularly upon the peak at m/z 1850.

mass (M+H ⁺)	mass (experimental)	position (APP α_{695} numbering)	missed cleavages	peptide sequence
752.31	752.24	122-127	1	ERMDVC
774.35	774.24	580-585	1	DAEFRH
935.46	935.32	491-498	0	EPRISYGN
997.40	997.39	166-173	0	EFVCCPLA(CM)
1154.66	1154.68	325-334	0	ERQAKNLPKA
1327.72	1327.24	268-280	0	EVVRVPTTAASTP*
1354.74	1354.79	323-334	1	EAERQAKNLPKA
1480.67	1480.86	312-322	2	ERMSQVMREWE
2245.18	2245.19	555-575	2	DRGLTTRPGSGLTNIKTEEIS
2334.19	2334.23	409-426	2	EQKDRQHTLKHFEHVRMV(MSO)

Table 86. Mascot search results from the MALDI-MS of the two-dimensional in-gel Asp-N digest of APP α_{695} shown (figure 137) covering 15% of the peptide sequence. The sequences highlighted in blue gave to best results when subjected to MS/MS analysis. Sequencing of the specific peptide EVVRVPTTAASTP (highlighted with a red asterisk), however, was unsuccessful.

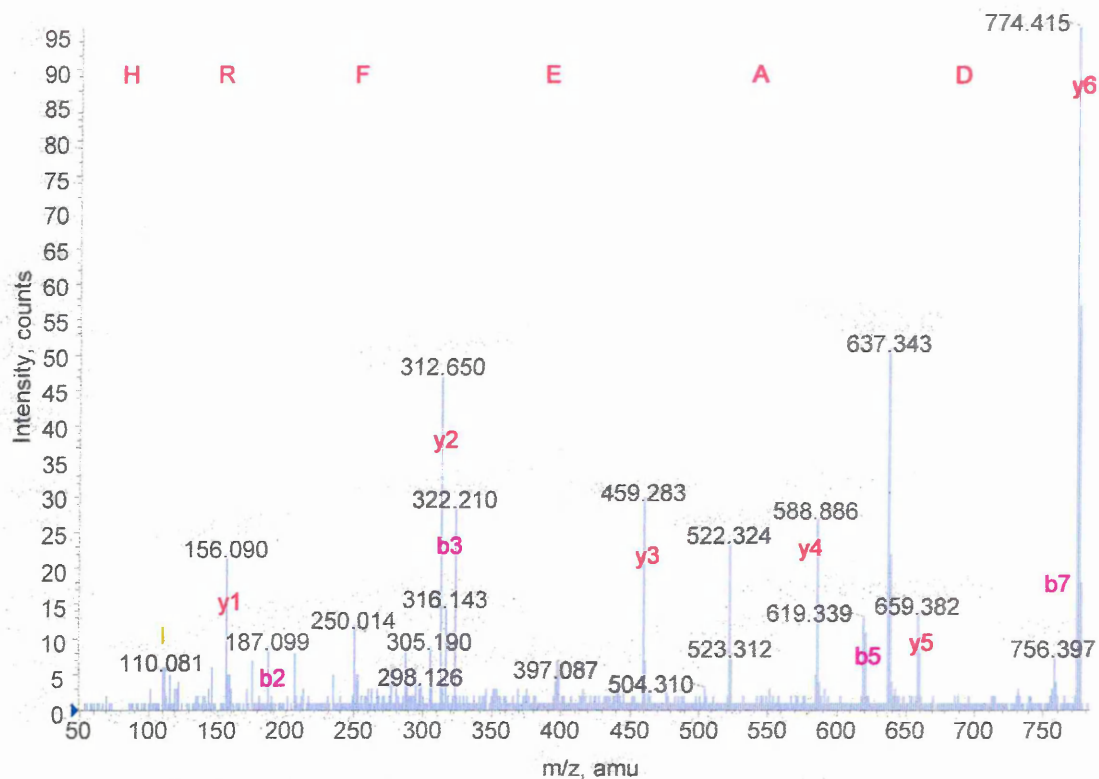


Figure 138. MALDI-MS/MS spectrum of peak at m/z 774.24 from the two-dimensional in-gel Asp-N digest of APP α_{695} in figure 137. This peak corresponds to the APP α_{695} Asp-N peptide DAEFRH, 773.25 MW and the MS/MS analysis results validate this by giving the full peptide sequence.

Amino acid		Ion type ($M+H^+$)						
residue	mass/Da	immonium	a	a-NH ₃	b	b-NH ₃	y	y-NH ₃
D, Asp	115.02	88.03	88.03	71.01	116.03	99.00	774.35	757.32
A, Ala	71.03	44.04	159.07	142.04	187.07	170.04	659.32	642.29
E, Glu	129.04	102.05	288.11	271.09	316.11	299.08	588.28	571.26
F, Phe	147.06	120.08	435.18	418.16	463.18	446.15	459.24	442.21
R, Arg	156.10	129.11	591.28	574.26	619.28	602.25	312.17	295.15
H, His	137.05	110.07	728.34	711.32	756.34	739.38	156.07	139.05

Table 87. BioAnalyst software results from the MALDI-MS/MS two-dimensional in-gel Asp-N digest of APP α_{695} shown in figure 138. Listed are all the possible 'a', 'b' and 'y' product ions for the peptide DAEFRH, highlighting the products ions present.

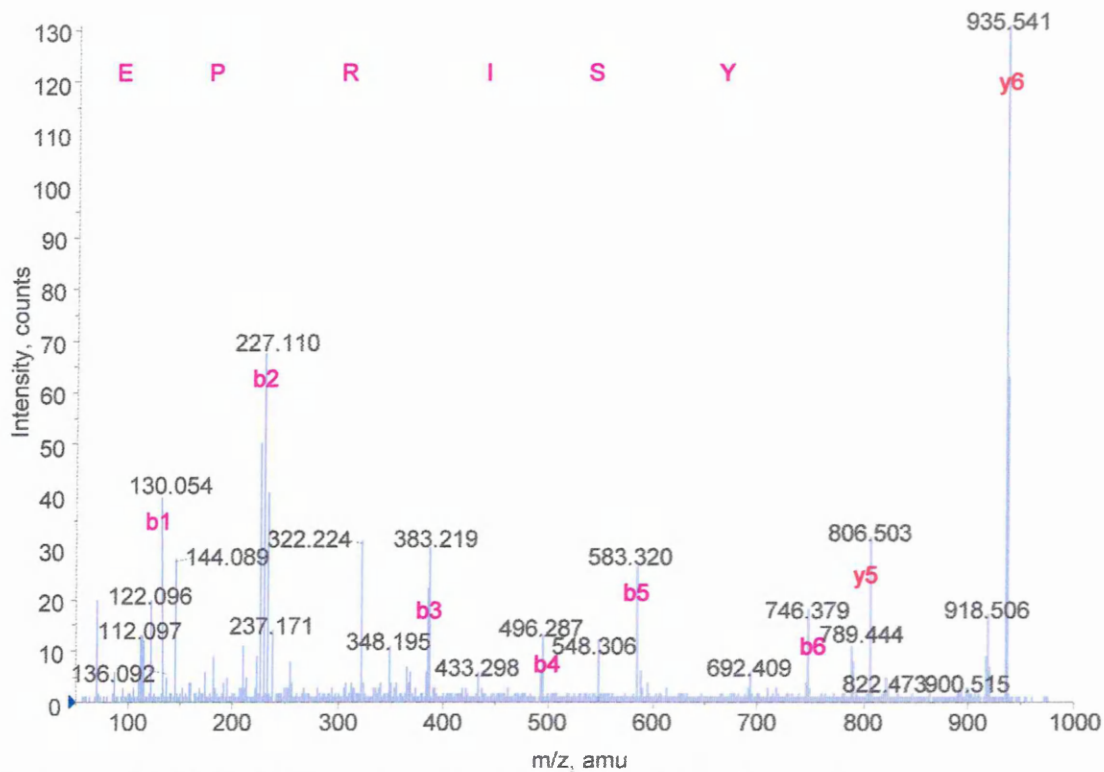


Figure 139. MALDI-MS/MS spectrum of peak at m/z 935.32 from the two-dimensional in-gel Asp-N digest of APP α_{695} in figure 137. This peak corresponds to the APP α_{695} Asp-N peptide EPRISYGN, 934.26 monoisotopic MW and the resulting 'b' ion sequence tag authenticates the peak.

Amino acid		Ion type ($M+H^+$)						
residue	mass/Da	immonium	a	a-NH ₃	b	b-NH ₃	y	y-NH ₃
E, Glu	129.04	102.05	102.05	85.02	130.04	113.02	935.45	918.43
P, Pro	97.05	70.06	199.10	182.08	227.10	210.07	806.41	789.38
R, Arg	156.10	129.11	355.20	338.18	383.20	366.17	709.36	693.33
I, Ile	113.08	86.09	468.29	451.26	496.28	479.26	553.26	536.23
S, Ser	87.03	60.04	555.32	538.29	583.31	566.29	440.17	423.14
Y, Tyr	163.06	136.07	718.38	701.36	746.38	729.35	353.14	336.11

Table 88. BioAnalyst software results from the MALDI-MS/MS two-dimensional in-gel Asp-N digest of APP α_{695} shown in figure 139. Listed are all the possible 'a', 'b' and 'y' product ions for the sequence EPRISY, highlighting the product ions present.

3.454 Capillary LC/MS analysis of a two-dimensional in-gel Asp-N digestion of standard APP α_{695} .

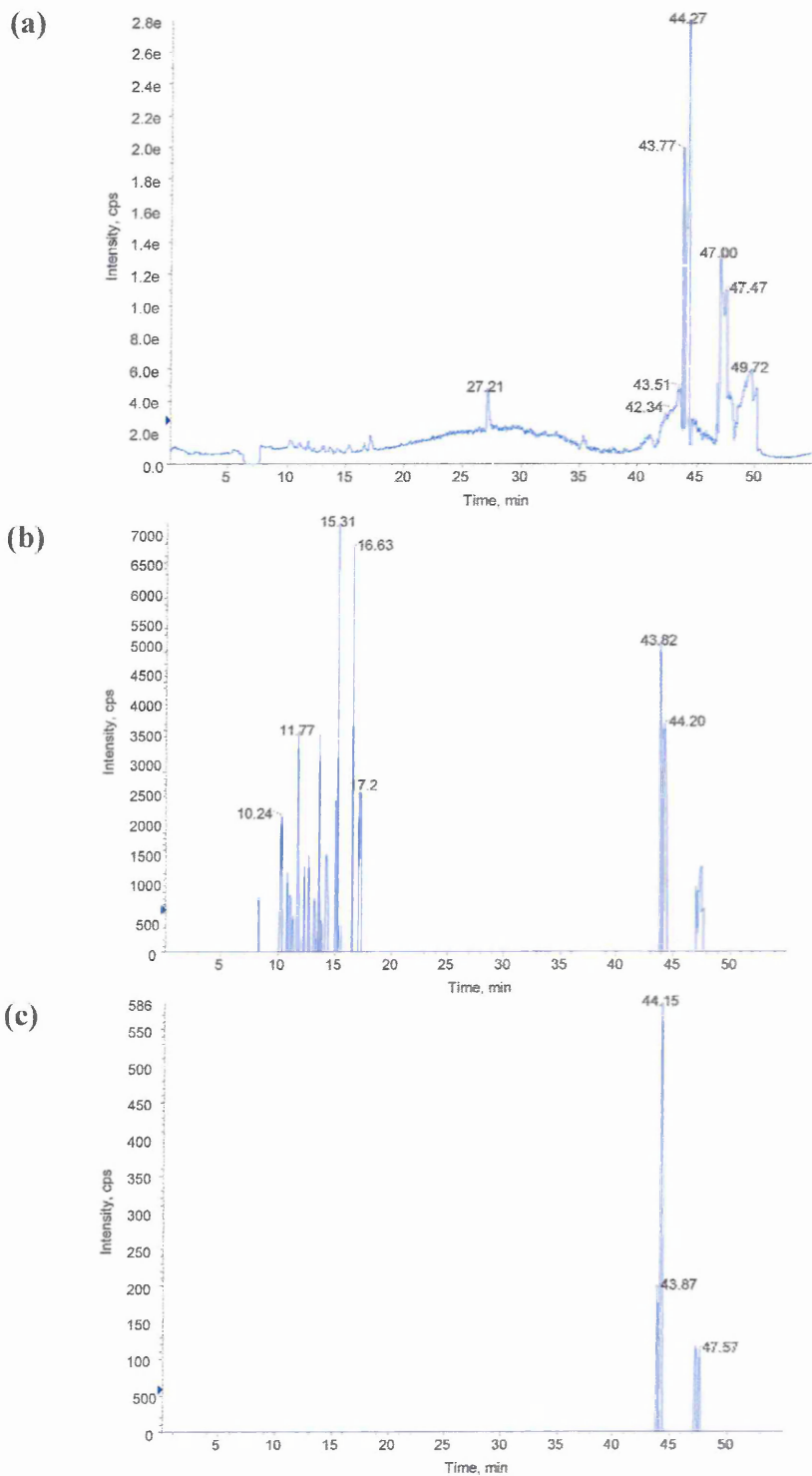


Figure 140. Capillary LC/MS run of an APP α_{695} two-dimensional in-gel Asp-N digest performed using information dependant acquisition (IDA) software. For experimental conditions see chapter 2.92, page 92. (a) Shows the survey scan or total ion chromatogram (TIC). (b) Shows the TIC for the product ion intensities generated by product ion scan of the most intense peak in the normal mass spectrum. (c) Shows the TIC for the product ion intensities generated by product ion scan of the second most intense peak in the normal mass spectrum, however, only mobile phase peaks can be seen. The peak list generated from trace (b) was sorted according to predefined parameters (chapter 2.92, page 93) and a selection of the most intense peaks automatically sent for MS/MS (figures 141 and 142).

mass observed	mass (experimental)	Position (APP α_{695} numbering)	missed cleavages	peptide sequence
395.67	789.33	190-196	0	DVWWGGA
461.72	921.43	284-291	1	DKYLETPG
489.23	976.44	482-490	1	DDVLANMIS
579.26	1156.51	525-534	0	DLQPWHSFGA
636.78	1271.59	524-534	1	DDLQPWHSFGA
664.35	1326.69	268-280	0	EVVRVPTTAASTP*
683.81	1365.61	471-481	2	DELLQKKEQNYS
494.40	1480.18	471-482	3	DELLQKKEQNYS
750.33	1498.65	535-548	3	DSVPANTENEVEPV
753.88	1505.74	499-512	1	DALMPSLTETKTTV

Table 89. BioAnalyst automatic data analysis (using Matrix Science software) of the chromatograms seen in figure 140 of a two-dimensional in-gel Asp-N digest of standard APP α_{695} gave 15% sequence coverage.

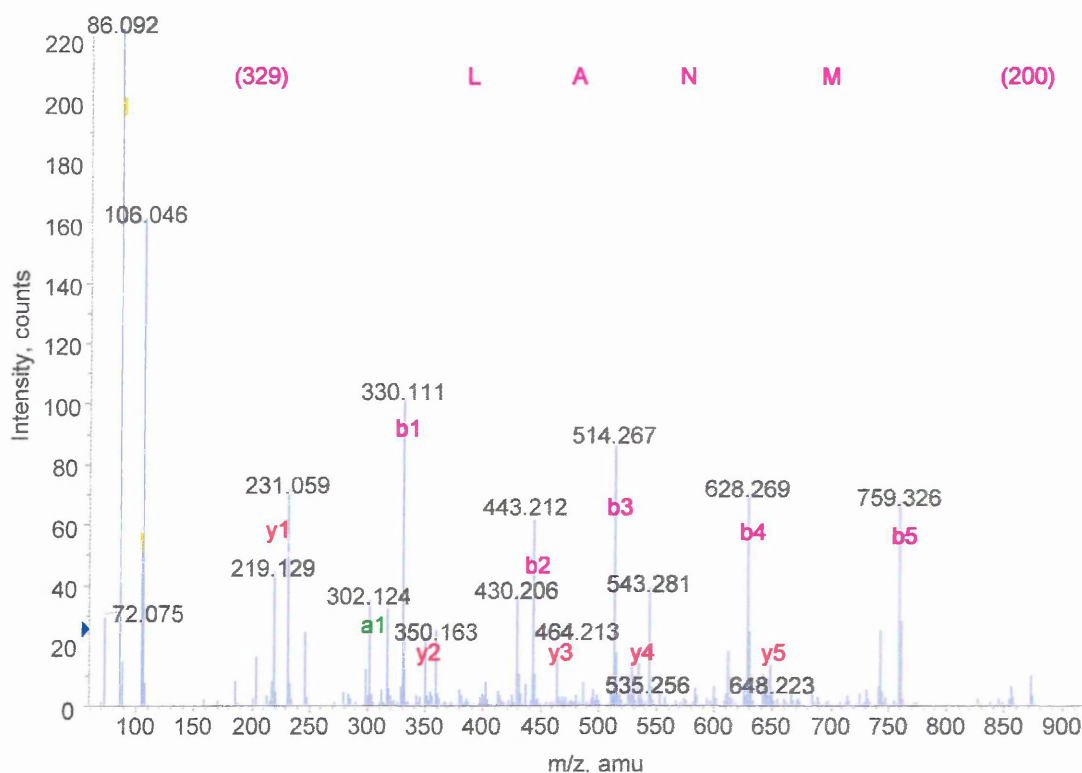


Figure 141. Capillary LC/MS/MS analysis of the doubly charged product ion at m/z 489.23, retention time 16.5 minutes from the LC/MS run of a two-dimensional in-gel Asp-N digest of standard APP α_{695} (figure 140b). This product is consistent with the APP α_{695} Asp-N peptide DDVLANMIS, 976.44 monoisotopic mass.

Amino acid		Ion type (M+H ⁺)						
residue	mass/Da	immonium	a	a-NH ₃	b	b-NH ₃	y	y-NH ₃
(329.12)	329.12	n/a	302.13	285.11	330.13	313.10	977.45	960.43
L, Leu	113.08	86.09	415.22	398.19	443.21	426.18	648.33	631.30

A, Ala	71.03	44.04	486.25	469.23	514.25	497.22	535.24	518.22
N, Asn	114.04	87.05	600.30	583.27	628.29	611.26	464.21	447.18
M, Met	131.04	104.05	731.34	714.31	759.33	742.30	350.16	333.14
(200.11)	200.11	n/a	931.45	914.42	959.44	942.42	219.12	202.10

Table 90. BioAnalyst software results of the capillary LC/MS/MS spectrum of the doubly charged product at 489.23 m/z from the two-dimensional in-gel Asp-N digest of standard APP α_{695} shown in figure 141.

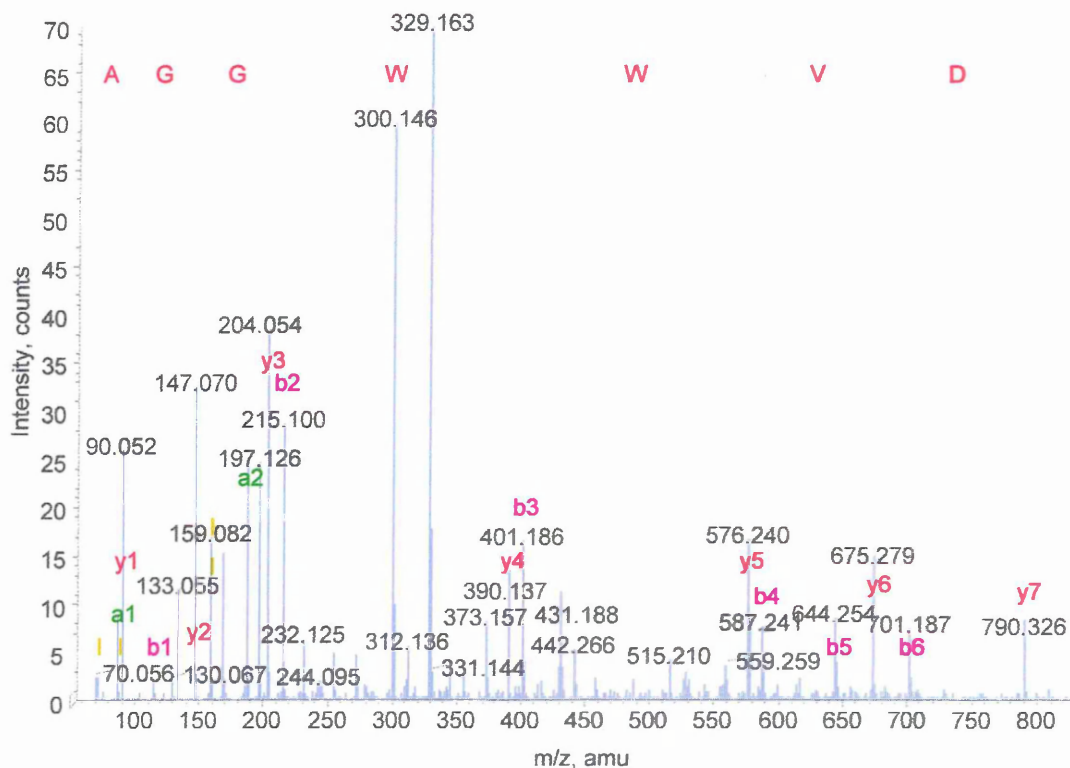


Figure 142. Capillary LC/MS/MS run of the doubly charged product ion at 395.67 m/z, retention time 17.3 minutes from the LC/MS run of a two-dimensional in-gel Asp-N digest of standard APP α_{695} (figure 140b). This product is consistent with the APP α_{695} Asp-N peptide DVWWGGA, 789.33 monoisotopic mass and MS/MS analysis revealing the full peptide sequence verifies this.

Amino acid	Ion type (M+H ⁺)								
	residue	mass/Da	immonium	a	a-NH ₃	b	b-NH ₃	y	y-NH ₃
D, Asp		115.02	88.03	88.03	71.01	116.03	99.00	790.30	773.28
V, Val		99.06	72.08	187.10	170.08	215.10	198.07	675.28	658.25
W, Trp		186.07	159.09	373.18	356.16	401.18	384.15	576.21	559.18
W, Trp		186.07	159.09	559.26	542.23	587.26	570.23	390.13	373.10
G, Gly		57.02	30.03	616.28	599.26	644.28	627.25	204.05	187.02
G, Gly		57.02	30.03	673.30	656.28	701.30	684.27	147.03	130.00
A, Ala		71.03	44.04	744.34	727.31	772.34	755.31	90.012	72.98

Table 91. BioAnalyst software results of the capillary LC/MS/MS spectrum of the doubly charged product at 395.67 m/z from the two-dimensional in-gel Asp-N digest of standard APP α_{695} shown in figure 142.

Amyloid precursor protein standard was purchased from Sigma for use as a direct comparison. The standard was the alpha secretase cleaved APP, isoform 695 (APP α_{695}) from E.coli origin.

The MALDI-MS determination of the two-dimensional in-gel Asp-N digestion of APP α_{695} (figure 137) gave amino acid sequence coverage of 15% of the APP α_{695} molecule from 10 Asp-N peptides. The sequence coverage achieved from the LC/MS (figure 140) was very similar covering 15% of the protein sequence from 10 peptides. MALDI-MS/MS analysis uncovered a full sequence (figure 138) and a generous sequence tag (figure 139), likewise for the LC/MS/MS examination (figures 141 and 142). The unique Asp-N peptide exhibited by APP α_{695} (position 268-280, MW 1326.6216, amino acid sequence EVVPTTAASTP) was present in both the MALDI-MS and LC/MS data. Observed as the peak at m/z 1327.24 in the MALDI-MS spectrum (figure 137) and its presence within the LC/MS chromatograms was highlighted in the BioAnalyst search results (table 88). MS/MS confirmation of this peptide, however, was not achieved.

3.455 MALDI-MS analysis of a two-dimensional in-gel Asp-N digestion of immunoprecipitated alpha secretase cleaved amyloid precursor protein, isoform 770 (APP α_{770}).

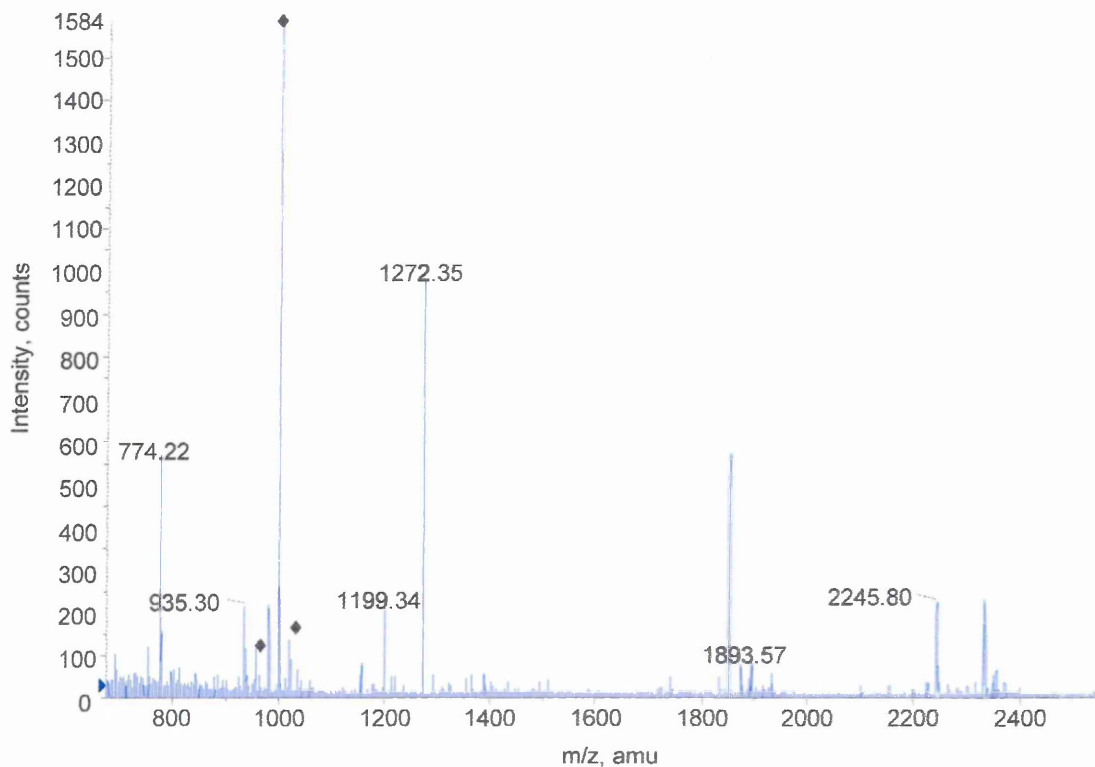


Figure 143. MALDI-MS spectrum of an in-gel Asp-N digest of APP α_{770} from a two-dimensional gel. There are several unknown peaks dominating the spectrum and as such need further investigation, however time restraints did not allow for this. Peaks thought to be due to keratin are marked with a black diamond. MS/MS analysis upon the annotated peaks present within the spectrum did not give any positive data.

mass (M+H ⁺)	mass (experimental)	position (APP α_{770} numbering)	missed cleavages	peptide sequence
774.35	774.22	655-660	1	DAEFRH
935.46	935.30	566-573	0	EPRISYGN
1199.54	1199.34	661-670	1	DSGYEVHHQK
1272.56	1272.35	599-609	1	DDLQPWHSFGA
1893.90	1893.57	557-573	2	DDVLANMISEPRISYGN
2245.18	2245.80	630-650	2	DRGLTTRPGSGLTNIKTEEIS

Table 92. Mascot search results from the MALDI-MS mass fingerprint of the two-dimensional in-gel Asp-N digest (figure 143) yielding 10% sequence coverage, although these results could not be confirmed by MS/MS.

3.456 Capillary LC/MS analysis of a two-dimensional in-gel Asp-N digestion of immunoprecipitated APP α_{770} .

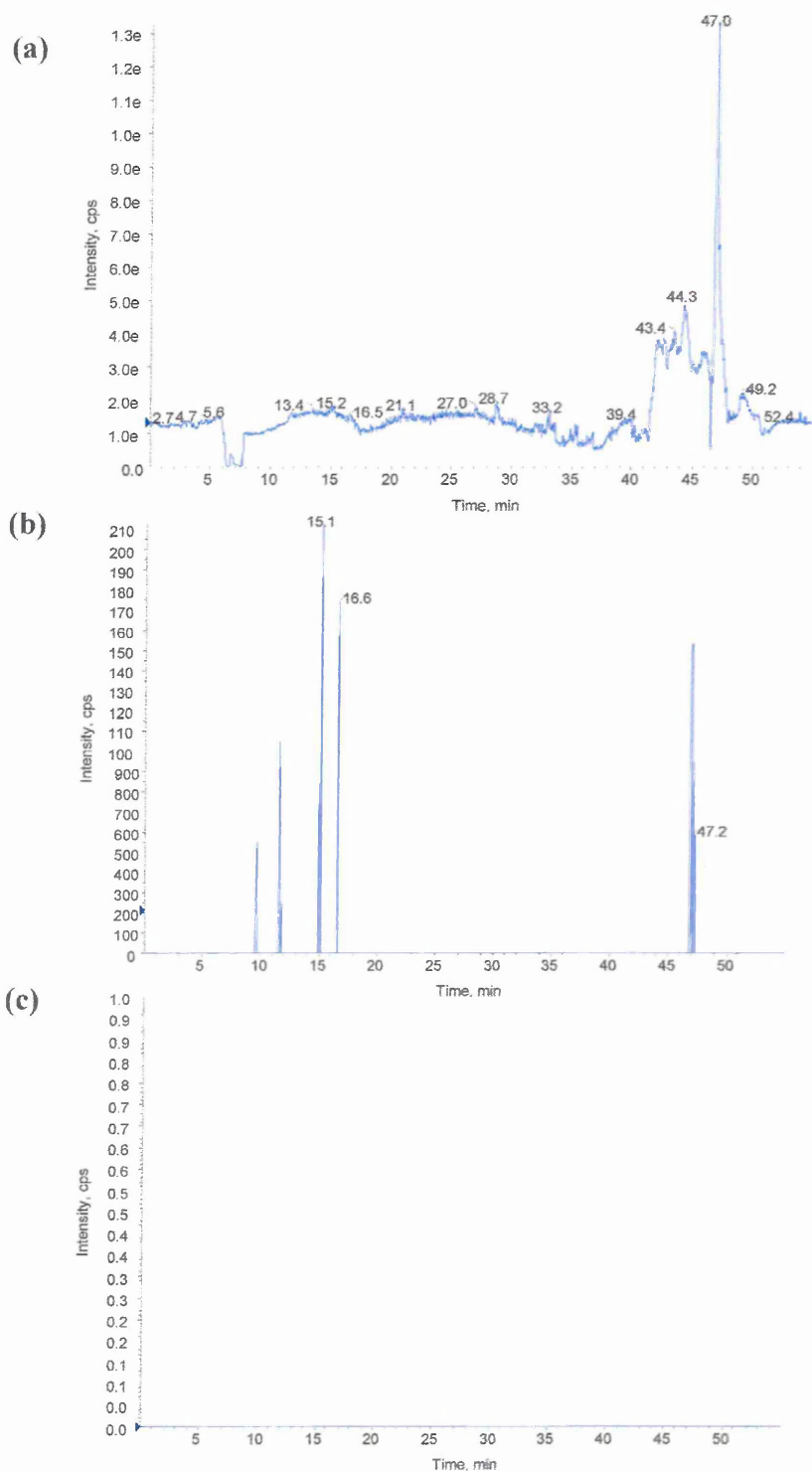


Figure 144. Capillary LC/MS run of an APP α_{770} two-dimensional in-gel Asp-N digest performed using information dependant acquisition (IDA) software. For experimental conditions see chapter 2.92, page 92. (a) Shows the survey scan or total ion chromatogram (TIC). (b) Shows the TIC for the product ion intensities generated by product ion scan of the most intense peak in the normal mass spectrum. (c) Should show the TIC for the product ion intensities generated by product ion scan of the second most intense peak in the normal mass spectrum, however, no data is present which is probably due to low sample concentration or poor sample quality. The peak list generated from trace (b) was sorted according to predefined parameters (chapter 2.92, page 93) and a selection of the most intense peaks automatically sent for MS/MS (figures 145 and 146).

mass observed	mass (experimental)	position	missed cleavages	peptide sequence
461.72	921.43	359-366	1	DKYLETPG
489.24	976.45	557-565	1	DDVLANMIS
636.79	1271.58	599-609	1	DDLQPWHSFGA
683.80	1365.60	546-556	2	DELLQKEQNYS

Table 93. BioAnalyst automatic data analysis (using Matrix Science software) of the chromatograms shown in figure 144 of a two-dimensional in-gel Asp-N digest of APP α_{770} gave 11 % sequence coverage.

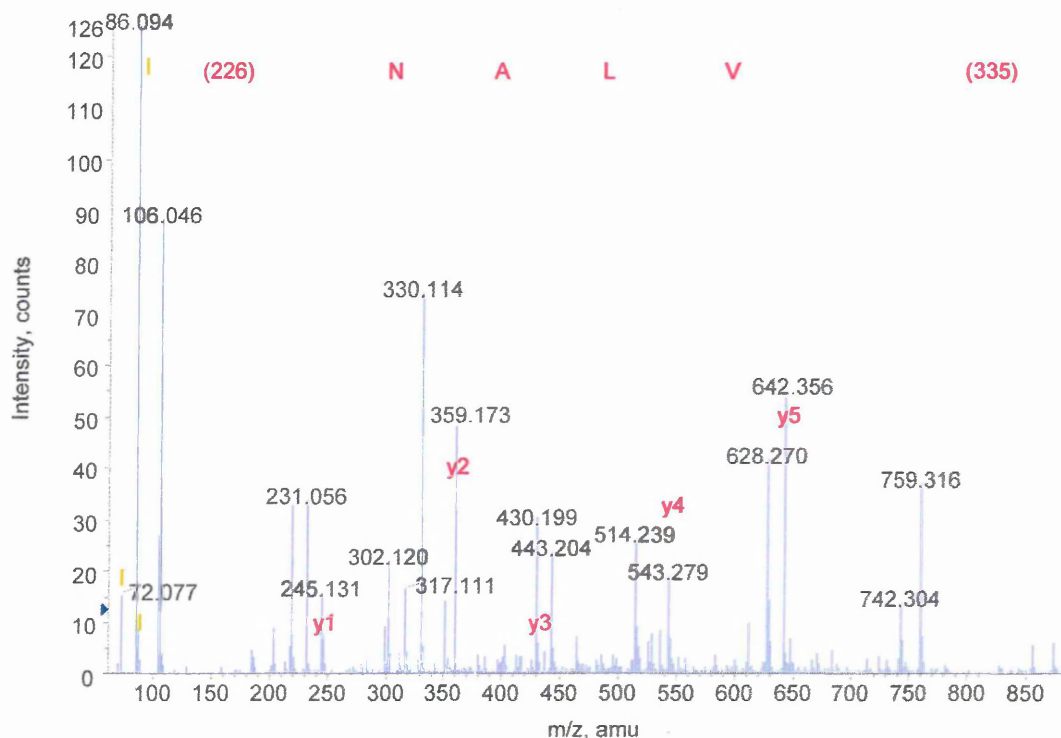


Figure 145. Capillary LC/MS/MS analysis of the doubly charged product ion at m/z 489.24 m/z , retention time 16.5 minutes from the LC/MS run of a two-dimensional in-gel Asp-N digest of APP α_{770} (figure 144b). This product is consistent with the APP α Asp-N peptide DDVLANMIS, 976.45 MW and the sequence tag VLAN expands this.

Amino acid		Ion type ($M+H^+$)						
residue	mass/Da	immonium	a	a-NH ₃	b	b-NH ₃	y	y-NH ₃
(335.12)	335.12	n/a	308.13	291.10	336.13	319.10	977.45	960.43
V, Val	99.06	72.08	407.20	390.17	435.19	418.17	642.33	625.30
L, Leu	113.03	86.09	520.28	503.26	548.28	531.25	543.26	526.23
A, Ala	71.03	44.04	591.32	574.29	619.32	602.29	430.18	413.15
N, Asn	114.04	87.05	705.36	688.34	733.36	716.33	359.14	342.11
(226.08)	226.08	n/a	931.45	914.42	959.44	942.42	245.10	228.07

Table 94. BioAnalyst automated searching of the capillary LC/MS/MS spectrum from the two-dimensional in-gel Asp-N digest of APP α_{770} in figure 144, shows the 'a', 'b' and 'y' product ions from the sequence tag VLAN.

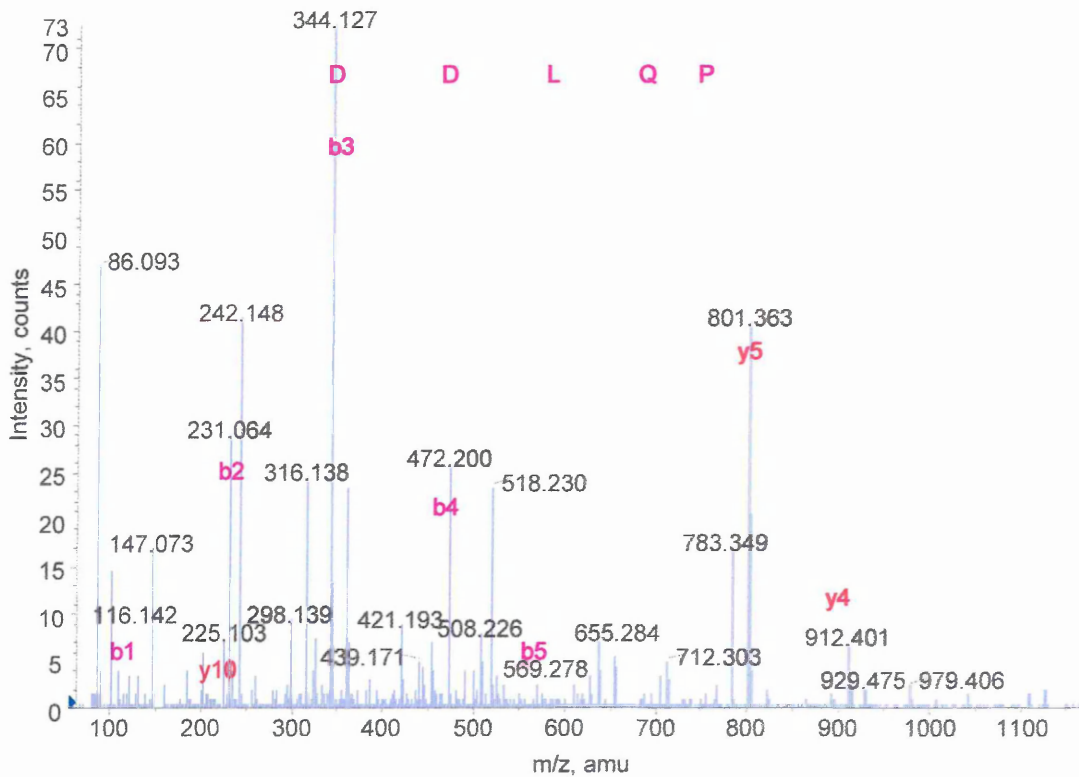


Figure 146. Capillary LC/MS/MS analysis of the doubly charged product ion at 636.79 m/z, retention time 15.1 minutes from the LC/MS run of a two-dimensional in-gel Asp-N digest of APP α_{770} (figure 144b). This product is consistent with the APP α_{770} Asp-N peptide DDLQPWHSFGA, 1271.58 monoisotopic mass and the sequence tag DDLQP expands this.

Amino acid		Ion type (M+H ⁺)						
residue	mass/Da	immonium	a	a-NH ₃	b	b-NH ₃	y	y-NH ₃
D, Asp	115.02	88.03	88.03	71.01	116.03	99.00	1272.56	1255.53
D, Asp	115.02	88.03	203.06	186.03	231.06	214.03	1157.53	1140.51
L, Leu	113.08	86.09	316.15	299.12	344.14	327.11	1042.51	1025.48
Q, Gln	128.05	101.09	444.20	427.18	472.20	455.17	929.42	912.39
P, Pro	97.05	70.06	541.26	524.23	569.25	552.23	801.36	784.34

Table 95. BioAnalyst automated searching of the capillary LC/MS/MS spectrum from the two-dimensional in-gel Asp-N digest of APP α_{770} shown in figure 146, shows the 'a', 'b' and 'y' product ions from the sequence tag DDLQP.

The alpha secretase cleaved amyloid precursor protein, isoform 770 (APP α_{770}) was immunoprecipitated from CHO 770 cell secretions.

The MALDI-MS examination of the two-dimensional in-gel Asp-N digestion of APP α_{770} (figure 143) gave amino acid sequence coverage of 10% of the APP α_{770} molecule from 6 Asp-N peptides. The sequence coverage achieved from the LC/MS analysis (figure 144) was 11% of the protein sequence from 4 peptides. Sequence coverage by both methods was low, however, this can be attributed to the low *in vitro* concentration of APP. The MALDI-MS spectrum (figure 143) was dominated by unknown contamination. The peaks believed to be due to keratin were assigned, however, further investigation would be needed to identify the other peaks. None of the MALDI-MS peaks yielded any sequence information, but the LC/MS/MS analysis was more successful resulting in two sequence tags (figures 145 and 146). APP α_{770} produces two unique Asp-N peptides (position 318-337, MW 2149.8589 and position 343-355, MW 1296.5998) regrettably neither of these peptides was detected by either technique.

3.457 MALDI-MS analysis of a two-dimensional in-gel Asp-N digestion of immunoprecipitated alpha secretase cleaved amyloid precursor protein (APP α).

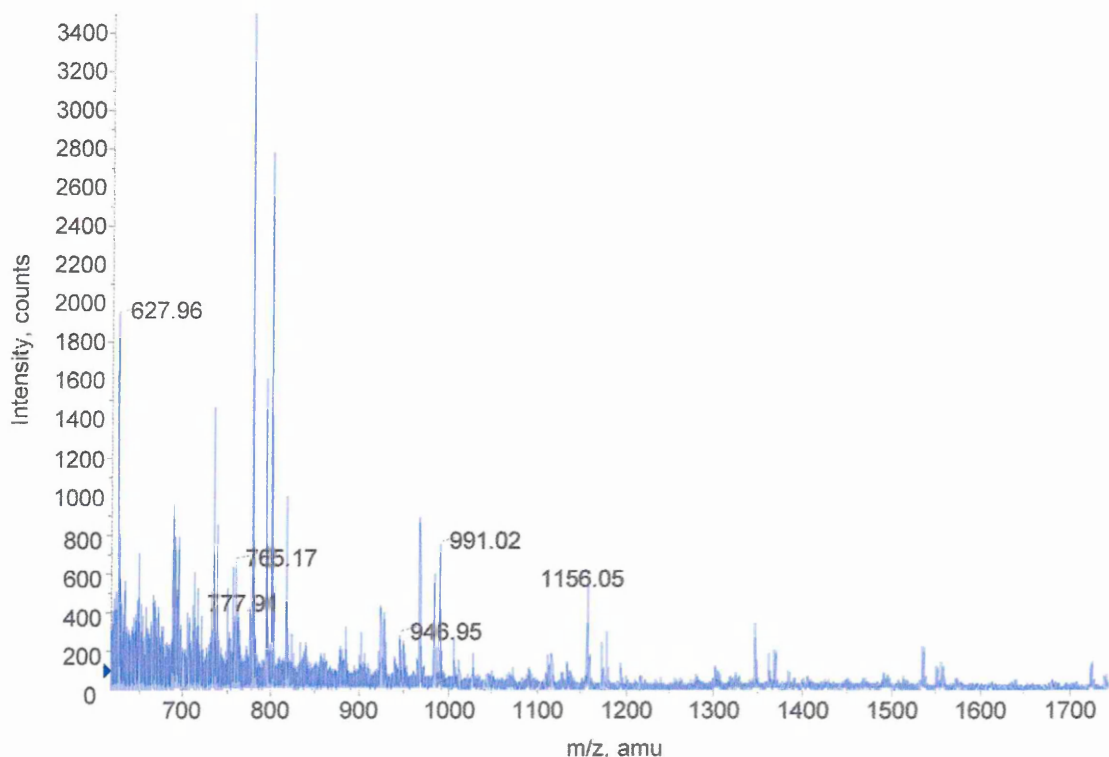


Figure 147. MALDI-MS spectrum of an in-gel Asp-N digest of APP α from a two-dimensional gel. None of the annotated peaks gave any MS/MS data. The spectrum appears to be contaminated by polymer adducts.

mass (M+H ⁺)	mass (experimental)	Position (APP α_{770} numbering)	missed cleavages	peptide sequence
627.37	627.96	108-113	0	DALLVP
765.31	765.17	272-278	1	EVCSEQA
777.40	777.91	665-670	0	EVHHQK
946.48	946.95	264-271	2	ESVEEVVR
990.44	991.02	423-431	2	ESLEQEAAN
1156.58	1156.05	2-13	1	EVPTDGNAGLLA

Table 96. Mascot search results from the MALDI-MS mass fingerprint of the two-dimensional in-gel Asp-N digest of APP α (figure 147), containing the three isoforms of interest (695, 751 and 770), giving coverage of 5% of the peptide sequence although no specific isoforms were seen and none of the sequences were confirmed by MALDI-MS/MS analysis.

3.458 Capillary LC/MS analysis of a two-dimensional in-gel Asp-N digestion of immunoprecipitated APP α .

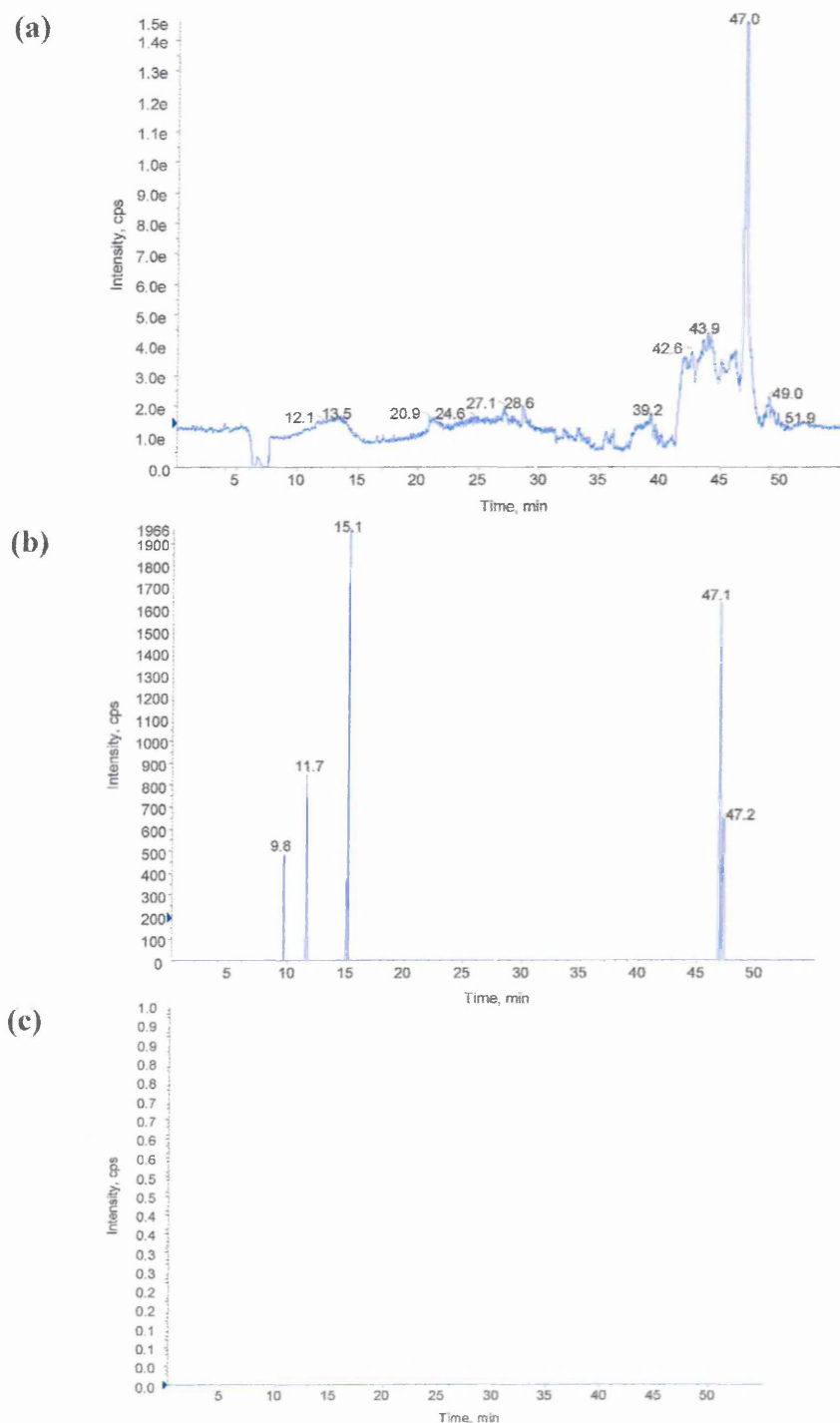


Figure 148. Capillary LC/MS run of an APP α two-dimensional in-gel Asp-N digest performed using information dependant acquisition (IDA) software. For experimental conditions see chapter 2.92, page 92. (a) Shows the survey scan or total ion chromatogram (TIC). (b) Shows the TIC for the product ion intensities generated by product ion scan of the most intense peak in the normal mass spectrum. (c) Should show the TIC for the product ion intensities generated by product ion scan of the second most intense peak in the normal mass spectrum, however, no data can be seen as this may be due to low sample concentration. The peak list generated from trace (b) was sorted according to predefined parameters (chapter 2.92, page 93) and a selection of the most intense peaks automatically sent for MS/MS (figures 149 and 150).

mass observed	mass (experimental)	position (APP α_{770} numbering)	missed cleavages	peptide sequence
636.78	1271.54	599-609	1	DDLQPWHSFGA
683.81	1365.61	546-556	2	DELLQKEQNYS

Table 97. BioAnalyst automatic data analysis (using Matrix Science software) of the chromatograms seen in figure 148 of a two-dimensional in-gel Asp-N digest of APP α gave sequence coverage of 6%. Both of the above peptides were analysed by LC/MS/MS the data shown in figures 149 and 150.

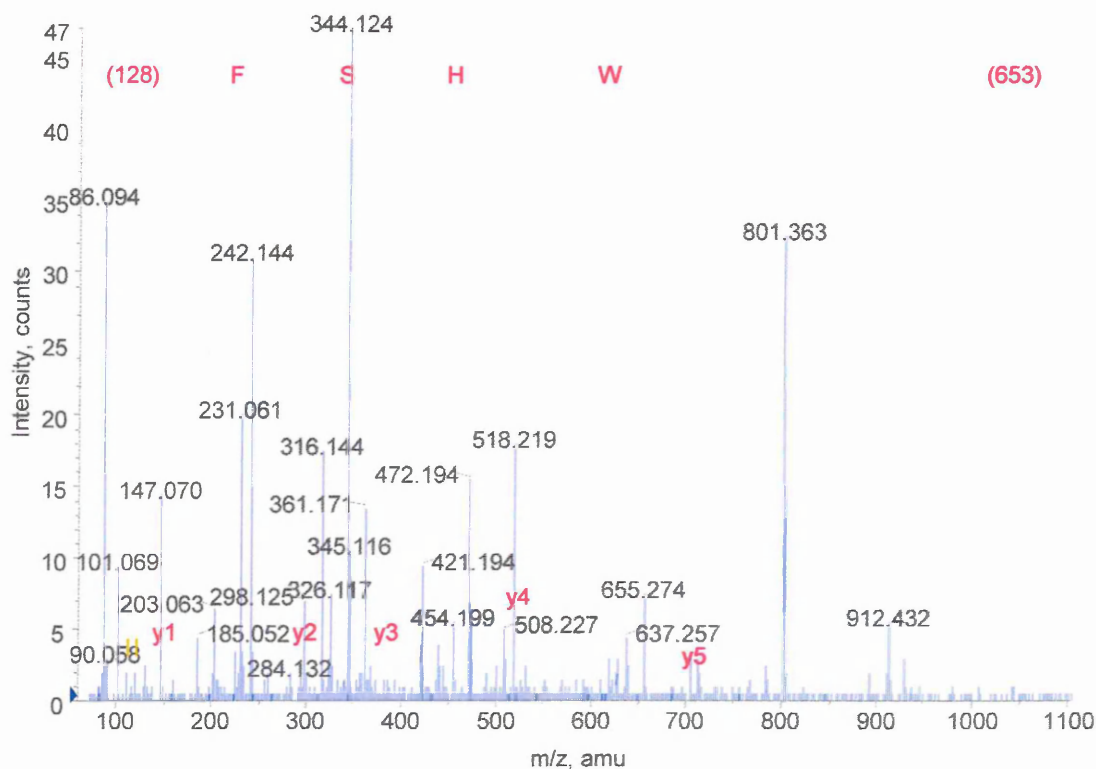


Figure 149. Capillary LC/MS/MS analysis of the doubly charged product ion at 636.78 m/z, retention time 15.1 minutes from the LC/MS run of a two-dimensional in-gel Asp-N digest of APP α (figure 148b). This product is consistent with the APP α Asp-N peptide, 1271.54 MW and the sequence tag WHSF verifies this.

residue	mass/Da	immonium	Ion type (M+H ⁺)					
			a	a-NH ₃	b	b-NH ₃	y	y-NH ₃
(653.38)	653.38	n/a	626.39	609.36	654.38	637.36	1357.63	1340.64
W, Trp	186.07	159.09	812.47	795.44	840.46	823.44	704.25	687.23
H, His	137.05	110.07	949.53	932.50	977.52	960.49	518.17	501.15
S, Ser	87.03	60.04	1036.56	1019.53	1064.55	1047.53	381.12	364.09
F, Phe	147.06	120.08	1183.63	1166.60	1211.62	1194.59	294.08	277.06
(128.00)	128.00	n/a	1311.63	1294.60	1339.62	1322.60	147.02	129.99

Table 98. BioAnalyst automated searching of the capillary LC/MS/MS spectrum from the two-dimensional in-gel Asp-N digest of APP α shown in figure 149, highlighting the 'y' product ions from the sequence tag WHSF.

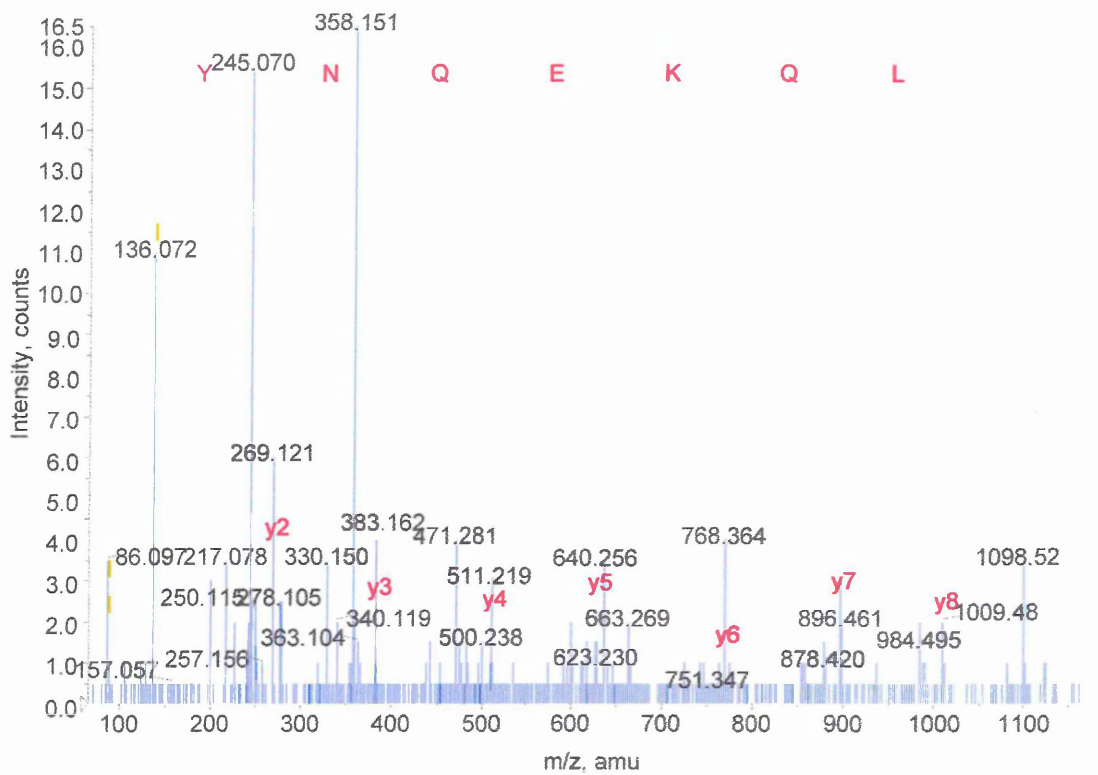


Figure 150. Capillary LC/MS/MS analysis of the doubly charged product ion at 683.81m/z, retention time 9.7 minutes from the LC/MS run of a two-dimensional in-gel Asp-N digest of APP α (figure 148b). This product is consistent with the APP α Asp-N peptide DELLQKEQNY, 1365.61 MW and the sequence tag LQKEQNY expands this.

Amino acid	Ion type ($M+H^+$)							
	residue	mass/Da	immonium	a	a-NH ₃	b	b-NH ₃	y
L, Leu	113.08	86.09	199.18	182.15	227.17	210.14	1009.49	992.46
Q, Gln	128.05	101.07	327.23	310.21	355.23	338.20	896.41	879.38
K, Lys	128.09	101.10	455.33	438.30	483.32	466.30	768.35	751.32
E, Glu	129.04	102.05	584.37	567.35	612.37	595.34	640.25	623.23
Q, Gln	128.05	101.07	712.43	695.40	740.43	723.40	511.21	494.18
N, Asn	114.04	87.05	826.47	809.45	854.47	837.44	383.15	366.12
Y, Tyr	163.06	136.07	989.54	972.51	1017.53	1000.50	269.11	252.06

Table 99. BioAnalyst automated searching of the capillary LC/MS/MS spectrum from the two-dimensional in-gel Asp-N digest of APP α in figure 150, highlighting the product ions present for the sequence tag LQKEQNY.

The alpha secretase cleaved amyloid precursor protein (APP α) used was immunoprecipitated from Ntera 2 cell secretions. APP α encompasses all three isoforms of interest (APP α_{695} , APP α_{751} , APP α_{770}) and as such is a more plausible model of *in vivo* conditions.

The MALDI-MS results from the two-dimensional in-gel Asp-N digestion of APP α (figure 147) gave amino acid sequence coverage of 5% of the APP α molecule from 6 Asp-N peptides. The sequence coverage achieved from the LC/MS (figure 148) analysis was poorer giving 6% of the protein sequence from only 2 peptides. MALDI-MS/MS analysis, however, was insufficient for sequencing but the LC/MS/MS data revealed two sequence tags from the peptides resolved (figure 149 and 150) allowing protein identification using the online search engine. Disappointingly none of the specific peptides was detected.

3.46 Two-dimensional in-gel formic acid digestion of BSA and APP.

3.461 MALDI-MS analysis of a two-dimensional in-gel formic acid digestion of BSA.

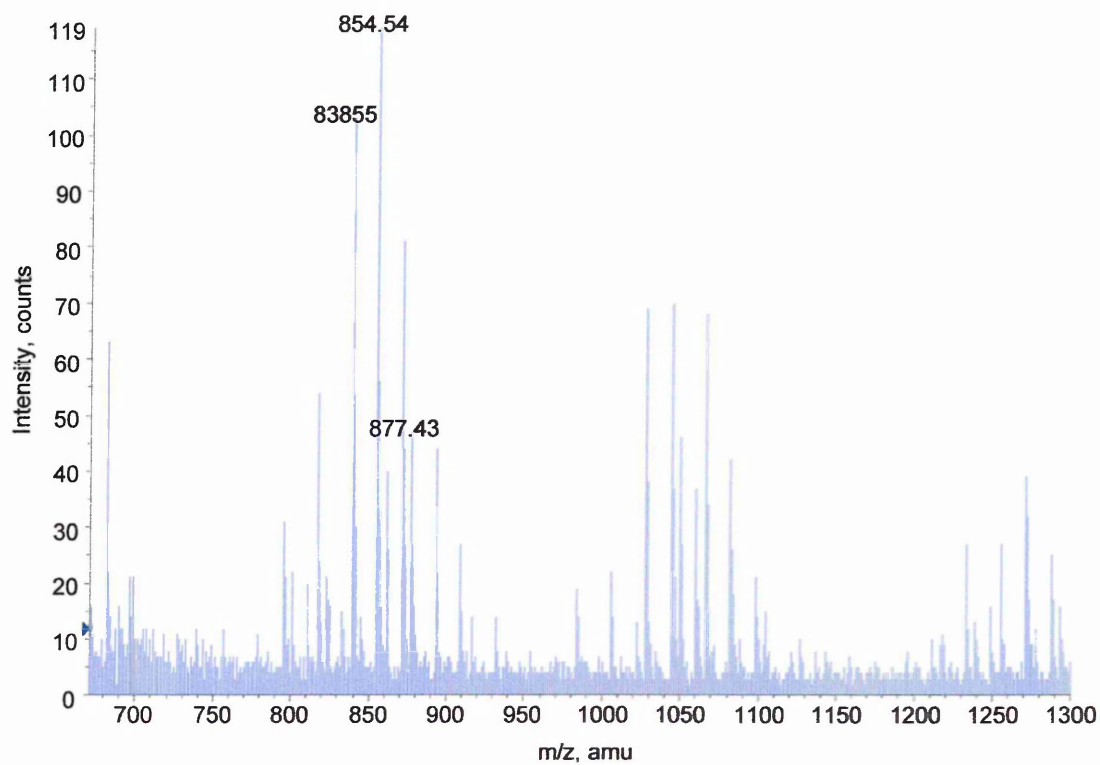


Figure 151. MALDI-MS spectrum of a two-dimensional in-gel formic acid digest of BSA dominated by the presence of contamination that may be caused by the formic acid digestion being too harsh and cleaving areas within the protein other than the specified bonds (N and C termini of aspartic acid) or perhaps the presence of intermediates present within the cleavage pathway. The formation of the peaks in equidistant clusters, however, suggests the presence of polymers or adducts very similar to those seen previously in the two-dimensional Asp-N in-digest of BSA. Further investigation of these peaks may help to establish the nature of the contaminating species and why sufficient cleavage by formic acid cleavage is not being achieved

mass (M+H ⁺)	mass (experimental)	position	missed cleavages	peptide sequence
838.48	838.55	62-68	0	EHVKLVN
854.46	854.54	323-330	0	ENLPPLTA
877.40	877.43	535-542	1	DICTLPDT

Table 100. Mascot search results from the two-dimensional in-gel formic acid digest of BSA (figure 151), showing 2% sequence coverage although the appearance of the MALDI-MS spectrum and lack of MS/MS data to validate these peptides may suggest that they are not real

3.462 Capillary LC/MS analysis of a two-dimensional in-gel formic acid digestion of BSA.

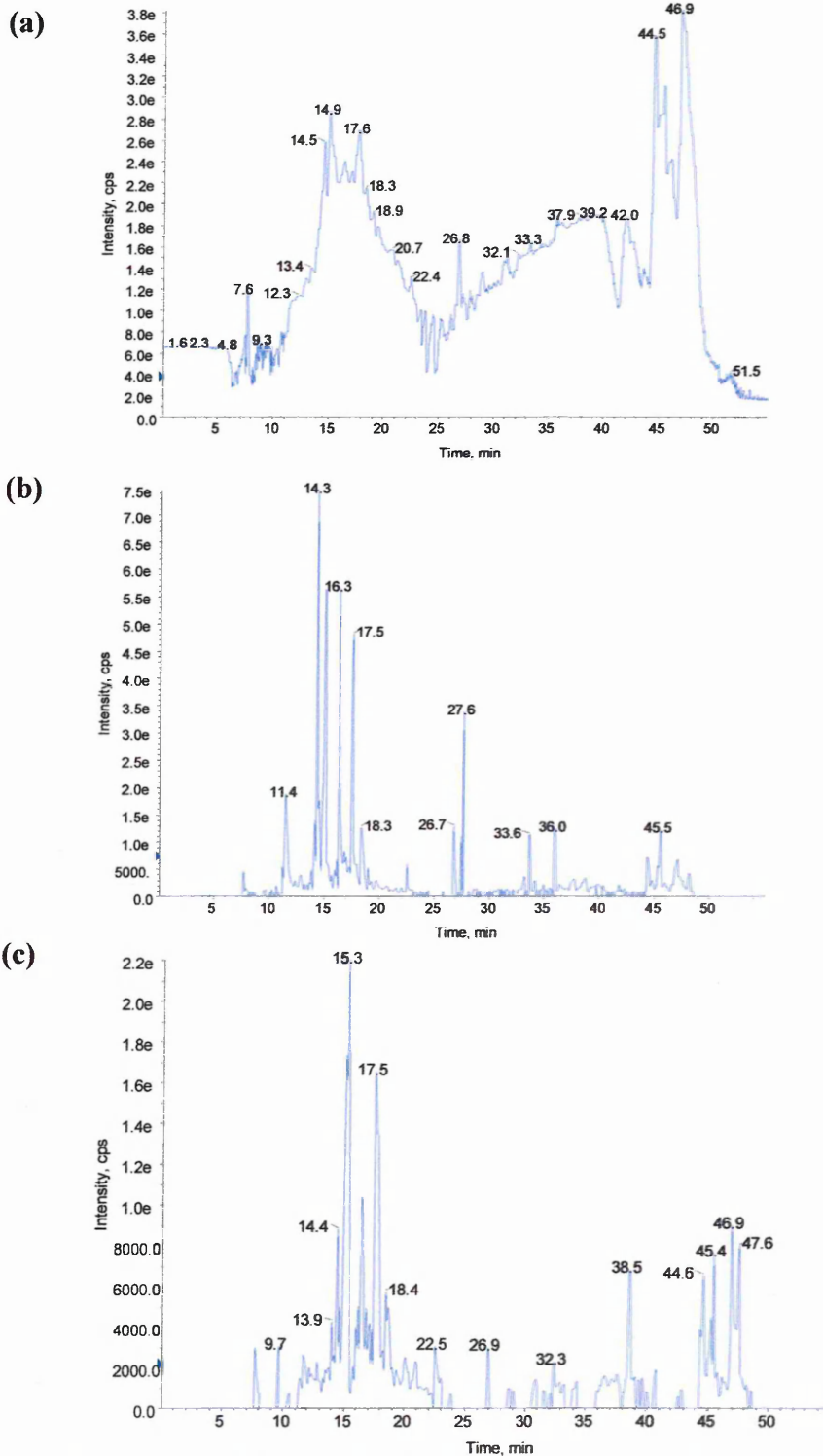


Figure 152. Capillary LC/MS run of a BSA two-dimensional in-gel formic acid digest performed using information dependant acquisition (IDA) software. For experimental conditions see chapter 2.92, page 92. (a) Shows the survey scan or total ion chromatogram (TIC). (b) Shows the TIC for the product ion intensities generated by product ion scan of the most intense peak in the normal mass spectrum. (c) Shows the TIC for the product ion intensities generated by product ion scan of the second most intense peak in the normal mass spectrum. The peak lists generated from (b) and (c), however, did not give MS/MS data relating to the sample.

mass observed	mass (experimental)	position	missed cleavages	peptide sequence
625.83	1249.65	319-330	1	DAIPENLPPLTA

Table 101. BioAnalyst automatic data analysis (using Matrix Science software) of the chromatograms shown in figure 152 of a two-dimensional in-gel formic acid digest of BSA gave 1% sequence coverage.

Bovine serum albumin (BSA, MW 66,432.96) was used as a standard due to its availability and similarity in molecular weight to the amyloid precursor protein isoforms (APP α_{695} , 67,708.02, APP α_{751} , 73,863.85, APP α_{770} , 75,988.34).

The MALDI-MS analysis of the two-dimensional in-gel formic acid digest of BSA (figure 151) resulted in 3 formic acid peptides covering 2% of the protein. LC/MS analysis (figure 152) of the same sample revealed 1 formic acid peptide for BSA, which covered 1% of the protein sequence. MALDI-MS/MS and LC/MS analysis of the peaks failed to determine any of the sequences. The poor spectral quality seen in figure 151 and lack of peak validation would suggest that the data provided here is indefinite. This experiment has been performed on several occasions previously and no reliable data has been achieved suggesting that the formic acid digest procedure taken from the literature¹⁹⁸ needs further investigation.

3.463 MALDI-MS analysis of a two-dimensional in-gel formic acid digestion of alpha secretase cleaved amyloid precursor protein standard, isoform 695 (APP α_{695}).

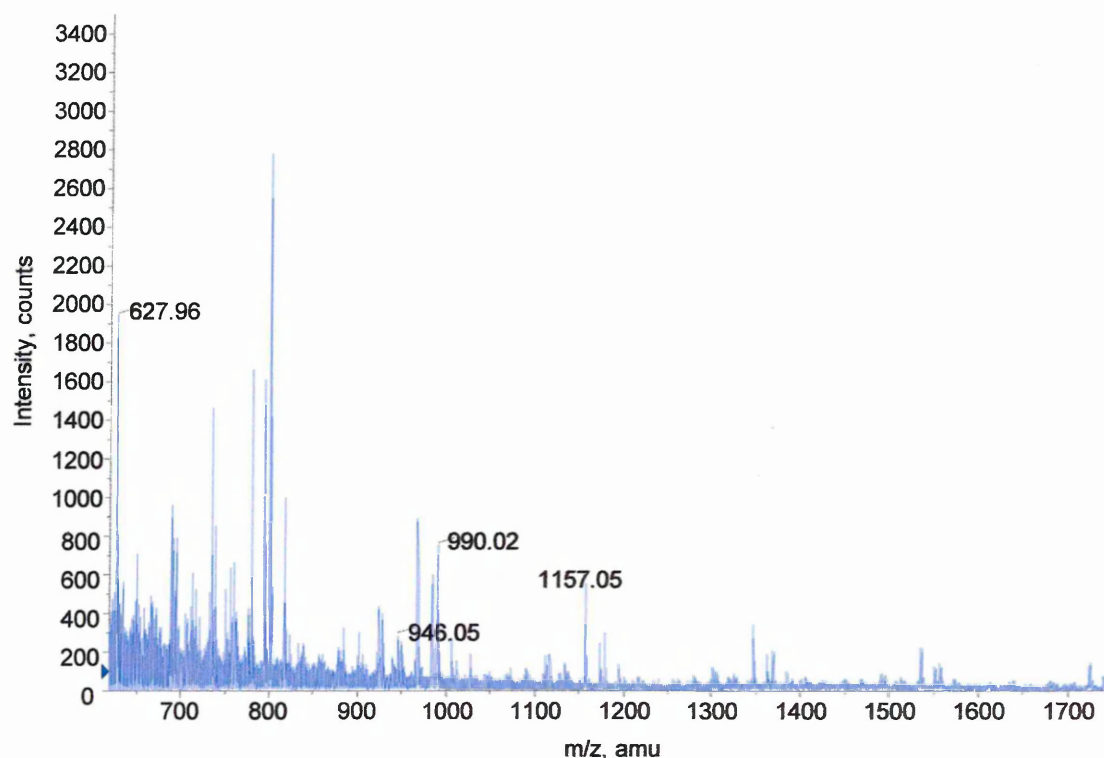


Figure 154. MALDI-MS spectrum of a two-dimensional in-gel formic acid digest of standard APP α_{695} . Dominant peaks in the spectrum due to contamination rather than desired peptide species.

mass (M+H ⁺)	mass (experimental)	position	missed cleavages	peptide sequence
627.37	627.96	108-113	0	DALLVP
946.48	946.05	264-271	2	ESVEEVVR
990.44	990.02	423-431	2	ESLEQEAAN
1157.54	1157.05	600-609	0	DLQPWHSFGA

Table 102. Mascot search results from the MALDI-MS of the two-dimensional in-gel formic acid digest of APP α_{695} shown (figure 154) covering 3% of the peptide sequence. Lack of MS/MS data to validate the peptides places uncertainty over their authenticity.

3.464 Capillary LC/MS analysis of a two-dimensional in-gel formic acid digestion of standard APP α_{695} .

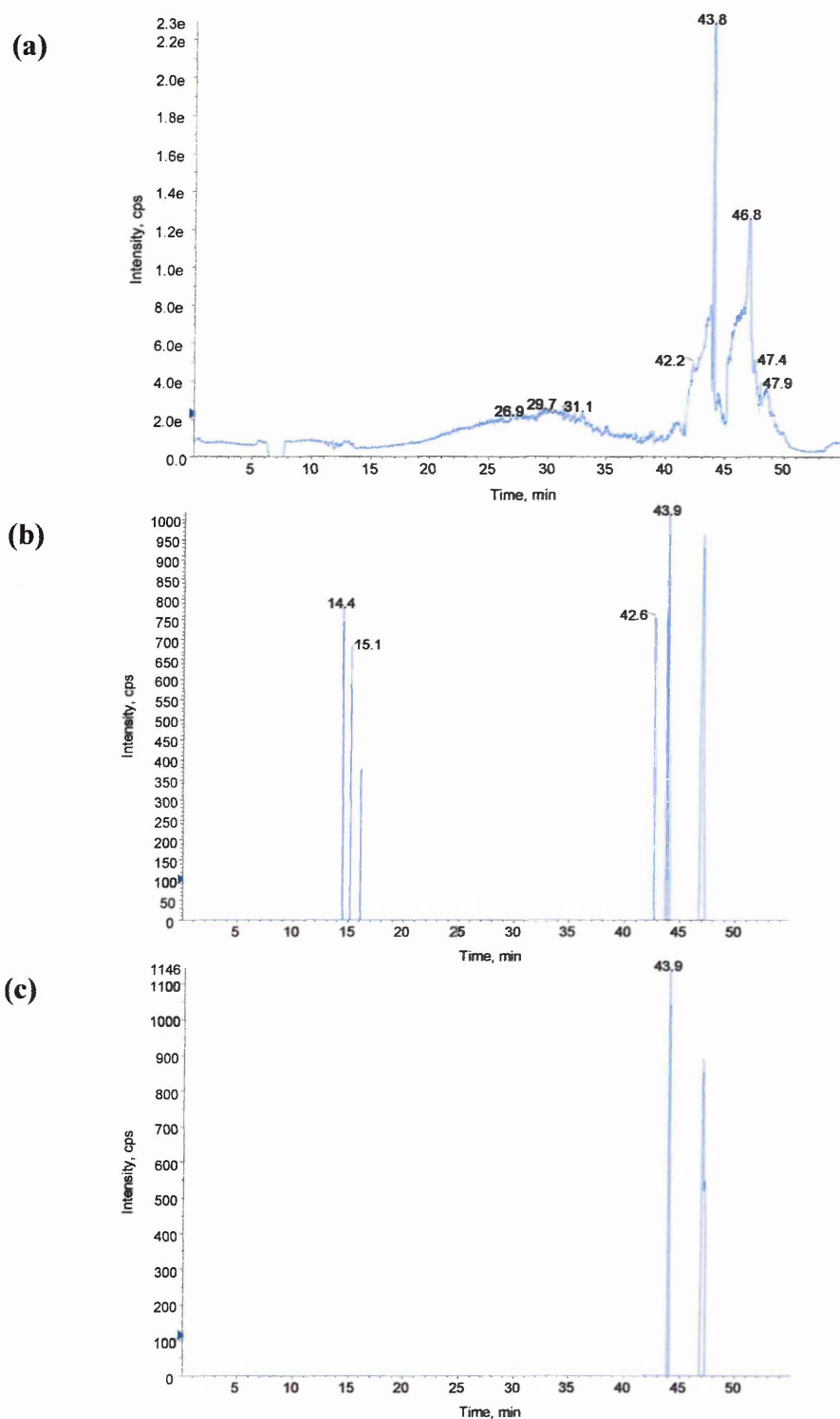


Figure 155. Capillary LC/MS run of an APP α_{695} two-dimensional in-gel formic acid digest performed using information dependant acquisition (IDA) software. For experimental conditions see chapter 2.92, page 92. (a) Shows the survey scan or total ion chromatogram (TIC). (b) Shows the TIC for the product ion intensities generated by product ion scan of the most intense peak in the normal mass spectrum. (c) Shows the TIC for the product ion intensities generated by product ion scan of the second most intense peak in the normal mass spectrum, however, only peaks due to the mobile phase are present. The peak list generated from (b) did not give MS/MS data relating to the sample

Amyloid precursor protein standard was purchased from Sigma for use as a direct comparison. The standard was the alpha secretase cleaved APP isoform 695 (APP α_{695}) from E.coli origin.

The MALDI-MS examination of the two-dimensional in-gel formic acid digestion of APP α_{695} (figure 154) gave amino acid sequence coverage of 3% of the APP α_{695} molecule from 4 formic acid peptides, however, MS/MS analysis of these peaks did not reveal any peptide sequences. The LC/MS analysis (figure 155) did not reveal any formic acid peptides for APP α_{695} and as such no LC/MS/MS data was achieved. The appearance of the MALDI-MS spectrum as well as the lack of MS/MS data shows the improbability of the results and further investigation of the contaminating species seen in the MALDI-MS spectrum (figure 154) may help to reveal why the formic acid digest procedure is not yielding the desired cleavage peptides. It is possible that the formic acid digest procedure is either hydrolysing at other positions within the peptide than stated or an incomplete reaction has occurred creating intermediates of the reaction pathway.

3.465 MALDI-MS analysis of a two-dimensional in-gel formic acid digestion of immunoprecipitated alpha secretase cleaved amyloid precursor protein, isoform 770 (APP α_{770}).

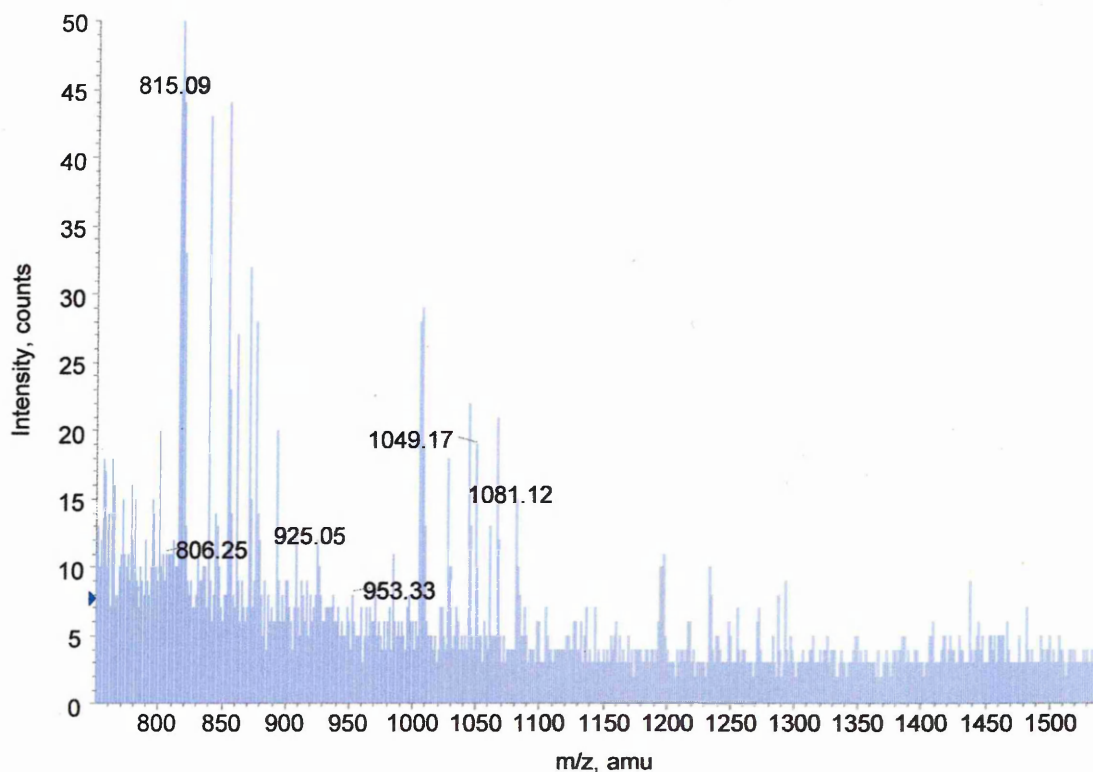


Figure 156. MALDI-MS spectrum of an in-gel formic acid digest of APP α_{770} from a two-dimensional gel. Spectrum dominated by noise and contamination. None of the annotated peaks were able to provide positive results when subjected to MS/MS analysis.

mass (M+H ⁺)	mass (experimental)	position (APP α_{770} numbering)	missed cleavages	peptide sequence
806.31	806.25	177-184	2	DNVDSADA
815.38	815.09	617-623	2	ENEVEPV
925.47	925.05	621-629	1	EPVDARPA
953.44	953.38	50-57	0	EGILQYCQ
1049.49	1049.17	267-275	2	EEVVVREVCS
1081.51	1081.12	150-159	0	DYGMLLPCGI

Table 103. Mascot search results from the MALDI-MS mass fingerprint of the two-dimensional in-gel formic acid digest (figure 156) yielding 5% sequence coverage, although appearance of the MALDI-MS spectra and lack of MS/MS data pose the credibility of the results.

3.466 Capillary LC/MS analysis of a two-dimensional in-gel formic acid digestion of immunoprecipitated APP α ₇₇₀.

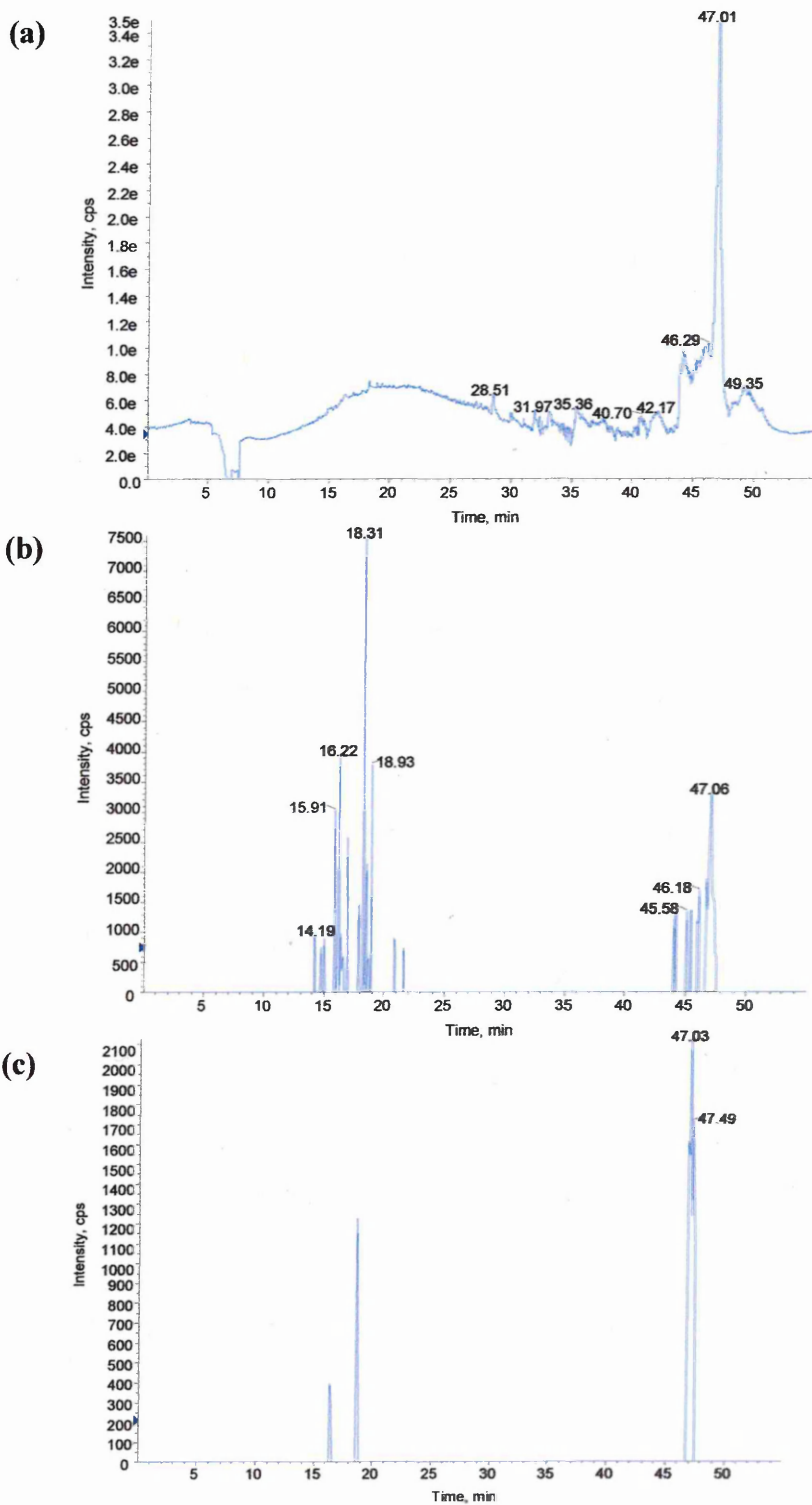


Figure 157. Capillary LC/MS run of an APP α ₇₇₀ two-dimensional in-gel formic acid digest performed using information dependant acquisition (IDA) software. For experimental conditions see chapter 2.92, page 92. (a) Shows the survey scan or total ion chromatogram (TIC). (b) Shows the TIC for the product ion intensities generated by product ion scan of the most intense peak in the normal mass spectrum. (c) Shows the TIC for the product ion intensities generated by product ion scan of the second most intense peak in the normal mass spectrum. The peak lists generated from (b) and (c), however, did not give MS/MS data relating to the sample.

The alpha secretase cleaved amyloid precursor protein, isoform 770 (APP α_{770}) was immunoprecipitated from CHO 770 cell secretions.

The MALDI-MS examination of the two-dimensional in-gel formic acid digestion of APP α_{770} (figure 156) gave amino acid sequence coverage of 5% of the APP α_{770} molecule from 6 formic acid peptides, however the appearance of the peaks, background 'noise' and lack of MS/MS data discredit their validity. Likewise for LC/MS analysis, which again failed to reveal any data and as such no MS/MS data was achieved. All the protein extraction and purification techniques were carried out in parallel keeping every step constant, the only difference being the variation in digest reagent. Due to the obvious advantages of this method adjustment of the formic acid digestion parameters such pH, time or temperature are well worth exploring as they may yield better results.

3.467 MALDI-MS analysis of a two-dimensional in-gel formic acid digestion of immunoprecipitated alpha secretase cleaved amyloid precursor protein (APP α).

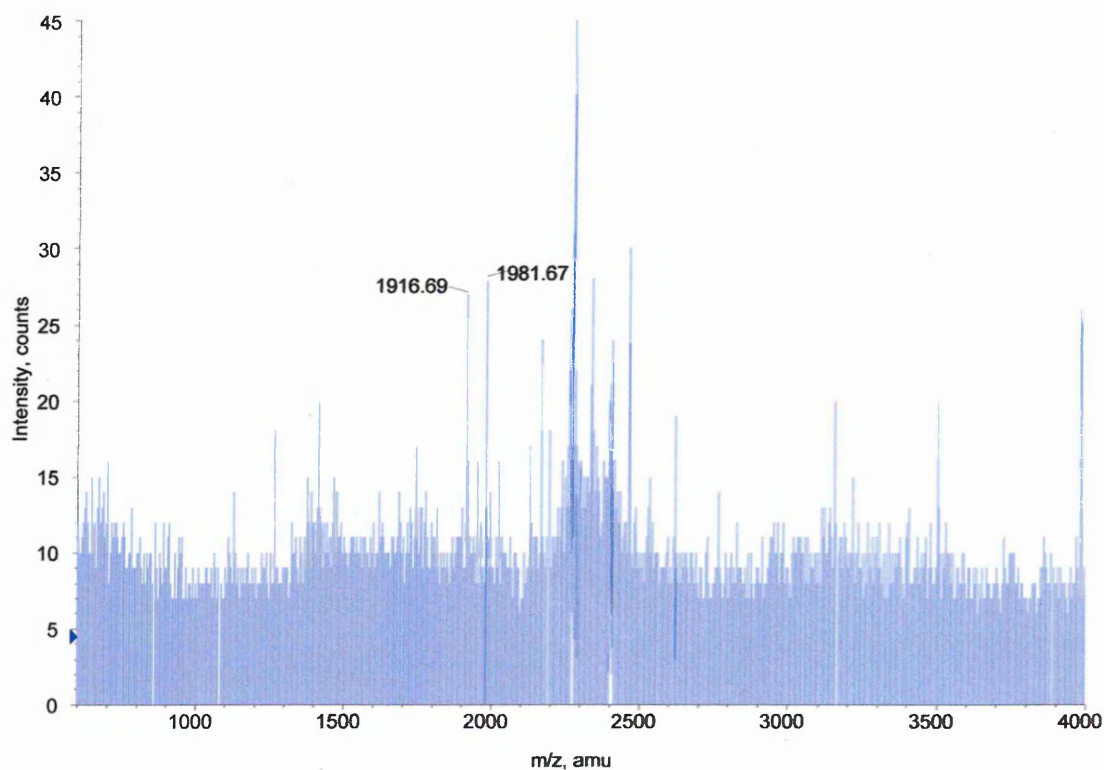


Figure 158. MALDI-MS spectrum of an in-gel formic acid digest of APP α from a two-dimensional gel. Very poor spectrum consisting mainly of background noise. The annotated peaks within the signal to noise ratio therefore low in credibility.

mass (M+H ⁺)	mass (experimental)	position (APP α_{695} numbering)	missed cleavages	peptide sequence
1916.02	1916.69	555-572	1	DRGLTTRPGSGLTNIKTE
1981.99	1981.67	352-369	2	EAANERQQLVETHMARV

Table 104. Mascot search results from the MALDI-MS mass fingerprint of the two-dimensional in-gel formic acid digest of APP α (figure 158), containing the three isoforms of interest (695, 751 and 770), giving coverage of 2% of the peptide sequence. As mentioned earlier in previous formic acid digest sections the poor spectral resolution and lack of MS/MS data to corroborate the authenticity of these results place a question mark over their validity.

3.468 Capillary LC/MS analysis of a two-dimensional in-gel formic acid digestion of immunoprecipitated APP α .

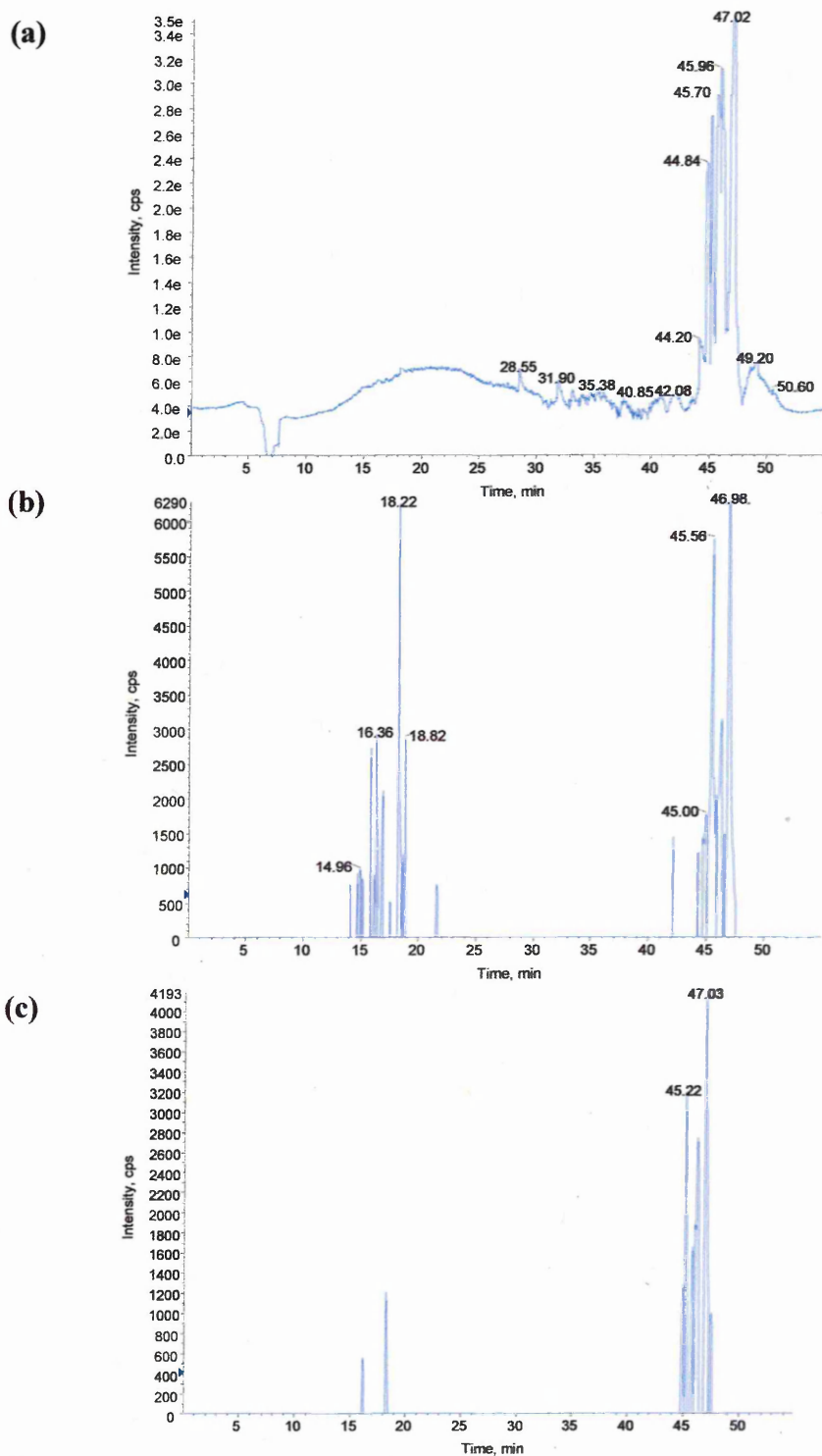


Figure 159. Capillary LC/MS run of an APP α two-dimensional in-gel formic acid digest performed using information dependant acquisition (IDA) software. For experimental conditions see chapter 2.92, page 92. (a) Shows the survey scan or total ion chromatogram (TIC). (b) Shows the TIC for the product ion intensities generated by product ion scan of the most intense peak in the normal mass spectrum. (c) Shows the TIC for the product ion intensities generated by product ion scan of the second most intense peak in the normal mass spectrum. The peak lists generated from (b) and (c), however, did not give MS/MS data relating to the sample.

The alpha secretase cleaved amyloid precursor protein (APP α) used was immunoprecipitated from Ntera 2 cell secretions. APP α encompasses all three isoforms of interest (APP α_{695} , APP α_{751} , APP α_{770}) and as such is a more plausible model of *in vivo* conditions.

The MALDI-MS results from the two-dimensional in-gel formic acid digestion of APP α (figure 158) gave amino acid sequence coverage of 2% of the APP α molecule from 2 formic acid peptides. LC/MS did not provide any formic acid peptides. Again the appearance of the MALDI-MS spectra, lack of LC/MS data and MS/MS data for both techniques does create uncertainty over the authenticity of the results achieved. The formic acid digest method has several advantages, cleavage occurs at both the amino and carboxy termini of aspartic acid residues. The abundance of aspartic acid residues in proteins is comparable to lysine and arginine and as such cleavage at these bonds creates peptides useful for sequencing. Cleavage by this method is unselective in that all groups of amino acids are cleaved equally for example trypsin is not as efficient in cleaving hydrophobic or basic protein. Finally the method is easy, none time consuming and the cost of the reagent is low. It may be worthwhile, therefore investigating experimental parameters of this method further looking at temperature, reaction time and pH.

Summary of Mass Spectroscopic Results from In-gel Digestions

Two-Dimensional Electrophoresis

Digest Reagent		Trypsin										
Sample	% sequence coverage	MALDI		LC		MALDI		LC				
		# MS/MS	# isoform specific peptides	% sequence coverage	# MS/MS data achieved	# isoform specific peptides	% sequence coverage	# MS/MS	# isoform specific peptides	% sequence coverage	# MS/MS	# isoform specific peptides
BSA	18	2	-	27	2	-	17	2	2	22	2	-
Standard APP α_{695}	33	2	1	16	2	1	29	2	2	10	2	1
IP APP α_{770}	19	2	1	11	2	0	21	2	2	12	2	2
IP APP α	17	2	0	4	2	0	19	2	2	8	2	0

Asp-N

Digest Reagent		Asp-N										
Sample	% sequence coverage	MALDI		LC		MALDI		LC				
		# MS/MS	# isoform specific peptides	% sequence coverage	# MS/MS	# isoform specific peptides	% sequence coverage	# MS/MS	# isoform specific peptides	% sequence coverage	# MS/MS	# isoform specific peptides
BSA	20	2	-	7	-	2	10	0	0	5	1	-
Standard APP α_{695}	18	2	1	17	1	1	15	2	2	15	2	1
IP APP α_{770}	6	0	0	3	0	2	10	0	0	11	2	0
IP APP α	5	0	0	2	0	1	5	0	0	6	2	0

Formic Acid

Digest Reagent		Formic Acid										
Sample	% sequence coverage	MALDI		LC		MALDI		LC				
		# MS/MS	# isoform specific peptides	% sequence coverage	# MS/MS	# isoform specific peptides	% sequence coverage	# MS/MS	# isoform specific peptides	% sequence coverage	# MS/MS	# isoform specific peptides
BSA	5	0	-	3	0	-	2	0	0	1	0	-
Standard APP α_{695}	2	0	0	0	0	0	3	0	0	0	0	0
IP APP α_{770}	2	0	0	0	0	0	5	0	0	0	0	0
IP APP α	4	0	0	0	0	0	2	0	0	0	0	0

Table 105. Protein coverage summary of all in-gel digestions (one-dimensional and two-dimensional) by all three digest reagents; trypsin, Asp-N and formic acid.

Three factors have been investigated within this chapter; the efficacy of different digest reagents; variation in results achieved from both one-dimensional and two-dimensional gel electrophoresis and the ability of two different mass spectroscopic techniques in analysing those results, all of which are summarised in table 105. The table is split into four main sections each one illustrating the results from the various samples used (BSA standard, APP α_{695} standard, immunoprecipitated APP α_{770} and immunoprecipitated APP α). With regards to *in vivo* experimental data the last section headed APP α is the most important as this is the best model of *in vivo* conditions. The best protein sequence coverage seen in this section is 19% seen from the two-dimensional in-gel tryptic digest analysed by MALDI-MS.

The digest reagents used were chosen for various reasons; trypsin because it is the most commonly utilised digest reagent in proteomics due its specificity, cost and availability. Trypsin is not without its drawbacks, however, and is known to suffer from autodigestion¹⁹⁹, that can be a significant problem in low-level protein examination and hence other digest reagents were investigated, namely endoproteinase Asp-N and formic acid. Asp-N is thought to be less troubled by autodigestion²⁰⁰ but is not as cost effective as trypsin and formic acid. One other requirement of all the digest reagents is the ability to create specific digest patterns for each of the APP isoforms in which peptides unique to each isoform could be seen. Examinations of the results show trypsin to be the most effective reagent, yielding the most peptides including isoform specific peptides. Asp-N works well when examining standard proteins (BSA and APP α_{695}) but seems less effective in the cleavage of sample proteins (APP α_{770} and APP α), possibly due to the lower concentration of

these proteins. The results for formic acid are negligible for both standard and sample proteins.

Comparison of one-dimensional and two-dimensional in-gel digests shows a divide in the results. The number of peptides cleaved from standard proteins run on one-dimensional gels is generally better than those from standard proteins run on two-dimensional gels. The opposite is true for the sample proteins and the best results, including the number of isoform specific peptides are achieved from the in-gel digests of two-dimensional gel separations. One possible answer for this may be that increased sample loss, which occurs in two-dimensional gel electrophoresis reduces the amount of protein available for digestion and as such lessens the concentration of the standard proteins present within the two-dimensional gel relative to that present in a one-dimensional gel. In the electrophoresis of sample proteins, however, it is possible that more than one protein is present in the one-dimensional gel bands and as such these contaminant proteins may obscure the protein of interest. Excision and digestion of the protein band therefore will include digest peptides of the contaminating species, which if in greater concentration than the desired protein may overshadow further analysis. Two-dimensional gel electrophoresis overcomes this problem by separating similar molecular weight species in the first dimension isoelectric focussing step.

The final area of discussion is the comparison of mass spectroscopic methods, MALDI-MS and LC/MS. Both are established techniques for the analysis of low-level proteins each having its own distinct advantages. Although the number of isoform specific peptides identified is similar for both methods the general pattern observed is

a slightly greater number of cleavage peptides detected by MALDI-MS compared to LC/MS. One explanation for this could be the variation between peptide peak detection in these experiments for each technique. Although automatic peak lists were generated from the MALDI-MS spectra closer manual examination of a spectrum quite often uncovered peaks of interest, which if considered real were then included in the data search lists. The LC/MS data on the other hand was fully automated and peak lists were sent directly for analysis by the online search engines. For MS/MS, however, LC/MS/MS gives better data compared to MALDI-MS/MS due to the increased internal energy present in the multiply charged species generated by ESI relative to the singly charged ions seen with MALDI.

4.0 Conclusions and Future Work

The most significant pathological feature of AD is the presence of neuritic plaques within post-mortem brain tissue. The chief protein constituent of these plaques is the A β peptide, subsequently a great deal of research is centred on causes for its seemingly increased levels. The presence and increase of APP isoforms found in the CNS is a major area of investigation in order to find out if the increase in A β peptide is due to defective APP processing. The strategic aim of this work has been the separation, detection and identification of the APP isoforms, APP α_{695} , APP α_{751} and APP α_{770} (due to their presence within the CNS) efficiently using proteomic techniques. Two protein models were employed; BSA due to its similarity in molecular weight to the APP isoforms and common knowledge of expected results¹⁹⁷ and standard APP α_{695} for use as a direct comparison. Other samples were immunoprecipitated directly from the cell media of CHO 770 cells, excreting APP α_{770} only and conditioned Ntera 2 cells able to mimic brain cells and excrete APP α , which comprises all three isoforms of interest (APP α_{695} , APP α_{751} , APP α_{770}) and as such is the most plausible model of *in vivo* conditions. Gel loading concentrations for the protein standards was 77fmol and 231fmol for BSA and APP α_{695} respectively. Comparison of staining density of samples verses standards showed the immunoprecipitated sample concentrations to be much lower than the standards, possibly within the low femtomole or attomole range.

Separation of the three isoforms was attempted by one and two-dimensional gel electrophoresis. One-dimensional electrophoresis gave only two bands, the faster running band consisting of APP α_{695} and the slower running band made up of both APP α_{751} and APP α_{770} running together due to their similarity in molecular weight.

Separation of all three isoforms was achieved by two-dimensional gel electrophoresis of APP α and is observed by Western blot (figure 43). The resolution of the two-dimensional separation was poor but optimisation of those results may be accomplished using narrower range pH strips to increase resolution in the IEF step and larger gels to aid resolution in the second step providing clearer more resolved protein spots, which could then be excised and digested individually. Attempts to identify large intact molecules such as proteins by mass spectrometry has always proved difficult and lacked resolution. Separation of APP isoforms, however, was attempted by both MALDI-MS and nanospray. Figure 53 shows three peaks that may be the separate isoforms but the peak resolution was very poor and overshadowed by the presence of noise making the viability of these results doubtful.

Mass fingerprinting is a technique that allows the separation of large molecules by creating resolvable peptides. Theoretical digestion of the three isoforms using trypsin, Asp-N and formic acid generates specific peptides for each isoform (figure 58). Mass fingerprinting, therefore, should in theory be able to reveal the presence of each isoform upon detection of isoform specific peptides. This technique was investigated looking at the differences between one-dimensional and two-dimensional in-gel digestion utilising the digest reagents trypsin, Asp-N and formic acid. The results from this work for all standards and samples are summarised in table 105. With regards to *in vivo* experimental data the last section headed APP α is the most important as this is the best model of *in vivo* conditions and as such only these results will be focused upon here.

The general trend visible in table 105 when comparing the results from both one-dimensional and two-dimensional in-gel digests for all three digest reagents is better sequence coverage for the model proteins (BSA and standard APP α_{695}) is achieved from the one-dimensional in-gel digests, whereas sequence coverage for the sample proteins (immunoprecipitated APP α_{770} and APP α) was better from the two-dimensional in-gel digests. One explanation for this could be increased sample loss occurring in two-dimensional gel electrophoresis ²⁰² reducing the amount of protein available for digestion lowering the concentration of the standard proteins present within the two-dimensional gel relative to that present in a one-dimensional gel. The solution of sample proteins, however, may contain more than one protein and if the contaminant proteins are similar in molecular weight to the sample proteins on a one-dimensional gel these contaminants may obscure the protein of interest. Excision and digestion of the protein band therefore will include digest peptides of the contaminating species, which if in greater concentration than the desired protein may overshadow further analysis. Two-dimensional gel electrophoresis overcomes this problem by separating similar molecular weight species in the first dimension isoelectric focussing step.

The most efficient digest reagent not only for APP α but all digested proteins investigated here was trypsin, proving itself to be consistent and yielding the greatest sequence coverage. Both MALDI-MS and LC/MS have their own distinct advantages; MALDI-MS gave better sequence coverage, whereas LC/MS gave better MS/MS results. As discussed earlier the desired outcome of this research was the ability to investigate APP isoforms by visualisation of isoform specific peptides, in view of APP α only one isoform specific peptide was observed in the MALDI-MS analysis of

the two-dimensional in-gel tryptic digest even though this sample is known to consist of all three isoforms. The peptide seen at m/z 1362.65 (figure 128) corresponds to the APP α_{695} specific peptide VPTTAASTPDAVDK and although MS/MS data would be preferred in order to fully substantiate its authenticity in this instance it was not achieved probably due to low concentration. Of the three isoforms APP α_{695} is known to be the most abundant form in brain tissue. Due to the low concentration of the APP α sample it may be that the APP α_{751} and APP α_{770} were present within the sample but in concentrations lower than the limits of detection.

The approach used in this research work is viable for the investigation of not only APP isoforms but also any closely related molecules compliant to digestion and the formation of specific fragments. Based upon the data created in this research the preferred strategy for APP isoform investigation would be two-dimensional gel separation, optimising the two dimensional step as previously stated in order to fully resolve each isoform. The separate isoform spots could then be excised and digested individually using trypsin as this was found to be the most efficient in this research, however, the benefits of both Asp-N²⁰⁰ and formic acid¹⁹⁸ previously described suggest that further investigation of these digest reagents may be worthwhile. Analysis of the digest peptides could then be performed by LC/MS and MALDI-MS as both methods offer their own distinct advantages followed by MS/MS investigation of peaks of interest. Overall the sequence coverage achieved for both model and sample proteins was poor in comparison to literature references¹⁹⁷ and this essentially needs to be the first point of any future investigation. Peptide recovery from in-gel digests is a frequent problem with low-level proteins, sample losses occurring at each stage in an experiment. Two of the major factors that limit peptide recoveries are

adsorptive losses and reduced protease activity at low substrate concentration^{197, 203}. Improvements in protein recovery should be investigated looking at parameters such as protein/enzyme solvent systems, derivitisation¹³³, protein adsorption and clean-up procedures. Time spent on initial method development in order to improve peptide recovery would be beneficial in the long term. Due to the low level of sample proteins any increase in peptide recovery could mean the difference between observing isoform specific peptides or not.

A continuation of this research using the results achieved, as a foundation would be the investigation of isoform expression in both stressed and non-stressed cells. Work carried out previously by Shepherd *et al*²⁰⁴ looked at changes in the isoform expression of cells subjected to heat shock using reverse transcription-polymerase chain reaction. Their research showed an increase in the APP₇₇₀ isoform under conditions of stress. This work could be repeated using the proteomics approach to reiterate or contradict those findings. Another area of interest would be the further investigation of *N*-glycosylation sites in order to fully determine the presence and type of sugar groups present again within both stressed and non-stressed cells.

5.1 Appendix 1 – Presentations and conferences attended

Oral Presentation

Isolation and Examination by Matrix Assisted Laser Desorption Ionisation-Mass Spectrometry of Alzheimer's Disease Amyloid Precursor Protein. British Mass Spectrometry Society (BMSS) 26th Annual Meeting, Loughborough University, 8th–11th September 2002.

Poster Presentations

Isolation and Examination by Matrix Assisted Laser Desorption Ionisation-Mass Spectrometry of Alzheimer's Disease Amyloid Precursor Protein. International Society for Mass Spectrometry (ISMS) 16th Annual Meeting, Edinburgh, U.K. August 31st – 5th September 2003.

Isolation and Examination by Matrix Assisted Laser Desorption Ionisation-Mass Spectrometry of Alzheimer's Disease Amyloid Precursor Protein. American Society for Mass Spectrometry (ASMS) 51st Annual Meeting, Montreal, Canada June 8th – 12th 2003.

Isolation and Examination by Matrix Assisted Laser Desorption Ionisation-Mass Spectrometry of the Amyloid Precursor Protein of Alzheimer's disease. Royal Society of Chemistry Analytical Division, Analytical research Forum (Incorporating R & D Topics), Kingston University, 15th-17th July 2002.

Isolation and Examination by Matrix Assisted Laser Desorption Ionisation-Mass Spectrometry of the Amyloid Precursor Protein of Alzheimer's disease. British Mass Spectrometry Society (BMSS) 25th Annual Meeting, University of Southampton, 9th-12th September 2001

Isolation and Examination by Matrix Assisted Laser Desorption Ionisation-Mass Spectrometry of the Amyloid Precursor Protein of Alzheimer's disease. Royal Society of Chemistry Analytical Division, Analytical research Forum (Incorporating R & D Topics), University of East Anglia, 16th-18th July 2001.

5.2 Appendix 2 - In-gel digestion

Bovine Trypsin (TRY1_BOVIN)

Residue number	Mass (mono, avg)	Mass (mono, avg)	Sequence
110-111	259.19	259.35	LK
157-159	362.20	362.49	CLK
238-243	632.31	632.67	QTIASN
64-69	658.38	658.76	SGIQVR
112-119	804.41	804.86	SAASLNSR
221-228	905.50	906.05	NKPGVYTK
160-169	1019.50	1020.17	APILSDSSCK
229-237	1110.55	1111.33	VCNYVSWIK
146-156	1152.57	1153.25	SSGTSYPDVLK
207-220	1432.71	1433.65	LQGIVSWGSGCAQK
191-206	1494.61	1495.61	DSCQGDSGGPVVCSGK
70-89	2162.05	2163.33	LGEDNINVEGNEQFISASK
170-190	2192.99	2194.47	SAYPGQITSNMFCAGYLEGGK
90-109	2272.15	2273.60	SIVHPSYNSNTLNDIMLIK
120-145	2551.24	2552.91	VASISILPTS...LISGWGNTK
21-63	4550.12	4553.14	IVGGYTCGA...VVSAAHCYK

Porcine Trypsin (TRYP_PIG)

52-53	261.14	261.28	SR
54-57	514.32	514.63	IQVR
108-115	841.50	842.01	VATVSLPR
209-216	905.50	906.05	NKPGVYTK
148-157	1005.48	1006.15	APVLSOSSCK
98-107	1044.56	1045.16	LSSPATLNSR
134-147	1468.72	1469.68	SSGSSYPSLLQCLK
217-231	1735.84	1736.97	VCNYVNWIQQTIAAN
116-133	1767.79	1768.99	SCAAAGTECLISGWGNTK
158-178	2157.02	2158.48	SSYPGQITGNMICVGFLEGGK

58-77	2210.10	2211.42	LGEHNIDVLEGNEQFINAAK
78-97	2282.17	2283.63	IITHPNFNGNTLDNDIMLIK
179-208	3012.32	3014.33	DSCQGDSGG...SWGYGCAQK

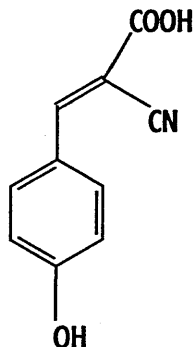
Table 1. Autolysis peaks for both bovine and porcine trypsin²⁰⁵. Quite often these peaks are used in MALDI-MS for internal calibration.

Keratin digest peaks (Da)			
804.410	1016.501	1277.710	1707.713
823.390	1033.516	1300.530	1716.851
832.489	1092.503	1302.715	1993.997
874.499	1125.542	1357.696	2383.952
910.415	1141.519	1383.690	2508.145
973.531	1179.600	1475.749	3312.308
999.445	1217.616	1475.785	
1006.430	1265.637	1657.793	

Table 2. Human keratin tryptic digest peaks²⁰⁶. All peaks are average values.

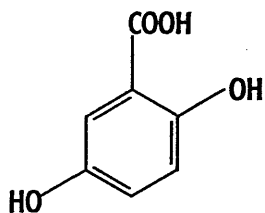
5.3 Appendix 3 – Mass spectrometry

Matrix	Application
α -cyano-4-hydroxycinnamic acid (α -CHCA)	Peptides, proteins, pharmaceutical products, polymers and DNA



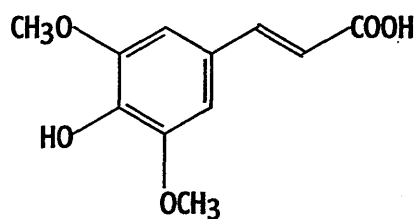
Solvents	Observed ions (Da)
50% acetonitrile/ 0.1% TFA	M^+ 189.04 $(M+H)^+$ 190.05
50% methanol/0.1% TFA	
50% ethanol	
50% isopropyl alcohol	

Matrix	Application
2,5-dihydroxybenzoic acid (DHB, gentisic acid)	Peptides, low molecular weight proteins, DNA, lipids and oligosaccharides



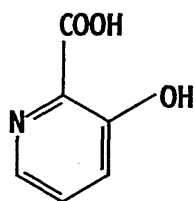
Solvents	Observed ions (Da)
50% acetonitrile/ 0.1% TFA	$(M+H-H_2O)^+$ 137.02
50% methanol/0.1% TFA	M^+ 154.03
50% ethanol	$(M+H)^+$ 155.03
50% isopropyl alcohol	$(M+Na)^+$ 177.02
Acetone	$(M+K)^+$ 192.99

Matrix	Application
Trans-3,5-dimethoxy-4-hydroxycinnamic acid (sinapinic acid)	Peptides, high molecular weight proteins, DNA and glycoproteins



Solvents	Observed ions (Da)
50% acetonitrile/ 0.1% TFA	M ⁺ 224.07
50% methanol/0.1% TFA	(M+H) ⁺ 225.08
50% ethanol	
50% isopropyl alcohol	

Matrix	Application
3-hydroxypicolinic acid (3-HPA)	Oligonucleotides, DNA and RNA



Solvents	Observed ions (Da)
50% acetonitrile/ 0.1% TFA	(M+H-CO ₂) ⁺ 96.04
	M ⁺ 139.03
	(M+H) ⁺ 140.03
	(2M+H-CO ₂) ⁺ 235.07

Table 1. Commonly used matrices and their applications. Matrices can be made up as saturated solutions but quite often a 10mg/ml concentration is used.

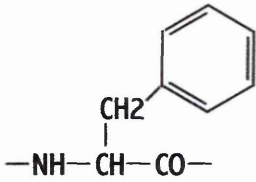
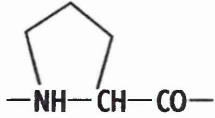
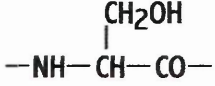
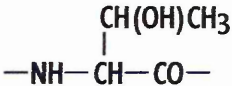
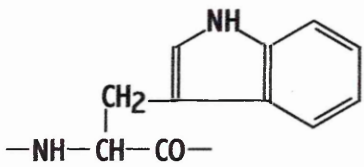
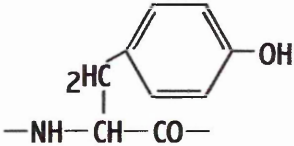
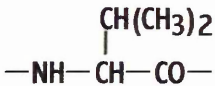
Phe	F	Phenylalanine		147.06841, 147.1766
		C ₉ H ₉ NO		
Pro	P	Proline		97.05276, 97.1167
		C ₅ H ₇ NO		
Ser	S	Serine		87.03203, 87.0782
		C ₃ H ₅ NO ₂		
Thr	T	Threonine		101.04768, 101.1051
		C ₄ H ₇ NO ₂		
Trp	W	Tryptophan		186.07931, 186.2133
		C ₁₁ H ₁₀ N ₂ O		
Tyr	Y	Tyrosine		163.06333, 163.1760
		C ₉ H ₉ NO ₂		
Val	V	Valine		99.06841, 99.1326
		C ₅ H ₉ NO		

Table 1. Most common amino acid residue structures and their masses.

Amino acid residue			Immonium ions (m/z)	Related ions (m/z)
Alanine	Ala	A	44	
Arginine	Arg	R	129	59, 70, 73, 87, 100, 112
Asparagine	Asn	N	87	70
Aspartic acid	Asp	D	88	70
Cysteine	Cys	C	76	
Acylamide modified cysteine	Cys	C	147	
Carboxyamidomethylated cysteine	Cys	C	133	
Carboxymethylated cysteine	Cys	C	134	

Pyridylethyl cysteine	Cys	C	106	
Glutamic acid	Glu	E	102	
Glutamine	Gln	Q	101	56, 84, 129
Glycine	Gly	G	30	82, 121, 123, 138, 166
Histidine	His	H	110	
Isoleucine	Iso	I	86	44, 72
Leucine	Leu	L	86	44, 72
Lysine	Lys	K	101	70, 84, 112, 129
Methionine	Met	M	104	61
Phenylalanine	Phe	F	120	91
Proline	Pro	P	70	
Serine	Ser	S	60	
Threonine	Thr	T	74	
Tryptophan	Try	W	159	77, 117, 130, 132, 170, 171
Tyrosine	Tyr	Y	136	91, 107
Phosphotyrosine	Tyr	Y		216
Valine	Val	V	72	41, 55, 69

Table 2. Common fragment ions of amino acids. Bold face indicating strong signals, italic indicating weak¹⁶⁵.

Ion type	Formulae	Ion type	Formulae
a	$[N]+[M]-CO$	D	a-partial side chain
a*	a-NH ₃	V	y-complete side chain
a°	a-H ₂ O	w	z-partial side chain
a++	$(a+H)/2$	X	$[C]+[M]+CO$
b	$[N]+[M]$	Y	$[C]+[M]+H_2$
b*	b-NH ₃	Y*	y-NH ₃
b°	b-H ₂ O	Y°	y-H ₂ O
b++	$(b+H)/2$	Y++	$(y+H)/2$
c	$[N]+[M]+NH_3$	Z	$[C]+[M]-NH$

Table 3. Formulae to calculate fragment ion masses. [N] is the mass of the N terminal group, [C] is the mass of the C terminal group and [M] is the mass sum of all the amino acid residue masses¹⁶⁵.

5.5 Appendix 5 – Protein modifications

Modification	Reagent	Site	Mass difference (mono, avg)
Acetylation		N-term K	42.01057, 42.037
Amidation		C-term	-0.98402, -0.985
Biotinylation		N-term K	226.07760, 226.293
Carbamidomethyl		C	57.02147, 57.052
Carbamyl	Cyanate from alkaline decomp. of urea	N-term K	43.00581, 43.025
Carboxymethyl	Iodoacetic acid	C	58.00548, 58.037
Deamidation		N,Q	0.98402, 0.985
Formylation		N-term	27.99492, 28.010
Homoserine	CNBr cleavage	C-term M	-29.99281, -30.087
Homoserine lactone	CNBr cleavage	C-term M	-48.00337, -48.103
ICAT d0		C	442.22500, 442.572
ICAT d8		C	450.27522, 450.622
Methyl ester		C-term D,E	14.01565, 14.027
NIPCAM	N-isopropyl iodoacetamide	C	99.06842, 99.132
¹⁸ O label		C-term	2.000424, 2.000
Oxidation		H,M,W	15.99492, 15.999
PEO biotin		C	414.19370, 414.519
Phosphorylation		S,T,Y	79.96633, 79.980
Propionamide	Acrylamide	C	71.03712, 71.079
Pyro-cys	Cyclisation of carboxyamidomethyl cys	N-term C	-17.2655, -17.030
Pyro-glu		N-term Q	-17.2655, -17.030
Pyro-glu		N-term E	-18.01057, -18.015
S-pyridylethyl		C	10.05785, 105.139
SMA	N-succinimidyl(3-morpholine acetate)	N-term K	127.06333, 127.143

Sodiation	C-term D,E	21.98194, 21.982
Sulphone	M	31.98983, 31.999

Table 1. Common protein modifications from natural sources²⁰⁷, accidental artifacts and sample preparation. It should be noted that glycosylation is not mentioned here as it is difficult to give an average mass difference due to the varying lengths of attached sugar groups.

5.6 Appendix 6 - Fluorescent stain, Ruthenium II bathophenanthroline¹⁹⁴

Potassium pentachloroaquoruthenate ($K_2Cl_5Ru.H_2O$, Alfa Aesar) 0.2g was dissolved in 20ml boiling water and kept under reflux until a deep red-brown colour resulted. Three molar equivalents of anhydrous bathophenanthroline disulphonate, disodium salt added and refluxing continued for 20 minutes at which time the solution turned greenish brown with some foaming. 5ml sodium ascorbate solution, 500mM was added to the reaction solution and refluxing continued for a further 20 min. Considerable foaming was seen and the solution turned orange-brown. Upon cooling the pH was adjusted to 7.0 with sodium hydroxide then dH_2O added to 26ml and the 20mM stock solution stored at 4°C.

Staining procedure

Gels were fixed overnight in 30% ethanol/ 10% acetic acid, before thorough rinsing for 4×30 min in 20% ethanol to remove acetic acid, known to have a quenching effect upon fluorescence. A staining solution of 5 to 10 μ l stock solution per 1L 20% ethanol was prepared and used to stain gels at room temperature for 3-6h. After staining the gels were washed in dH_2O for 2 × 10 min before imaging on a UV table and image capture.

5.7 Appendix 7- Theoretical digest lists for APP isoforms²⁰⁸

mass (M+H ⁺)	position	# missed cleavages	artificial.modification(s)		peptide sequence
5105.43	510-556	0			TTVELLPVNGEFSLDDLQPWHSFGADSV PAN TENEEPVDARPAADR
5057.98	208-251	0			VVEVAEEEEVAEVEEEEADDEDEDGDEVE EEAEEPYEEATER
4712.84	164-207	0	Cys_CM: 169, 170	4828.85	GVEFVCCPLAEESDNVDSADAEEDSDVWW GGADTDYADGSEDK
3849.88	50-82	0	Cys_CM: 56, 81	3965.89	EGILQYCQEVYPELQITNVVEANQPVTIQNWC K
3188.60	449-476	0	MSO: 449	3204.59	MNQSLSLLYNVPVAVEEIQD EVDLLQK
2402.18	1-23	0	Cys_CM: 21 MSO: 19	2460.18 2418.17	LEVPTDGNAGLLAEPQIAMFCGR
2127.06	252-271	0			TTSIATTTTTTTESVEEVVR
2022.14	379-396	0			LALENYITALQAVPPRPR
1980.89	477-493	0	MSO: 488	1996.89	EQNYSDDVLANMISEPR
1914.86	286-301	0			YLETGPDENEHAHFQK
1876.89	145-161	0	Cys_CM: 157 MSO: 153	1934.89 1892.88	STNLHDYGMLLPCGIDK
1806.84	124-138	0	Cys_CM: 127 MSO: 124	1864.84 1822.83	MDVCETHLHWHTVAK
1739.85	494-509	0	MSO: 502	1755.84	ISYGDALMPSLTETK
1704.88	100-115	0	Cys_CM: 100	1762.89	CLVGEFVSDALLVPDK
1414.80	557-570	0			GLTRPGSGLTNIK
1374.64	347-358	0			VESLEQEAAANER
1372.69	272-285	0			VPTTAASTPDAVDK
1336.60	585-595	0			HDSGYEVHHQK
1285.61	24-34	0	MSO: 26, 28	1317.60	LNMHMNVQNGK
1266.67	90-99	0			THPHFVIPYR
1212.61	359-368	0	MSO: 366	1228.61	QQLVETHMAR
1099.58	338-346	0			AVIQHFQEK
992.43	35-43	0			WSDPSGTK
971.50	436-443	0	MSO: 439	987.50	SQVMTHLR
948.40	320-326	0			EWEEAER
947.46	369-376	0	MSO: 372	963.45	VEAMLNDR
934.47	571-578	0			TEEISEVK
888.47	397-403	0	MSO: 401	904.47	HVFNMLK
829.43	118-123	0			FLHQER
824.41	419-424	0			HFEHVR
768.33	579-584	0	MSO: 579	784.32	MDAEFR
751.35	314-319	0	MSO: 314, 318	783.34	MSQVMR
696.28	139-144	0	Cys_CM: 141	754.29	ETCSEK

680.32	44-49	0	Cys_CM: 45	738.33	TCIDTK
679.37	444-448	0			VIYER
626.36	414-418	0			QHTLK
589.30	425-429	0	MSO: 425	605.29	MVDPK
558.33	431-435	0			AAQIR

Table 1. Theoretical tryptic digest peptides for APP α_{695} . All cysteines have been treated with iodoacetic acid to form carboxymethyl-cysteine (Cys_CM) and methionines oxidised to form methionine sulphoxide (MSO). All masses shown are monoisotopic M+H⁺. Isoform specific peptides are highlighted in blue.

mass (M+H ⁺)	position	# missed cleavages	artificial modification(s)		peptide sequence
5105.43	566-612	0			TTVELLPVNGEFLDDLQPWHSFGADSVANTENEVEPVD ARPAADR
5057.98	208-251	0			VVEVAEEEEVAEVEEEEADDEDEDGDEVEEEAEPEYEE ATER
4712.84	164-207	0	Cys_CM: 169, 170	4828.85	GVEFVCCPLAEESDNVDSADAEEEDSDVWVGADTDYADG SEDK
3849.88	50-82	0	Cys_CM: 56, 81	3965.89	EGILQYCQEVPELQITNVV EANQPVTIQNWCK
3188.60	505-532	0	MSO: 505	3204.59	MNQSLSLLYNVPVAEEIQD EVDELLQK
3121.34	312-341	0	Cys_CM: 320, 324 MSO: 321	3237.35 3137.33	NNFDTEEYCMVCGSAIPTT AASTPDAVDK
2402.18	1-23	0	Cys_CM: 21 MSO: 19	2460.18 2418.17	LEVPTDGNAGLLAEPQIAMF CGR
2127.06	252-271	0			TTSIATTTTTTTESVEEVVR
2022.14	435-452	0			LALENYITALQAVPPRPR
1980.89	533-549	0	MSO: 544	1996.89	EQNYSDDVLANMISEPR
1914.86	342-357	0			YLETPGDENEHAHFQK
1876.89	145-161	0	Cys_CM: 157 MSO: 153	1934.89 1892.88	STNLHDYGMLLPCGIDK
1806.81	124-138	0	Cys_CM: 127 MSO: 124	1864.84 1822.83	MDVCETHLHWHTVAK
1739.85	550-565	0	MSO: 558	1755.84	ISYGN DALMPSLTETK
1704.88	100-115	0	Cys_CM: 100	1762.89	CLVGEFVSDALLVPDK
1414.80	613-626	0			GLTTRPGSGLTNIK
1408.58	272-284	0	Cys_CM: 274, 283	1524.59	EVCSEQAETGPCR
1374.64	403-414	0			VESLEQEAANER
1348.55	299-311	0	Cys_CM: 299, 307	1464.56	CAPFFYGGCGGNR
1336.60	641-651	0			HDSGYEVHHQK
1285.61	24-34	0	MSO: 26, 28	1317.60	LNMHMNVQNGK
1266.67	90-99	0			THPHFVIPYR
1212.61	415-424	0	MSO: 422	1228.61	QQLVETHMAR
1144.53	290-298	0			WYFDVTEGK
1099.58	394-402	0			AVIQHFQEK

992.43	35-43	0		WSDSPSGTK
971.50	492-499	0	MSO: 495	987.50 SQVMTHLR
948.40	376-382	0		EWEEAER
947.46	425-432	0	MSO: 428	963.45 VEAMLNDR
934.47	627-634	0		TEEISEVK
888.47	453-459	0	MSO: 457	904.47 HVFNMLK
829.43	118-123	0		FLHQER
824.41	475-480	0		HFEHVR
768.33	635-640	0	MSO: 635	784.32 MDAEFR
751.35	370-375	0	MSO: 370, 374	783.34 MSQVMR
696.28	139-144	0	Cys_CM: 141	754.29 ETCSEK
680.32	44-49	0	Cys_CM: 45	738.33 TCIDTK
679.37	500-504	0		VIYER
626.36	470-474	0		QHTLK
589.30	481-485	0	MSO: 481	605.29 MVDPK
577.31	285-289	0	MSO: 286	593.30 AMISR
558.33	487-491	0		AAQIR

Table 2. Theoretical tryptic digest peptides for APP α_{751} . All cysteines have been treated with iodoacetic acid to form carboxymethyl-cysteine (Cys_CM) and methionines oxidised to form methionine sulphoxide (MSO). All masses shown are monoisotopic M+H⁺. Isoform specific peptides are highlighted in blue.

mass (M+H ⁺)	position	# missed cleavages	artificial .modification(s)	peptide sequence
5105.43	585-631	0		TTVELLPVNGEFSLDDLQPWHSFGADSV PANTENEVEPVDAP AADR
5057.98	208-251	0		VVEVAEEEEV AEVEEEEADDEDEDGDEVEEEAEPEYEETE R
4712.84	164-207	0	Cys_CM: 169, 170	4828.85 GVEFVCCPLAEESDNVDSADAEEDSDVWWGGADTDYADG SEDK
3849.88	50-82	0	Cys_CM: 56, 81	3965.89 EGILQYCQEVYPELQITNVV EANQPVTIQNWCK
3188.60	524-551	0	MSO: 524	3204.59 MNQSLSLLYNPAVAEEIQD EVDELLQK
2541.07	312-334	0	Cys_CM: 320, 324 MSO: 321, 328	2657.08 NNFDTEEYCMVCGSAMSQS LLK 2573.06
2402.18	1-23	0	Cys_CM: 21 MSO: 19	2460.18 LEVPTDGNAGLLAEPQIAMF CGR 2418.17
2127.06	252-271	0		TTSIATTTTTTTESVEEVVR
2022.14	454-471	0		LALENYITALQAVPPRPR
1980.89	552-568	0	MSO: 563	1996.89 EQNYSDDVLANMISEPR
1914.86	361-376	0		YLETPGDENEHAHFQK
1876.89	145-161	0	Cys_CM: 157 MSO: 153	1934.89 STNLHDYGMLLPCGIDK 1892.88
1806.84	124-138	0	Cys_CM: 127 MSO: 124	1864.84 MDVCETHLHWHTVAK 1822.83
1739.85	569-584	0	MSO: 577	1755.84 ISYGN DALMPSLTETK
1704.88	100-115	0	Cys_CM: 100	1762.89 CLVGEFVSDALLVPDK
1414.80	632-645	0		GLTTRPGSGLTNIK
1408.58	272-284	0	Cys_CM: 274, 283	1524.59 EVCSEQAETGPCR
1386.71	347-360	0		LPTTAASTPDAVDK
1374.64	422-433	0		VESLEQEAANER
1348.55	299-311	0	Cys_CM: 299, 307	1464.56 CAPFFYGGCGGGR
1336.60	660-670	0		HDSGYEVHHQK
1285.61	24-34	0	MSO: 26, 28	1317.60 LNMHMNVQNGK
1266.67	90-99	0		THPHFVIPYR
1212.61	434-443	0	MSO: 441	1228.61 QQLVETHMAR
1144.53	290-298	0		WYFDVTEGK
1099.58	413-421	0		AVIQHFQEK
992.43	35-43	0		WSDPSGTK
971.50	511-518	0	MSO: 514	987.50 SQVMTHLR
948.40	395-401	0		EWEEAER
947.46	444-451	0	MSO: 447	963.45 VEAMLNDR
934.47	646-653	0		TEEISEVK
915.48	335-342	0		TTQEPLAR
888.47	472-478	0	MSO: 476	904.47 HVFNMLK
829.43	118-123	0		FLHQR
824.41	494-499	0		HFEHVR
768.33	654-659	0	MSO: 654	784.32 MDAEFR
751.35	389-394	0	MSO: 389, 393	783.34 MSQVMR
696.28	139-144	0	Cys_CM: 141	754.29 ETCSEK
680.32	44-49	0	Cys_CM: 45	738.33 TCIDTK

679.37	519-523	0		VIYER
626.36	489-493	0		QHTLK
589.30	500-504	0	MSO: 500	605.29 MVDPK
577.31	285-289	0	MSO: 286	593.30 AMISR
558.33	506-510	0		AAQIR

Table 3. Theoretical tryptic digest peptides for APP α_{770} . All cysteines have been treated with iodoacetic acid to form carboxymethyl-cysteine (Cys_CM) and methionines oxidised to form methionine sulphoxide (MSO). All masses shown are monoisotopic M+H⁺. Isoform specific peptides are highlighted in blue.

mass (M+H ⁺)	position	#MC	artif.modification(s)	peptide sequence
4007.05	70-103	0	Cys_CM: 81, 88, 100	4181.07 EANQPVTIQNWCKRGRKQCKTHPHFVIPYRCLVG
3211.76	382-408	0	MSO: 401	3227.76 ENYITALQAVPPRPRHVFNM LKKYVRA
2604.20	14-35	0	Cys_CM: 21 MSO: 19, 26, 28	2662.21 EPQIAMFCGRLNMHMNVQNG KW 2652.19
2354.31	427-446	0	MSO: 439	2370.30 DPKAAQIRSQVMTHLRVIY
1904.98	447-463	0	MSO: 449	1920.98 ERMNQLSLLYNVPAVA
1786.97	555-571	0		DRGLTTRPGSGLTNIKT
1484.74	250-263	0		ERTTSIATTTTTTT
1358.69	128-138	0		ETHLHWHTVAK
1327.72	268-280	0		EVVRVPTTAASTP
1213.66	335-344	0		DKKAVIQHFQ
1181.61	412-420	0		DRQHTLKHf
1157.53	525-534	0		DLQPWHSFGA
1154.66	325-334	0		ERQAKNLPKA
1095.56	295-303	0		EHAHFQKAK
1081.50	150-159	0	Cys_CM: 157 MSO: 153	1139.51 DYGMLLPCGI 1097.50
1036.50	312-319	0	MSO: 314, 318	1068.49 ERMSQVMR
1018.51	114-121	0	Cys_CM: 116	1076.51 DKCKFLHQ
953.43	50-57	0	Cys_CM: 56	1011.44 EGILQYCQ
935.45	491-498	0		EPRISYGN
921.43	38-46	0	Cys_CM: 45	979.44 DPSGKTICI
915.51	62-69	0		ELQITNVV
899.55	375-381	0		DRRRLAL
881.38	166-173	0	Cys_CM: 169, 170	997.40 EFVCCPLA
862.43	483-490	0	MSO: 488	878.42 DVLANMIS
847.42	499-506	0	MSO: 502	863.41 DALMPSLT
843.41	363-369	0	MSO: 366	859.40 ETHMARV
828.42	143-149	0		EKSTNLH
790.35	190-196	0		DVWWGGA

777.40	590-595	0			EVHHQK
772.43	357-362	0			ERQQLV
770.39	421-426	0	MSO: 425	786.39	EHVRMV
741.41	513-519	0			ELLPVNG
730.37	6-13	0			DGNAGLLA
721.39	160-165	0			DKFRGV
703.32	535-541	0			DSVPANT
678.36	507-512	0			ETKTTV
640.35	307-311	0			EAKHR
640.25	477-481	0			EQNYS
630.38	472-476	0			ELLQK
627.37	108-113	0			DALLVP
600.31	549-554	0			DARPAA
588.28	582-585	0			EFRH
577.26	370-374	0	MSO: 372	593.25	EAMLN
538.28	284-287	0			DKYL
507.24	58-61	0			EVYP
506.26	576-579	0	MSO: 579	522.25	EVKM

Table 4. Theoretical Asp-N digest peptides for APP α_{695} . All cysteines have been treated with iodoacetic acid to form carboxymethyl-cysteine (Cys_CM) and methionines oxidised to form methionine sulphoxide (MSO). All masses shown are monoisotopic M+H⁺. It should be noted that formic acid has the same cleavage pattern as Asp-N. Isoform specific peptides are highlighted in blue.

mass (M+H ⁺)	position	#MC	artif.modification(s)		peptide sequence
4007.05	70-103	0	Cys_CM: 81, 88, 100	4181.07	EANQPVTIQNWCKRGRKQCK THPHFVIPYRCLVG
3211.76	438-464	0	MSO: 457	3227.76	ENYITALQAVPPRPRHVFNM LKKYVRA
2604.20	14-35	0	Cys_CM: 21 MSO: 19, 26, 28	2662.21 2652.19	EPQIAMFCGRLNMHMNVQNG KW
2354.31	483-502	0	MSO: 495	2370.30	DPKKAQAQIRSQVMTHLRVIY
2037.86	296-314	0	Cys_CM: 299, 307	2153.88	EGKCAPFFYGGCGGNRNNF
1904.98	503-519	0	MSO: 505	1920.98	ERMNQSLSLLYNPAVA
1872.81	318-336	0	Cys_CM: 320, 324 MSO: 321	1988.82 1888.81	EYCMAVCGSAIPTTAASTP
1786.97	611-627	0			DRGLTTRPGSGLTNIKT
1716.79	279-292	0	Cys_CM: 283 MSO: 286	1774.80 1732.79	ETGPCRAMISRWFYF
1484.74	250-263	0			ERTTSIATTTTTTT
1358.69	128-138	0			ETHLHWHTVAK
1213.66	391-400	0			DKKAVIQHFQ
1181.61	468-476	0			DRQHTLKHF
1157.53	581-590	0			DLQPWHSFGA
1154.66	381-390	0			ERQAKNLPKA
1095.56	351-359	0			EHAHFQKAK
1081.50	150-159	0	Cys_CM: 157 MSO: 153	1139.51 1097.50	DYGMILLPCGI
1036.50	368-375	0	MSO: 370, 374	1068.49	ERMSQVMR
1018.51	114-121	0	Cys_CM: 116	1076.51	DKCKFLHQ
953.43	50-57	0	Cys_CM: 56	1011.44	EGILQYCQ
935.45	547-554	0			EPRISYGN
921.43	38-46	0	Cys_CM: 45	979.44	DPSGKTICI
915.51	62-69	0			ELQITNVV
899.55	431-437	0			DRRRLAL
881.38	166-173	0	Cys_CM: 169, 170	997.40	EFVCCPLA
862.43	539-546	0	MSO: 544	878.42	DVLANMIS
847.42	555-562	0	MSO: 558	863.41	DALMPSLT

843.41	419-425	0	MSO: 422	859.40	ETHMARV
828.42	143-149	0			EKSTNLH
790.35	190-196	0			DVWWGGA
777.40	646-651	0			EVHHQK
772.43	413-418	0			ERQQLV
770.39	477-482	0	MSO: 481	786.39	EHVRMV
741.41	569-575	0			ELLPVNG
730.37	6-13	0			DGNAGLLA
721.39	160-165	0			DKFRGV
703.32	591-597	0			DSVPANT
678.36	563-568	0			ETKTTV
640.35	363-367	0			EAKHR
640.25	533-537	0			EQNYS
630.38	528-532	0			ELLQK
627.37	108-113	0			DALLVP
600.31	605-610	0			DARPAA
588.28	638-641	0			EFRH
577.26	426-430	0	MSO: 428	593.25	EAMLN
538.28	340-343	0			DKYL
507.24	58-61	0			EVYP
506.26	632-635	0	MSO: 635	522.25	EVKM
502.29	268-271	0			EVVR

Table 5. Theoretical Asp-N digest peptides for APP α_{751} . All cysteines have been treated with iodoacetic acid to form carboxymethyl-cysteine (Cys_CM) and methionines oxidised to form methionine sulphoxide (MSO). All masses shown are monoisotopic M+H⁺. It should be noted that formic acid has the same cleavage pattern as Asp-N. Isoform specific peptides are highlighted in blue.

mass (M+H ⁺)	position	#MC	artif.modification(s)	peptide sequence
4007.05	70-103	0	Cys_CM: 81, 88, 100	4181.07 EANQPVTIQNWCKRGRKQCKTHPHFVIPYRCLVG
3211.76	457-483	0	MSO: 476	3227.76 ENYITALQAVPPRPRHVFNM LKKYVRA
2604.20	14-35	0	Cys_CM: 21 MSO: 19, 26, 28	2662.21 EPQIAMFCGRLNMHMNVQNG KW 2652.19
2354.31	502-521	0	MSO: 514	2370.30 DPKKAAQIRSQVMTHLRVIY
2150.95	318-337	0	Cys_CM: 320, 324 MSO: 321, 328	2266.96 EYCMVCGSAMSQSLKTTQ 2182.94
2037.86	296-314	0	Cys_CM: 299, 307	2153.88 EGKCAPFFYGGCGGNRRNF
1904.98	522-538	0	MSO: 524	1920.98 ERMNQSLSLLYNPAVA
1786.97	630-646	0		DRGLTTRPGSGLTNIKT
1716.79	279-292	0	Cys_CM: 283 MSO: 286	1774.80 ETGPCRAMISRWYF 1732.79
1484.74	250-263	0		ERTTSIATTTTTTT
1358.69	128-138	0		ETHLHWHTVAK
1297.69	343-355	0		DPVKLPPTAASTP
1213.66	410-419	0		DKKAVIQHFQ
1181.61	487-495	0		DRQHTLKHf
1157.53	600-609	0		DLQPWHSFGA
1154.66	400-409	0		ERQAKNLPKA
1095.56	370-378	0		EHAHFQKAK
1081.50	150-159	0	Cys_CM: 157 MSO: 153	1139.51 DYGMLLPCGI 1097.50
1036.50	387-394	0	MSO: 389, 393	1068.49 ERMSQVMR
1018.51	114-121	0	Cys_CM: 116	1076.51 DKCKFLHQ
953.43	50-57	0	Cys_CM: 56	1011.44 EGILQYCQ
935.45	566-573	0		EPRISYGN
921.43	38-46	0	Cys_CM: 45	979.44 DPSGKTICI
915.51	62-69	0		ELQITNVV
899.55	450-456	0		DRRRLAL
881.38	166-173	0	Cys_CM: 169, 170	997.40 EFVCCPLA

862.43	558-565	0	MSO: 563	878.42	DVLANMIS
847.42	574-581	0	MSO: 577	863.41	DALMPSLT
843.41	438-444	0	MSO: 441	859.40	ETHMARV
828.42	143-149	0			EKSTNLH
790.35	190-196	0			DVWWGGA
777.40	665-670	0			EVHHQK
772.43	432-437	0			ERQQLV
770.39	496-501	0	MSO: 500	786.39	EHVRMV
741.41	588-594	0			ELLPVNG
730.37	6-13	0			DGNAGLLA
721.39	160-165	0			DKFRGV
703.32	610-616	0			DSVPANT
678.36	582-587	0			ETKTTV
640.35	382-386	0			EAKHR
640.25	552-556	0			EQNYS
630.38	547-551	0			ELLQK
627.37	108-113	0			DALLVP
600.31	624-629	0			DARPAA
588.28	657-660	0			EFRH
585.33	338-342	0			EPLAR
577.26	445-449	0	MSO: 447	593.25	EAMLN
538.28	359-362	0			DKYL
507.24	58-61	0			EVYP
506.26	651-654	0	MSO: 654	522.25	EVKM
502.29	268-271	0			EVVR

Table 6. Theoretical Asp-N digest peptides for APP α_{770} . All cysteines have been treated with iodoacetic acid to form carboxymethyl-cysteine (Cys_{CM}) and methionines oxidised to form methionine sulphoxide (MSO). All masses shown are monoisotopic M+H⁺. It should be noted that formic acid has the same cleavage pattern as Asp-N. Isoform specific peptides are highlighted in blue.

1. Alzheimer A. Über einen eigenartigen schweren Krankheitsprozess der Hirnrinde. *Zentralblatt für Nervenkrankheiten* 1906,25:1134.
2. Praticò D. & Trojanowski J.Q. Inflammatory hypotheses: novel mechanisms of Alzheimer's neurodegeneration and new therapeutic targets. *Neurobiology of Aging* 2000; 21:441-445.
3. Dorrell S. Untangling Alzheimer's disease with β -secretase inhibitors. *Drug Discovery Today* 2000; 8:316-317.
4. Alzheimer's Disease Mutation Database, URL <http://molgen-www.uia.ac.be/>
5. Goedert M., Trojanowski J.Q., Lee V.M.Y. & Smith M.J. The neurofibrillary pathology of Alzheimer's disease. *Molecular and Genetic Basis of Neurological Disease* 2nd ed. 1996, pp613-627.
6. Selkoe D.J. The cell biology of beta amyloid precursor protein and presenilin in Alzheimer's disease. *Trends in Cell Biology* 1998; 8: 448-453.
7. Goedert M., Jakes R., Spillantni M.G., Hasegawa M., Smith M.J. & Crowther R.A. Assembly of microtubule associated protein tau into Alzheimer-like filaments induced by sulphated glycosaminoglycans. *Nature* 1996; 383:550-553.
8. St.George-Hyslop P.H. Molecular genetics of Alzheimer's disease. *Biological Psychiatry* 2000; 47:183-199.

9. Lu P.J., Wulf G., Zhou X.Z., Davies P. & Lu K.P. The prolyl isomerase Pin 1 restores the function of Alzheimer's associated phosphorylated tau protein. *Nature* 1999; 399: 784-788.
10. Glenner G.G & Wong C.W. Alzheimer's disease: initial report of the purification and characterisation of a novel cerebrovascular amyloid protein. *Biochemical and Biophysical Research Communications* 1984; 120:885-890.
11. Shoji M., Golde T.E. & Ghiso J. Production of the Alzheimer amyloid β protein by normal proteolytic processing. *Science* 1992; 258:126-129.
12. Iwatsubo T., Odaka A., Suzuki N., Mizusawa H.M., Nukina N. & Ihara Y. Visualisation of amyloid beta 42 and amyloid beta 40 in senile plaques with end specific amyloid beta monoclonals: evidence that an initially deposited species is amyloid beta. *Neuron* 1994; 13: 45-53.
13. Cai X.D., Golde T.E. & Younkin S.G. Release of excess amyloid β protein from a mutant amyloid β precursor. *Science* 1993; 259: 514-516.
14. Schellenburg G.D., Clarenz O. & Schmidt R. Genetic linkage evidence for a familial Alzheimer's disease locus on chromosome 14. *Science* 1992; 258:668-671.
15. Fan W., Acquati F., Nucci C. & Taramelli R. BACE maps to chromosome 11 and a BACE homolog, BACE2, reside in the obligate Down syndrome region of chromosome 21. *Science* 1999; 286:1255a.

16. Heintz N. & Zoghbi H. Alpha-synuclein- a link between Parkinson's and Alzheimer's disease. *Nature Genetics* 1997; 16: 325-327.
17. Percy M.E., Mankovic V.D., Crapper T.E., McLachlan D.R. & Stevens T. Family with a 22 derived marker chromosome and late onset dementia of the Alzheimer's type I. Application on a new model for estimation of the risk factor of the disease associated with the marker. *Journal of Medical Genetics* 1991; 39: 307-313.
18. Corder E.H., Saunders A.M., Strittmatter W.J., Schmechel D.E., Gaskell P.C., Small G.W., Roses A.D., Haines J.L. & Perical-Vance M.A. Gene dose of apolipoprotein E type 4 allele and the risk of Alzheimer's disease in late onset families. *Science* 1993; 261: 921-923.
19. Campion D., Dumanch C., Hannequin D., Shanoi L. & Li X. Early onset Alzheimer's disease: prevalence, genetics, heterogeneity and mutation spectrum. *American Journal of Human Genetics* 1999; 65: 664-670.
20. Patterson D., Gardiner K., Kao F.T., Tanzi R., Watkins P. & Gusella J.F. Mapping of the gene encoding the beta amyloid precursor protein and its relationship to the Down syndrome region of chromosome 21. *Proceedings of the National Academy of Science* 1988; 85: 8266-8270.
21. Tanzi R.E., Gusella J.F., Watkins P.C., Bruns G.A., St George-Hyslop P. Van Keuren Neve R.L. Amyloid β protein gene: cDNA, mRNA distribution and genetic linkage near the Alzheimer locus. *Science* 1987; 235:880-884.

22. Delabar J.M., Goldgaber D., Lamour Y. Nicole A., Huret J.L., de Grouchy J., Brown P. Gajdusek D.C. & Sinet P.M. Beta amyloid gene duplication in Alzheimer's disease and karyotypically normal Down syndrome. *Science* 1987; 236: 1390-1392.
23. Tanzi R., St George Hyslop P., Haines J., Drachman D. & Growden J. Genetic linkage analysis of the Alzheimer's associated amyloid beta protein gene with familial Alzheimer's disease and chromosome 21. *Cellular Genetics* 1987; 46: 703.
24. Engidawork E., Balic N., Fountoulakis M., Unstan R., Travini S.T. & Octave J. Beta amyloid precursor protein, ETS and collagen alpha I (VI) chain precursor, encoded on chromosome 21, are not over expressed in fetal Down syndrome: further evidence against the gene dosage effect. *Journal of Neural Transmission* 2001; 61: 335-346.
25. Kang J., Lemaire H.G., Unterbeck A. & Kramer G.E. The precursor of Alzheimer's disease amyloid A4 protein resembles a cell surface receptor. *Nature* 1987; 325:733-736.
26. .Specher C.A., Grant F.J. & Grimm G. Amyloid precursor protein homology: evidence for a multi-gene family. *Biochemistry* 1993; 32: 4481-4486.
27. Kang J. & Muller-Hill B. Differential splicing of Alzheimer's disease A4 precursor mRNA in rat tissue: precursor A4-695 mRNA is predominantly produced in rat and human brain. *Biochemical and Biophysical Research Communications* 1989; 166: 1192-1200.

28. Harrison P.J. & Porter-Smithe T. Amyloid precursor protein mRNA's in Alzheimer's disease. *Neurodegeneration* 1996; 5:409-415.
29. de Sauvage F. & Octave J. A novel mRNA of the A4 amyloid precursor gene coding for a possibly secreted protein. *Science* 1989; 245: 651-653.
30. Jitaguchi N., Takahashi Y., Tokushima Y. & Li S. Novel precursor of Alzheimer's disease amyloid protein shows protease inhibitory activity. *Nature* 1988; 331: 530-532.
31. Konig G., Monning U., Czech C. & Fensau L. Identification and differential expression of a novel alternative splice isoform of the beta A4 amyloid precursor protein mRNA in leukocytes and brain microglial cells. *Journal of Biological Chemistry* 1992; 267: 804-810.
32. Ohgami T., Kitamoto T. & Tateishi J. Alzheimer's amyloid precursor protein mRNA without exon 15 is ubiquitously expressed except in the central nervous system. *Molecular Brain Research* 1993; 20: 240-244.
33. Pangalos M.N., Efthimiopoulos S., Shioi J., Theodopolous A. R. & Zhoi S. The chondroitin sulphate attachment site of appican is formed by splicing out exon 15 of the amyloid precursor gene. *Journal of Biological chemistry* 1995; 270:10388-10391.
34. Caporaso G.L., Gandy S.E., Buxbaum J.D. & Brown D.B. Cloroquin inhibits intracellular degradation but not secretion of Alzheimer's B/A4 amyloid precursor protein. *Proc National Acad Sci* 1992; 82: 2252-2256.

35. St. George-Hyslop P.H. Molecular genetics of Alzheimer's disease. *Biological Psychiatry* 2000; 47:183-199.
36. Haas C., Koo E.H., Mellon A., Hung A.Y. & Selkoe D.J. Targeting of cell surface beta amyloid precursor protein to lysosomes: alternative processing into amyloid bearing fragments. *Nature* 1992; 357: 500-503.
37. Sisodia S.S., Koo E., Beyreuther K., Unterbeck A. & Price D.L. Evidence that beta amyloid protein in A beta is not derived by normal processing. *Science* 1990; 248: 492-495.
38. Shoji M., Golde T.E., Ghiso J., Cheung T.T., Estus S., Shaffer L.M., Cai X.D., McKay D.M., Tintner R. & Frangione B. Production of Alzheimer's amyloid beta protein by normal proteolytic processing. *Science* 1992; 258: 129-129.
39. Cook D.G., Forman M.S., Sung J.C. & Golde T.E. Alzheimer's A beta (1-42) is generated in the ER/intermediate compartment of NT2N cells. *Nature Medicine*. 1997; 3: 1021-1023.
40. Lammich S., Kojro E., Postina S., Gilbert S., Pfeiffer R., Jasionowski M., Haas C. & Fahrenholz F. Constitutive and regulated alpha secretase cleavage of Alzheimer's precursor protein by a disintegrin metalloprotease. *Proceedings of the National Academy of Science* 1999; 96: 3922-3927.

41. Hotoda N., Koike H., Sasagawa N. & Ishiura S. A secreted form of human ADAM 9 has an alpha secretase activity for APP. *Biochemical and Biophysical Research Communications* 2002; 293: 800-805.
42. Buxbaum J.D., Liu K.N., Luo Y.X. & Schultz P. Evidence that tumour necrosis factor α converting enzyme is involved in regulated alpha secretase cleavage of the Alzheimer's protein precursor. *Journal of Biological Chemistry* 1998; 27765-27767.
43. Vassar R., Bennet B.D., Babu-Khan S., Molde T.E. & Esterez E. Beta secretase cleavage of Alzheimer's amyloid precursor protein by the transmembrane aspartic protease BACE. *Science* 1999; 286: 735-741.
44. Hussain I., Powell D., Howlett D.R., Tew D.G., Meek T.D., Chapman C., Gloger I.S., Murphy K.E., Southan C.D., Ryan D.M., Smith T.S., Simmons D.L., Walsh F.S., Dingwall C. & Christie G. Identification of a novel aspartic protease (Asp2) as beta secretase. *Molecular and Cellular Neuroscience* 1999; 14: 419-427.
45. Sinha S., Anderson J.P., Barbour R., Basi G.S., Caccavello R., Davis D., Doan M., Dovey H.F., Frigon N., Hong J., Jacobson-Croak K., Jewett N., Keim P., & Knops J. Purification and cloning of the amyloid precursor protein beta secretase from human brain. *Nature* 1999; 40: 537-540.
46. Yan R., Bienkowski M.J., Shuck M.E., Miao H., Tory M.C., Pauley A.M., Brashier J.R., Stratman N.C., Mathews W.R., Buhl A.E., Carter D.B., Tomasselli

A.G., Parodi L.A. & Henrikson L.A. Membrane anchored aspartyl protease with Alzheimer's disease beta secretase activity. *Nature* 1999; 402: 533-537.

47. Li Y.M., Xu M.T., Lai Q., Thinakaran G, & Luo W.J. Photoactivated γ -secretase inhibitors directed to the active site covalently label presenilin 1. *Science* 2000; 405: 689-694.

48. De Strooper B., Annaert W., Cupers P., Saftig P. & Craessaerts K. Deficiency of presenilin-1 inhibits the normal cleavage of amyloid precursor protein. *Nature* 1998; 391: 387-390.

49. Yu G., Talli L. & Zhou G. The presenilin 1 protein is a component of a high molecular weight intracellular complex that contains beta catenin. *Journal of Biological Chemistry* 1998; 272: 16470-16476.

50. Wolfe M.S. Therapeutic strategies of Alzheimer's disease. *Nature Reviews* 2002; 1: 859-866.

51. Storey E & Cappai R. The amyloid precursor protein of Alzheimer's disease and the A β peptide. *Neuropathology and Applied Neurobiology* 1999; 25:81-97.

52. Rossjohn J., Cappai R., Feil S., Davies M.C. & Steinburg T. Crystal structure of the N-terminus growth like factor domain of Alzheimer's amyloid precursor protein. *Nature Structural Biology* 1999; 6: 327-331.

53. Sambamurti K., Shioi J., Anderson A.P., Carter H.T. & Laitham P. Evidence for intracellular cleavage of the Alzheimer's amyloid precursor protein in PC12 cells. *Journal of Neuroscience Research* 1992; 33: 319-329.
54. Jung S.S., Nalbantoglu J. & Cashman N.R. Alzheimer's beta amyloid precursor protein is expressed on the surface of immediately ex-vivo brain cells: a flow cytometry study. *Journal of Neuroscience Research* 1996; 46: 336-348.
55. Mattson M.P., Cheng B., Culwell A.R., Esch F.S., Lieberburg I. & Rydel R.E. Evidence for excitoprotective and intraneuronal calcium regulating roles for secreted forms of the beta amyloid precursor protein. *Neuron* 1993; 10: 243-254.
56. Ninomiya H., Roch J.M., Sundsmo M.P. & Samsol L. Amino acid sequence RERMS represents the active domain of amyloid beta/A4 protein precursor that promotes fibroblast growth. *Journal of Cell biology* 1993; 121: 879-886.
57. Small D.H., Nurcombe V., Reed G. & Smith S. A heparin binding domain in the amyloid protein precursor of Alzheimer's disease is involved in the regulation of neurite outgrowth. *Journal of Neuroscience* 1994; 14: 2117-2127.
58. Multhaup G. Identification and regulation of the high affinity binding site of the Alzheimer's disease amyloid precursor protein (APP) to glycosaminoglycans. *Biochimie* 1994; 76: 304-311.

59. Williamson T.G., Mok S.S., Henry T. & White A.R. Secreted glypican bind to the amyloid precursor protein of Alzheimer's disease and inhibits APP induced neurite outgrowth. *Journal of Biological Chemistry* 1996; 271: 31215-31221.
60. Bush A.I., Multhaup G., Moir R.D. & Tanzi R.E. A novel Zinc (II) binding site modulates the function of the beta A4 amyloid precursor protein of Alzheimer's disease. *Journal of Biological Chemistry* 1993; 268: 16109-16112.
61. Franceschi C., Chiricolo M., Licastro F. & Lannetti A.P. Oral zinc supplementation in Down's syndrome: restoration of thymic endocrine activity and some immune deficits. *Journal of Mental Deficiency Research* 1988; 32: 169-181.
62. Snow A.D., Kinsella M.G., Parks E., Sekiguchi R.T., Miller J.D., Kimata K. & Wight T.N. Differential binding of vascular cell-derived proteoglycans (perlecan, biglycan, decorin and versican) to the beta amyloid protein of Alzheimer's disease. *Archives in Biochemistry and Biophysical Research* 1995; 320: 84-95.
63. Multhaup G., Ruppert T., Schlicksupp A., Hesse L., Bill E., Pipkorn K., Masters C.L. & Beyreuther K. Copper binding amyloid precursor protein undergoes a site-specific fragmentation in the reduction of hydrogen peroxide. *Biochemistry* 1998; 37: 7224-7230.
64. Johnson S.A., McNeill T., Cordell B. & Finch C.E. Relation of neuronal APP751/APP695 mRNA ratio and neuritic plaque density in Alzheimer's disease. *Science* 1990; 248:854-857.

65. Bush A.E., Pettingell W.H., Multhaup G., Moir R.D. & de Paradis M. Rapid induction of Alzheimer's amyloid beta formation by zinc. *Science* 1994; 265: 1464-1467.
66. Saunderson J.M., Arthur J.W. & Dunbrack J.R. Modelling of substrate specificity of the Alzheimer's disease amyloid precursor protein β secretase. *Journal of Molecular Biology* 2000; 300: 756-763.
67. Ghosh J., Stein R. & Hessian P. Structure based design: potent inhibitors of human brain memapsin 2 (beta secretase). *Journal of Medicinal Chemistry* 2001; 44: 2865-2868.
68. Hadland B.K. Corder V., Smith R.P., Roberts A.D. & Rossjohn E. Gamma secretase inhibitors repress thymocyte development. *Proceedings of the National Academy of Science*. 2001; 98: 7487-7491.
69. Weggen S., Eriksen J.L., Das P., Sagi S.A., Wang R., Pietrzik C.U., Findlay K.A., Smith T.E., Murphy M.P., Butler T., Kang D.E., Marquez-Sterling N., Golde T.E. & Koo E.H. A subset of NSAID's lower amyloidogenic A β 42 independently of cyclooxygenase activity. *Nature* 2001; 414: 212-216.
70. Nitsch R.M., Slack B.E., Wurtman R.J. & Growdon J.H. Release of Alzheimer amyloid precursor derivatives stimulated by activation of muscarinic acetylcholine receptors. *Science* 1992; 258: 304-307.

71. Schenk D., Barber R., Dunn W., Gordon G., Grajeda H., Guido T., Hu K., Huang J., Johnson-Wood K., Khan K., Kholodenko D., Lee M., Liao Z. & Wogulis M. Immunisation with amyloid beta attenuates Alzheimer's disease-like pathology in the PDAPP mouse. *Nature* 1999; 400: 173-177.

72. Bard F. & Powis D. Peripherally administered antibodies against amyloid beta enter the central nervous system and reduce pathology in a mouse model of Alzheimer's disease. *Nature Medicine* 2000; 6: 916-919.

73. Pepys M.B., Herhert J., Hutchinson W.L., Tennet G.A., Lachmann H.J., Gallimore J.R., Lovat L.B., Bartfai T., Murray S., Thompson D. & Purvis A. Targeted pharmacological depletion of serum amyloid P component for treatment of human amyloidosis. *Nature* 2002; 417: 254-259.

74. Kivipelto M., Saunderson T. & Johnson S.A. Midlife vascular risk factors and Alzheimer's disease in later life: longitudinal population based study. *British Medical Journal* 2001; 322: 1447-1451.

75. Jick H., Zornberg G.L., Jick S.S., Sheshadri S. & Drachman D.A. Statins and the risk of dementia. *Lancet* 2000; 356: 1627-1631.

76. Fassbender K., Simmons M., Bergmann C., Stroick M., Lutjohann D., Keller P., Runz H., Kuhl S., Bertsch T., von Bergmann K. & Beyreuther K. Simvastatin strongly reduces levels of Alzheimer's disease beta amyloid peptides A β 40 and A β 42

in vitro and in vivo. *Proceedings of the National Academy of Science* 2001; 98:5856-5861.

77. Sparks D.L., Scheff S.W., Hunsaker J.C. 3rd, Liu H., Landers T. & Gross J.R. Induction of Alzheimer-like beta amyloid immunoreactivity in the brains of rabbits with dietary cholesterol. *Experiments in Neurology* 1994; 126: 88-94

78. Cherney R.A., Atwood C.S., Xilinas M.E., Gray D.N., Jones W.D., McLean C.A., Barnham K.J., Volitakis I. & Fraser F.W. Treatment with copper-zinc chelator markedly and rapidly inhibits B amyloid accumulation in Alzheimer's disease transgenic mice. *Neuron* 2001; 30: 655.

79. Rogers J.T., Randall J.D., Eder P.S., Huang X., Bush A.I., Tanzi R.E., Venti A., Payton S.M. & Giodano T. Alzheimer's disease drug discovery targeted to the APP mRNA 5' untranslated region. *Journal of Molecular Neuroscience* 2002; 19: 77-82.

80. www.thebiotechclub.org/industry/emerging/proteomics.php

81. Pennisi E. Human genome: reaching their goal early, sequencing labs celebrate. *Science* 2003; 300:409.

82. Laemmli U.K. Cleavage of structural proteins during the assembly of the head of bacteriophage T4. *Nature* 1970; 227: 680-685.

83. O'Farrel P.H. High resolution two-dimensional electrophoresis of proteins. *Journal of Biological Chemistry* 1975; 250: 4007-4021.

84. Lauber W.M., Carroll J.A., Dufield D.R., Kiesel J.R., Radabaugh M.R. & Malone J.P. Mass spectrometry compatibility of two-dimensional gel protein stains. *Electrophoresis* 2001; 22: 906-918.
85. Lopez M.F., Berggren K., Chernokalskaya E., Lazarev A., Robinson M. & Patton W.F. A comparison of silver stain and Sypro ruby protein gel stain with respect to protein detection in two-dimensional gels and identification by peptide mass profiling. *Electrophoresis* 2000; 21: 3673-3683.
86. Naidong W., Hua S., Roets E. & Hoogmartens J. Assay and purity control of tetracycline and oxytetracycline in animal feeds and premixes by TLC densitometry with fluorescent detection. *Journal of Pharmaceutical and Biomedical Analysis* 2003; 33: 85-93.
87. Southern E.M. Detection of specific sequences among DNA fragments separated by gel electrophoresis. *Journal of Molecular Biology* 1975; 98: 503-517.
88. Ogorzalek Loo R.R., Mitchel C., Stevenson T.I., Loo J.A. & Andrews P.C. Diffusive transfer to membranes as an effective interface between gel electrophoresis and mass spectrometry. *International Journal of Mass Spectrometry and Ion Processes* 1997; 169/170: 273-290.
89. Towbin H., Ozbey. & Zingel O. An immunoblotting method for high resolution isoelectric focussing of protein isoforms in immobilised pH gradients. *Electrophoresis* 2001; 22: 1887-1893.

90. Vestling M.M. & Fenselau C. Poly(vinylidene difluoride) membranes as the interface between laser desorption mass spectrometry, gel electrophoresis and in situ proteolysis. *Analytical Chemistry* 1994; 66: 471-477.
91. Abersold R. *Advances in Electrophoresis*. 1990; 1st ed., Weinheim publishing.
92. Strupat K., Karas M., Hillenkamp f., Eckerskorn C. & Lottspeich F. Matrix assisted laser desorption of proteins electroblotted after polyacrylamide gel electrophoresis *Analytical Chemistry* 1994; 66: 464-470.
93. Western blot processing technical manual at URL <http://www.apbiotech.com>
94. Mann M., Hojrup P. & Roepstorff P. Advances in Mass Spectrometry *Journal of Biological Mass Spectrometry* 1993; 22: 338-345.
95. Henzel W.J., Billeci T.M., Stults J.T., Wong S.C., Grimley C. & Watanabe C. A new technique for protein identification. *Proc National Acad Science* 1993; 90: 5011-5015.
96. Pappin D.J.C., Hojrup P. & Bleasby A.J. Peptide mass mapping. *Current Opinions in Biology* 1993; 3: 327-332.
97. James P.M., Quadroni J.D.C., Carafoli E. & Gonner G. Enzyme digest reagents and their use in mass spectrometry. *Biochemistry and Biophysical Research Communications* 1993; 195; 58-64.

98. Beynon R.J. & Bond J.S. *Proteolytic Enzymes: A Practical Approach* 1989, Oxford University Press, Oxford.
99. Keil B. *Enzymic Cleavage of Proteins: Methods in Protein Sequence Analysis* 1981, Humana Press, Clifton, New Jersey.
100. Patterson D.H., Tarr G.E., Regnier F.E. & Martin S.A. C-terminal ladder sequencing via MALDI-MS coupled with carboxy peptidase Y time dependant and concentration dependant digestions. *Analytical Chemistry* 1995; 67: 3971-3978.
101. Parker K.C, Garrels J.I., Hines W., Butler E.M., McKee A.H., Patterson D. & Martin S. Identification of yeast proteins from two-dimensional gels. *Electrophoresis* 1998; 19: 1920-1932.
102. Barber M., Bordoli R.S., Sedgwick R.D. & Tyler A.N. Fast atom bombardment in the analysis of large molecules. *Nature* 1981; 293:270-275.
103. Macfarlane R.D. *Methods in Enzymology* 1990; 193:263-279.
104. Gross J. & Strupat K. Matrix assisted laser desorption ionisation-mass spectrometry applied to biological macromolecules. *Trends in Analytical Chemistry* 1998;17: 470-484.
105. Fenn J.B., Mann M., Meng C.K., Wong S.F. & Whitehouse C.M. Electrospray ionisation for mass spectrometry of large biomolecules. *Science* 1989; 246: 64-71.

106. Karas M. & Hillenkamp F. Laser desorption ionisation of proteins with molecular masses exceeding 10,000 daltons. *Analytical Chemistry* 1988; 60: 2299-2301.
107. Tanaka K., Ido Y., Akita S., Yoshida Y. & Yoshida T. Presented at the Second Japan-China Joint Symposium on Mass Spectrometry (abstract) Takarazuka Hotel, Osaka, Japan; Sept 15-18, 1987.
108. Beavis R.C. & Chait B.T., High accuracy molecular mass determination of proteins using matrix assisted laser desorption ionisation-mass spectrometry. *Analytical Chemistry* 1990; 62:1836-1840.
109. Beavis R.C., Chaudhary T. & Chait B.T. α -cyano-4-hydroxycinnamic acid as a matrix for matrix-assisted laser desorption ionisation-mass spectrometry. *Organic Mass Spectrometry* 1992; 27:156-158.
110. Strupat K., Karas M. & Hillenkamp F. 2,5-dihydroxybenzoic acid: a new matrix for laser desorption ionisation mass spectrometry. *International Journal of Mass Spectrometry and Ion Processes* 1991; 111:89-102.
111. Karas M., Bahr U. & Hillenkamp F. UV laser matrix desorption/ionisation mass spectrometry of proteins in the 100,000 dalton range. *International Journal of Mass Spectrometry and Ion Processes* 1991; 92: 231-242.

112. Schleuder D., Hillenkamp F. & Strupat K. IR-MALDI-mass analysis of electroblotted proteins directly from membranes, application to on-membrane digestion and protein identification by database searching. *Analytical Chemistry* 1999; 71: 3238-3247.
113. Asara J. & Allison J. Enhanced detection of oligonucleotides in UV MALDI-MS using tetraamine spermine as a matrix additive. *Analytical Chemistry* 1999; 71 2866-2870.
114. Stimson E., Truong O., Richter W.J., Waterfield M.D. & Bulingame A.L. Enhancement of charge remote fragmentation in protonated peptides by high energy CID MALD-TOF-MS using cold matrices. *International Journal of Mass Spectrometry and Ion Processes*. 1997; 169/170:231-240.
115. Yongseong K., Hurst G.B., Doktycz M.J. & Buchanan M.V. Improving spot homogeneity by using polymer substrates in matrix-assisted laser desorption ionisation mass spectrometry of oligonucleotides. *Analytical Chemistry* 2001; 67: 191-210.
116. Yates III J.R. Mass Spectrometry and the age of the proteome. *Journal of Mass Spectrometry* 1998; 33:1-19.
117. Johnstone R.A.W. & Rose M.E. Mass spectrometry for chemists and biochemists. 1996; 2nd ed., Cambridge University Press.
118. Carr S.A. & Annan R.S. Current Protocols in Protein Science. Supplement 4; John Wiley & Sons 1996.

119. MALDI-TOF at URL <http://www.chem.cmu.edu/oma/maldiscience>
120. Vorm O., Roepstorff P. & Mann M. Improved resolution and very high sensitivity in matrix assisted laser desorption ionisation of matrix surfaces made by fast evaporation. *Analytical Chemistry* 1994; 66: 3281-3287.
121. Jéspersen S., Niessen W.M., Tjaden U.R., Van der Greef J., Litborn E., Lindenburg U. & Roerade J. Attomole detection of proteins by matrix assisted laser desorption ionisation mass spectrometry with the use of picolitre vials. *Rapid Communications in Mass Spectrometry* 1994; 8: 581-584.
122. Brown R.S & Lennon J.J. Mass resolution improvement by incorporation of pulsed ion extraction in a matrix assisted laser desorption ionisation linear time of flight mass spectrometer. *Analytical Chemistry* 1995; 67: 1998-2003.
123. Brown R.S. & Lennon J.J. Sequence specific fragmentation of matrix assisted laser desorbed protein/peptide ions. *Analytical Chemistry* 1995; 67: 3990-3999.
124. Wiley W.C. & McLaren I.H. Time of flight mass spectrometer with improved resolution. *Revue in Scientific Instruments* 1955; 26:1150.
125. Vorm O. & Mann M. Improved mass accuracy in matrix assisted laser desorption ionisation time of flight mass spectrometry of peptides. *Journal of the American Society of Mass Spectrometry* 1994; 5:955-958.

126. Chernushevich I.V., Loboda A.V. & Thompson B.A. An introduction to quadrupole time of flight mass spectrometry. *Journal of Mass Spectrometry* 2001; 36: 849-865.
127. Krutchinsky A.N., Loboda A.V., Spicer V.L., Dworschak R., Ens W. & Standing K.G. Increased resolution seen with orthogonal MALDI-TOF. *Rapid Communications in Mass Spectrometry* 1998; 12: 508-512.
128. Mirgorodskaya O.A. & Shevchenko A.A. Electrospray time of flight mass spectrometry in protein chemistry. *Analytical Chemistry* 1994; 66: 99-107.
129. Verentchikov A.N., Ens W. & Standing K.G. Reflecting time of flight mass spectrometer with an electrospray source and orthogonal extraction. *Analytical Chemistry* 1994; 66: 126-133.
130. Kaufmann R., Kirsch D. & Spengler B. Sequencing of peptides in a time of flight mass spectrometer: Evaluation of post source decay following matrix assisted laser desorption ionisation. *International Journal of Mass Spectrometry and Ion Processes* 1994; 131:355-385.
131. Carr S.A. & Annan R.S. *Current Protocols in Protein Science. Supplement 4*; John Wiley & Sons 1996.
132. Sherman N.E., Yates N.A., Shabanowitz J., Hunt D.F., Jeffrey W., Jones M.B. & Pappin D.J. A novel N terminal derivative designed to simplify peptide fragmentation. In Proceedings of the 43rd ASMS conference on mass spectrometry and allied topics. 1995 Atlanta Ga.

133. Keough T., Youngquist R.S. & Lacey P. A method for high sensitivity peptide sequencing using post source decay matrix assisted laser desorption ionisation mass spectrometry. *Proceedings of the National Academy of Science* 1999; 96:7131-7136.
134. Castoro J.A., Wilkins C.L., Wood A.S. & Cotter R.J. Peptide amino acid sequence analysis using matrix-assisted laser desorption ionisation and fourier transform mass spectrometry. *Journal of Mass Spectrometry* 1995; 30: 94-98.
135. Dorochenko V.M. & Cotter R.J. High performance collision induced dissociation of peptides formed by matrix-assisted laser desorption ionisation in an ion trap mass spectrometer. *Analytical Chemistry* 1995; 67: 2180-2187.
136. Lee H. & Lubman D.M. Sequence specific fragmentation generated by matrix-assisted laser desorption ionisation in a quadrupole ion trap reflectron time of flight device. *Analytical Chemistry* 1995; 67: 1400-1408.
137. Krutchinsky A.N., Loboda A.V., Spicer V.L., Dworschak R., Ens W. & Standing K.C. Coupling of the MALDI source to a quadrupole time of flight mass spectrometer. *Rapid Communications in Mass Spectrometry* 1997; 11: 1015-1024.
138. Krutchinsky A.N., Zhang W. & Chait B.T. Rapidly switchable MALDI and electrospray quadrupole time of flight mass spectrometer for protein identification. *Journal of the American Society for Mass Spectrometry* 2000; 11: 493-504.

139. Shevchenko A., Lobodo A., Shevchenko A., Ens W. & Standing K.G. MALDI quadrupole time of flight mass spectrometry: A powerful tool for proteomic research. *Analytical Chemistry* 2000; 72: 2132-2141.
140. Beuhler R.J., Flanigan E., Green L.J. & Freidman L. A new method of ionisation by electrospray. *Journal of the American Chemical Society* 1974; 96: 3600-3609.
141. Fenn J.B., Mann M., Meng C.K., Wong S.F. & Whitehouse C.M. Electrospray ionisation for mass spectrometry of large biomolecules. *Science* 1989; 246: 64-71.
142. Taylor G. *Proceedings of the National Academy of Science*. Tip cone formation of charged droplets. 1964; 280: 383-397.
143. Johnson T. *Current Protocols in Protein Science*. Supplement 4; John Wiley & Sons 1996.
144. Smith R.D. & Light-Wahl K.J. Multiple charging via the charged residue mechanism. *Biological Mass Spectrometry* 1993; 22:493.
145. Thompson B.A. & Iribarne J.V. Ion evaporation causes multiple charging of ions. *Journal of Chemistry and Physics* 1979; 71: 4451-4458.
146. Mann M., Meng C.K. & Fenn J.B. Interpreting mass spectra of multiply charged ions. *Analytical Chemistry* 1989; 61: 1702-1708.

147. Van Berkel G.J., Glish G.L. & McLuckey S.A. Electrospray ionisation coupled to ion trap mass spectrometry. *Analytical Chemistry* 1990; 63: 1284.
148. March R.E. & Todd J.F.J. (Eds.) *Practical Aspects of Ion Mass Spectrometry: Modern Mass Spectrometry Series*, C.R.C., Boca Raton, Florida, 1995.
149. Verentchikov A.N., Ens W. & Standing K.G. Reflecting time of flight mass spectrometer with an electrospray ion source and orthogonal extraction. *Analytical Chemistry* 1994; 66: 126-133.
150. Boyle J.G. & Whitehouse C.M. Electrospray ionisation and fourier transform ion cyclotron mass spectrometry *Analytical Chemistry* 1992; 64: 2084.
151. Franklin Smyth W. The use of electrospray mass spectrometry in the detection and determination of molecules of biological significance. *Trends in Analytical Chemistry* 1999; 18: 335-345.
152. Mass Spectrometry at URL <http://www.spectroscopynow.com/Spy/basehtml>
153. Dawson P.H. (Ed.) *Quadrupole Mass Spectrometry and its Applications*, Elsevier, Amsterdam, 1976, reissued by A.I.P. Press, Woddbury, New York, 1996.
154. Collings B.A. & Douglas D.J. An extended mass range quadrupole for electrospray mass spectrometry. *International Journal of Mass Spectrometry and Ion Processes* 1997; 162: 121-127.

155. Bruin A.P., Covey T.R. & Henion J.D. Ionspray: An interface to liquid chromatography. *Analytical Chemistry* 1987; 59: 2641.
156. Dulcks T. & Juraschek R. Electrospray as an ionisation method for mass spectrometry. *Journal of Aerosol Science* 1999; 30:927-943.
157. Advantages of nanospray at URL <http://www.electrospray.com>
158. Wilm M. & Mann M. Nanolitre sample analysis. *International Journal of Mass Spectrometry and Ion Processes* 1994; 136: 167.
159. Niessen W.M.A. Advances in instrumentation in liquid chromatography-mass spectrometry and related liquid introduction techniques. *Journal of Chromatography A* 1998; 794:407-435.
160. Smith R.D., Barinaga C.J. & Udseth H.R. The coupling of capillary electrophoresis to electrospray ionisation. *Analytical Chemistry* 1988; 60: 1948.
161. Yates J.R. *Methods in Enzymology* 1996; 271: 351.
162. Yost R.A. & Boyd R.K. *Methods in Enzymology* 1990; 193: 154.
163. Dongr'e A.R. Somogyi A. & Wysocki V.H. New approaches in mass spectrometry. *Journal of Mass Spectrometry* 1996; 31: 339.

164. Schwartz J.C., Wade A.P., Enke C.G. & Cooks R.G. Tandem quadrupole mass spectrometry. *Analytical Chemistry* 1990; 62:1809.
165. Morris H.R., Paxton T., Dell A., Langhorne J., Berg M., Bordoli R.S., Hoyes J. & Bateman R.H. High sensitivity collisionally activated decomposition tandem mass spectrometry on a novel quadrupole orthogonal acceleration time of flight mass spectrometer. *Rapid Communication in Mass Spectrometry* 1996; 10: 889-896.
166. Krutchinsky A.N., Zhang W. & Chait B.T. Rapidly switchable MALDI and electrospray quadrupole time of flight mass spectrometry for protein identification. *Journal of the American Society for Mass Spectrometry* 2000; 11: 493-504.
167. Shevchenko A., Loboda A., Shevchenko A., Ens W. & Standing K.G. Maldi quadrupole time of flight mass spectrometry: a powerful tool for proteomics research. *Analytical Chemistry* 2000; 72: 2132-2141.
168. Biemann K. *Methods in Enzymology* 193; 455-479 1990
169. Roepstorff P. & Fohlmann J. Proposal for a common nomenclature for sequence ions in mass spectra of peptides. *Biomedical mass Spectrometry* 1984; 11: 601.
170. Johnson T. *Current Protocols in Protein Science. Supplement 5*; John Wiley & Sons 1996.
171. Peptide fragmentation at URL <http://www.matrixscience.com/>

172. Hernandez L.M., Ballou L., Alvarado E., Gillece-Castro B.L., Burlingame A.L. & Ballou C.E. A new *saccharomyces cerevisiae mnn* mutant N-linked oligosaccharide structure. *Journal of Biological Chemistry* 1989; 269: 11849-11856.

173. Settineri C.A. & Burlingame A.L. Mass spectrometry of carbohydrates and glycoconjugates. *Modern Chromatographic and Electrophoretic Methods in Carbohydrate Analysis*. Elsevier, 1995, 447-514.

174. Post-translational modifications at URL <http://www-isu.indstate.edu/thsmc>

175. Msfit at URL <http://prospector.ucsf.edu/ucsfhtml3.4/msfit.htm>

176. Pappin D.J.C., Hojrup P. & Bleasby A.J. at URL <http://www.hgmp.mrc.ac.uk>

177. Hutchens T.W. & Yip T.T. New desorption strategies for the mass spectrometric analysis of macromolecules. *Rapid Communications in Mass Spectrometry* 1993; 7:576-580.

178. Davies H. Lomas L & Austen B. Profiling of amyloid B peptide variants using SELDI Protein Chip Array biotechniques. 1999; 27: 1258-1261.

179. Goldstein L.E., Muffat J.A., Cherny R.A., Mar R.D., Ericsson M.H., Huang X., Mavros C., Coccia S.A., Faget N.Y., Fitch K.A., Masters C.L., Tanzi R.E., Chylack L.T. & Bush A.I. Cytosolic beta amyloid deposition and supranuclear cataracts in lenses from people with Alzheimer's disease. *The Lancet* 2003; 361: 1258-1265.

180. Carrette O., Demalte I., Sherle A., Yalkimoglu O., Corthals G., Burkhard P., Hochstrasser D.F. & Sanchez J.C. Cerebrospinal fluid potential biomarkers for the diagnosis of Alzheimer's disease. *Proteomics* 2003; 8: 1486-1494.

181. Puchades M., Hansson S.F., Nilsson C.L., Andreasen N., Blennow K. & Davidsson P. Proteomic studies of potential cerebrospinal fluid protein markers for Alzheimer's disease. *Molecular Brain Research* 2003; 118: 140-146.

182. Lewis H.D., Beher D., Smith D., Hewson L., Cookson N., Reynolds D.S., Dawson G.R., Jiang M., Van der Ploeg L.H.T., Qian S., Rosahl T.W., Kalaria R.N. & Shearman M.S. *Neurobiology of Aging* 2004; 25:1175-1185.

183. Kanninen K., Goldstein G., Auriola S., Alafuzoff I. & Koistinaho J. Glycosylation changes in Alzheimer's disease as revealed by a proteomic approach. *Neuroscience Letters* 2004. Article in Press.

184. Castegna A., Aksenov M.Y., Aksenova M.V., Thongboonkerd V., Klein J.B., Pierce W.M., Booze R., Markesbury W.R. & Butterfield D.A. Proteomic identification of oxidatively modified proteins in Alzheimer's disease. *Radical Biological Medicine* 2002; 33:562-571.

185. Butterfield D.A & Castegna A. Proteomic analysis of oxidatively modified proteins in Alzheimer's disease: insights into neurodegeneration *Cellular Molecular biology* 2003; 49: 747-751.

186. Drake J., Link C.D. & Butterfield D.A. Oxidative stress precedes fibrillar deposition of Alzheimer's disease A beta peptide (1-42) in transgenic caenorhabditis elegans model. *Neurobiology of Aging* 2003; 24: 415-420.
187. Lee Y., Aono M., Laskowitz D., Warner D.S. & Pearlstein R.D. Apolipoprotein E protects against oxidative stress in mixed neuronal-glial culture by reducing glutamate toxicity. *Neurochemical International* 2004; 44: 107-118.
188. Poon H.F., Castegna A., Farr S.A., Thongboonkerd V., Lynn B.C., Banks W.A., Morly J.E., Klein J.B. & Butterfield D.A. Quantitative proteomics analysis of specific protein expression and oxidative modification in aged senescence-accelerated-prone 8 mice brain. *Neuroscience* 2004; 126: 915-926.
189. Choi J., Forster M.J., McDonald S.R., Weintraub S.T., Caroll C.A. & Gracy R.W. Proteomic identification of specific oxidised proteins in ApoE-knockout mice: relevance to Alzheimer's disease. *Free Radical biology and Medicine* 2004; 36: 1155-1162.
190. Bagshaw R.D., Pasternak S.H., Mahuran D.J. & Callahan J.W. Nicastrin is a residual lysosomal membrane protein. *Biochemical and Biophysical Research Communications* 2003; 300: 615-618.
191. Terry D.E., Umstot E & Desidero D.M. Optimised sample processing time and peptide recovery for the mass spectrometry analysis of protein digests. *Journal of the American Society of Mass Spectrometry* 2004; 15: 784-794.

192. Kienlen-Campard P., Tasiaux B. & Octave J.N. The processing and biological function of the human amyloid precursor protein: lessons from different cellular models. *Experimental Gerontology* 2000; 35: 843-850.
193. Hanspeter S., Fischer I.B., Dieter S, Schatz C.H. & Saria A. Retinoic acid treatment enhances the acetylcholine contents in the human teratocarcinoma cell line Ntera-2. *Regulatory Peptides* 200; 96: 59-63.
194. Rabilloud T., Strub J.M., Luche S., Dorsselaer A. & Lunardi J. A comparison between Sypro Ruby and ruthenium II tris (bathophenanthroline disulfonate) as fluorescent stains for protein detection in gels. *Proteomics* 2001;1: 699-704.
195. Gobom J., Nordhoff E, Ekmann R. & Roepstorff P. Rapid micro-scale proteolysis of proteins for MALDI-MS peptide mapping using immobilised trypsin . *International Journal of Mass Spectrometry* 1997; 169/170: 153-163.
196. Shevchenko A., Loboda A., Shevchenko A., Ens W. & Standing K.G. MALDI quadrupole time of flight mass spectrometry: a powerful tool for proteomic research. *Analytical Chemistry* 2000; 72: 2132-2141.
197. Finehout E.J. & Lee K.H. Comparison of automated in-gel digest methods for femtomole level samples. *Electrophoresis* 2003; 24: 3508-3516.

198. Li A., Sowder R.C., Henderson L.E., Moore S.P., Garfinkel D.J. & Fisher R.J. Chemical cleavage at aspartyl residues for protein identification. *Analytical Chemistry* 2001; 73: 5395-5402.
199. Li G., Waltham M., Anderson N.L., Unsworth E., Treston A. & Weinstein J.N. Rapid mass spectrometric identification of proteins from two-dimensional polyacrylamide gels after in-gel proteolytic digestion. *Electrophoresis* 1997; 18: 391-402.
200. Johnson T. Current Protocols in Protein Science. Supplement 6; John Wiley & Sons 1996.
201. Baczek T. Fractionation of peptides in proteomics with the use of pI based approach and ZipTip pipettes. *Journal of Pharmaceutical and Biomedical Analysis* 2004; 34: 851-860.
202. Stasyk T., Hellman U. & Souchelnytsky S. Optimising sample preparation for 2-D electrophoresis *Electrophoresis* 2001; 9: 3217-3221.
203. Speicher K.D., Kolbas O., Harper S & Speicher D.W. Systematic analysis of peptide recoveries from in-gel digestions for protein identifications in proteome studies. <http://www.abrf.org>

204. Shepherd C.E., Bowes S., Parkinson D., Cambray-Deakin M. & Pearson C.A.

Expression of amyloid precursor protein in human astrocytes in vitro: Isoform specific increases following heat shock. *Neuroscience* 2000; 99: 317-325.

205. Autolysis at URL <http://www.matrixscience.com/>

206. Keratin at URL <http://www.matrixscience.com/>

207. Modifications at URL <http://www.matrixscience.com/>

208. Peptide mass at URL <http://www.matrixscience.com/>

Acknowledgments

I would like to thank Dr D.Parkinson for all his help with protein purification techniques and Alzheimer's disease research and Dr M.R.Clench for his enthusiasm, ideas, help with mass spectrometry and general support throughout the whole project.